ROCK FRACTURE UNDER STATIC STRESS CONDITIONS

by

E. HOEK, B.Sc (Eng), M.Sc Eng.

A Thesis submitted to

The Faculty of Engineering of the
UNIVERSITY OF CAPE TOWN

in fulfillment of the requirements
for the degree of

DOCTOR OF PHILOSOPHY IN ENGINEERING

October, 1965

D E C L A R A T I O N

I declare that this thesis, entitled "Rock Fracture under Static Stress Conditions" is my own work and that it has not been submitted, as a whole or in part, to any other University for the purpose of obtaining a degree.

With the permission of the University of Cape Town, several parts of this study have been published prior to the submission of this thesis.

Signed by candidate
Signature removed

E. HOEK

Pretoria, 1st October, 1965.

ROCK FRACTURE UNDER STATIC STRESS CONDITIONS

ABSTRACT

A knowledge of the strength of a material is an essential prerequisite to the successful design of a structure in that material. Consequently, in designing deep level mining excavations and large civil engineering structures, an understanding of the mechanics of rock fracture, particularly under compressive stress conditions, is of fundamental importance.

This thesis contains details of an investigation into the applicability of Griffith's brittle fracture theory, modified to account for the effects of crack closure in compression, to the prediction of rock fracture behaviour. It is shown that this theory provides a reliable basis for the analysis of hard rock fracture under static stress conditions.

The application of the Griffith's theory to the prediction of rock fracture initiation and propagation in a complex stress field is illustrated by means of a detailed analysis of the behaviour of the rock around a circular hole in a biaxial stress field.

While this study is primarily concerned with rock fracture problems associated with deep level mining, it is believed that the general principles are equally useful in the analysis of rock and concrete fracture problems encountered in civil engineering.

ACKNOWLEDGMENTS

The author wishes to record his indebtedness to the South African Council for Scientific and Industrial Research and the Transvaal and Orange Free State Chamber of Mines for the opportunity to carry out this work and for permission to publish parts of it and to submit the whole as a thesis.

Particular acknowledgments are due to Dr H.G. Denkhaus, Director of the National Mechanical Engineering Research Institute, for his continued guidance, support and encouragement. Dr R.S. Loubser and Mr E.R. Leeman, as heads of divisions in which this work was carried out, played a significant part in encouraging the development of this research. The author's colleagues who contributed in the form of discussion, ideas and assistance.

Amongst those who have contributed freely from their experience and who have advised and encouraged the author are Professor W.M. Brace of Massachusetts Institute of Technology (who also carried out a series of tests on chert dyke), Dr J.B. Walsh of Wood's Hole Oceanographic Institute and Dr J.R. Hoskins of the U. S. Bureau of Mines.

Particular thanks are due to Mrs J.J. Lötter who has typed this thesis as well as the hundreds of pages of preliminary work and publication manuscripts. Also the National Mechanical Engineering Research Institute's drawing office and the CSIR's Graphic Arts Division who were responsible for processing the drawings and photographs.

Finally, the author wishes to thank his wife and family for their encouragement and patience during the course of this research.

TABLE OF CONTENTS

LIST OF SYMBOLS

a	spacing between neighbouring atomic planes
a	radius of circular hole
b	fissure or crack spacing in specimen
c	half-length of crack
d	diameter of specimen
k	principal stress ratio σ_3/σ_1
m	coefficient relating strength of specimen to strength of rock mass
r	radius of crack-tip
x, z	Cartesian co-ordinates
r, θ	polar co-ordinates
ξ, η	elliptical co-ordinates
A_o	area of crack opened by pore pressure
D	hole diameter
D_L	load piston diameter
D_p	pressure piston diameter
D_s	specimen diameter
E	Young's modulus or modulus of elasticity
L	crack length
P	pore pressure
P	vertical applied stress
Q	lateral applied stress
R	radius of curvature of parabola
R_{apex}	radius of apex of parabola
W	total potential energy
W_e	excess strain energy
W_k	total kinetic energy
W_{pl}	plastic work

V	voltage
γ	specific surface energy
ν	Poisson's ratio
ψ	angle between axis of crack and major principal stress direction
ψ_c	critical crack orientation
ε_r	radial strain
ε_n	normal strain
μ	coefficient of friction between crack surfaces
ξ_o	value of elliptical co-ordinate ξ on crack boundary
σ_a	applied tensile stress
σ_c	uniaxial compressive strength
σ_m	mean stress $\frac{1}{2}(\sigma_1 + \sigma_3)$
σ_n	normal stress
σ_o	maximum value of σ_η for ψ_c
σ_o	molecular cohesive strength
σ_p	major principal stress in model plane
σ_q	minor principal stress in model plane
σ_r	radial stress
σ_s	strength of specimen
σ_t	uniaxial tensile strength
σ_M	strength of rock mass
σ_N	maximum value of σ_η for any ψ
σ_{cp}	uniaxial compressive strength of primary crack system
σ_{cs}	uniaxial compressive strength of secondary crack system
C_{tp}	uniaxial tensile strength of primary crack system
σ_{ts}	uniaxial tensile strength of secondary crack system
σ_{cr}	critical stress required to close cracks
$\bar{\sigma}_n$	average normal stress
σ_{xx}	stress normal to xx in xz plane

σ_η tangential stress on crack boundary

σ_θ tangential stress

σ_1 major (algebraically largest) principal stress

σ_2 intermediate principal stress

σ_3 minor (algebraically smallest) principal stress

τ_n shear resistance = $\mu\sigma_n$

$\bar{\tau}_n$ average shear resistance

τ_{xz} shear stress in xz plane.

ROCK FRACTURE UNDER STATIC STRESS CONDITIONS

1. INTRODUCTION

The successful mining of an ore body or coal seam depends largely upon the extent to which fracture and movement of the rock around the excavations can be controlled.

Controlled rock fracture, achieved by careful planning of the geometrical layout of the excavations and the correct choice of support and other operational factors, results in safe and efficient operation of the mine. Uncontrolled rock fracture, manifesting itself in such phenomena as rockbursts, disrupts mining operations and constitutes a serious hazard to men and machines in the mine.

Current mining methods and strata control techniques, evolved almost entirely from practical experience, have proved remarkably effective and will continue to form the basis of mining practice. However, improved operational efficiency requires that these techniques be supplemented with a more fundamental understanding of the mechanism of deformation and fracture of the rock around mining excavations. This is particularly true in areas where the richest and most accessible ore bodies have been mined out and future mining operations are faced with mining lower grade ore at greater working depths.

In civil engineering, a knowledge of rock deformation and failure is particularly important in the design of foundations for large dam structures. Improved design techniques have resulted in a steady increase in the size and complexity of these structures but continued progress depends upon the provision of adequate foundations which, in turn, depends upon the successful application of rock mechanics.

The results of laboratory tests indicate that many rock types exhibit elastic stress-strain relationships up to fracture*.

---

* Elasticity implies a reversible stress-strain curve which may, or may not, be linear. In the case of most hard rocks the stress-strain curve is, in fact, usually linear up to fracture.

Since a material which behaves elastically up to fracture is defined as brittle, it is evident that a study of the basic mechanism of brittle fracture is a useful starting point for any investigation into the phenomena associated with the fracture of rock.

The present study is an attempt to collect the relevant information from available literature on brittle fracture, to extend it where necessary and to present it in a form which is directly applicable to the solution of practical rock mechanics problems. It is concerned with the problem of fracture initiation under static load conditions only; the problems of fracture propagation and fracture initiation under dynamic stress conditions are beyond its scope.

This study is presented in three parts:

Part I - Theoretical considerations of brittle fracture initiation under static load conditions.

Part II - The fracture of brittle rock and the influence of additional factors, such as anisotropy, specimen selection and preparation and environmental conditions during testing, upon the fracture of rock.

Part III - The practical application of rock fracture criteria to the analysis of observed fracture phenomena.

The development and even the experimental verification of a brittle fracture criterion for rock is of little value unless it can be demonstrated that this criterion can be effectively applied to the solution of practical engineering problems. Consequently, one of the most important parts of this study is that which deals with attempts to apply the fracture criterion, dealt with in Part I, to the analysis of observed rock fracture phenomena.

The study forms part of an extensive research project which is being carried out in the Rock Mechanics Division of the National Mechanical Engineering Research Institute on behalf of the Transvaal and Orange Free State Chamber of Mines.

PART I - THEORETICAL CONSIDERATIONS OF BRITTLE FRACTURE INITIATION UNDER STATIC LOAD CONDITIONS

In 1920, A.A. Griffith of the Royal Aircraft Establishment at Farnborough presented a brittle fracture hypothesis in a paper to the Royal Society[150]*. In this paper he postulated that fracture of a brittle material, subjected to pure tensile stress, initiates at microscopic cracks and discontinuities within the material.

In a second paper, presented in 1924[151], Griffith extended this concept of fracture initiation to the case of multiaxial compression. In both papers he derived equations which could be used to predict the fracture stress.

In mechanical engineering, interest in brittle fracture has been mainly confined to steel. In this field, important contributions have been made by Irwin[208], Orowan[288], Wells[368] and many others. These authors have dealt with such problems as fracture initiation from dislocations and plastic slip planes, velocity of crack growth and energy changes associated with brittle fracture.

In mining engineering and particularly in rock mechanics, the fracture of rock subjected to various states of multiaxial stress is of vital interest. The hypothesis postulated in Griffith's second paper[151] has only been applied to this problem within the past few years. The most important contributions to this work have been made by Murrell[270], Brace[52] and McClintock and Walsh[249]. The work of the last named authors is particularly important since it extends Griffith's theory which deals with open cracks only to cracks which have closed in compression.

A review, by Barenblatt[23], of Russian literature on brittle fracture has recently become available. It is interesting to note that a considerable amount of attention has been paid to the fracture of rock, particularly oil-bearing strata subjected to pressure from a permeating liquid[24, 25, 26, 380, 381].

The Russian work is based upon the Griffith hypothesis of

---

* Superscripts refer to items listed in the bibliography at the end of this study.

fracture initiation from existing cracks but the theoretical approach used in deriving the equations for the fracture stress is somewhat different from that used by British and American authors. Since the final equations which are of interest in this study are identical in the two approaches, no useful purpose would be served by including details of the Russian work.

2. THE THEORETICAL STRENGTH OF AN ELASTIC MATERIAL

According to Orowan[286], an estimate of the molecular cohesion of a solid can be obtained from its surface energy which, in turn, can be used to calculate the order of magnitude of the fracture stress by means of the following equation:

$$\sigma_o = \sqrt{\frac{2\gamma E}{a}} \quad \ldots\ldots\ldots\ldots\ldots\ldots \quad (1)$$

where σ_o is the magnitude of the uniaxial tensile stress required to overcome the molecular cohesion of the material = interatomic fracture strength

γ is the specific surface energy of the material

E is the Young's modulus and

a is the spacing between neighbouring atomic planes.
= distance between two planes at right angles to the fracture

For brittle materials such as hard rock the value of E lies between 10×10^6 and 15×10^6 lb/sq. in, a is of the order of 1.2×10^{-7} in and the order of magnitude of the specific surface energy is 6×10^{-4} lb in/sq. in. Hence the theoretical strength of these materials is approximately 3.5×10^6 lb/sq. in.

Under certain conditions, tensile strengths of glass fibres approaching this order of magnitude have been measured[150] but, in general, materials fail at a stress level several orders of magnitude lower than that predicted from equation (1). Griffith's theory of brittle fracture initiation is generally regarded as an acceptable explanation for the discrepancy between the observed and theoretical strengths of brittle materials.

3. GRIFFITH THEORY OF BRITTLE FRACTURE INITIATION

Griffith[150] assumed that the discrepancy between the theoretically estimated and the observed value of the tensile strength of brittle materials is due to the presence of small cracks, flaws and other discontinuities around which high stress concentrations occur when the material is stressed.

By assuming that a crack in a two-dimensional (plane) body can be approximated by an ellipse of large eccentricity, Griffith was able to calculate, from the analytical solution of the stress distribution around elliptical openings in a plane body under stress[207], that the maximum stress at the end of a crack orientated at right angles to the direction of applied tension is given by

$$\sigma_o \simeq 2\sigma_a\sqrt{\frac{c}{r}} \qquad \ldots\ldots\ldots\ldots\ldots\ldots (2)$$

where σ_a is the applied tensile stress

$2c$ is the length of the crack and

r is the radius of the end of the crack.

Since, in 1920, Griffith had no experimental techniques at his disposal for the determination of the actual values of the crack dimensions c and r, he based his calculations upon assumptions concerning the energy required to propagate the crack. It will be shown later that the final results obtained by Griffith can be arrived at without making these assumptions but, since the original calculations are instructive, the concepts upon which they were based are included here.

3.1 Energy changes associated with crack propagation

If a crack of length 2c in a body subjected to static external tension is to propagate by a small increment dc, the energy present in the system is redistributed. The changes involved are as follows:

(1) A loss in potential energy of the externally applied forces due to displacements induced

by the crack propagation. If the total potential energy of the external forces is denoted by W, the change in W due to a change of dc in crack length is $-dW/dc$.

(2) A gain in the excess strain energy in the material around the crack. This excess strain energy is given by the difference between the strain energy in the cracked body and that in the same body without a crack. If the excess strain energy is W_e, the gain in W_e due to a change of dc in crack length is dW_e/dc.

(3) A gain in surface energy of the crack due to the breaking of the molecular bonds along the crack path. If the total surface energy is W_s, then the change in W_s due to a change of dc in crack length is dW_s/dc.

(4) A gain in the kinetic energy of the system due to the propagation of the crack. If the total kinetic energy in the system is W_k*, the increase in W_k due to an increase dc in the crack length is dW_k/dc.

(5) An expenditure of potential energy on plastic deformation at the crack tip in the case of a material which does not exhibit ideal elastic behaviour. The amount of energy expended on plastic deformation, for an increase of dc in crack length, is $+dW_{pl}/dc$.

Since the energy balance of the system must be maintained, the five energy changes listed above can be related by the following equation:

$$dW/dc = dW_e/dc + dW_s/dc + dW_k/dc + dW_{pl}/dc \quad \ldots\ldots\ldots (3)$$

A useful summary of the role of the four energy terms, contained in the right hand side of equation (3), in the fracture of

---

* In the case of a static system, the initial kinetic energy $W_k = 0$.

actual engineering materials has been given by Corten and Park[89].

In the case of materials which exhibit considerable plasticity, such as mild steel, the plastic energy term dW_{pl}/dc can dominate the energy balance of the system[128]. On the other hand, in brittle materials this term is assumed to be negligibly small in comparison with the other terms and can be ignored.

Since this study is concerned primarily with fracture initiation under static load conditions, it can be assumed that the kinetic energy changes involved are so small that they can be neglected in the following analysis.

Consequently, the energy balance governing fracture initiation in a brittle material under static load conditions can be simplified to the following equation:

$$dW / dc = dW_e/dc + dW_s/dc \quad \ldots\ldots\ldots (4)$$

It can be shown* that the gain in excess strain energy around the crack is equal to half the loss in potential energy of the external forces:

$$dW_e/dc = \tfrac{1}{2}\, dW/dc \quad \ldots\ldots\ldots\ldots\ldots (5)$$

Hence, equation (4) can be written as

$$dW_e/dc = dW_s/dc \quad \ldots\ldots\ldots\ldots\ldots (6)$$

In other words, the surface energy gained in rupturing the molecular bonds along the crack path must be equal to the net reduction in the strain energy of the system in order that the crack may propagate. If the strain energy reduction is smaller than the surface energy requirements, the crack will be stable and will not propagate.

---

* LOVE, A.E.H. A treatise on the mathematical theory of elasticity, 2nd edition, Cambridge Univ. Press, London, 1906, p. 170.

3.2 Derivation of fracture stress in a plane body

In order to evaluate equation (6), the excess strain energy in a plane body containing an elliptical crack is calculated. For a thin plate under plane stress conditions it is found to be

$$W_e = \frac{c^2 \pi \sigma_a^2}{E} \quad \ldots\ldots\ldots\ldots\ldots\ldots \quad (7a)$$

If the plate is thick compared with the dimensions of the crack, then plane strain conditions exist and the excess strain energy in the system is given by

$$W_e = \frac{c^2 \pi \sigma_a^2 (1 - \nu^2)}{E} \quad \ldots\ldots\ldots \quad (7b)$$

where ν is the Poisson's ratio of the material.

The surface energy of the crack per unit thickness of plate is given by

$$W_s = 4 \gamma c \quad \ldots\ldots\ldots\ldots\ldots\ldots \quad (8)$$

where γ is the specific surface energy, i.e. the quantity of energy per unit area of crack surface, and

$2c$ is the length of the crack.

According to equation (6), the condition for fracture initiation is that the change in excess strain energy is equal to the change in surface energy for a change dc in crack length. Hence, differentiation of equations (7) and (8) with respect to c and solving for the applied stress σ_a leads to the following condition for crack initiation under plane stress conditions:

$$\sigma_a = \sqrt{\frac{2 \gamma E}{\pi c}} \quad \ldots\ldots\ldots\ldots \quad (9a)$$

And for plane strain*

$$\sigma_a = \sqrt{\frac{2\gamma E}{\pi c(1-\nu^2)}} \quad \ldots\ldots\ldots\ldots (9b)$$

3.3 Derivation of fracture stress from atomic considerations

Orowans interpretation of Griffith's fracture theory is that a sufficient condition for crack propagation is that the tensile ~~stres~~ stress induced at the tip of the crack is equal to the molecular cohesive strength of the material[2 8 6].

Assuming that the radius of curvature (r) of the crack tip is of the order of magnitude of the atomic spacing a, equation (2) becomes

$$\sigma_o = 2\sigma_a \sqrt{\frac{c}{a}} \quad \ldots\ldots\ldots\ldots\ldots (10)$$

Dividing this equation by equation (1) which defines the theoretical strength due to molecular cohesion, the following relationship is obtained

$$\sigma_a = \sqrt{\frac{\gamma E}{2c}} \quad \ldots\ldots\ldots\ldots\ldots (11)$$

Within the accuracy of the assumption that the material behaves elastically up to fracture and that the crack can be represented by a two-dimensional ellipse, equation (12) is in good agreement with Griffith's original equations (9a) and (9b).

3.4 Derivation of fracture stress in a three-dimensional system

One of the principal objections to Griffith's original work is that his solution is a two-dimensional simplification of a three-dimensional problem. Actual cracks are almost certainly three-

---

* This equation was incorrectly stated in Griffith's original paper.

dimensional in shape and, moreover, they are acted upon by three principal stresses. Sack[32] has extended Griffith's work to the case of a crack which has the shape of a very flat oblate ellipsoid ("penny shaped" crack). He has shown that the most dangerous cracks lie in planes parallel to the direction of the intermediate principal stress which has negligible influence upon the stress distribution at the crack tip. The magnitude of the applied stress required to cause propagation of this particular crack was found to be

$$\sigma_a = \sqrt{\frac{\pi \gamma E}{2c\,(1 - \nu^2)}} \quad \ldots\ldots\ldots\ldots (12)$$

3.5 Comparison between theoretical conditions for brittle fracture

TABLE I

Equn.	Derived by	Conditions	Value assuming $\nu = 0.2$*
9a	Griffith	Plane stress, plane body	$\sigma_a = 0.795\sqrt{\gamma E/c}$
9b	Griffith	Plane strain, plane body	$\sigma_a = 0.815\sqrt{\gamma E/c}$
11	Orowan	Atomic considerations, plane body	$\sigma_a = 0.707\sqrt{\gamma E/c}$
12	Sack	Three-dimensional	$\sigma_a = 1.280\sqrt{\gamma E/c}$

The conditions for brittle fracture, obtained by Griffith, Sack and Orowan have been listed in Table I for the sake of comparison. Table I shows that the three predictions referring to a plane body are in good agreement.

The assumption that the initial cracks from which fracture

---

* This is an average value for the Poisson's ratio of the brittle materials with which this study is primarily concerned.

propagates can be treated as a two-dimensional problem is obviously an over-simplification of the actual problem. Internal cracks in a brittle material such as rock are probably more correctly approximated by the very flat oblate ellipsoid ("penny"shape) assumed by Sack. As can be expected from considerations of the additional restraint imposed by the material surrounding such a crack, compared with a two-dimensional crack, the stress required to propagate the "penny" shaped crack is greater than that derived by Griffith and Orowan for plane bodies.

4. EXPERIMENTAL EVIDENCE IN SUPPORT OF GRIFFITH'S HYPOTHESIS

According to Griffith's hypothesis, the observed tensile strength of a brittle material is lower than the theoretical strength due to the presence of cracks. Consequently, if these cracks can be eliminated or rendered ineffective, it should be possible greatly to increase the strength of the material.

Griffith himself demonstrated that this is the case by testing freshly drawn glass fibres in the diameter range 0.00013 to 0.040 inches. He found that, as the diameter of the specimen decreased and hence the probability of a crack being present decreased, the tensile strength increased. In the case of the finest fibres, he measured tensile strengths of up to 480 000 lb/sq. in as compared with the usual value of about 25 000 lb/sq. in.

Reinkober[307] carried out an interesting experiment in which he fractured silica glass fibres, then fractured the two fragments and then the fragments of the fragments and so on. He reasoned that in this way the most dangerous cracks would be progressively eliminated and he found that the tensile strength increased from "generation to generation". In one case, a fibre of 4.7 inches length fractured at 40 000 lb/sq. in while one of its fragments, 0.25 inches long, fractured at 110 000 lb/sq. in.

Orowan[286] argued that, since the perfect cleavage planes of mica could hardly contain effective cracks, fracture of mica lamella must originate at edge cracks. Consequently, if the edges of a mica sheet could be relieved of stress, a great increase in strength should be observed. By gripping the mica lamella with

grips which were narrower than the width of the specimen, so that no stress was transmitted along the edges, Orowan measured tensile strengths of 440 000 lb/sq. in compared with the normal value of 30 000 lb/sq. in.

Direct evidence of submicroscopic flaws has been sought by using the electron microscope. Gordon, Marsh and Parraft[142], using a sodium vapour decoration technique, found convincing evidence of small flaws which exist in unstressed glass and which multiply with application of stress. Their photographs reveal surface cracks of 2×10^{-3} inches long, 8×10^{-7} inches wide and 4×10^{-6} inches deep. Cracks of this order of magnitude can easily account for strength reductions to approximately ten percent of the theoretical strength.

5. ESTIMATE OF THE CRITICAL CRACK LENGTH IN ROCK

Brace[51], using measured values of tensile strength, Young's modulus and specific surface energy, calculated from equation (9a), the critical crack length which could be anticipated in several types of rock. Detailed measurements on these rocks, particularly on limestone specimens, revealed a remarkably close correlation between the calculated crack length and the maximum grain diameter of the material.

In order to eliminate the uncertainty involved in the determination of the specific surface energy, Brace compared two samples of limestone which, apart from having different grain sizes were, for all practical purposes, identical.

It can be deduced from equation (9a) that, provided the Young's modulus and specific surface energy remain unchanged, the tensile strength of the material should be inversely proportional to the square root of the crack length. Substituting the maximum grain diameter of the limestone specimens for crack length in equation (9a), Brace found near perfect agreement between the ratio of observed and anticipated strengths.

Although the results presented by Brace are only applicable to limestone, it is reasonable to assume that the critical cracks which give rise to brittle fracture in hard rock are of the same order of magnitude as the maximum grain diameter of the material.

6. FRACTURE OF BRITTLE MATERIALS SUBJECTED TO TRIAXIAL STRESS

In 1924 Griffith extended his original fracture hypothesis to include the behaviour of a brittle material subjected to triaxial compressive stress[151]. The currently accepted interpretation of this extension is that the fracture of a body containing randomly oriented cracks, subjected to any condition of applied load, occurs when the maximum tensile stress at tips of favourably oriented cracks exceeds the molecular cohesive strength of the material[286].

In order to obtain the conditions for brittle fracture in the case of a material subjected to triaxial stress, it is necessary to consider the stress distribution around the boundary of a crack under these conditions. In order to simplify the mathematical analyses involved in this study, the crack is approximated by a flat ellipse in a two-dimensional stress field as illustrated in Figure 1.

Sack[321], in his theoretical considerations of the stresses around a penny shaped crack in a triaxial stress field, showed that the highest tensile stresses occur at the boundary of the crack which lies in the plane of the intermediate principal stress. He found that the magnitude of these tensile stresses was not markedly influenced by this intermediate principal stress.

Murrell[271] has discussed the influence of the intermediate principal stress and, using the experimental results of Von Kármán[357] and Boker[45], has shown that the maximum effect of the intermediate principal stress on the axial stress at fracture is approximately 15%.

Consequently, the two-dimensional treatment of the stresses around a crack, presented in this study, is considered sufficiently accurate for practical purposes.

Although more elegant calculations of the stress distribution around cracks have been carried out, notably by Williams[369] and Barenblatt[23], the author feels that much of the clarity of the physical reasoning for which the mathematics is a model is lost if too many refinements are attempted. In any event even the

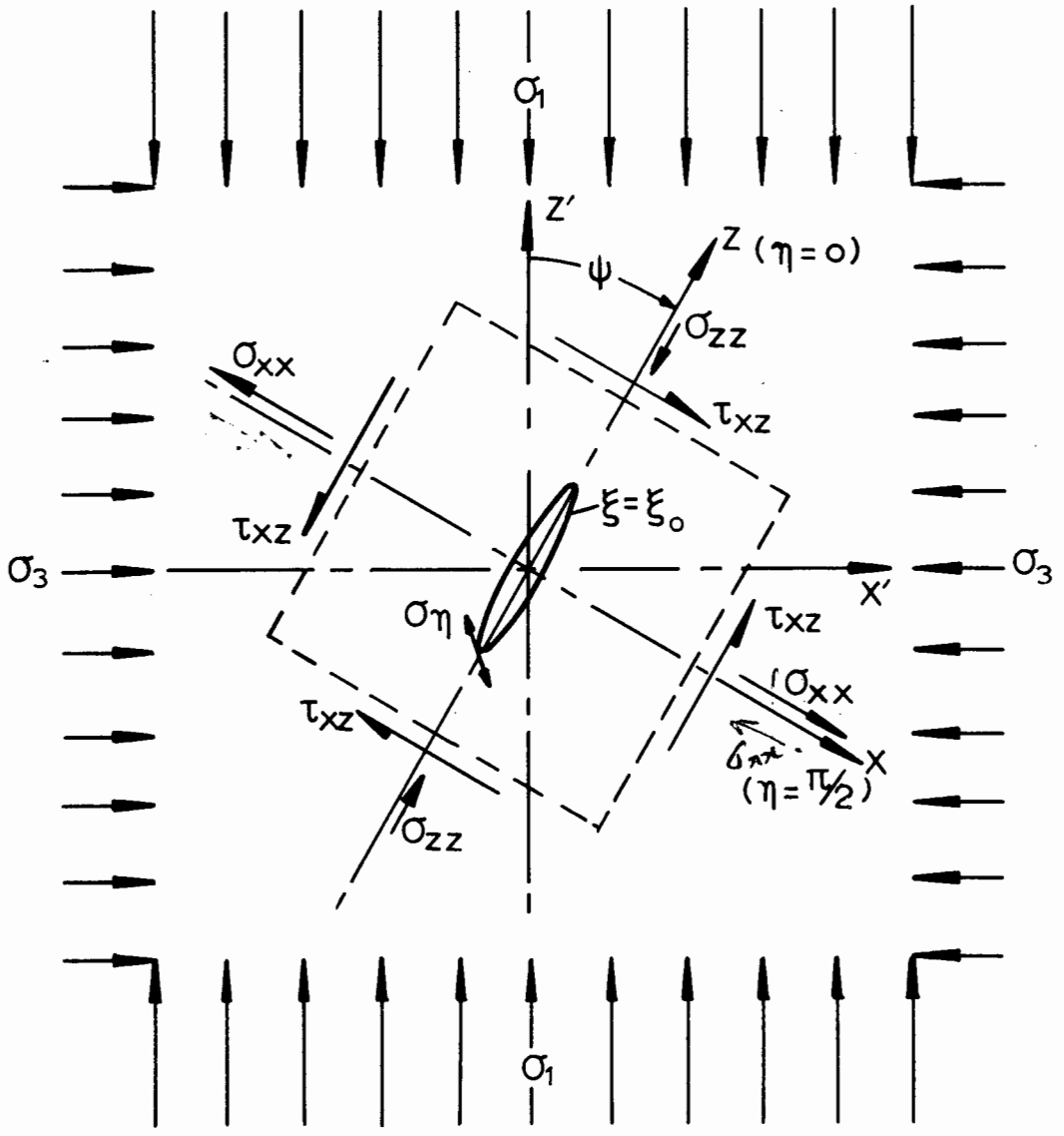

FIGURE 1

Stresses acting upon a crack which is inclined at an angle Ψ to the direction of the major principal stress σ_1

most involved calculations can only predict an overall pattern of behaviour and the parameters which govern the fracture behaviour of a particular material must be determined experimentally. It will be demonstrated in this study that the simple mathematical approach outlined hereunder offers an adequate prediction of the rock fracture phenomena which are of interest to the science of rock mechanics in its present state of development.

6.1 Stresses acting upon an elliptical crack

The two-dimensional stress field in the material surrounding an elliptical opening is most conveniently expressed in terms of the elliptical co-ordinates ξ and η which are defined by the following equations of transformation from a rectangular Cartesian system of co-ordinates x and z.

$$x = c \text{ Sinh } \xi \text{ Sin } \eta$$

$$z = c \text{ Cosh } \xi \text{ Cos } \eta$$

In Figure 1, the system of rectangular co-ordinates x, z is parallel to the axes of the elliptical opening: it is inclined at an angle ψ with respect to the system of rectangular co-ordinates x', z' which is parallel to the directions of the principal stresses σ_1 and σ_3. σ_1 denotes the algebraically largest and σ_3 the algebraically smallest of the three principal stresses.

Note that, throughout this study, compressive stress is taken as positive. This sign convention has been adopted because of the predominance of compressive stresses in rock mechanics problems.

The normal stress σ_{xx}, parallel to the minor axis of the elliptical crack, and the shear stress τ_{xz} are related to the principal stresses σ_1 and σ_3 by the following equations:

$$2\sigma_{xx} = (\sigma_1 + \sigma_3) - (\sigma_1 - \sigma_3) \text{ Cos } 2\psi \quad \ldots\ldots (13)$$

$$2\tau_{xz} = (\sigma_1 - \sigma_3) \text{ Sin } 2\psi \quad \ldots\ldots\ldots\ldots\ldots (14)$$

The normal stress σ_{zz}, parallel to the major axis of the crack, has a negligible influence upon the stresses induced near the crack tip and is, therefore, not considered in the following analysis.

6.2 Griffith's fracture criterion for open cracks

The tangential stress σ_η at the boundary of an open elliptical crack, due to the stresses σ_{xx} and τ_{xz}, can be calculated from the results presented by Inglis[207] and is found to be:

$$\sigma_\eta = \frac{\sigma_{xx}(\text{Sinh } 2\xi_o + e^{2\xi_o}.\text{Cos } 2\eta - 1) + 2\tau_{xz}.e^{2\xi_o}.\text{Sin } 2\eta}{\text{Cosh } 2\xi_o - \text{Cos } 2\eta} \quad .. \quad (15)$$

where ξ_o is the value of the elliptical co-ordinate ξ on the crack boundary.

The maximum boundary stresses occur near the ends of the crack, i.e. when the value of the elliptical co-ordinate η is small. Since the value of $\xi = \xi_o$ (the ellipse in elliptical co-ordinates) is also small for a very flat ellipse, equation (15) may be simplified by series expansion in which terms of the second order and higher which appear in the numerator are neglected*. This simplification results in the following equation, valid only for the stresses near the crack tip:

$$\sigma_\eta = \frac{2(\sigma_{xx}.\xi_o + \tau_{xz}.\eta)}{\xi_o^2 + \eta^2} \quad \ldots\ldots\ldots\ldots \quad (16)$$

Differentiation of equation (16) with respect to η and equating $\partial\sigma_\eta/\partial\eta$ to zero results in a quadratic equation in η from which the positions on the crack boundary at which the maximum and minimum stresses occur can be determined. Substituting these values of η into equation (16) gives the maximum and minimum stresses on the boundary of the crack as

---

* A complete derivation of the equations governing fracture initiation according to the original Griffith theory is given in Appendix A1.

$$\sigma_N \cdot \xi_o = \sigma_{xx} \pm \sqrt{\sigma_{xx}^2 + \tau_{xz}^2} \quad \ldots\ldots\ldots (17)$$

where σ_N is the maximum or minimum value of the tangential stress σ_η of the ellipse boundary.

Expressing equation (17) in terms of the principal stresses σ_1 and σ_3 from equations (13) and (14) gives

$$\sigma_N \cdot \xi_o = \tfrac{1}{2}\left\{(\sigma_1+\sigma_3) - (\sigma_1-\sigma_3)\text{Cos } 2\psi\right\} \pm \sqrt{\tfrac{1}{2}\left\{(\sigma_1^2+\sigma_3^2)-(\sigma_1^2-\sigma_3^2)\text{ Cos } 2\psi\right\}} \quad (18a)$$

or

$$\sigma_N \cdot \xi_o = \tfrac{1}{2}\sigma_1\left\{(1+k) - (1-k)\text{ Cos } 2\psi\right\} \pm \sqrt{\tfrac{1}{2}\left\{(1+k^2)-(1-k^2)\text{ Cos } 2\psi\right\}} \quad (18b)$$

where $k = \sigma_3/\sigma_1$

The critical crack orientation ψ_c at which the maximum and minimum stresses are induced near the crack tip is found by differentiating equations (18) with respect to ψ and letting $\partial\sigma_N/\partial\psi = 0$. This gives

$$\text{Cos } 2\psi_c = \frac{\sigma_1 - \sigma_3}{2(\sigma_1+\sigma_3)} = \frac{1 - k}{2(1+k)} \quad \ldots\ldots\ldots (19)$$

Note that this equation is only meaningful for values of $\sigma_3 \geq -\sigma_1/3$ or $k \geq -0.33$. The critical crack orientation for algebraically smaller values of k must be determined from other considerations which will be dealt with later.

The maximum and minimum stresses at the boundary of a crack oriented at the critical angle ψ_c under conditions where $k \geq -0.33$ are found by substituting ψ_c from equation (19) for ψ in equations (18). If it is accepted that fracture occurs as a result of tensile stress at or near the crack tip, only the minimum (negative)

stress given by this substitution need be considered. Hence

$$\sigma_o \cdot \xi_o = \frac{-(\sigma_1 - \sigma_3)^2}{4(\sigma_1 + \sigma_3)} = \frac{-\sigma_1(1 - k)^2}{4(1 + k)} \quad \ldots\ldots\ldots (20)$$

where σ_o denotes the minimum (algebraically smallest value of the tangential stress on the boundary of the ellipse.

If it is postulated that the fracture of a brittle material initiates when the maximum tensile stress at the crack tip is equal to the molecular cohesive strength of the material [286], then equation (20) expresses a fracture criterion for a brittle material under conditions where $k \geq -0.33$, if σ_o is taken as the molecular cohesive strength of the material.

The molecular strength, σ_o, and the crack geometry, ξ_o, cannot be determined by direct physical measurements. However, their product can be expressed in terms of the uniaxial tensile strength, σ_t, determined on a laboratory specimen. Since, for uniaxial tension ($\sigma_3 < 0$, $\sigma_1 = 0$), $k = -\infty$, equations (19) and (20), which are only valid for $k \geq -0.33$, cannot be used to find a relationship between $\sigma_o \cdot \xi_o$ and σ_t and equation (18) must be resorted to for finding this relationship.

6.2.1 Fracture under uniaxial tensile stress conditions

If the plane body containing the crack, illustrated in Figure 1, is subjected to a uniaxial tensile stress (i.e. $\sigma_3 < 0$, $\sigma_1 = 0$), the maximum stress at the crack tip (σ_N) is dependent upon the minor principal stress σ_3 only. Hence, equation (18) simplifies to

$$\sigma_N \cdot \xi_o = \sigma_3\left(\tfrac{1}{2}(1 + \text{Cos } 2\psi) \pm \sqrt{\tfrac{1}{2}(1 + \text{Cos } 2\psi)}\right) \quad \ldots\ldots (21)$$

The maximum tensile stress at the crack tip occurs when the bracketted term on the right hand side of equation (21) is a maximum. This occurs when Cos $2\psi = 1$ or when $\psi = 0$,

giving

$$\sigma_o.\xi_o = 2\sigma_{3(\sigma_1 = 0,\ \psi = 0)} \quad \ldots\ldots (22)$$

If the minor principal stress σ_3 is tensile (negative), equation (22) defines the fracture criterion for uniaxial tensile stress conditions in terms of the molecular cohesive strength of the material (σ_o) and the crack geometry (ξ_o). Denoting the uniaxial tensile strength of the material, measured on a laboratory specimen, as σ_t*, equation (22) may, with $\sigma_3 = \sigma_t$, be re-written as:

$$\sigma_o.\xi_o = 2\sigma_t \quad \ldots\ldots\ldots\ldots\ldots\ldots (23)$$

6.2.2 Fracture conditions for $k > -0.33$

Equation (20), which is valid for $k \geq -0.33$, is of limited practical use because the term $\sigma_o.\xi_o$ cannot be evaluated in the laboratory. If, however, this term is expressed in terms of the uniaxial tensile strength of the material (σ_t), according to equation (23), the fracture criterion becomes

$$\frac{(\sigma_1 - \sigma_3)^2}{(\sigma_1 + \sigma_3)} = \frac{\sigma_1(1 - k)^2}{(1 + k)} = -8\sigma_t \quad \ldots\ldots (24a)$$

The author has found that the most useful interpretation of this equation is in expressing the major principal stress (σ_1), at fracture, in terms of the principal stress ratio (k) and the uniaxial tensile strength (σ_t):

$$\sigma_1 = \frac{-8\sigma_t\ (1 + k)}{(1 - k)^2} \quad \ldots\ldots\ldots\ldots\ldots (24b)$$

---

* Note that the uniaxial tensile strength is negative by definition. Hence, in substituting a numerical value for σ_t, the negative sign must be shown e.g. σ_t = - 100 lb/sq. in.

6.2.3 Fracture conditions for k = -0.33

When k = -0.33 then, from equation (19), Cos 2ψ = 1. Substituting this value into equation (18) gives

$$\sigma_o \xi_o = 2\sigma_{3_{(k = -0.33)}} \quad \ldots\ldots\ldots\ldots (25)$$

which is identical to equation (22).

In other words, the fracture conditions for k = -0.33 are identical to those for uniaxial tension and the fracture criterion for this case may be expressed as

$$\sigma_{3_{(k = -0.33)}} = \sigma_t \quad \ldots\ldots\ldots\ldots (26)$$

6.2.4 Fracture conditions for k < -0.33

Since fracture for both k = $-\infty$ and k = -0.33 occurs when the minor principal stress σ_3 equals the uniaxial tensile strength of the material σ_t, according to equations (22), (23) and (26), it can be deduced by interpolation that the same condition must hold for the entire range $-\infty < k \leq -0.33$. In other words, equation (26) may be written as*

$$\sigma_{3_{(-\infty < k \leq -0.33)}} = \sigma_t \quad \ldots\ldots (27)$$

Similarly, since ψ = 0 for both k = $-\infty$ and k = -0.33, the critical crack orientation for $-\infty < k \leq -0.33$ remains unchanged at ψ = 0.

7. MODIFIED FRACTURE CRITERION FOR CLOSED CRACKS

One of the principal deficiencies of the original Griffith theory,

* An alternate proof for the validity of equation (27) is given in section 9.3.2.

when applied to the prediction of brittle fracture initiation under compressive stress conditions, lies in the fact that it does not make provision for the closure of very flat cracks before the tensile stresses at their tips have reached sufficient magnitude to cause them to propagate. The frictional forces which occur when the crack faces are forced into contact can exert a marked influence upon the subsequent crack behaviour.

A difficulty associated with the theoretical consideration of the effects of crack closure is to decide upon the exact stress level at which crack closure occurs. Obviously, this stress is governed by the physical characteristics of the material under consideration and it is unlikely that it will have a single clearly defined value in the case of a material such as rock.

In the following analysis, based on the modification to Griffith's fracture theory by McClintock and Walsh[249], it is assumed that the initial crack in an unstressed body is uniformly closed over its entire length, i.e. the stress required to cause crack closure is zero. The effects of this closure stress having a value other than zero will be discussed in a later section dealing with the influence of additional factors upon fracture initiation.

The stress system acting upon a closed crack is given in Figure 2. Note that this stress system differs from that for an open crack, illustrated in Figure 1, in that a normal and a shear stress (σ_n and τ_n respectively) act on the crack surfaces.

When the stress σ_{xx} acting across the crack becomes compressive (positive) a normal stress $\sigma_n = \sigma_{xx}$ results from the reaction between the crack surfaces. Under these conditions, the normal stress σ_{xx} is transmitted across the crack surfaces without influencing the stresses induced at the crack tips and, hence, it plays no direct part in the fracture process.

In addition, however, frictional shear resistance τ_n occurs parallel to the crack as a result of the contact pressure between

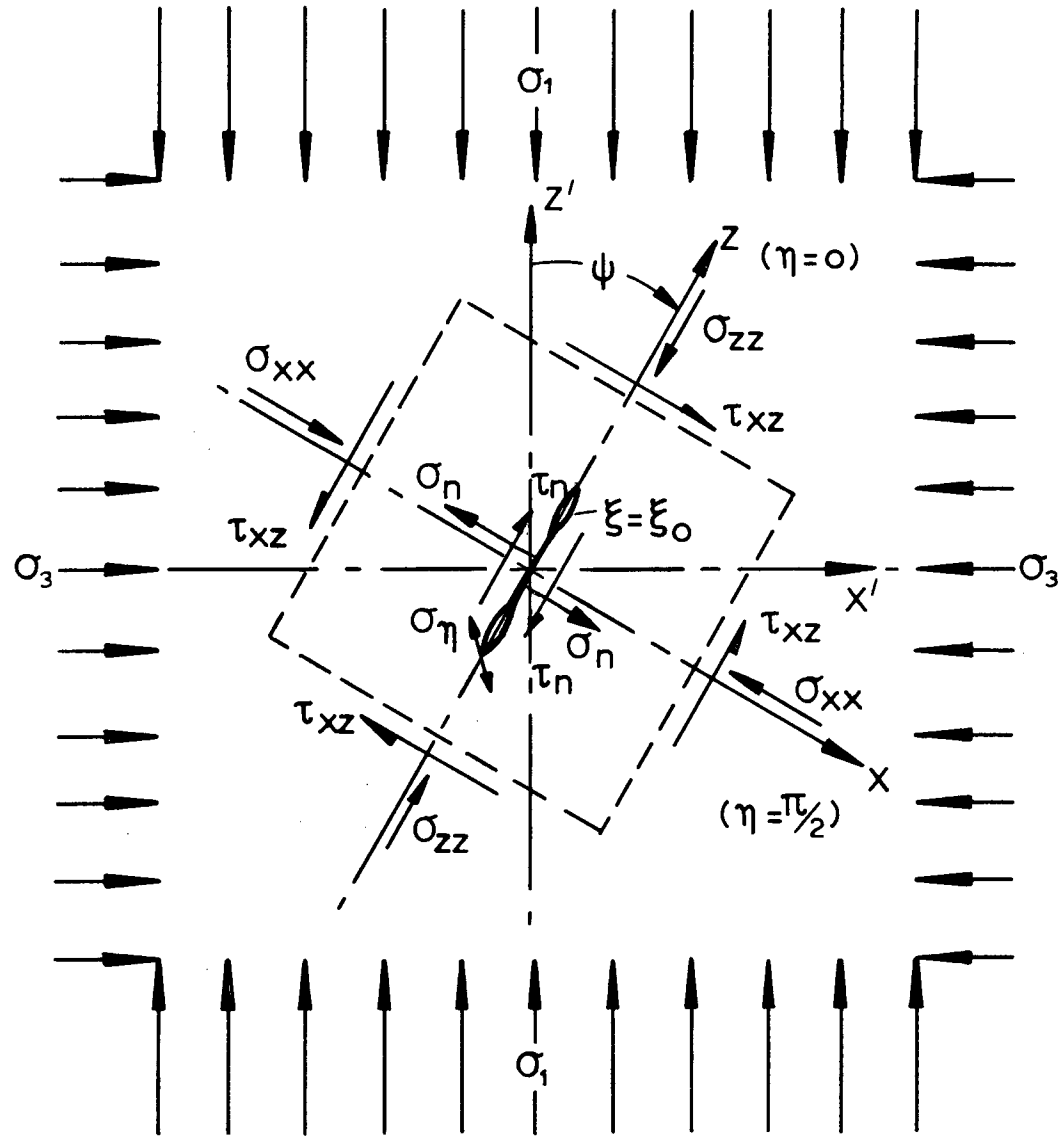

FIGURE 2

Stresses acting upon a closed crack which is inclined at an angle Ψ to the direction of the major principal stress σ_1

the crack surfaces*. Defining the ratio of the frictional shear resistance τ_n to the normal stress σ_n as the coefficient of internal friction μ :

$$\frac{\tau_n}{\sigma_n} = \frac{\tau_n}{\sigma_{xx}} = \mu \qquad \ldots\ldots\ldots (28)$$

The shear stress τ_{xz} can only induce tensile stresses at the crack tip when this frictional resistance has been overcome and when relative movement between the crack surfaces can occur. Consequently, the net shear stress which is effective in inducing tensile stresses on the crack boundary is

$$\tau_{xz} - \tau_n \quad \text{or} \quad \text{(from equation (28))} \quad \tau_{xz} - \mu\sigma_{xx}$$

The tangential stress on the boundary of the closed crack (σ_η), due to the net shear stress ($\tau_{xz} - \mu\sigma_{xx}$), can be determined by replacing τ_{xz} by ($\tau_{xz} - \mu\sigma_{xx}$) and $\sigma_{xx}\xi_o$ by $(\sigma_{xx} - \sigma_n)\xi_o = (\sigma_{xx} - \sigma_{xx})\xi_o = 0$ in equation (16):

$$\sigma_\eta = \frac{2\eta(\tau_{xz} - \mu\sigma_{xx})}{\xi_o^2 + \eta^2} \qquad \ldots\ldots\ldots (29)$$

Differentiating equation (29) with respect to η and equating $\partial\sigma_\eta/\partial\eta$ to zero gives the position on the crack boundary at which the maximum and minimum stresses occur as $\eta = \pm\xi_o$. Substituting this value into equation (29) gives the maximum and minimum

---

* Note that, in addition to the frictional shear resistance which occurs as a result of the contact pressure between the crack surfaces, interlocking of projections and irregularities on the crack surfaces may also occur and, as a result, the total shear resistance τ_n may be greater than the normal stress σ_n. In other words, the coefficient of friction μ may have a value greater than unity.

The mechanism of crack propagation in a material having a coefficient of internal friction of greater than unity will be discussed in Part II of this study.

tangential stresses σ_N on the boundary of the crack as

$$\sigma_N \xi_o = \pm (\tau_{xz} - \mu\sigma_{xx}) \quad \ldots\ldots\ldots\ldots (30)$$

Since crack propagation occurs as a result of tensile stress, only the negative value of equation (30) need be considered.

Expressing this equation in terms of the major principal stress σ_1 and the principal stress ratio k, from equations (13) and (14):

$$\sigma_N \cdot \xi_o = -\tfrac{1}{2}\sigma_1\{(1-k)\sin 2\psi - \mu\{(1+k) - (1-k)\cos 2\psi\}\} \quad \ldots\ldots (31)$$

Differentiating equation (31) with respect to ψ and equating $\partial\sigma_N/\partial\psi$ to zero gives the critical crack orientation ψ_c for a closed crack as

$$\tan 2\psi_c = {}^1/\mu \quad \ldots\ldots\ldots\ldots\ldots (32)$$

The highest tensile stress on the boundary of a crack oriented at the critical angle ψ_c is given by substituting $\psi = \frac{1}{2}\arctan({}^1/\mu)$ (from equation (32)) into equation (31). As in the case of the original Griffith's theory, this stress can be related to the uniaxial tensile strength of the material by means of equation (23). The resulting fracture criterion for a brittle material with initially closed cracks is then given by

$$\sigma_1 = \frac{-4\sigma_t}{(1-k)\sqrt{1+\mu^2} - \mu(1+k)} \quad \ldots\ldots (33)$$

This criterion is only valid when the normal stress σ_{xx} is compressive, i.e. when $\sigma_{xx} > 0$.

8. TRANSITION FROM ORIGINAL TO MODIFIED GRIFFITH CRITERION

It has been assumed that, in the hard rocks under consideration in this study, the Griffith cracks in the unstressed material are initially closed. Consequently, the original Griffith fracture criterion for open cracks is only applicable when the normal stress σ_{xx} acting across the crack is tensile (negative).

The crack orientation at which this stress becomes tensile is given by substituting $\sigma_{xx} = 0$ in equation (13):

$$\text{Cos } 2\psi = \frac{1 + k}{1 - k} \quad \ldots\ldots\ldots\ldots\ldots\ldots \quad (34)$$

8.1 Limit of validity of original Griffith theory

The derivation of the original Griffith fracture criterion for open cracks is dependent upon the fact that the critical crack orientation ψ_c can be determined from equation (19). Since this equation is only valid when the crack is open, i.e. when σ_{xx} is tensile, the limit of validity of the original Griffith criterion occurs when the crack orientation ψ given by equation (34) is equal to the critical crack orientation ψ_c given by equation (19). Equating equations (34) and (19) and solving for k gives

$$k = -0.17 \quad \ldots\ldots\ldots\ldots\ldots\ldots \quad (35)$$

which defines the upper limit of validity of the original Griffith theory under these conditions.

8.2 Limit of validity of modified fracture theory

The critical crack orientation for the modified fracture theory is defined by equation (32) which is only valid when the normal stress σ_{xx} acting across the crack is compressive. Hence the lower limit of validity of the modified fracture criterion occurs when ψ_c given by equation (32) is equal to the crack orientation ψ at which σ_{xx} becomes compressive, given by equation (34).

Expressing equation (32) in terms of Cos $2\psi_c$ and equating it to equation (34) gives

$$\text{Cos } 2\psi_c = \frac{\mu}{\sqrt{1 + \mu^2}} = \frac{1 + k}{1 - k} \quad \ldots\ldots\ldots (36)$$

Solving for k :

$$k = \frac{\mu - \sqrt{1 + \mu^2}}{\mu + \sqrt{1 + \mu^2}} \quad \ldots\ldots\ldots\ldots\ldots (37)$$

It follows from equation (37) that the lower limit of validity of the modified fracture criterion can only coincide with the upper limit of validity of Griffith's criterion (which is at k = - 0.17) when μ = 1.00. Hence, for any other value of μ, there must be a region of transition between the upper limiting value of k for the Griffith criterion and the lower limit for the modified criterion.

8.3 Transition when μ < 1.00

When μ < 1.00, the limiting value of k for the modified fracture theory, given by equation (37), is algebraically smaller than - 0.17 and the two fracture theories overlap. McClintock and Walsh suggest that fracture occurs at the lowest fracture stress predicted by either theory and hence, that the limiting value of k is that for which the fracture stress is the same for both criteria. Hence, equating the fracture stresses from equations (24b) and (33), this limiting value of k is given by:

$$k = \frac{-1}{2\sqrt{1 + \mu^2} + 2\mu + 1} \quad \ldots\ldots\ldots\ldots (38)$$

Below this value of k, the original Griffith criterion represented by equation (24b) is applicable while, for greater values of k, the modified fracture criterion represented by equation (33) should be used.

8.4 Transition when $\mu > 1.00$

When $\mu > 1.00$, the limiting value of k for the modified fracture criterion, given by equation (37), is algebraically greater than - 0.17 and a zone of k-values exists in which neither fracture criterion is valid. This transition zone is due to the fact that cracks oriented at an angle defined by equation (19) are closed while those with an orientation given by equation (32) are open. Consequently, neither equation (19) nor equation (32) hold in this region.

If it is assumed that, under these conditions, fracture initiates at those cracks which have just opened, i.e. those which are oriented at the angle ψ defined by equation (34), then, from equations (34) and (18), the fracture criterion in this transition zone is found to be

$$\sigma_1 = \frac{-2\sigma_t}{\sqrt{-k}} \qquad \ldots\ldots\ldots\ldots\ldots\ldots \quad (39)$$

Since the value of k is always negative within this transition zone, this equation has physical meaning.

8.5 Limiting value of k above which fracture cannot occur

Examination of equation (33) reveals that, for a given value of μ, a value of k will be reached at which the stress σ_1 required to cause fracture is infinite. This occurs when

$$(1 - k)\sqrt{1 + \mu^2} = \mu(1 + k)$$

or when

$$k = \frac{\sqrt{1 + \mu^2} - \mu}{\sqrt{1 + \mu^2} + \mu} \qquad \ldots\ldots\ldots\ldots\ldots\ldots \quad (40)$$

For a greater value of k than that given by equation (40) for a given coefficient of friction μ, the material will not fracture if it behaves in accordance with the modified Griffith's fracture criterion.

9. GRAPHICAL REPRESENTATION OF ORIGINAL AND MODIFIED GRIFFITH FRACTURE CRITERIA

The equations which have been derived on the preceding pages offer a number of possibilities for the graphical representation of the state of stress at which fracture of a brittle material initiates under static load conditions. A detailed discussion of the merits of these various graphical representations does not fall within the scope of this study and has already been adequately dealt with in standard texts such as that by Nadai[277].

Three graphical representations of the state of stress at which brittle fracture initiates will be used in this study:

(a) The relationship between the major principal stress (σ_1) at fracture and the minor principal stress (σ_3).

(b) The relationship between the major principal stress (σ_1) at fracture and the principal stress ratio (k).

(c) The Mohr envelope for fracture initiation.

It should be noted that these three graphical representations are in terms of the major and minor principal stresses (σ_1 and σ_3) only. As already discussed (section 6), the influence of the intermediate principal stress (σ_2) is assumed to be sufficiently small to permit its omission from this analysis. A more complete analysis[93] would include the effects of the intermediate principle stress which would be plotted as a third axis on the above graphs. The complete fracture criterion would then be represented by a three-dimensional diagram. The two-dimensional graphical representations of the state of stress at fracture discussed in this study are sections through the three-dimensional fracture diagram.

In deriving the conditions for fracture initiation in a brittle material, the uniaxial tensile strength (σ_t) has been chosen as a basic material constant. The reason for this choice is that the uniaxial tensile strength (σ_t) is theoretically related to the molecular cohesive strength of the material (σ_o) (equation (23)) which is assumed to govern the mechanism of brittle fracture initiation.

In spite of the theoretical advantage of expressing the strength of a brittle material in terms of its uniaxial tensile strength, the practical difficulties associated with its accurate determination impose a serious limitation upon the usefulness of this means of expression.

On the other hand, the uniaxial compressive strength (σ_c) of a material is probably the easiest strength value to determine experimentally and it is advantageous to use this value as the basic material constant in place of the uniaxial tensile strength.

If it is assumed that the cracks from which fracture of a brittle material initiates are initially open and that they remain open under compressive stress conditions, then the original Griffith fracture theory can be used to relate the uniaxial tensile and compressive strengths. Substituting $k = 0$ and $\sigma_c = \sigma_{1_{(k = 0)}}$ in equation (24b),

$$\sigma_c = -8\sigma_t \qquad \text{..... (41)}$$

In this study, however, it has been assumed that the cracks from which fracture propagates are initially closed and that the modified Griffith's theory must be applied when the normal stress σ_{xx} across the crack is compressive. Consequently, the relationship between the uniaxial tensile and compressive strengths which will be used in the following discussion is obtained by substituting $k = 0$ and $\sigma_c = \sigma_{1_{(k = 0)}}$ in equation (33):

$$\sigma_c = \frac{-4\sigma_t}{\sqrt{1 + \mu^2} - \mu} \qquad \text{..... (42)}$$

In the following discussion on the graphical representation of the original and modified Griffith's fracture criteria, the equations will be derived in terms of the uniaxial tensile strength (σ_t). However, to facilitate practical application of

these equations, they will also be given (in Figures 5, 7 and 10 and Table II) in terms of the uniaxial compressive strength (σ_c).

In addition to the graphs of the state of stress at fracture, it is useful to plot the critical crack orientation (ψ_c) against the principal stress ratio (k) for the various conditions discussed in the preceding sections. This graph, representing equations (19), (38), (32) and (34) is presented in Figure 3.

It is important to note that the critical crack orientation (ψ_c) given in equations (19), (38), (32) and (34) and shown in Figure 3 refers to the direction of the crack which has the highest tensile stress at its tip. Theoretically, fracture will propagate from the tip of this crack but the direction of fracture propagation need not coincide with the direction of the initial crack (defined by ψ_c). Experimental evidence presented by Brace and Bombolakis[50] indicates that, under compressive stress conditions, the crack propagation may follow a complex path and that the inclination of the final fracture surface may differ markedly from the inclination of the initial crack. A discussion of fracture propagation is included in Part II of this study.

9.1 Relationship between the major principal stress (σ_1) at fracture and the principal stress ratio (k)

The original Griffith criterion for fracture initiation is expressed by equation (24a) which relates the major principal stress (σ_1) and the principal stress ratio (k).

$$\sigma_1/\sigma_t = \frac{-8\,(1 + k)}{(1 - k)^2} \qquad \ldots\ldots\ldots\ldots\ldots\ldots \quad (24a)$$

This equation is only valid for $k > -0.33$.

The relationship between the major principal stress and the principal stress ratio for the modified fracture criterion is given by equation (33):

$$\sigma_1/\sigma_t = \frac{-4}{(1 - k)\sqrt{1 + \mu^2} - \mu(1 + k)} \qquad \ldots\ldots \quad (33)$$

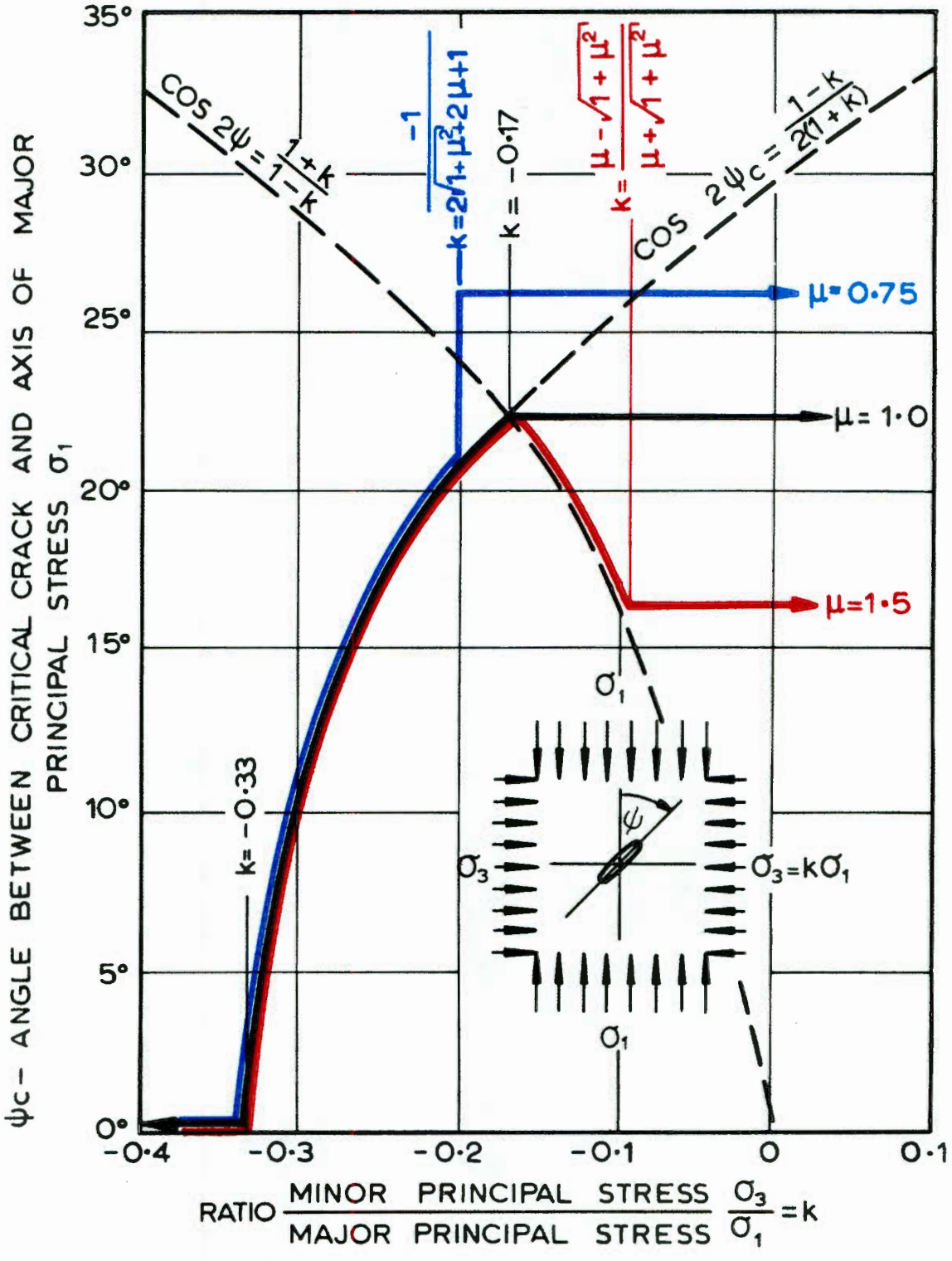

FIGURE 3

Relationship between the critical crack orientation Ψ_c and the principal stess ration k

The limits of validity of equations (24a) and (33) and the transition from the original to the modified Griffith's theory have been fully discussed in section 8.4. The equations governing the relationship between the major principal stress (σ_1) at fracture and the principal stress ratio (k) are graphically represented in Figures 4 and 5. Note that, in the graphs, it has been found convenient to plot the major principal stress (σ_1) on a logarithmic scale.

The author has found this particular representation of the original and modified Griffith's criteria the most useful for the analysis of practical brittle fracture problems.

9.2 Relationship between major principal stress (σ_1) at fracture and minor principal stress (σ_3)

From equation (24), the Griffith relationship between the major and minor principal stresses at the initiation of fracture can be written as follows:

$$\sigma_1/\sigma_t = \sigma_3/\sigma_t - 4\left\{1 \pm \sqrt{1 - \sigma_3/\sigma_t}\right\} \quad \ldots\ldots (43)$$

Since equation (24) is only valid for $k > -0.33$, equation (43) is also only valid within this region and only the positive sign in equation (43) is meaningful.

As shown previously, for $k < -0.33$,

$$\sigma_{3(-\infty < k \leq -0.33)} = \sigma_t \quad \ldots\ldots\ldots\ldots (27)$$

In the case of the modified fracture criterion, the relationship between the major and minor principal stresses at fracture is derived from equation (33) and is found to be

$$\sigma_1/\sigma_t = \frac{\sigma_3/\sigma_t \left(\sqrt{1 + \mu^2} + \mu\right) - 4}{\sqrt{1 + \mu^2} - \mu} \quad \ldots\ldots\ldots\ldots (44)$$

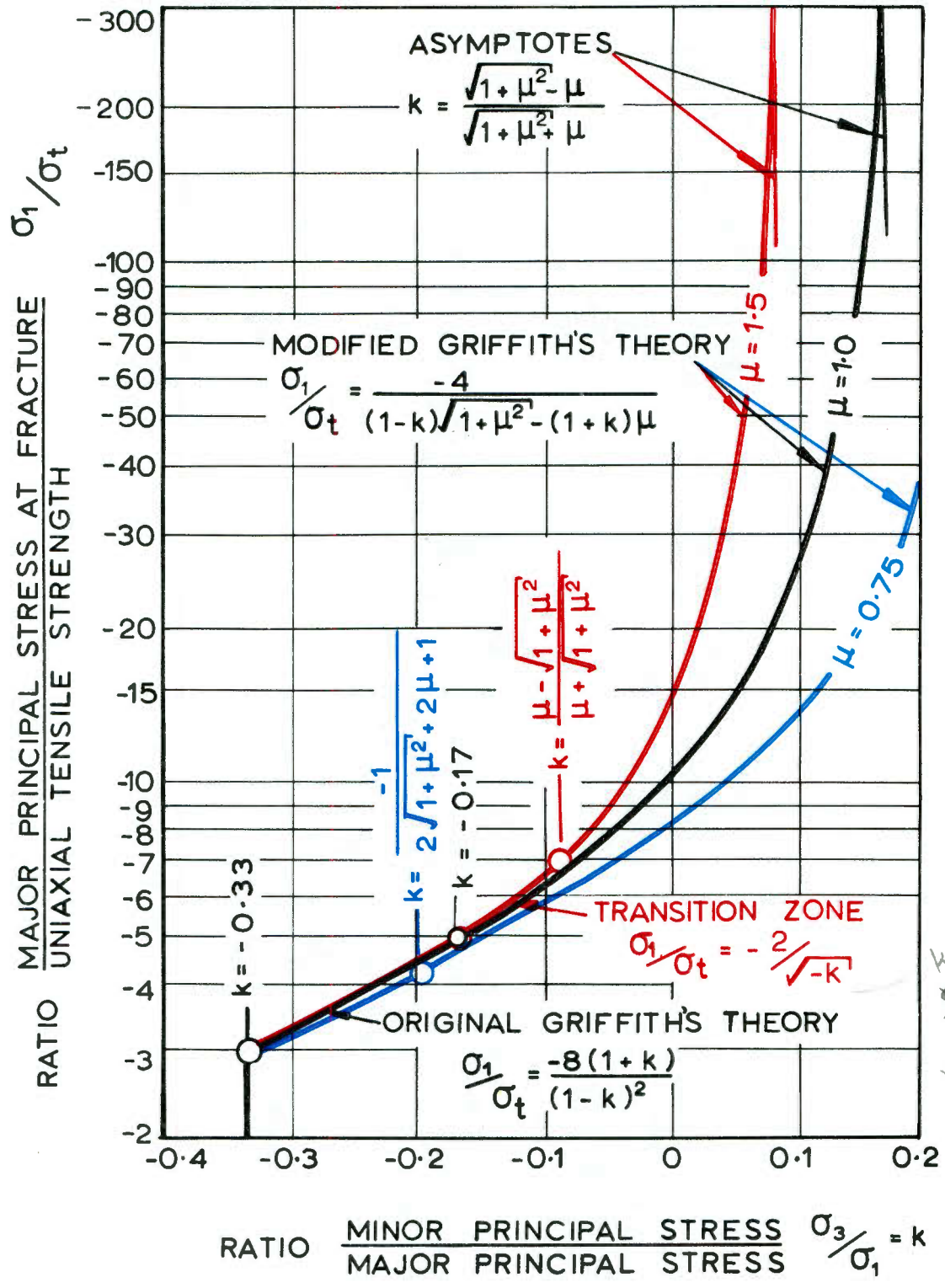

FIGURE 4

Relationship between the major principal stress σ_1 at fracture and the principal stress ratio k in terms of the uniaxial tensile strength σ_t

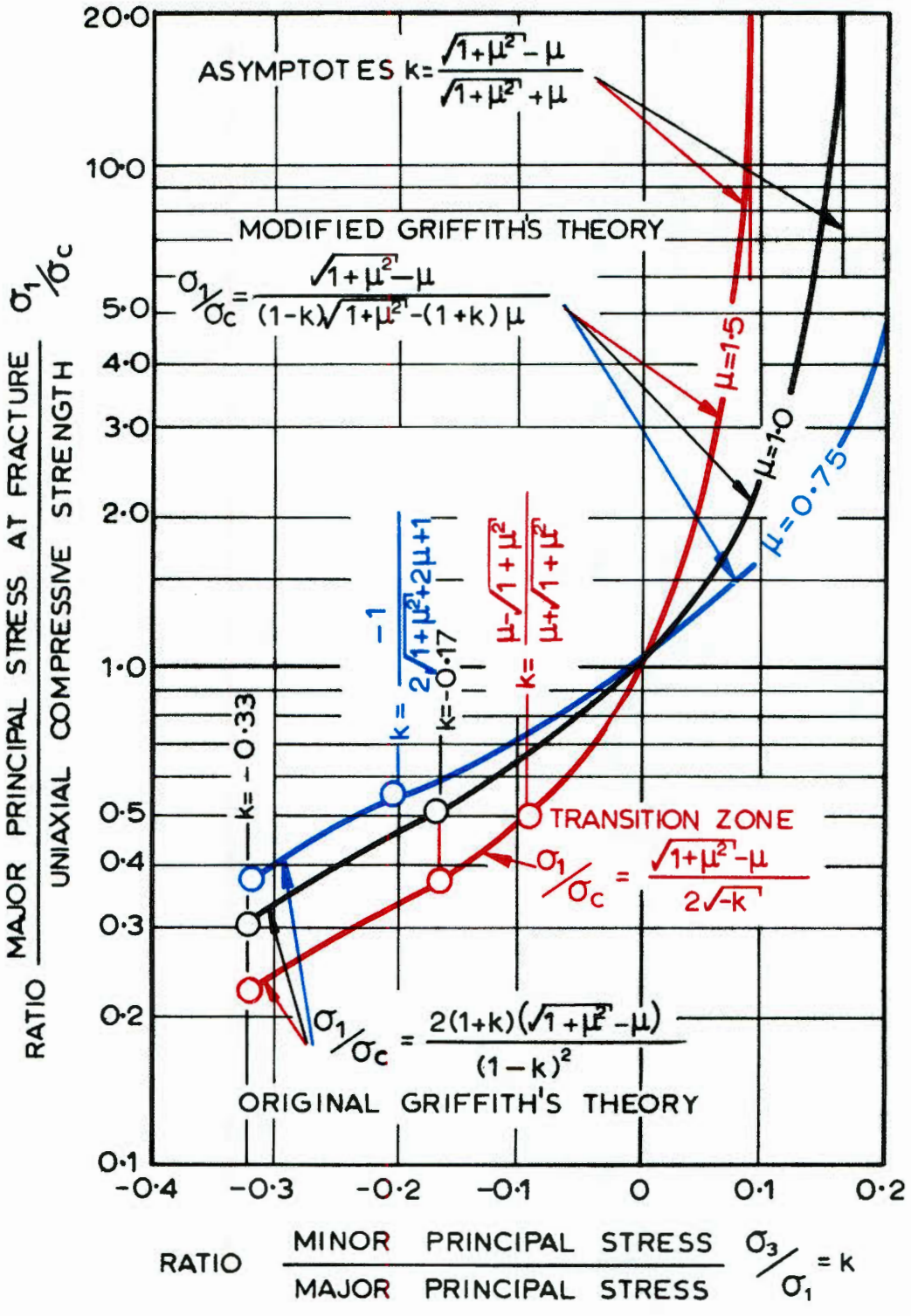

FIGURE 5

Relationship between the major principal stress σ_1 at fracture and the principal stress ratio k in terms of the uniaxial compressive strength σ_c

Equation (43) is the equation of a parabola with its apex at the origin and with its axis of symmetry defined by $\sigma_1 = \sigma_3$.

Equation (27) defines a vertical straight line which is tangential to the parabola (equation (43)) at k = -0.33.

Equation (44) is also that of a straight line. The transition from the parabola (equation (43)) to the straight line (equation (44)) depends upon the value of the coefficient of friction (μ) as discussed in sections 8.3 and 8.4.

When $\mu < 1.00$, the transition from the parabola (equation (43)) to the straight line (equation (44)) occurs at

$$k = \frac{-1}{2\sqrt{1+\mu^2} + 2\mu + 1} \quad \ldots\ldots\ldots\ldots (38)$$

When $\mu = 1.00$, the straight line (equation (44)) is tangential (i.e. it has the same slope) to the parabola (equation (43)) at k = - 0.17.

When $\mu > 1.00$, equation (43) is only valid up to k = - 0.17 and equation (44) is only valid down to

$$k = \frac{\mu - \sqrt{1+\mu^2}}{\mu + \sqrt{1+\mu^2}} \quad \ldots\ldots\ldots\ldots\ldots\ldots (37)$$

The transition curve between these two limits is defined by equation (39) which may be written as

pg 27.

$$\frac{\sigma_1}{\sigma_t^2} = \frac{-4}{\sigma_3} \quad \ldots\ldots\ldots\ldots\ldots\ldots (45)$$

The equations defining the relationship between the major and the minor principal stresses at fracture, in terms of the

uniaxial tensile strength, are represented graphically in Figure 6. Graphical representation of these equations, in terms of the uniaxial compressive strength, is given in Figure 7.

9.3 Limiting Mohr envelopes for brittle fracture initiation

The graphical representation of stress proposed by Mohr[257], in addition to being familiar to most engineers, is a useful aid in visualising some of the stress phenomena which are associated with the fracture of a brittle material.

The two-dimensional stress at a point can be specified by the two principal stresses σ_1 and σ_3 and by the inclination of σ_1 to a given reference direction. In practice, it is often useful to know the stress across a plane oriented at an angle ψ with respect to the direction of σ_1. It is convenient to specify the stress across a plane by two components, the stress component σ_{xx} normal to the plane and the shear stress component τ_{xz} parallel to the plane. The components σ_{xx} and τ_{xz} are related to the principal stresses σ_1 and σ_3 and to the angle ψ by equations (13) and (14):

$$2\sigma_{xx} = (\sigma_1 + \sigma_3) - (\sigma_1 - \sigma_3) \cos 2\psi \quad \ldots\ldots (13)$$

$$2\tau_{xz} = (\sigma_1 - \sigma_3) \sin 2\psi \quad \ldots\ldots\ldots\ldots\ldots\ldots (14)$$

These equations specify a circle in a $\tau - \sigma$ system of rectangular Cartesian co-ordinates. The radius of the circle is $\frac{1}{2}(\sigma_1 - \sigma_3)$ and its centre is located at $\tau = 0$, $\sigma = \frac{1}{2}(\sigma_1 + \sigma_3)$, as illustrated in Figure 8.

From the geometry of the circle illustrated in Figure 8 it will be seen that

$$\left(\tfrac{1}{2}(\sigma_1 + \sigma_3) - \sigma_{xx}\right)^2 + \tau_{xz}^2 = \left(\tfrac{1}{2}(\sigma_1 - \sigma_3)\right)^2 \quad \ldots (46)$$

Hence, any two-dimensional state of stress (σ_1, σ_3) can be graphically represented by such a circle, called a Mohr circle. As will be noted from Figure 8, the stress components σ_{xx} and τ_{xz}

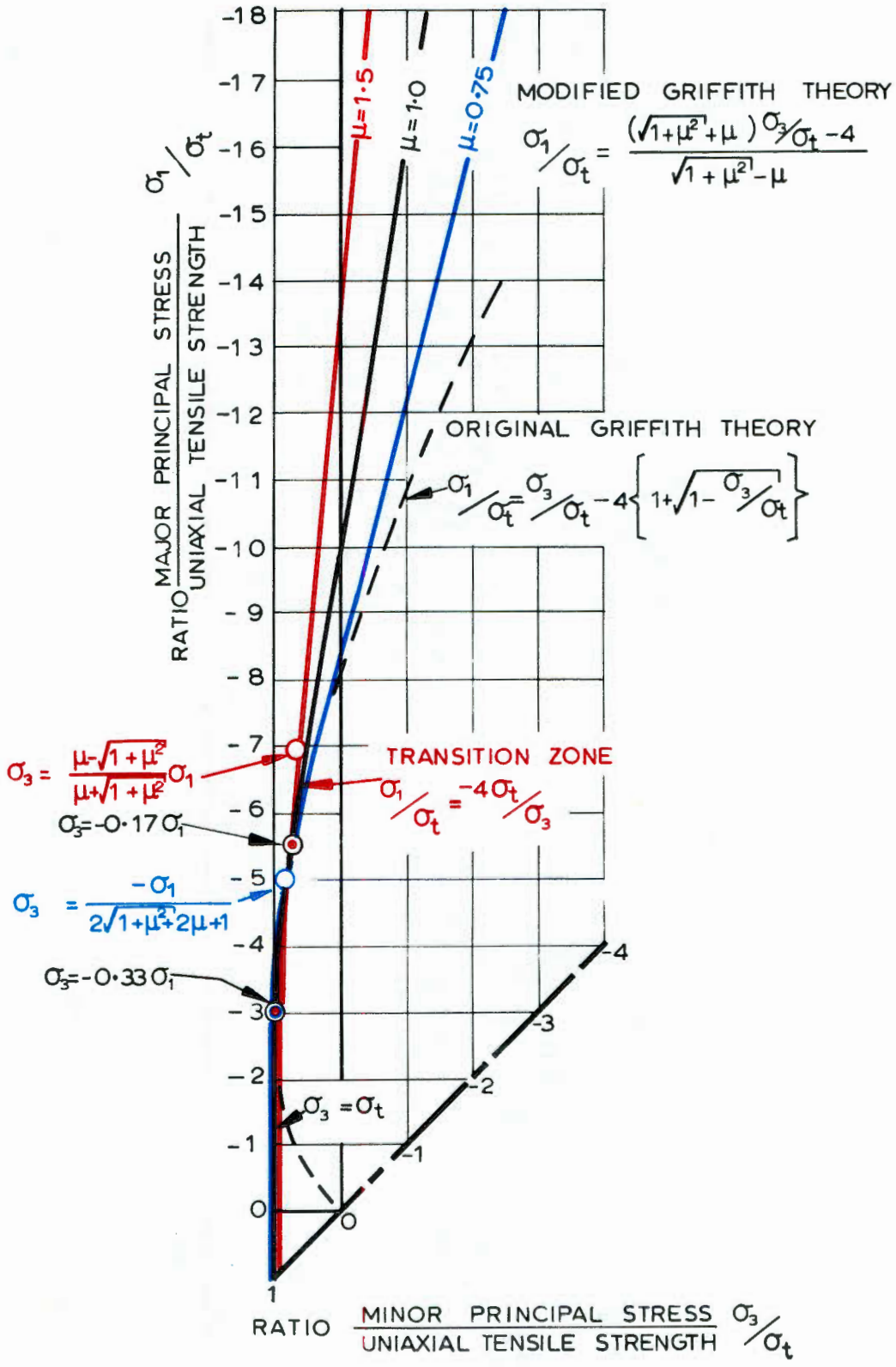

FIGURE 6

Relationship between the major principal stress σ_1 at fracture and the minor principal stress σ_3 in terms of the uniaxial tensile strength σ_t

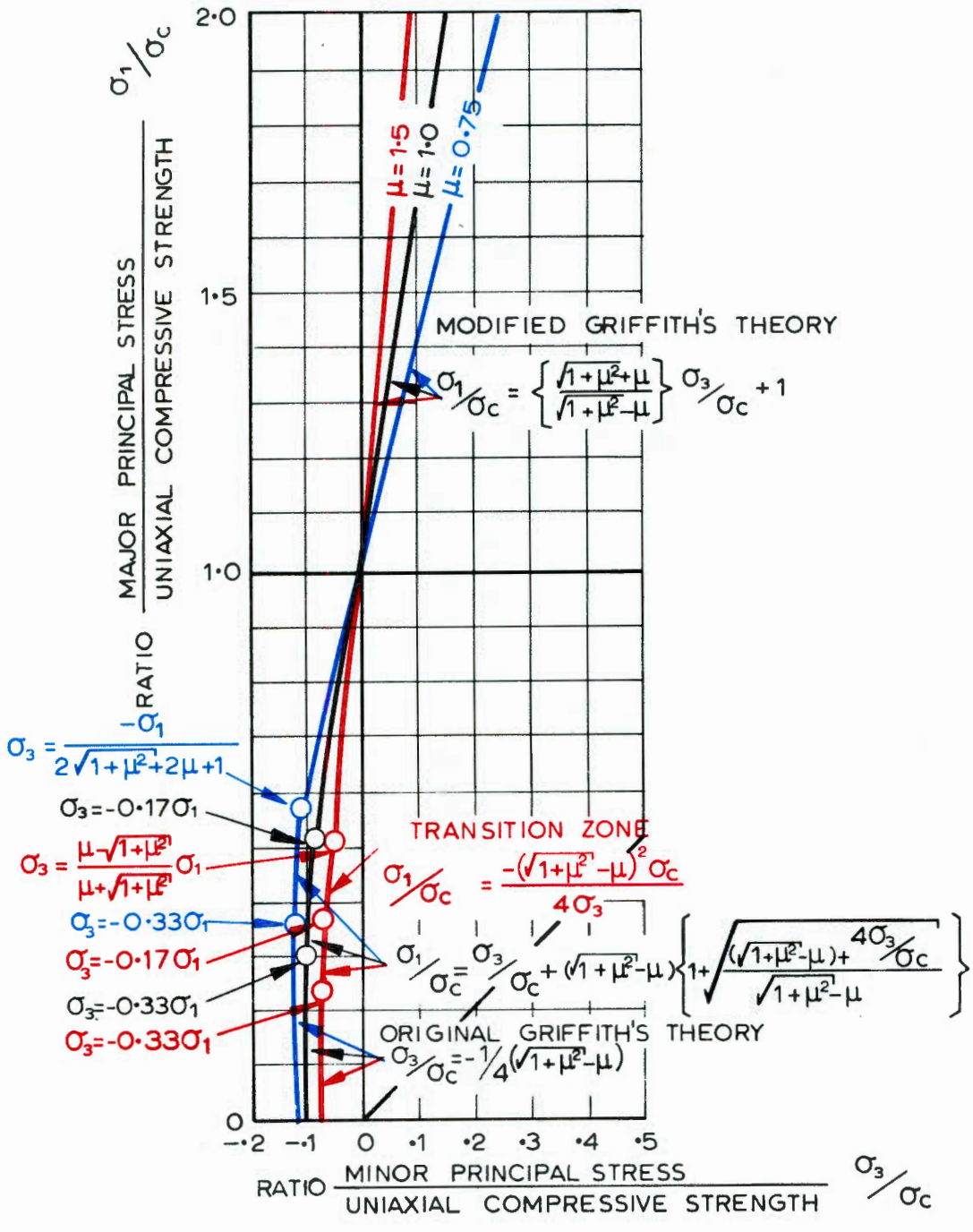

FIGURE 7

Relationship between the major principal stress σ_1 at fracture and the minor principal stress σ_3 in terms of the uniaxial compressive strength σ_c

across a plane at an angle ψ to the direction of the principal stress σ_1 can be determined directly from the Mohr diagram.

A fracture hypothesis which specifies the state of stress at fracture can now be graphically represented by an infinite number of Mohr circles for the states of stress at which fracture occurs. The envelope to these circles, called the Mohr envelope, can be described by an equation $\tau = f(\sigma)$.

9.3.1 Envelope to a family of Mohr circles defined by the original Griffith theory for $k > -0.33$

According to the original Griffith theory, the principal stresses σ_1 and σ_3 at fracture, for $k > -0.33$, are related by equation (24a) which may be written in the following form:

$$\left(\tfrac{1}{2}(\sigma_1 - \sigma_3)\right)^2 = -4\sigma_t\left(\tfrac{1}{2}(\sigma_1 + \sigma_3)\right) \quad \ldots\ldots (47)$$

From equations (46) and (47), the family of Mohr circles representing the fracture of a brittle material which behaves in accordance with the original Griffith theory (for $k > -0.33$) is defined by the following equation:

$$(\sigma_m - \sigma_{xx})^2 + \tau_{xz}^2 + 4\sigma_t\sigma_m = 0 \quad \ldots\ldots\ldots (48)$$

where $\sigma_m = \tfrac{1}{2}(\sigma_1 + \sigma_3)$, is the mean stress.

The general method of fitting an envelope to a family of curves, defined by an equation $f(\sigma_{xx}, \tau_{xz}, \sigma_m) = 0$, is to eliminate the variable parameter σ_m between this equation and $\partial f / \partial \sigma_m = 0$.*

Equating the partial derivative with respect to σ_m ($\partial f / \partial \sigma_m$) of equation (48), to zero gives

---

* PIAGGIO, H.T.H.
An elementary treatise on differential equations
G. Bell and Sons Ltd., London. Revised edition 1952, p. 66.

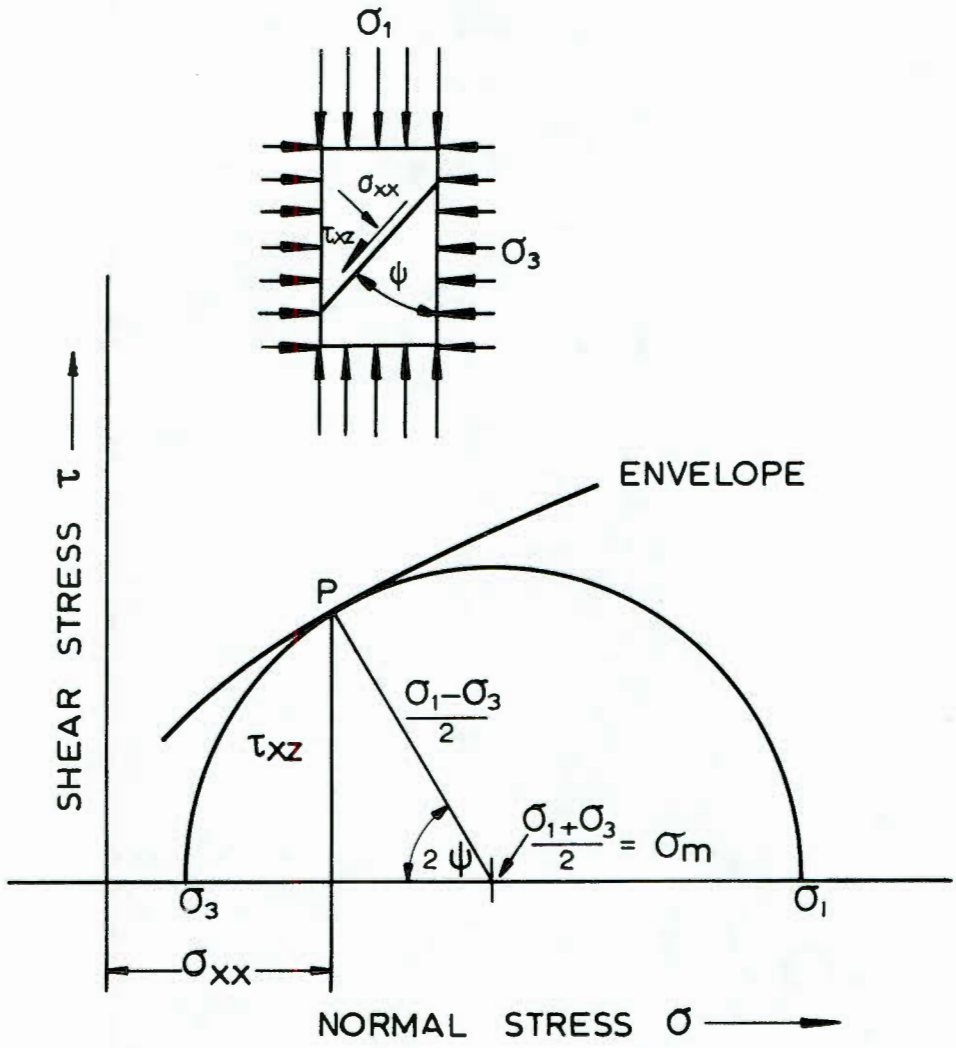

FIGURE 8

Mohr's graphical representation of stress.

$$\sigma_m = \sigma_{xx} - 2\sigma_t \quad \ldots\ldots\ldots\ldots\ldots\ldots (49)$$

Eliminating σ_m between equations (48) and (49) gives

$$\tau_{xz}^2 = 4\sigma_t (\sigma_t - \sigma_{xx}) \quad \ldots\ldots\ldots\ldots (50a)$$

This is the equation to a parabolic Mohr envelope representing the conditions for fracture initiation in an ideal Griffith material for $k > -0.33$.

The subscripts $_{xx}$ and $_{xz}$ have been retained in the above derivation to conform with the nomenclature used in the earlier part of this study. However, for practical application, it is convenient to omit these subscripts and to write equation (50a) as

$$\tau^2 = 4\sigma_t (\sigma_t - \sigma) \quad \ldots\ldots\ldots\ldots\ldots\ldots (50b)$$

or

$$\frac{\tau}{\sigma_t} = 2\sqrt{1 - \frac{\sigma}{\sigma_t}} \quad \ldots\ldots\ldots\ldots (50c)$$

The inclination of the plane (x, z) in which the shear stress (τ) acts, in relation to the direction of the major principal stress (σ_1) is given by equation (19):

$$\text{Cos } 2\psi_c = \frac{\sigma_1 - \sigma_3}{2(\sigma_1 + \sigma_3)} \quad \ldots\ldots\ldots\ldots\ldots (19)$$

9.3.2 Envelope to a family of Mohr's circles defined by the original Griffith theory for $k \leq -0.33$

The radius of curvature (R) of the parabolic envelope defined by equation (50b) can be determined from the following general

relationship*:

$$R = \frac{(1 + (d\sigma/d\tau)^2)^{\frac{3}{2}}}{-d^2\sigma/d\tau^2} \quad \ldots\ldots\ldots\ldots (51)$$

Substituting the first and second derivatives of equation (50b) into equation (51) gives

$$R = \frac{(4\sigma_t^2 + \tau^2)^{\frac{3}{2}}}{4\sigma_t^2} \quad \ldots\ldots\ldots\ldots (52)$$

The radius of curvature of the apex of the parabolic Mohr envelope, defined by equation (50b), is obtained by substituting $\tau = 0$ in equation (52):

$$R_{apex} = 2\sigma_t \quad \ldots\ldots\ldots\ldots\ldots (53)$$

From equation (50b), the apex of the envelope, when $\tau = 0$, is located at $\sigma = \sigma_t$. Since $\sigma = \sigma_3$ when $\tau = 0$ (by definition), it follows that the apex of the envelope lies at

$$\sigma = \sigma_3 = \sigma_t \quad \ldots\ldots\ldots\ldots (54)$$

From Figure 9 it can be seen that the centre of the circle of curvature lies at $-\sigma_t$ while the major principal stress $\sigma_1 = -3\sigma_t$. Consequently, the circle of curvature of the apex of the parabolic Mohr envelope defined by equation (50b) coincides with the condition $\sigma_3/\sigma_1 = k = -0.33$.

---

* GRANVILLE, W.A., SMITH, P.F. and LONGLEY, W.M.
Elements of differential and integral calculus
Ginn and Company, New York, 1941, p. 152

Since the Mohr circles for $k < -0.33$ all lie within the circle of curvature of the apex, they can only touch the envelope at a single point i.e. $\sigma = \sigma_3 = \sigma_t$ and the condition for fracture initiation within the range $-\infty < k \leq -0.33$ is given by

$$\sigma_{3(-\infty < k \leq -0.33)} = \sigma_t \quad \ldots\ldots\ldots (27)$$

This equation is identical to equation (27) which was derived in section 6.2.4 and the above argument can, in fact, be used as an alternate proof for the validity of equation (27).

Since $\tau = 0$ for $k \leq -0.33$, it follows from Figure 9, that

$$\psi_{c(k \leq -0.33)} = 0 \quad \ldots\ldots\ldots\ldots (55)$$

9.3.3 Envelope to a family of Mohr's circles defined by the modified Griffith theory

According to the modified Griffith theory, the principal stresses σ_1 and σ_3 at fracture are related by equation (33) which may be re-written as:

$$\left(\tfrac{1}{2}(\sigma_1 - \sigma_3)\right)^2 = \frac{(\mu\sigma_m - 2\sigma_t)^2}{(1 + \mu^2)} \quad \ldots\ldots\ldots (56)$$

From equations (46) and (56), the family of Mohr circles representing the fracture of a brittle material which behaves in accordance with the modified Griffith theory is defined by the following equation

$$(\sigma_m - \sigma_{xx})^2 + \tau_{xz}^2 = \frac{(\mu\sigma_m - 2\sigma_t)^2}{(1 + \mu^2)} \quad \ldots\ldots (57)$$

Equating the partial derivative of equation (57), with respect to σ_m, to zero and solving for σ_m gives

$$\sigma_m = (1 + \mu^2)\sigma_{xx} - 2\mu\sigma_t \quad \ldots\ldots\ldots\ldots (58)$$

Eliminating σ_m between equations (57) and (58):

$$\tau_{xz} = \mu\sigma_{xx} - 2\sigma_t \quad \ldots\ldots\ldots\ldots\ldots\ldots (59a)$$

Equation (59a) is the equation of a straight line Mohr envelope which defines the condition for fracture initiation in a brittle material containing initially closed cracks, when the normal stress across the cracks (σ_{xx}) is compressive.

As in the case of the original Griffith theory, for practical application it is convenient to omit the subscripts $_{xx}$ and $_{xz}$ and to write equation (59a) simply as

$$\tau = \mu\sigma - 2\sigma_t \quad \ldots\ldots\ldots\ldots\ldots\ldots (59b)$$

or

$$\tau/\sigma_t = \mu\tau/\sigma_t - 2 \quad \ldots\ldots\ldots\ldots\ldots\ldots (59c)$$

The inclination of the Mohr envelope defined by equation (59b) is given by equation (32):

$$\text{Tan } 2\psi_c = 1/\mu \quad \ldots\ldots\ldots\ldots\ldots\ldots (32)$$

9.3.4 Transition between Mohr envelopes for the original and modified Griffith's theories

In deriving the fracture criteria discussed in the preceding sections of this study, it has been assumed that the cracks from which fracture initiates are initially closed. When the normal stress σ_{xx} acting across a crack (see Figure 1) is tensile, the crack opens and the original Griffith theory applies. When the normal stress σ_{xx} acting across the crack

(see Figure 2) is compressive, a shear resistance is induced parallel to the crack surfaces and the modified fracture criterion becomes operative.

Since the normal stress σ_{xx} is plotted as the ordinate of the Mohr diagram (see Figure 8), the transition between the Mohr envelopes representing the original and modified Griffith's criteria occurs at $\sigma_{xx} = 0$.

Examination of equations (50) and (59) shows that, in both cases, when $\sigma_{xx} = 0$:

$$\tau_{xz(\sigma_{xx} = 0)} = -2\sigma_t \quad \ldots\ldots\ldots\ldots\ldots\ldots (60)$$

Consequently, the transition between the Mohr envelopes representing the original and modified Griffith criteria occurs at a point defined by (σ = 0, τ = $-2\sigma_t$).

It is evident from Figure 3.31 that the slope of the Mohr envelopes for the original and modified theories, at the point of transition, can only be identical for $\mu = 1.00$. If the coefficient of friction (μ) has any value other than 1.00, the Mohr envelope defining the fracture behaviour of the material is discontinuous at the point of transition. This is illustrated for the cases $\mu = 0.75$ and $\mu = 1.5$ in Figure 9.

Although the degree of discontinuity is not large, the fact that the Mohr envelope is discontinuous, for values of μ other than 1.00, suggests that the limits of validity imposed upon the original and modified theories (see section 8) should not be too rigidly adhered to for practical application. These limits have been derived on the assumption that all the cracks within the stressed body behave in an identical manner. This assumption is obviously an over-simplification of the actual situation as, in a material such as rock, the transition from the original to the modified criterion will occur gradually over a stress range rather than at a specific stress level.

9.3.5 Graphical representation of equations defining the Mohr envelopes representing the original and modified Griffith's criteria

The equations which define the Mohr envelopes representing the original and modified Griffith's fracture criteria are presented graphically in Figures 9 and 10. As in the case of the other graphical representations, the equations are presented in terms of both the uniaxial tensile and the uniaxial compressive strength of the material. Mohr circles for particular stress states which are of interest in this study are included in these Figures.

10. SUMMARY OF EQUATIONS DEFINING FRACTURE INITIATION IN A BRITTLE MATERIAL CONTAINING INITIALLY CLOSED CRACKS

The equations defining fracture initiation in a brittle material containing initially closed cracks, discussed in the previous section and represented graphically in Figures 3 to 7 and 9 and 10, are summarised in Table II.

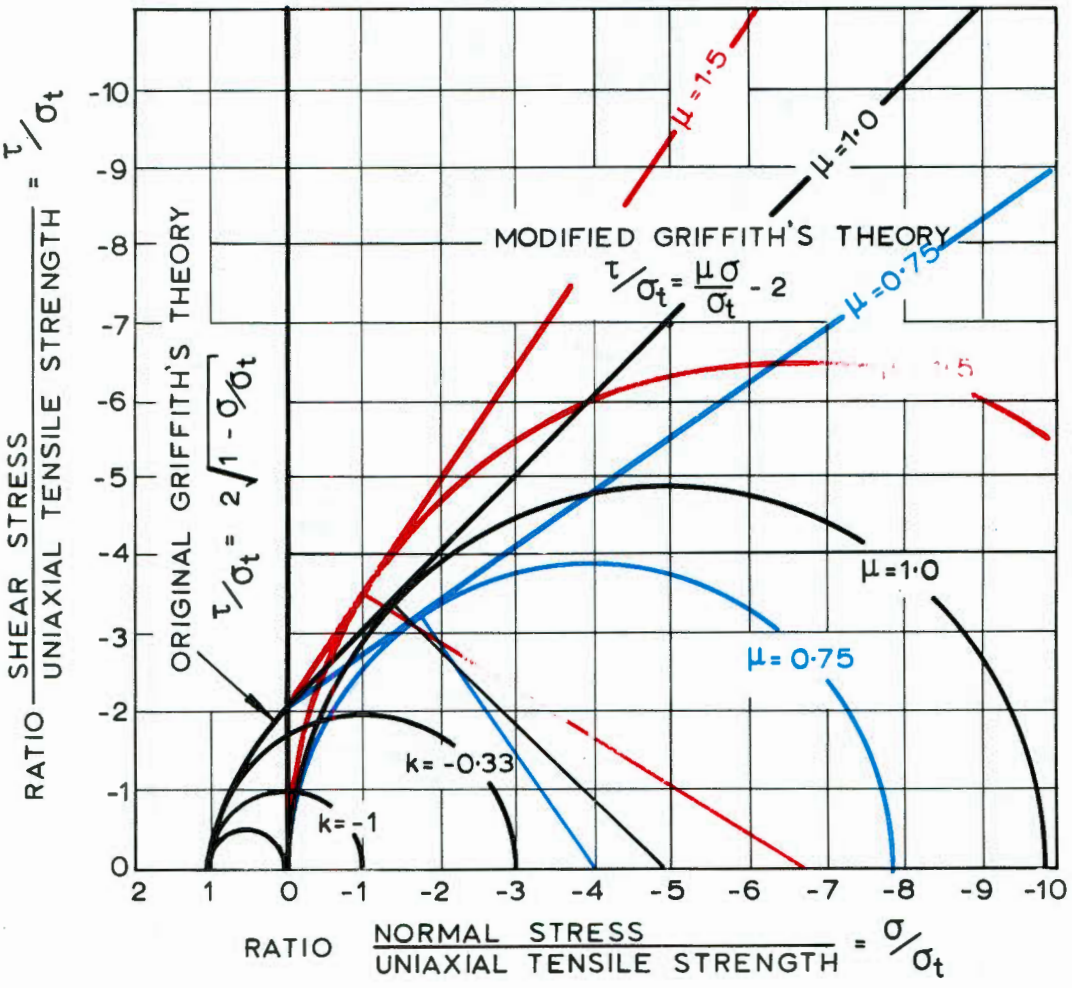

FIGURE 9

Mohr envelopes for original and modified Griffith's brittle fracture in terms of the uniaxial tensile strength σ_t

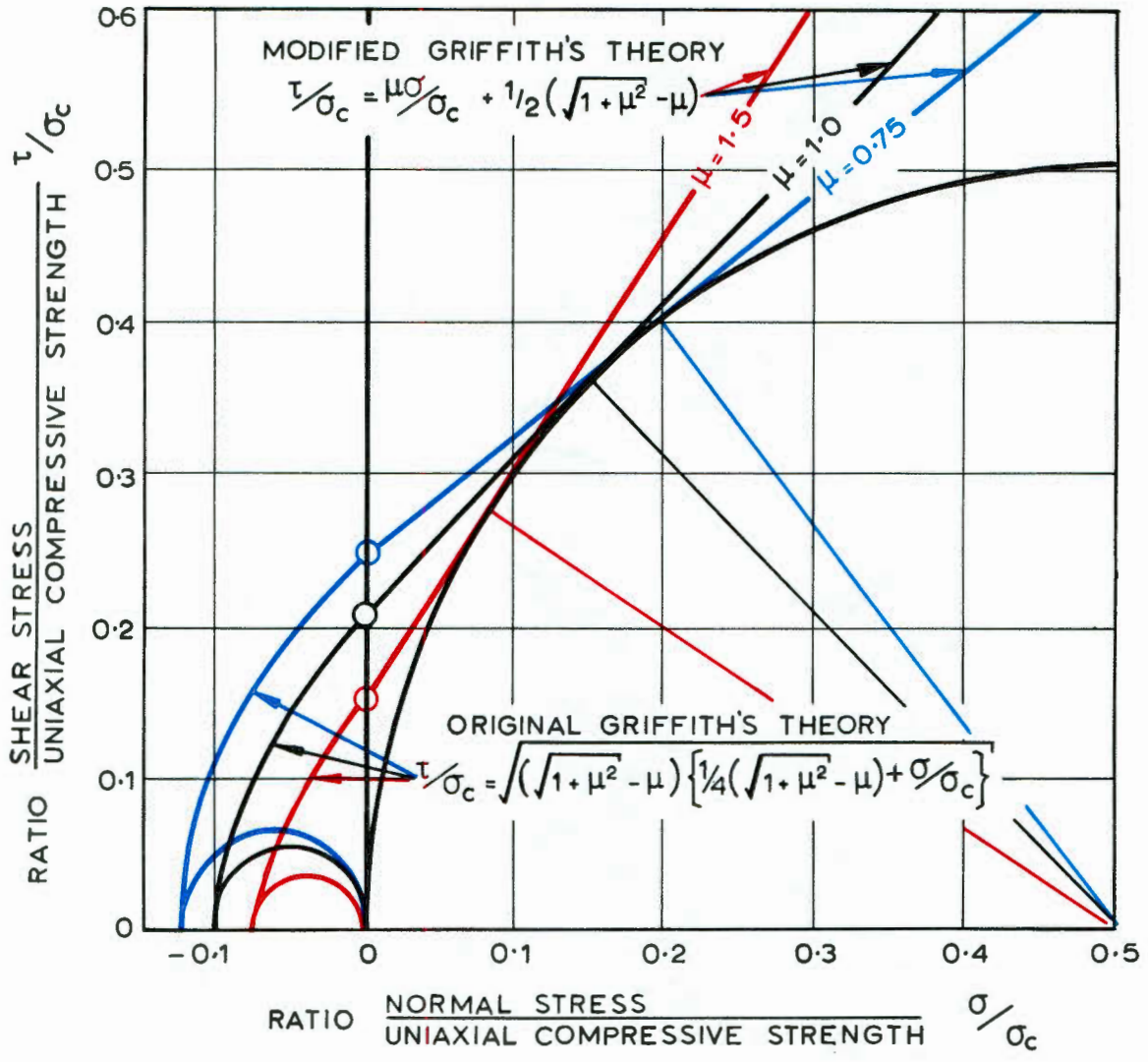

FIGURE 10

Mohr envelopes for original and modified Griffith's brittle fracture criteria in terms of the uniaxial compressive strength σ_c

TABLE II :

FRACTURE CRITERION	ORIGINAL GRIFFITH BRITTLE FRACTURE CRITERION FOR CLOSED CRACKS			FIGURE NUMBER
COEFFICIENT OF INTERNAL FRICTION μ	OPEN CRACK WITHOUT FRICTION	INITIALLY CLOSED CRACK $\mu = 1$	INITIALLY CLOSED CRACK $\mu > 1$	
LIMITS OF VALIDITY DEPENDING UPON AND SPECIFIED BY k AND μ	$-\infty \leq k \leq -0{\cdot}33$	$-\infty \leq k \leq \frac{\sqrt{1+\mu^2}-\mu}{\sqrt{1+\mu^2}+\mu}$	$\frac{\mu-\sqrt{1+\mu^2}}{\mu+\sqrt{1+\mu^2}} \leq k \leq \frac{\sqrt{1+\mu^2}-\mu}{\sqrt{1+\mu^2}+\mu}$	
CRITICAL CRACK ORIENTATION ψ_c	$\psi_c = 0$	ARCTAN $1/\mu$		3
FRACTURE INITIATION CRITERIA IN TERMS OF:				
$\sigma_1\ (\sigma_t, \mu, k)$	FRACTURE INITIATION IN THE RANGE $-\infty \leq k \leq -0{\cdot}33$ OCCURS WHEN THE MINOR PRINCIPAL STRESS EQUALS THE UNIAXIAL TENSILE STRENGTH; $\sigma_3 = \sigma_t$	$\frac{-4}{\mu^2 - (1+k)\mu}$		4
$\sigma_1\ (\sigma_c, \mu, k)$		$\frac{\sqrt{\mu^2} - \mu}{\mu^2 - (1+k)\mu}$		5
$\sigma_1\ (\sigma_t, \mu, \sigma_3)$		$\frac{(\sqrt{\mu^2}+\mu)\sigma_3/\sigma_t - 4}{\sqrt{1+\mu^2} - \mu}$		6
$\sigma_1\ (\sigma_c, \mu, \sigma_3)$		$\left\{\frac{\sqrt{\mu^2}+\mu}{\sqrt{\mu^2}-\mu}\right\}\sigma_3/\sigma_c + 1$		7
$\tau\ (\sigma_t, \mu, \sigma)$		$\tau/\sigma_t = \mu\,\sigma/\sigma_t - 2$		9
$\tau\ (\sigma_c, \mu, \sigma)$		$\tau/\sigma_c = \sqrt{(\ldots} + \frac{1}{2}(\sqrt{1+\mu^2} - \mu)$		10

PART II - THE FRACTURE OF BRITTLE ROCK AND THE INFLUENCE OF ADDITIONAL FACTORS UPON FRACTURE

11. ROCK FRACTURE

The theoretical considerations presented in part I of this study were based upon fracture initiation at the boundary of an isolated crack in a uniform stress field. The immediate question which arises is - can this theory be used to predict fracture in a crystalline material such as rock which, according to Brace[51], contains a multitude of randomly oriented cracks in the form of grain boundaries?

In an attempt to provide an answer to this question, a survey of published fracture data on rock and concrete was undertaken. A similar, but less extensive, survey was carried out by McClintock and Walsh[249] in order to substantiate their modification to the original Griffith's theory. The results of their survey are included in the present study.

A comparison of the results of triaxial tests on different rock materials necessitates reducing these results to a dimensionless form. This is most conveniently done by expressing all the strength results as ratios of the uniaxial compressive strength (σ_c). The uniaxial compressive strength is the only value, presented by all the authors whose work is included in this survey, which can be accepted as a reliable basis for comparison.

The procedure for reducing the strength results to dimensionless ratios has the additional advantage that factors of influence, such as the geometry, moisture content and rate of loading of the specimen are presumably the same in both numerator and denominator and are thereby eliminated from the dimensionless strength values.

The materials included in this survey are listed in Table III and the results are plotted in Figure 11. These experimental results are compared with the original and modified Griffith's fracture loci obtained from Figure 7.

It is evident from Figure 11 that, in spite of the wide

TABLE III : SUMMARY OF TRIAXIAL TEST RESULTS ON ROCK AND CONCRETE

Graph Point	Material	σ_c * lb/sq.in	Tested by	Ref.
1	Marble	13 700	Ros and Eichinger	319
2	Marble	18 000	Ros and Eichinger	319
3	Marble	20 000	Von Karman	357
4	Carthage Marble	10 000	Bredthauer	53
5	Carthage Marble	7 500	Bredthauer	55
6	Wombeyan Marble	10 000	Jaeger	215
7	Concrete	2 380	McHenry and Karni	250
8	Concrete	3 200	Akroyd	7
9	Concrete	6 000	Jaeger	215
10	Concrete	5 700	Fumagalli	134
11	Concrete (28 day)	3 510	Balmer	17
12	Concrete (90 day)	4 000	Balmer	17
13	Granite Gneiss	25 500	Jaeger	215
14	Barre Granite	24 200	Robertson	312
15	Granite (slightly alt)	10 000	Wreuker	375
16	Westerly Granite	33 800	Brace	52
17	Iwaki Sandstone	1 780	Horibe and Kobayashi	202
18	Rush Springs Sandstone	26 000	Bredthauer	55
19	Pennant Sandstone	22 500	Price	297
20	Darley Dale Sandstone	5 780	Price	297
21	Sandstone	9 000	Jaeger	215
22	Oil Creek Sandstone	**	Handin	249
23	Dolomite	24 000	Bredthauer	55
24	White Dolomite	12 000	Bredthauer	55
25	Clear Fork Dolomite	**	Handin	249
26	Blair Dolomite	**	Handin	249
27	Blair Dolomite	75 000	Brace	52
28	Webtuck Dolomite	22 000	Brace	52
29	Chico Limestone	10 000	Bredthauer	55
30	Virginia Limestone	48 000	Bredthauer	55
31	Limestone	20 000	Jaeger	215
32	Anhydrite	6 000	Bredthauer	55
33	Knippa Basalt	38 000	Bredthauer	55
34	Sandy shale	8 000	Bredthauer	55
35	Shale	15 000	Bredthauer	55
36	Porphry	40 000	Jaeger	215
37	Sioux Quartzite	**	Handin	249
38	Frederick Diabase	71 000	Brace	52
39	Cheshire Quartzite	68 000	Brace	52
40	Chert dyke material	83 000	Hoek	194
41	Quartzitic shale (Dry)	30 900	Colback and Wiid	83
42	Quartzitic shale (Wet)	17 100	Colback and Wiid	83
43	Quartzitic sandstone (dry)	9 070	Colback and Wiid	83
44	Quartzitic sandstone (wet)	4 970	Colback and Wiid	83
45	Slate (primary cracks)	4 300	Hoek	193
46	Slate (secondary cracks)	15 900	Hoek	193
47	Dolerite	37 000	CSIR	-
48	Quartzite (ERPM Footwall)	31 000	CSIR	-
49	Quartzite (ERPM Hanging wall)	43 200	CSIR	-
50	Glass	91 000	CSIR	-

* Uniaxial compressive strength

** Presented in dimensionless form by McClintock and Walsh

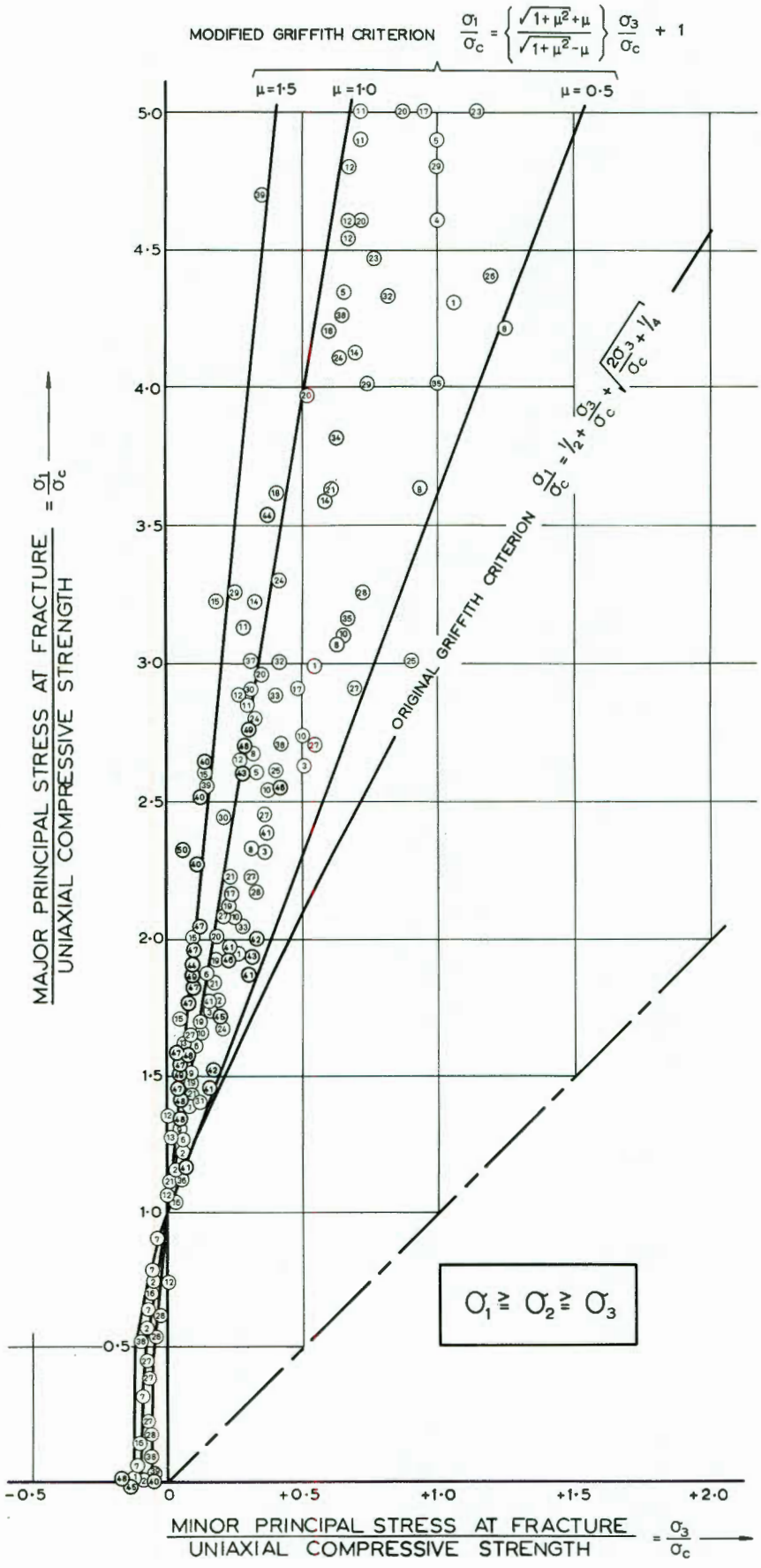

FIGURE 11

Triaxial fracture data for rock materials

variety of materials included in this survey, there is a remarkable agreement between these results and the fracture initiation behaviour predicted by the modified Griffith theory. On the basis of this agreement one may be tempted to conclude that this theory is substantially correct. Closer inspection, however, reveals an anomaly which suggests that the picture is not as simple as one may wish to believe.

Investigations by Jaeger[216] indicate that the coefficient of friction of rock against rock is of the order of 0.8. Many of the materials included in Figure 11 appear to have coefficients of friction considerably in excess of unity. This suggests that there must be interlocking of projections on the crack faces and that propagation of the crack can only occur when these projections have been sheared off. Alternately, because of the interlocking of the grains themselves, the crack may be forced to follow a complex path. This propagation may require an increase in the coefficient of internal friction.

Consequently, the results presented in Figure 11, although most encouraging, suggest that the mechanism of fracture propagation requires further investigation.

12. BRITTLE FRACTURE PROPAGATION IN COMPRESSION

In studying the fracture of brittle materials subjected to tension, fracture is normally expected in a direction perpendicular to the applied tension, in other words, in the plane of the critically oriented crack. In the case of a brittle material subjected to compressive stress, one might therefore expect that fracture propagation will also follow the direction of the most critically oriented crack, i.e. one which is inclined at 20-30° to the direction of the major principal applied stress.

Detailed examination of equation (15)[283] shows that the maximum tensile stress on the boundary of an inclined crack does not occur at the actual crack tip. Experimental results presented by Brace and Bombolakis[50] confirm this finding and reveal that fracture propagation does not follow the direction of the initial crack.

In order to study these effects in greater detail, an experimental study on glass plates containing initial cracks was carried out by Hoek and Bieniawski[383] and the results are summarised below.

12.1 Fracture propagation from an open "Griffith crack"

The edges of 6 inch square by ¼ inch thick plates of annealed glass were carefully ground. Open "Griffith Cracks" were machined into these plates by means of a Mullard 60 watt ultrasonic drill. The length of these cracks was kept constant at ½ inch and the axis ratio at 25:1. The cracks were oriented at their critical angles as determined from equation (19).

The plates were subjected to uniformly distributed edge loading in the tension and compression loading devices described in Appendices II and III to this study. The specimens were studied photoelastically while under load and the stresses at which fracture initiated were noted. A typical isochromatic pattern obtained in a plate subjected to uniaxial compression is reproduced in Figure 12.

The stresses at which fracture initiated are plotted, in terms of the major and minor applied principal stresses, in

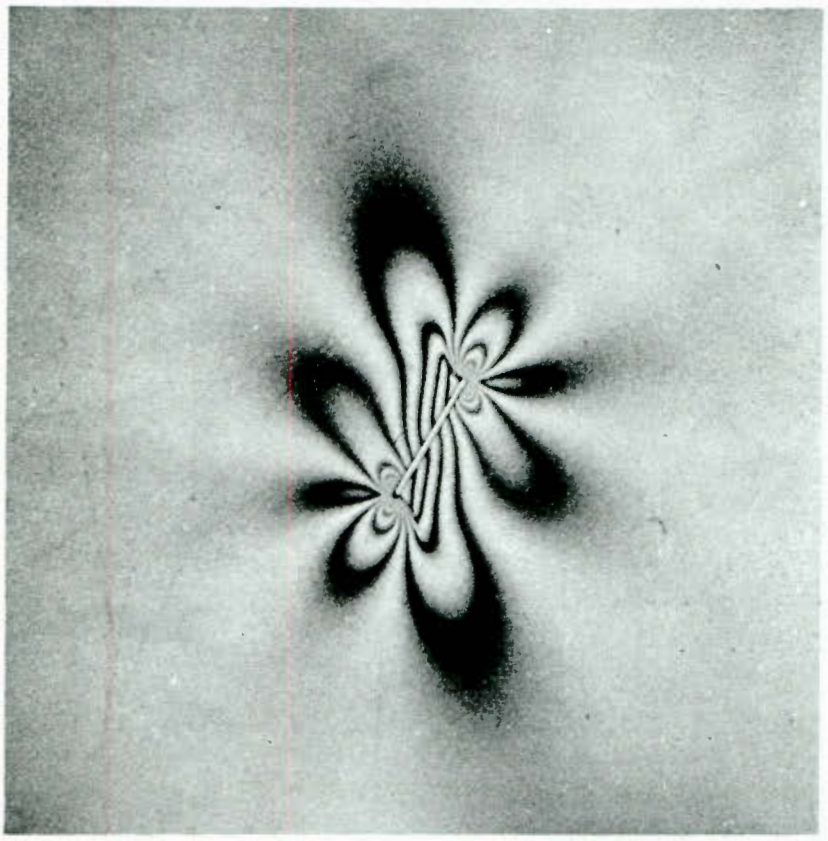

FIGURE 12

Isochromatic pattern in a glass plate containing an open "Griffith" crack from which fracture has propagated under uniaxial compressive applied stress

Number the fringes?
What did bi-axial pattern look like?
Show more detail of thinner in zone of interest at crack tip!!

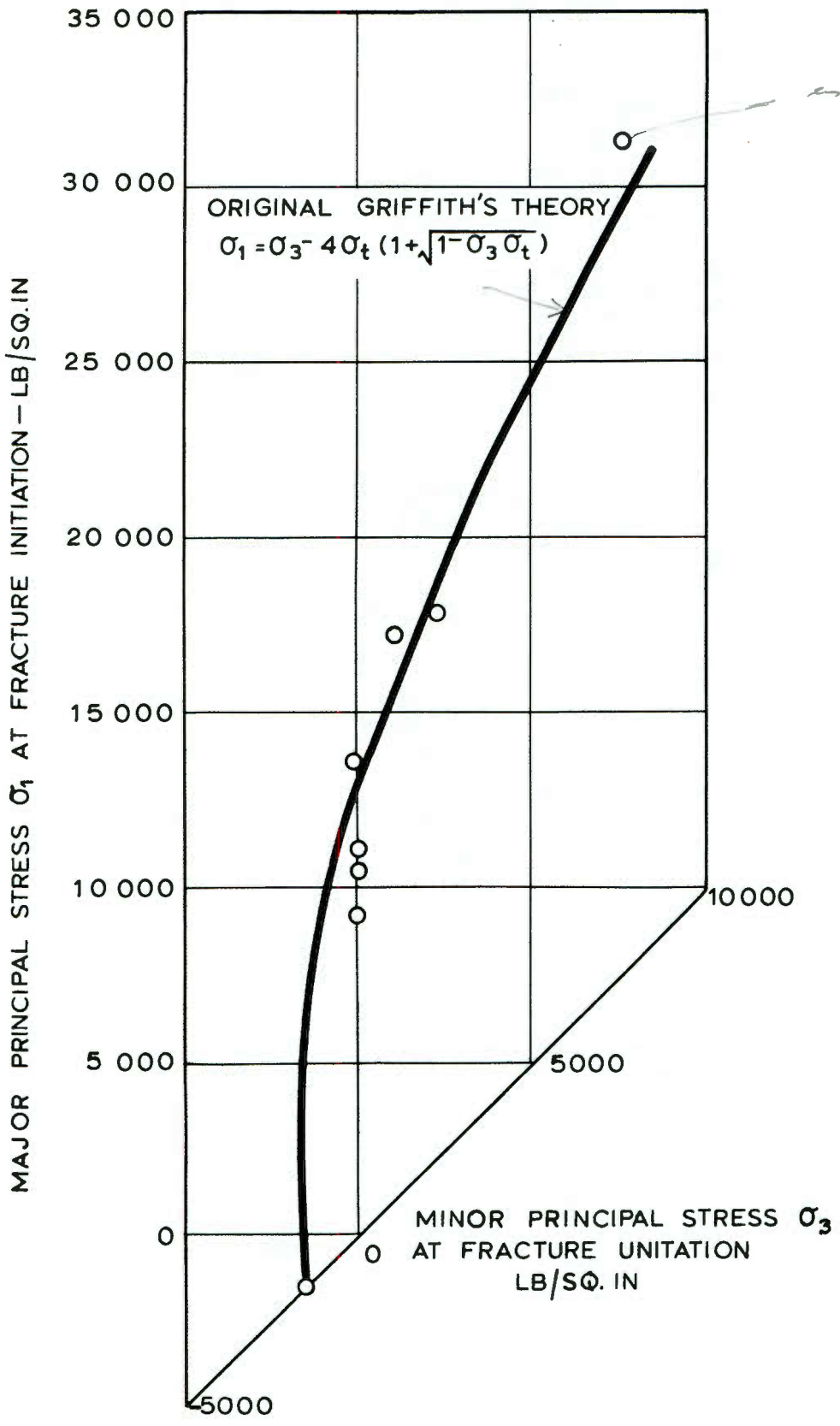

FIGURE 13

Relationship between the principal stresses at fracture initiation from the boundary of an open crack

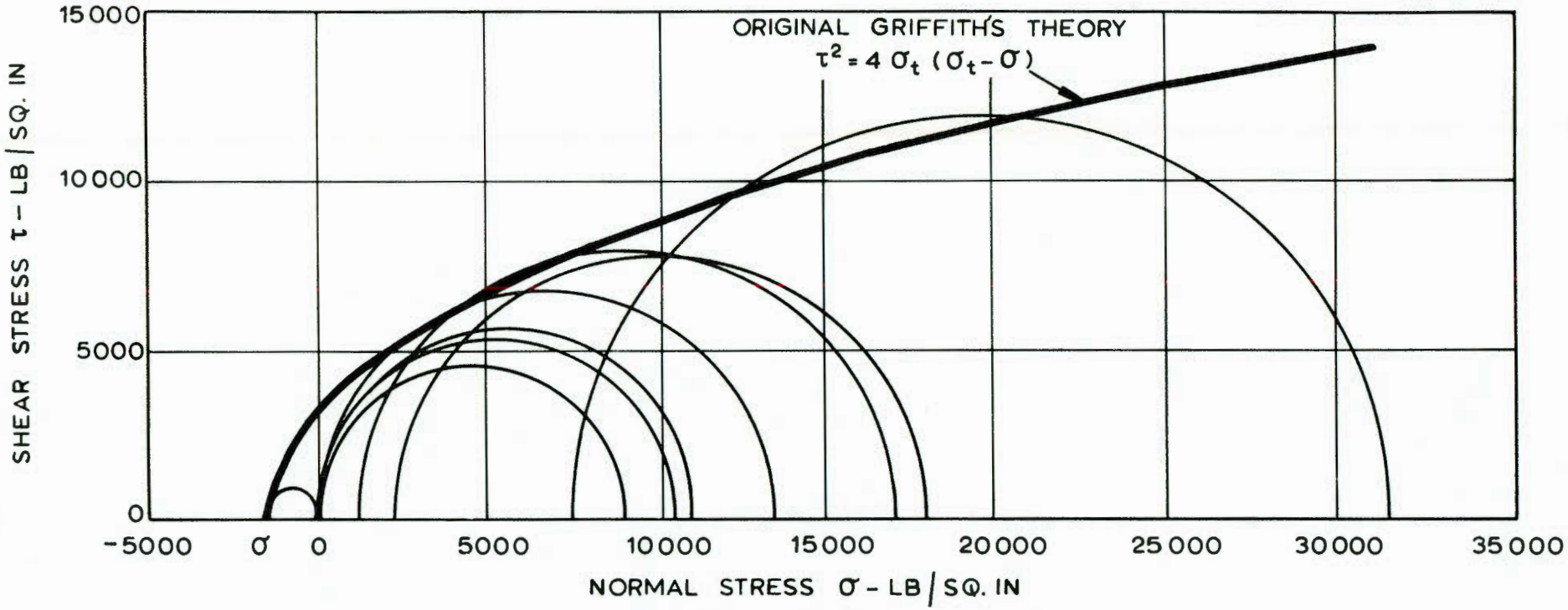

FIGURE 14

Mohr circles for fracture initiation at the boundary of an open crack

How valid are all these circles for a material 25"×25" with a 2" crack?

Figure 13 and as Mohr circles in Figure 14. The experimental results are compared, in these figures, with the theoretical Griffith fracture loci defined by equations (43) and (50b).

From the agreement between the experimental and theoretical applied stresses at fracture initiation, one must conclude that the original Griffith theory provides an accurate basis for the prediction of fracture initiation from an open crack in a plane stress field.

In uniaxial tension, as can be expected, fracture propagation occurred in a direction perpendicular to the direction of applied tension.

In biaxial compression, the fracture propagation followed a consistent pattern. As revealed by careful examination of Figure 12, fracture initiated at a point on the crack boundary near but not at the crack tip and propagated along a curved path. Fracture propagation ceased when the crack path had become parallel to the major principal applied stress direction. In all cases, the applied stress was increased to at least three times the fracture initiation stress and, if the cracks showed no tendency to propagate further, the test was discontinued on the assumption that fracture of the specimen would not occur except at much higher stress levels.

The lengths of the stable cracks were found to be related to the ratio of the applied principal stresses as illustrated in Figure 15. These findings are similar to those previously reported by the author[195] for the propagation of cracks from a circular hole in a biaxial compressive stress field.

Under uniaxial compressive stress conditions, fracture propagation commenced with the sudden appearance of a small crack of approximately 0.2 times the initial crack length. Normally, this crack would appear at only one end of the initial crack but would be followed, within a period of a few seconds* and at the same applied stress level, by a mirror image crack at the other end of the initial crack. Further propagation of these cracks

---

* In many of these tests on glass, the fracture process was observed to be significantly time-dependent but no conclusion can be drawn from the present results because of a lack of adequate records in this respect.

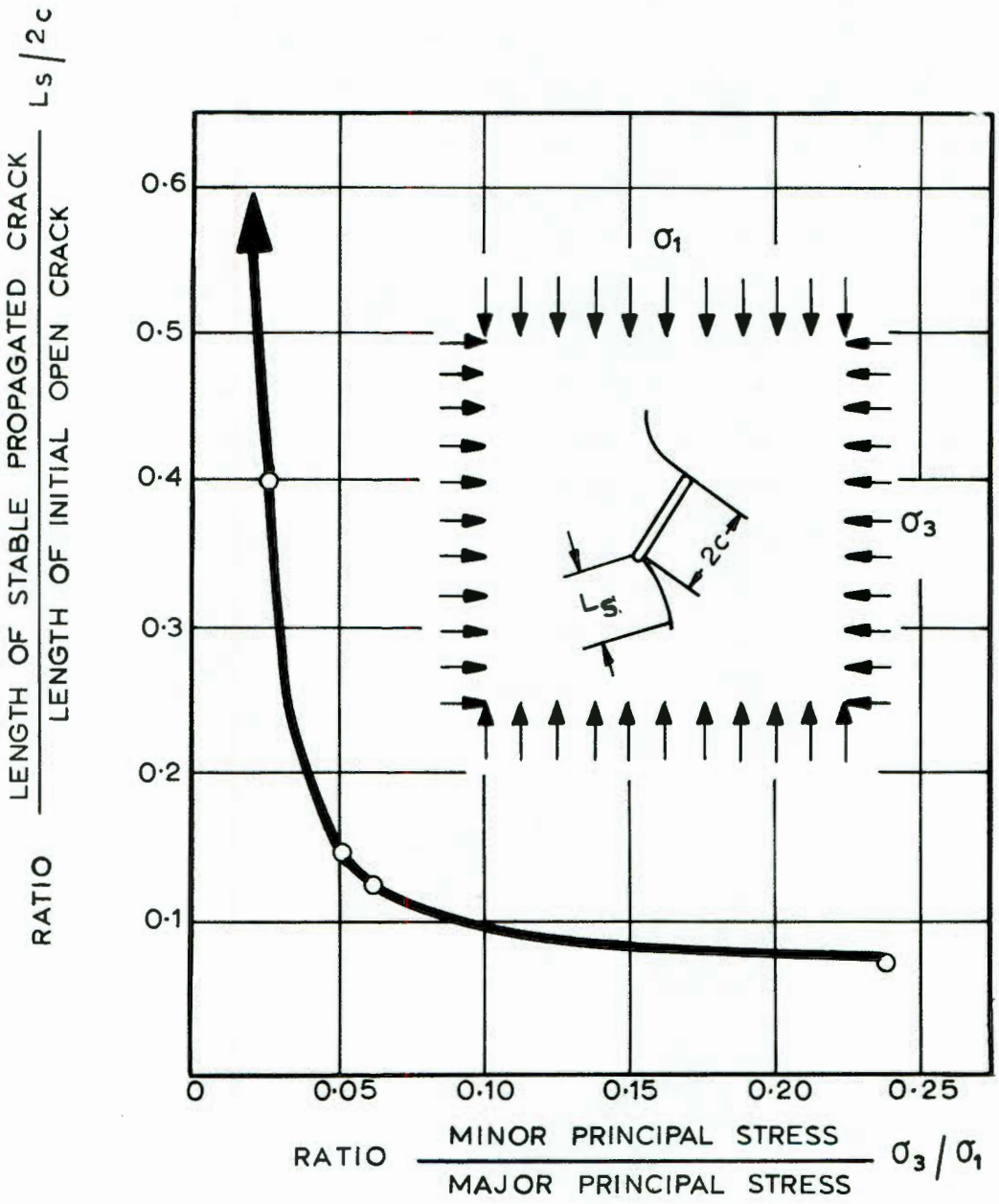

FIGURE 15

Relationship between stable crack length and ratio of applied stresses (glass).

required an increase in the applied stress and this applied stress is plotted, against crack length, in Figure 16.

In the case of biaxial compression, insufficient information is available to permit the plotting of graphs similar to that shown in Figure 16. From examination of available records, however, it appears that the length of the initial and final cracks do not differ by more than a few percent. This implies that, if the crack can be propagated, the stress required to do so would be many times greater than the initiation stress and, as such, is of little practical interest.

From these results it can be concluded that a single open "Griffith crack" cannot account for the failure of a specimen unless the ratio of the applied principal stresses is equal to or less than zero i.e. in uniaxial compression or when one of the principal stresses is tensile. It is also suggested that, when failure of the specimen originates from a single crack, the direction of the macroscopic fracture surface will always tend to be parallel to the direction of the major applied principal stress.

12.2 Fracture propagation from an initially closed "Griffith crack"

Since it appears reasonable to assume that the cracks from which the fracture of hard rock initiates are initially closed[49], an attempt was made to produce closed cracks in glass plates.

The method used to produce these cracks involved inducing a hairline crack of the required length on the surface of the glass plate. A hardened roller type glass tool which induces this crack as a result of the stress distribution under the contact point has been found preferable to a diamond tool which scores the glass surface. The shallow hairline crack is propagated through the thickness of the plate by reflected tensile stress waves generated by impacting the plate on the face opposite to that containing the crack.

Preliminary tests carried out on closed cracks showed that the mechanism of fracture differs significantly from that of open cracks. An example of fracture initiation and propagation

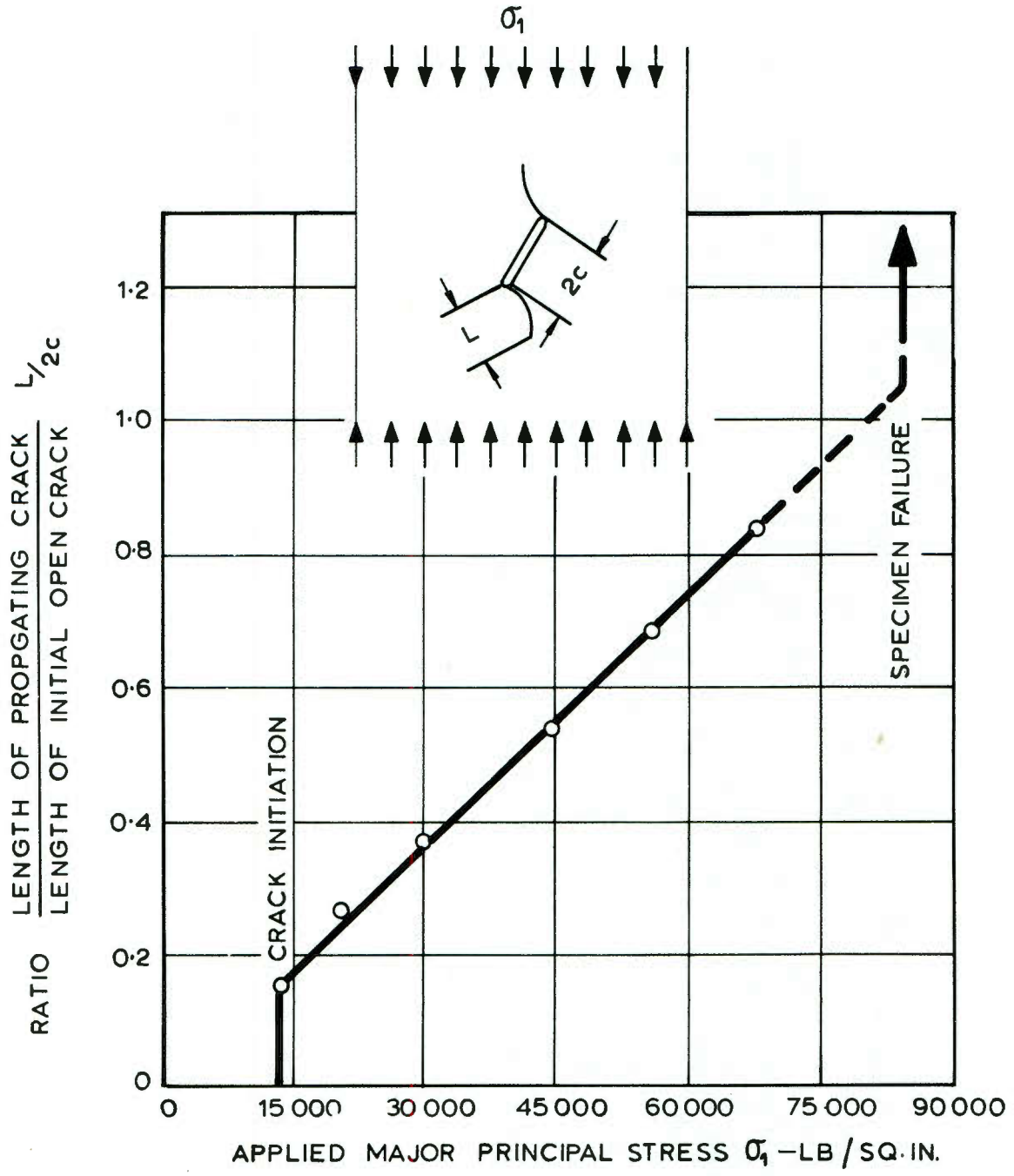

FIGURE 16

Relationship between the propagating crack length and the applied uniaxial compressive stress (glass).

from a closed crack in glass is illustrated in the photograph reproduced in Figure 17.

Careful observation of the crack, during loading of the specimen, revealed the formation of short vertical cracks along the length of the initial crack. These cracks multiplied with increasing applied load until the cracks closest to the initial crack tip started to propagate. At this stage, the formation of the short cracks ceased. In most cases, the cracks which finally propagated, although nearest to the crack tips, were a significant distance away from it as illustrated in Figure 17. It will also be noted that all the cracks lie parallel to the direction of the major principal applied stress.

In order to determine the coefficient of friction μ and the critical crack orientation ψ_c for closed cracks in glass, a series of tests was carried out in which plate models containing cracks at various orientations were loaded in uniaxial compression. The applied stress at which fracture initiated is plotted for various crack orientations in Figure 18. It will be noted that the lowest stress required to initiate fracture occurs at a crack orientation of approximately $27\frac{1}{2}^{\circ}$ which, from equation (32), coincides with a coefficient of friction μ of 0.7.

From equations (31) and (42) the following equation can be derived, relating the applied uniaxial compressive stress σ_1, the uniaxial compressive strength σ_c and the crack orientation ψ:

$$\frac{\sigma_1}{\sigma_c} = \frac{\sqrt{1 + \mu^2} - \mu}{\sin 2\psi - \mu(1 - \cos 2\psi)} \quad \ldots\ldots\ldots\ldots (61)$$

Substituting $\mu = 0.7$ into this equation results in the curve illustrated in Figure 18 and, from the agreement between this curve and the experimental results, it can be concluded that the estimate of $\mu = 0.7$ is sufficiently accurate for practical purposes.

Having established that the critical orientation ψ_c for closed cracks in glass is $27\frac{1}{2}^{\circ}$, plates containing cracks with

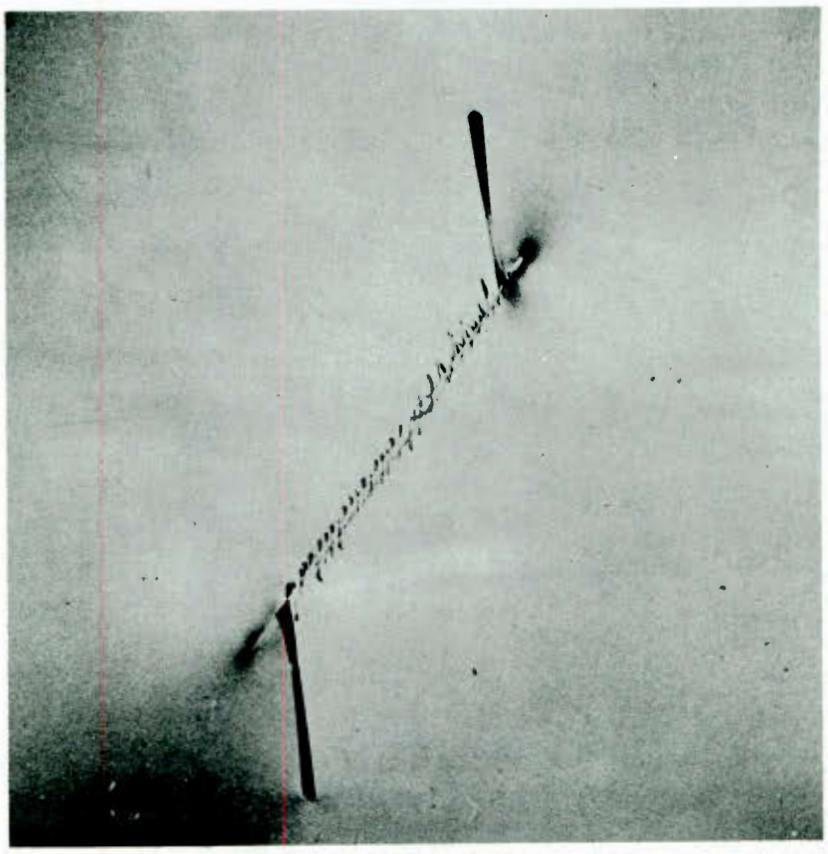

FIGURE 17

Fracture propagation from a closed crack in glass subjected to uniaxial compressive stress conditions

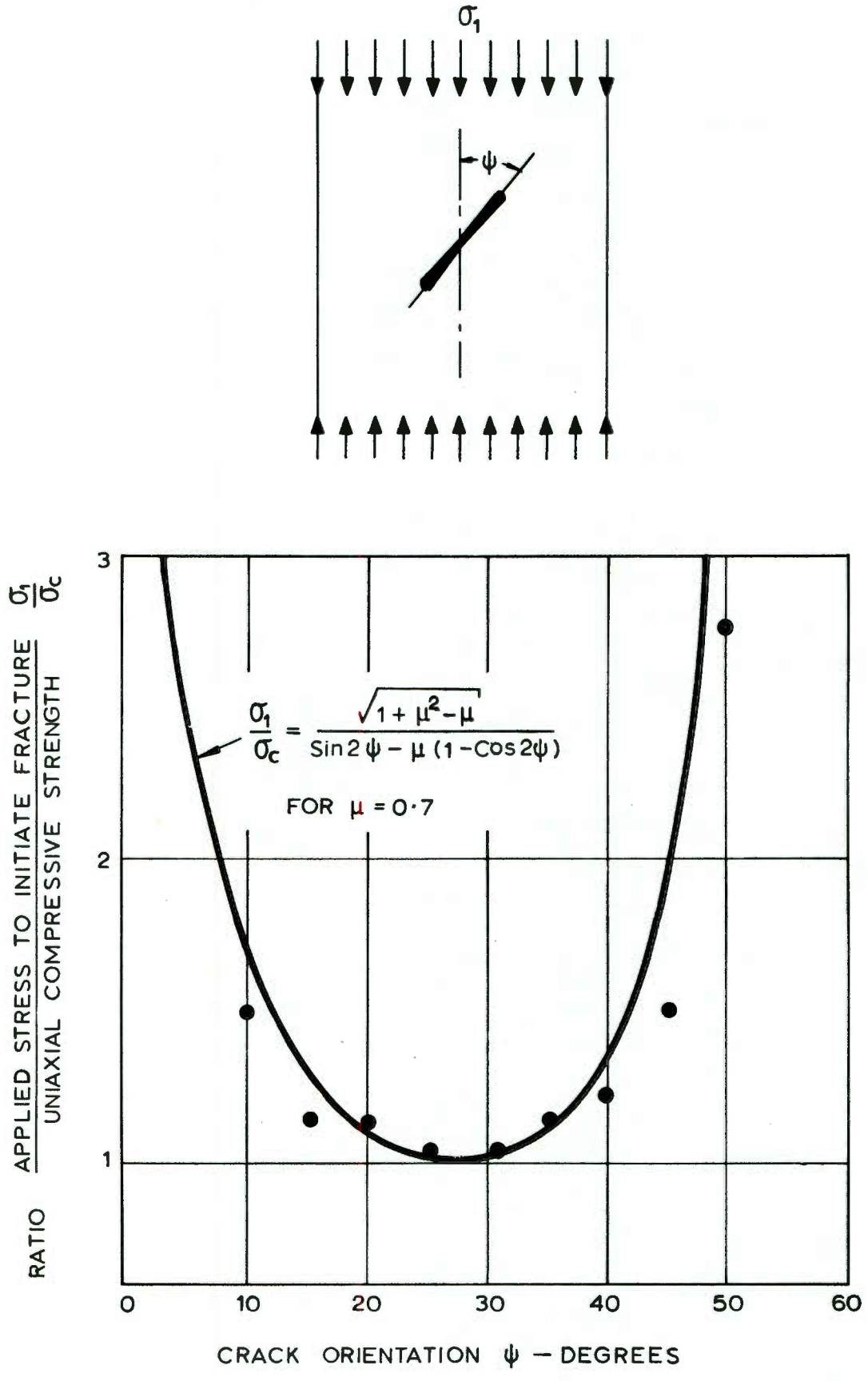

FIGURE 18

Relationship between applied stress required to initiate fracture and orientation of closed cracks in glass

this orientation were tested at various ratios of applied principal stresses.

It was immediately obvious in carrying out these tests that two distinct phases of fracture behaviour can be distinguished.

Firstly, the short cracks illustrated in Figure 17 appear at a well defined stress level. These cracks, all of approximately the same length, increase in number with increasing applied stress.

Secondly, also at a well defined stress level, the short cracks closest to the tips of the initial crack started to propagate. As in the case of the open cracks, the length to which these cracks could be propagated was found to depend upon the ratio of applied stresses.

The results of these tests are plotted, as the relationship between the principal stresses, in Figure 19 and, as Mohr circles, in Figures 20 and 21. These experimental results are compared with the original and modified Griffith fracture loci, calculated on the basis of the uniaxial compressive strength σ_c and, in the case of the modified theory, using a coefficient of friction μ of 0.7

Comparison of the theoretical and experimental results in Figures 19, 20 and 21 suggests a fracture mechanism which would account for the observed behaviour. This fracture mechanism is diagrammatically illustrated in Figure 22.

Due to irregularities in crack surface, sections of the crack are forced into intimate contact and develop a high frictional shear resistance when the crack is subjected to compressive stress. Between these sections of high shear resistance, one can visualise short open "Griffith cracks" as illustrated in Figure 22. Since these cracks do not exert a significant influence upon each other, as illustrated in Figure 23, it can be anticipated that fracture initiation from these cracks will be reasonably accurately defined by the original Griffith theory. Examination of Figures 19 and 20 reveals that this is, in fact, the case.

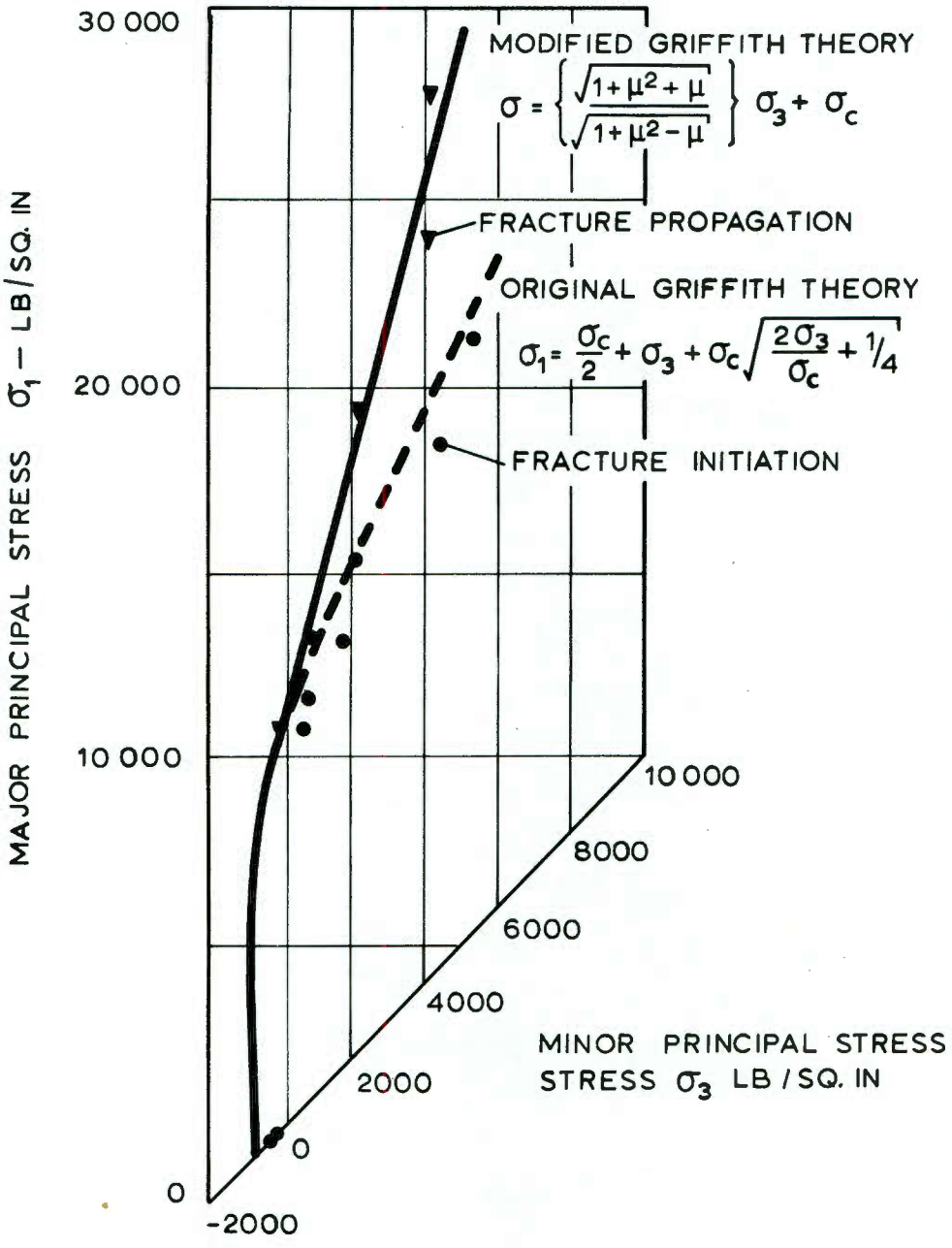

FIGURE 19

Relationship between principal stresses for fracture initiation and propagation from closed cracks in glass

compr. stresses fort.

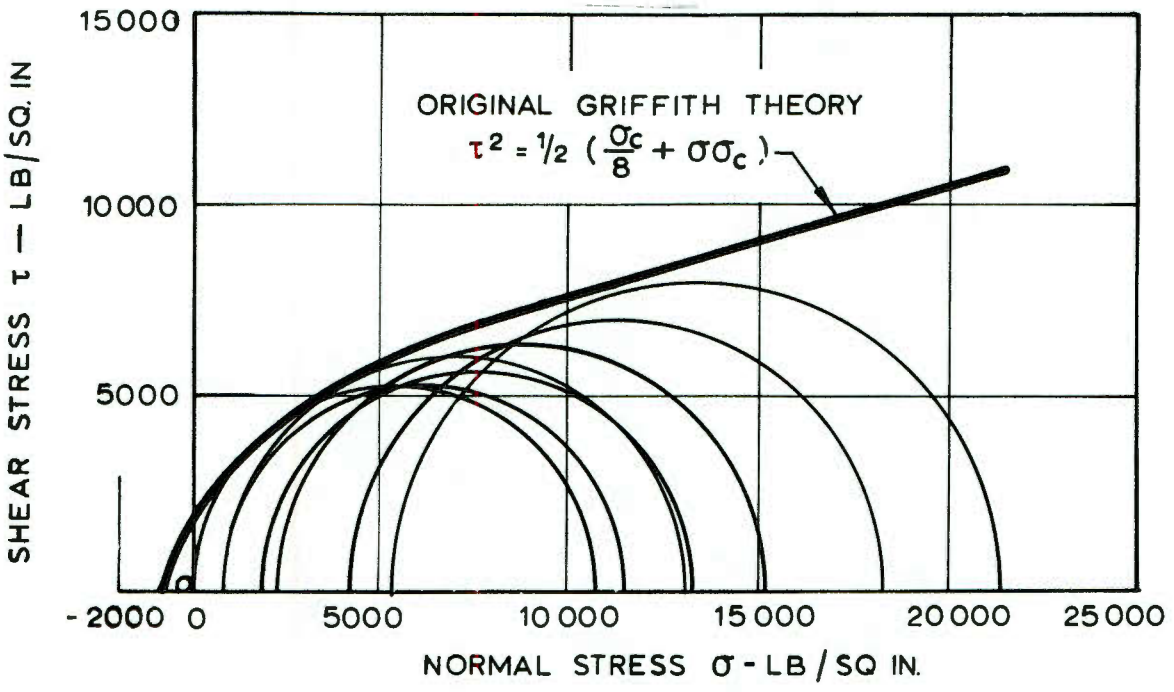

FIGURE 20

Mohr diagram for fracture initiation
from closed cracks in glass

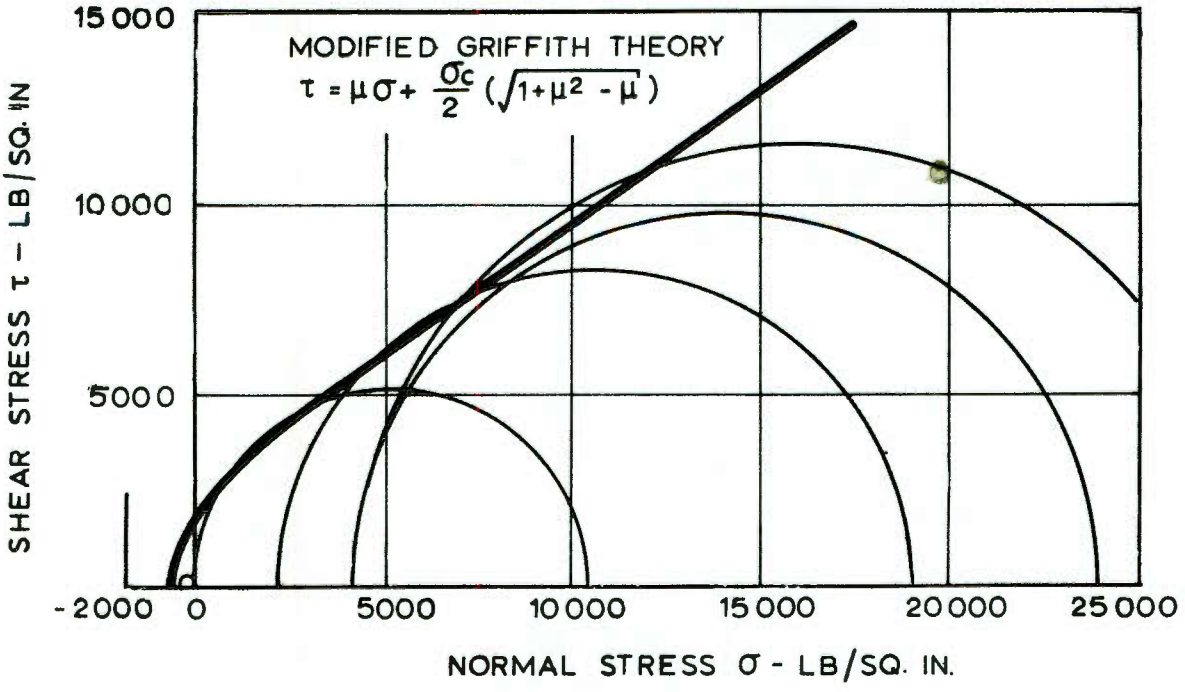

FIGURE 21

Mohr diagram for fracture propagation
from closed cracks in glass

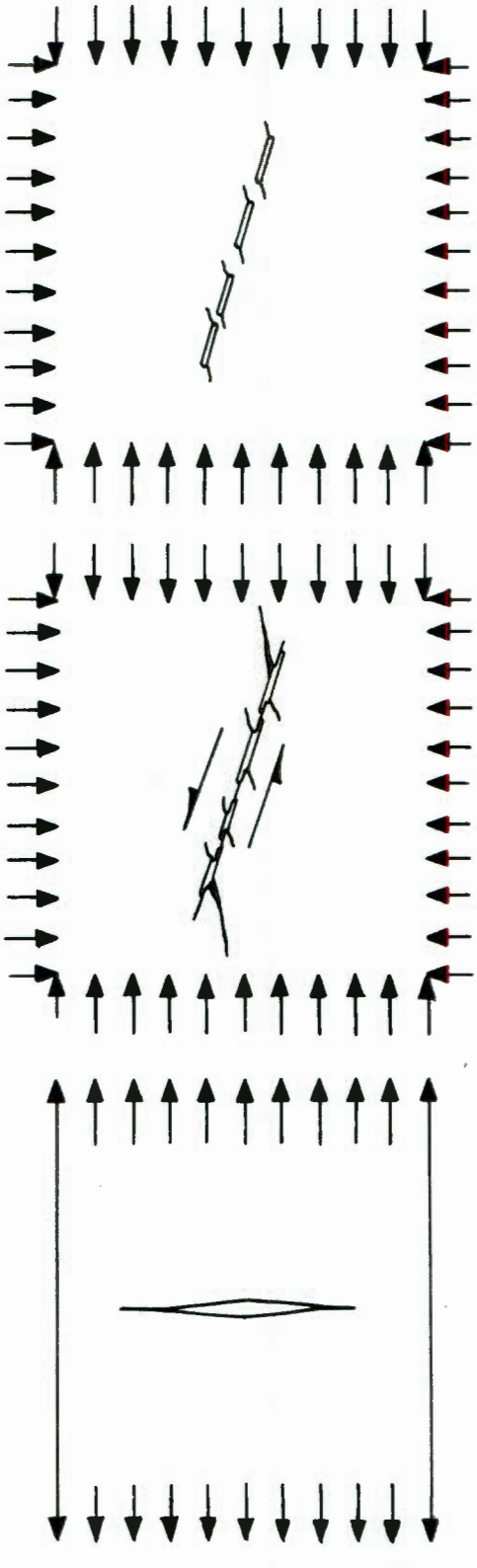

PHASE 1: FRACTURE INITIATION FROM SHORT OPEN CRACKS SEPARATED BY SECTIONS WITH HIGH FRICTIONAL SHEAR RESISTANCE

PHASE 2: FRACTURE PROPAGATION OF CRACKS NEAREST TIPS OF INITIAL CRACK WHEN FRICTIONAL SHEAR RESISTANCE OF CRACK SURFACES HAS BEEN OVERCOME.

CRACK OPENS UNDER TENSILE STRESS CONDITIONS.

FIGURE 22

Diagrammatic representation of the probable fracture mechanism of a closed crack in glass

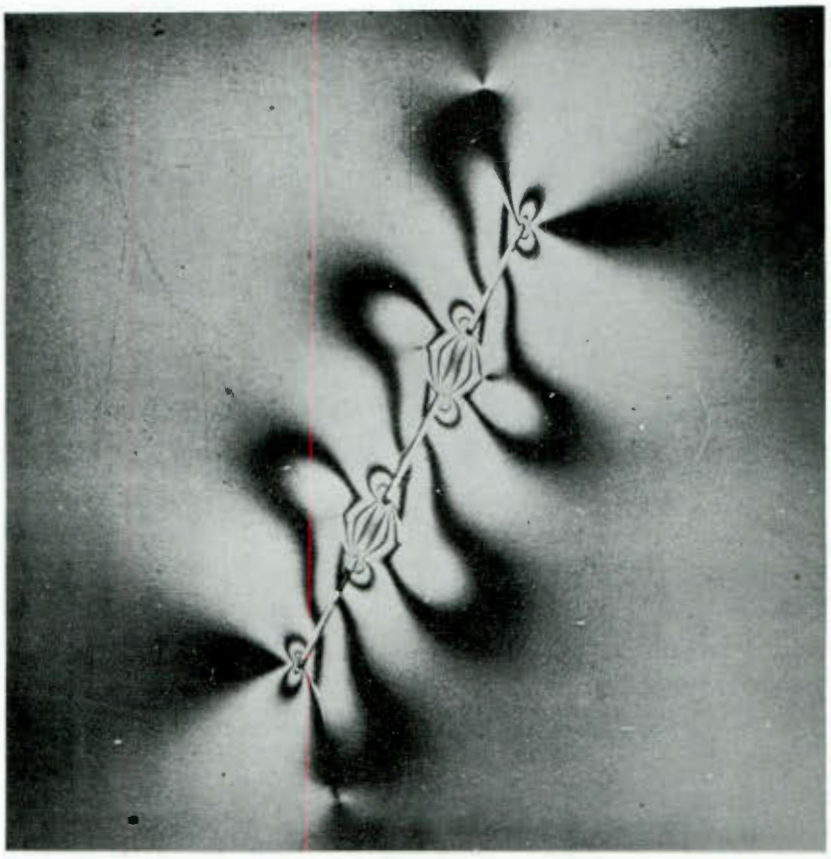

FIGURE 23

Fracture behaviour of an "in-line"
array of cracks in glass

stress pattern ?

As the applied stress level is increased, a stage will be reached at which the frictional shear resistance due to contact between the crack surfaces is overcome. At this stage, fracture propagation occurs as a result of extension of the existing cracks near the tips of the initial crack. Since the stress level at which shear movement of the crack surfaces can take place is dependent upon the normal stress σ_{xx} across the crack and the coefficient of friction μ, it can be anticipated that this stress level can be predicted by the modified Griffith theory. Again, comparison of the experimental and theoretical results presented in Figures 19 and 21 shows that this is the case.

Figures 19, 20 and 21 show that the fracture stress in uniaxial tension is approximately one half of that anticipated theoretically from equation (42). It is proposed that the reason for this discrepancy lies in the fact that equation (29), from which equation (42) is derived, is not sufficiently accurate when applied to cracks in which the radius of the tip approaches zero, i.e. both ξ_o and $\eta \to 0$.

From the results of these tests, it can be concluded that the original and modified Griffith's fracture criterion provide a good description of fracture initiation and the initial propagation of fracture from closed cracks in glass. As in the case of the open cracks, the presence of a single crack cannot account for failure of the specimen if $\sigma_3/\sigma_1 > 0$.

12.3 Brittle fracture propagation in rock

Studies on the behaviour of isolated cracks, discussed in the previous sections, have shown that, except for $\sigma_3/\sigma_1 \leq 0$, failure of a specimen cannot occur as a result of the presence of a single crack. It must therefore be concluded that the presence of a favourable array of cracks is an essential prerequisite for rock fracture on a macroscopic scale.

Figure 24 illustrates the crack path in a typical quartzite specimen in which fracture was arrested just before the specimen became unstable. It will be noted that this crack has propagated along the grain boundaries which, in this case, constitute

FIGURE 24

Crack path in a quartzite specimen subjected to uniaxial compression

$\frac{\sigma_3}{\sigma_1} = 0$

the favourable crack array which is necessary to cause failure of the specimen.

The photograph reproduced in Figure 25 shows the multitude of cracks which have developed in a quartzite specimen in which fracture was arrested by removal of the applied compressive stress just before the specimen became unstable.

A detailed examination of fracture patterns such as those illustrated in Figures 24 and 25 and the evidence presented earlier in this section has led the author to the belief that fracture in hard rock follows the sequence illustrated diagrammatically in Figure 26.

Phase 1 : Fracture initiation occurs at microcracks within grain boundaries which are oriented at between 20 and 30 degrees to the direction of the major principal applied stress. This fracture initiation can probably be accurately predicted by the original Griffith fracture theory. Experimental evidence accumulated from tests on quartzite specimens, in which fracture was arrested at various percentages of the ultimate strength, suggests that fracture initiation from grain boundary microcracks occurs at between 70 and 80% of the ultimate compressive strength.

Phase 2 : At approximately 85% of the compressive strength of quartzite, the frictional shear resistance of the potential grain boundary crack is overcome and sliding along this crack occurs as predicted by the modified Griffith theory. This sliding is, however, soon arrested by interlocking of the grains of the material.

If this interlocking is severe, as illustrated in Figure 26, a considerable increase in the applied stress is necessary before propagation of this crack can occur. Consequently, similar cracks will form in other suitably oriented grain boundaries as illustrated in Figure 25.

Phase 3 : Fracture propagation and fracture of the specimen occurs when the interlocking grains fail and allow the numerous cracks which have formed to join. Final fracture

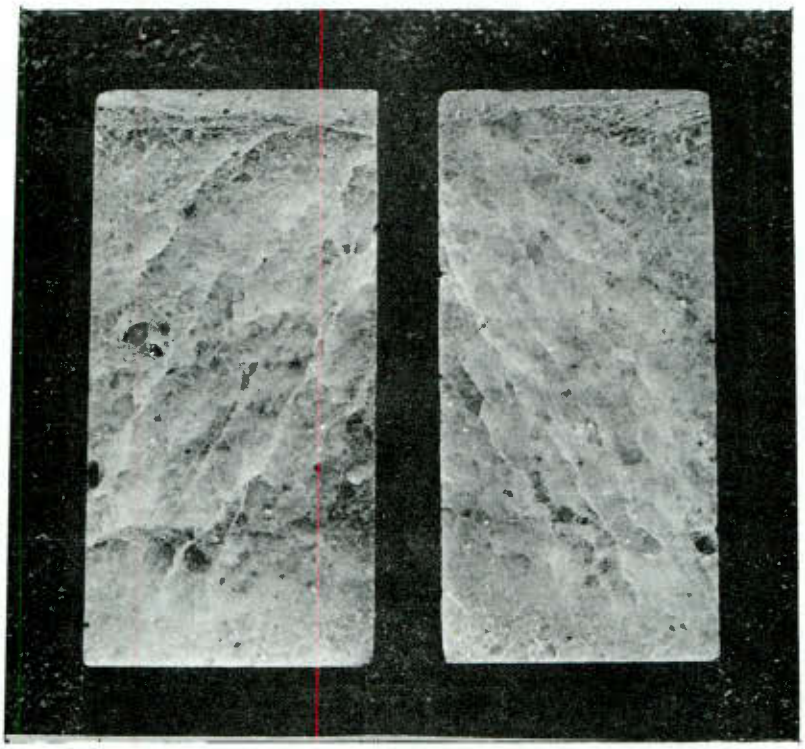

FIGURE 25

uni-axial?

Development of fracture in compression specimens from which the load was removed just before final failure

$\frac{\sigma_3}{\sigma_1} = 0$!

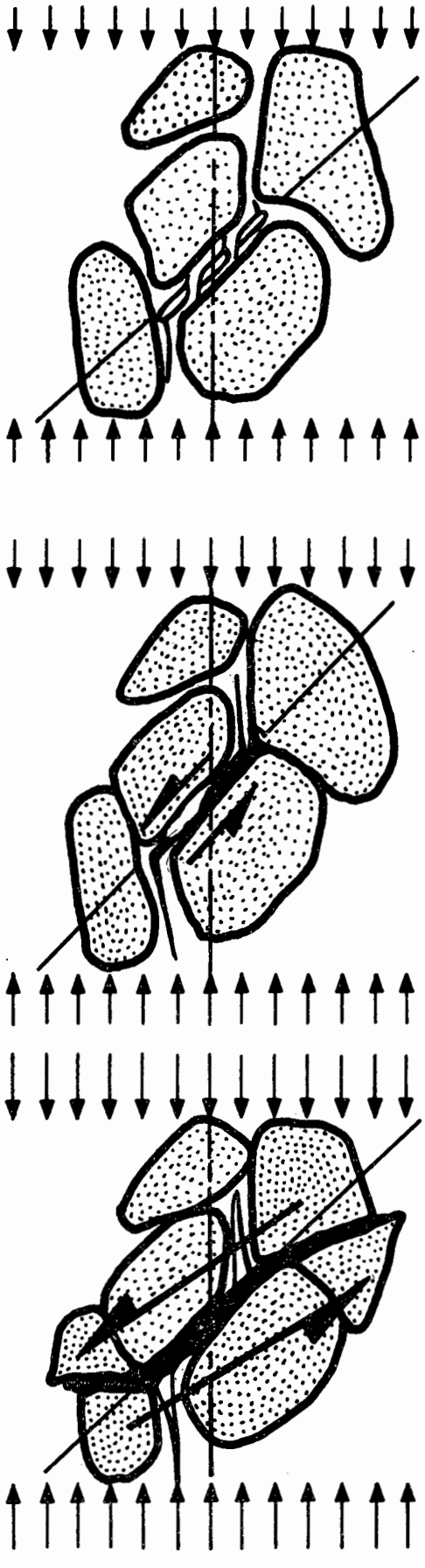

PHASE 1: FRACTURE INITIATION FROM MICROCRACKS IN GRAIN BOUNDARIES ACCORDING TO ORIGINAL GRIFFITH'S THEORY.

PHASE 2: SLIDING ALONG GRAIN BOUNDARY WHEN FRICTIONAL SHEAR RESISTANCE IS OVERCOME ACCORDING TO MODIFIED GRIFFITH THEORY. FRACTURE ARRESTED BY INTERLOCKING GRAINS.

PHASE 3: FRACTURE PROPAGATION OCCURS WHEN INTERLOCKING GRAINS FAIL AND ALLOW SHEAR MOVEMENT. INCLINATION OF FINAL FRACTURE SURFACE NEED NOT COINCIDE WITH CRITICAL CRACK ORIENTATION PREDICTED BY MODIFIED GRIFFITH THEORY.

FIGURE 26

Proposed rock fracture mechanism

occurs as a result of shear movement along an array of cracks.

Since the interlocking grains fail as a result of complex stress distributions induced by point loading, the final fracture direction need not coincide with the orientation of the individual grain boundary cracks. Examination of fractured hard rock specimens reveals that the macroscopic fracture surface usually lies at approximately 30° to the direction of the major principal stress as compared with a critical crack orientation of $22\frac{1}{2}^{\circ}$ predicted by the modified Griffith theory for a rock with a coefficient of friction of unity.

The final fracture phase postulated above is markedly dependent upon the grain structure of the rock. In igneous and metamorphosed sedimentary rocks, in which the grains have been tightly packed and well cemented, severe interlocking of the grains can occur. This would result in a considerable increase in the applied stress required to propagate the grain boundary cracks and would manifest itself as an apparently high coefficient of internal friction.

On the other hand, in sedimentary rocks, in which the grains are loosely bonded, phase 2 and phase 3 are probably almost coincident and the fracture conditions more nearly those predicted by the modified Griffith fracture theory.

Careful examination of Figure 11 (page 52.) shows that, in fact, the igneous and metamorphosed sedimentary rocks are characterised by a coefficient of friction in excess of unity while the sedimentary rocks have coefficients of friction of less than 1.00.

12.4 The application of the original and modified Griffith's theories to rock fracture

On the basis of the evidence presented in the preceeding sections, it is suggested that, with certain limitations, the original and modified Griffith's fracture theories offer an adequate basis for the solution of practical rock fracture problems.

The limitations are due to the fact that failure of a specimen requires propagation of cracks and this propagation does

not necessarily occur at the same stress level nor follow the same direction as the fracture initiation process predicted by the theories. However, on a macroscopic scale, fracture propagation follows the general trends predicted by the original and modified Griffith's fracture theories and, consequently, these theories constitute an acceptable practical rock mechanics tool.

13. THE STUDY OF THE FRACTURE OF ROCK SPECIMENS

In studying the fracture of rock specimens in the laboratory, an exact knowledge of the state of stress in the specimen is essential. This requires careful design of the loading apparatus as well as careful preparation of the specimen.

Before discussing details of the equipment and techniques used by the author, the principal features of triaxial test equipment used by other research workers will be considered.

13.1 Triaxial compression testing of rock specimens

Most of the apparatus described in publications on triaxial compression testing[17, 52, 57, 166, 174, 189, 202, 203, 270, 277, 297, 301, 312, 329, 355] has several features in common. The most important of these common features are:

(i) Generally, cylindrical rock specimens are used for compression testing. The choice of this specimen geometry is governed by the availability of core specimens and the ease of specimen preparation. The length to diameter ratio of specimens and the method of end preparation differ considerably.

(ii) In most triaxial tests, the specimen is subjected to an axial load in a compression testing machine and the lateral stress is applied by means of a fluid under pressure which surrounds the specimen. This stress state can be expresses as $\sigma_1 > \sigma_2 = \sigma_3$ where σ_1 is the axial stress in the specimen and $\sigma_2 = \sigma_3$ the lateral hydraulic pressure. The specimen must be sleeved in order to prevent ingress of the surrounding fluid.

(iii) In most cases, the specimen is subjected to a fixed lateral pressure and the axial stress is increased until failure of the specimen occurs.

Most of the common features described above have been chosen as a result of sound practical reasoning and, with the exception of inevitable differences created by the details of a particular design, there does not appear to be any valid reason for departing

from common practice.

13.2 Stress distribution in a compression specimen

Theoretical studies of the stress distribution in cylindrical compression specimens[129, 90, 15, 16, 293] show that the stress distribution can deviate considerably from uniformity, depending upon the length to diameter ratio of the specimen, the coefficient of friction between the plattens and the ends of the specimen and the Poisson's ratio of the specimen material.

The solution of Balla's equations[15, 16] for various typical cases* reveals that the main factor which induces a non-uniform stress distribution in the specimen is the frictional restraint imposed upon the specimen ends. When the specimen is compressed between semi-infinite rigid plattens, the specimen assumes a barrel shape due to the shear stresses between its ends and the plattens**.

Under the worst conditions - assuming a coefficient of friction of unity between the specimen and the semi-infinite rigid plattens - the length to diameter ratio of the specimen should be at least 2:1 in order that the stress distribution in the centre third of the specimen should be uniform.

Two possible means for improving the stress distribution suggest themselves:

(a) To reduce the coefficient of friction between the specimen and platten and

(b) To design the platten to deform radially with the specimen.

Both of these steps are aimed at reducing the shear stresses between the specimen and platten.

The principal objections to reducing the coefficient of friction between the specimen and platten by lubrication are the

---

* HOEK, E. Unpublished CSIR internal report on the analysis of fracture in a cylindrical compression specimen November 1963

** In a private communication to the author (1964) Dr J.R. Hoskins of the U.S. Bureau of Mines pointed out certain errors in Balla's equations. These errors do not, however, invalidate the above argument.

uncertainty of the process and the danger of extrusion of the layer of lubricant. This extrusion can induce radial tensile stresses in the specimen end which can cause the specimen to split along its axis. This danger is particularly pronounced if a layer of rubber on plastic is inserted between the specimen and platten in an effort to reduce the effects of friction.

The approach adopted by the author was to design the specimen and platten as a unit in such a way that both deform radially to a similar extent. In this case the ends of the specimen are unlubricated and it is assumed that the coefficient of friction between specimen and platten approaches unity.

The principal features of this design are illustrated in Figure 27 which shows that the specimen is the same diameter as the steel platten through which it is loaded.

The radial strain in a cylindrical specimen subjected to triaxial compressive stress can be approximated by the following equation

$$\varepsilon_r = \frac{\sigma_1}{E}\left\{\frac{\sigma_3}{\sigma_1} - \nu\left[1 + \frac{\sigma_3}{\sigma_1}\right]\right\} \quad \ldots\ldots\ldots\ldots\ldots (62)$$

A survey of the properties of typical hard rocks, in which most gold mining in South Africa is carried out, shows that the average Young's Modulus is 12×10^6 lb/sq. in and the average Poisson's ratio is 0.15. Substituting these values into equation (62) results in the curve plotted in Figure 27. The radial strain of the steel plattens is compared with that of the rock specimen and it will be noted that, at low principal stress ratios, these strains are reasonably similar. Since hard rocks will only fail at principal stress ratios smaller than approximately 0.25 (see section 8.5 of part I), the radial strains in specimen and platten are sufficiently similar to induce an acceptably uniform stress distribution in the specimen.

Figure 25, which shows the fracture pattern in a cylindrical specimen from which the load was removed just before complete failure, justifies the above assumptions since it reveals that

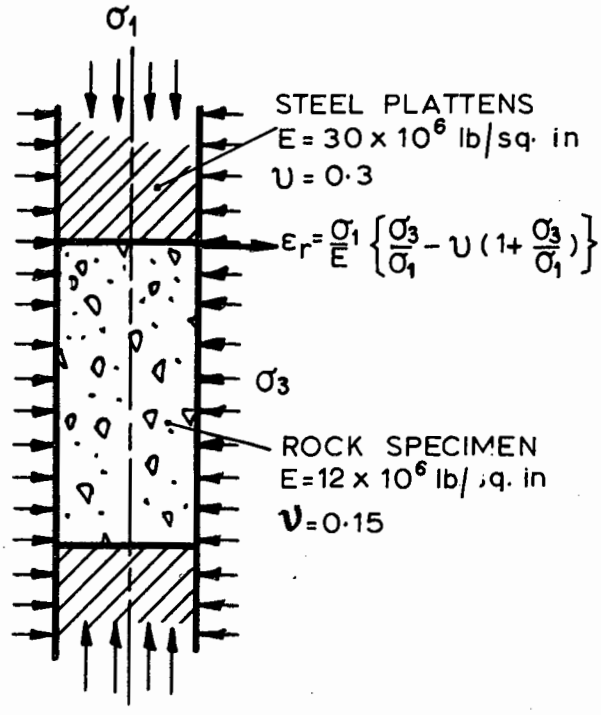

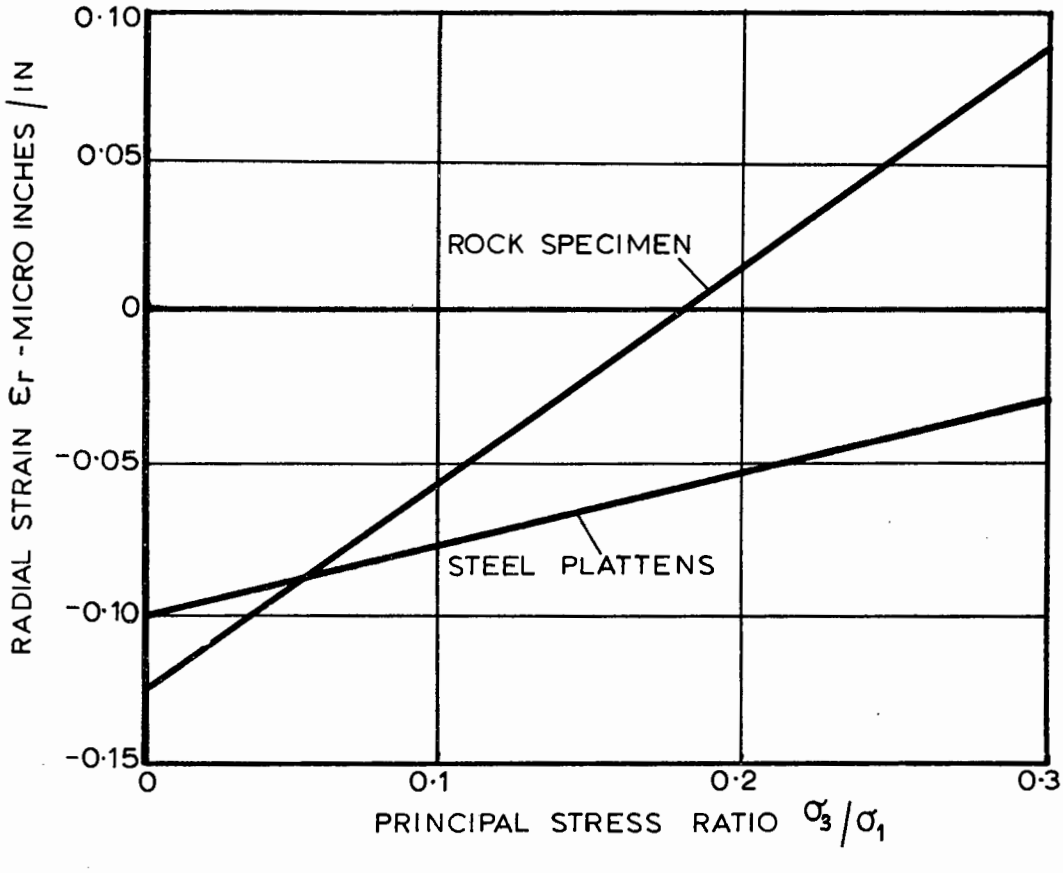

FIGURE 27

Radial strain in a hard rock specimen loaded through steel plattens of the same diameter

fracture is uniformly distributed throughout the body of the specimen.

In addition to these efforts to improve the stress distribution in the specimen, a specimen length to diameter ratio of 2:1 is used. Hence, even in softer materials in which the radial strain may differ considerably from that in the plattens, the stress distribution in the centre portion of the specimen will still be approximately uniform.

13.3 Triaxial compression testing equipment

Details of the apparatus designed by the author for the triaxial compression testing of rock specimens are given in Appendix IV. The principal features of this apparatus are:

(i) The specimen is loaded between steel plattens of the same diameter as the specimen.

(ii) Spherical seats are provided at each end of the specimen to minimise eccentricity of loading.

(iii) The specimen is subjected to axial loading and lateral hydraulic pressure so that the stress state in the specimen can be experessed as $\sigma_1 > \sigma_2 = \sigma_3$.

(iv) The specimen is sleeved with latex rubber to prevent ingress of the hydraulic fluid.

(v) The ratio of lateral to axial stress in the specimen remains constant throughout the loading cycle.

(vi) Strain gauge lead wires can be brought out through the axial loading piston for measurements of the elastic moduli.

Triaxial apparatus is at present available for testing EX (0.85 inch diameter), BX (1.66 inch diameter) and NX (2.13 inch diameter) specimens. The length to diameter ratio of the specimens is always 2:1.

13.4 Tensile testing of rock specimens

In order to obtain a complete fracture diagram for a rock sample it is desirable to measure its uniaxial tensile strength.

Numerous experimental techniques have been used in attempts to obtain reliable values for the tensile strength of brittle materials and some of these techniques are discussed briefly hereunder.

The simplest experimental technique involves bonding a rock specimen between steel end-pieces and subjecting it to direct tension. The extremely unreliable results obtained from this type of test are due to the high stress concentrations which occur in the adhesive layer and to the difficulty of eliminating eccentricity from the loading. In an attempt to overcome these difficulties, the author has experimented with various end fixings and specimen shapes and, while a considerable improvement in the consistency of results has been obtained, the problem of bending in the specimen has proved almost impossible to overcome when mechanical loading is used*.

Indirect tension tests have been fairly extensively used in the study of rock properties. Beam specimens subjected to bending and hollow cylinders subjected to internal pressure[56] have been used, particularly in concrete testing. The so-called "Brazilian" test which involves subjecting a disc specimen to diametral compression[192] is also a convenient and simple method for obtaining an estimate of the tensile strength of rock.

The principal objection to these indirect methods is that the tensile stress from which fracture initiates is confined to a small portion of the test specimen. In the case of the beam and hollow cylinder, the tensile stress occurs on the specimen surface and, depending upon the geometry of the specimen, the stress gradient into the body of the specimen can be relatively steep. In the case of the disc subjected to diametral compression, true tensile fracture is only theoretically possible at the centre of the disc where the principal stress ratio $\sigma_3/\sigma_1 = -0.33$**.

Since the influence of stress gradient upon the fracture of rock is, at this stage, largely unknown, it is felt that, while

---

* It is understood that an American research organisation uses air bearings in an effort to eliminate bending from ceramic tensile specimens.

** COLBACK, P.S.B. Unpublished CSIR internal report on the fracture of a disc subjected to diametral compression.

these indirect methods may be useful for obtaining estimates and for comparative studies, they should not be used in an effort to determine the actual uniaxial tensile strength of rock.

The technique used by the author for the determination of the uniaxial tensile strength of rock specimens is an adaptation of that used by Brace[52] for his rock strength tests. This technique involves subjecting a sleeved "dog-bone" specimen to hydraulic pressure in the apparatus illustrated diagrammatically in Figure 28. The test section of the specimen is subjected to a state of triaxial stress in which the axial stress (σ_3) is tensile and the radial stress ($\sigma_1 = \sigma_2$) is compressive. By varying the ratio of test section to specimen end diameter, various principal stress ratios (σ_3/σ_1) can be induced in the specimen. The principal advantage of this technique is that bending of the specimen is virtually impossible, provided that the specimen is accurately machined. Details of the specimen preparation will be discussed in a later section of this study.

A three-dimensional photoelastic model of the "dog-bone" tensile specimen illustrated in Figure 28 was used to check the stress distribution in the test section and fillets. It was found that, when $d_2 = 2d_1$, no stress concentration could be detected for fillet radii in excess of $4d_1$.

13.4 Specimen size and selection

It is well known that the strength of brittle materials is markedly dependent upon the size of the test specimen. Very little reliable information on this effect is available in literature and the discussion which follows is based upon the work of Protodiakonov[299].

According to Protodiakonov, the relationship between the strength of a rock specimen and the strength of the rock in situ is given by the following relationship:

$$\sigma_s = \frac{\sigma_M \cdot b\,(m - 1)}{d + b} + \sigma_M \quad \ldots\ldots\ldots\ldots \quad (63)$$

where σ_s is the strength of the specimen

σ_M is the strength of the rock mass in situ

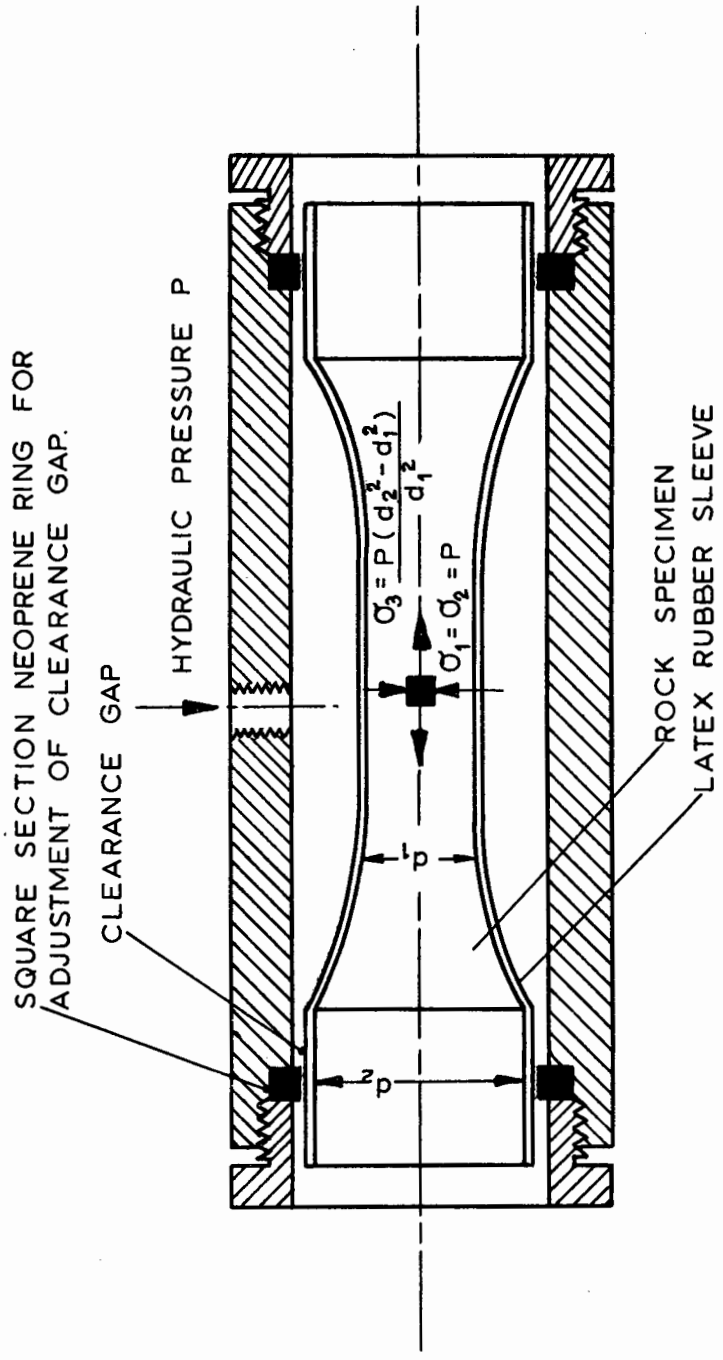

FIGURE 28

Apparatus for the determination of the uniaxial tensile strength of rock specimens

d is the diameter of the specimen
b is a constant which depends upon the spacing between fissures or inherent cracks and
m is a coefficient which indicates how many times the strength of the crack free material exceeds the strength of the rock in situ.

Since the exact definition of the constant b is not clear in Protodiakonov's paper (presented in Russian), the author has presumed that b is, in fact, equal to the average spacing between the discontinuities from which fracture initiates. In the case of hard rock, b is approximately equal to the average grain size[51] while, in the case of coal, b is probably equal to the cleat spacing.

Rewriting equation (63) in dimensionless form:

$$\frac{\sigma_s}{\sigma_M} = \frac{m - 1}{d/b + 1} + 1 \quad \ldots\ldots\ldots\ldots\ldots (64)$$

The solution to this equation, for various values of m and d/b is presented graphically in Figure 29 in which, for the sake of clarity, logarithmic scales have been used. Note that equation (64) is that of a hyperbola.

From the curves plotted in Figure 29, some interesting conclusions can be reached. For a given rock type, for which m and b are constant, the strength of the specimen σ_s approaches the strength of the rock mass σ_M fairly rapidly with increasing specimen size. The specimen size, expressed in multiples of the crack spacing b, required to give a strength value within 10% of that of the rock mass depends upon the magnitude of the coefficient m.

Very few experimental determinations of the size effect in rocks, covering a sufficiently wide range of sizes, have been reported in literature. Consequently, an accurate estimate of m is, at present, difficult to obtain. Protodiakonov gives a method for the determination of σ_M, b and m from strength measurements on three specimen sizes but obviously, in order to obtain accurate

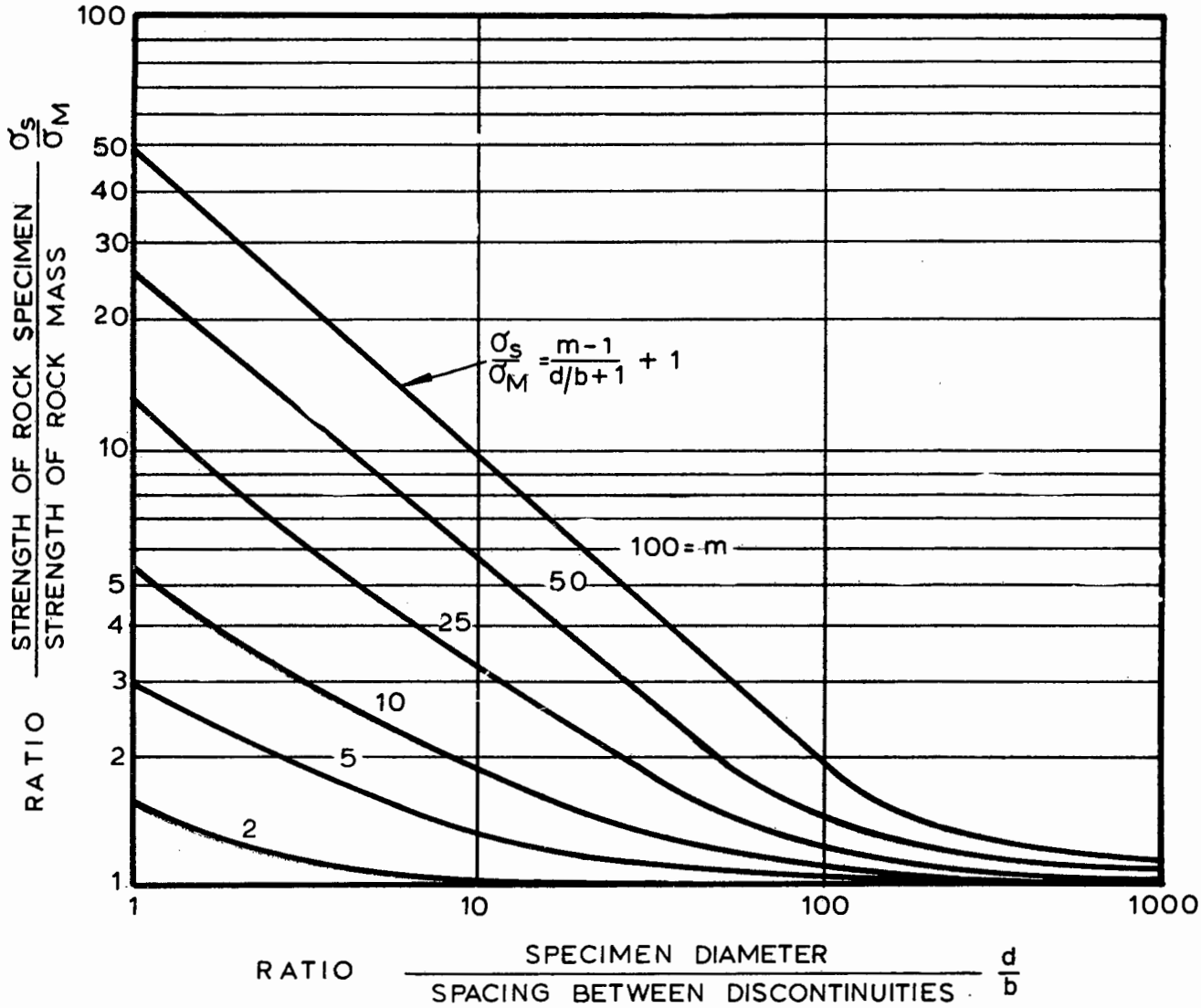

FIGURE 29

Relationship between specimen size and strength according to Protodiakonov

estimates of these constants, the specimen sizes should cover as wide a range as possible.

From the limited number of experimental results available[136, 299] it is possible to arrive at some very crude estimates for the value of m.

From these results, it is evident that the value of m depends upon the stress state to which the specimen is subjected. The frictional effects due to crack closure in compression reduce the difference in strength between small and large specimens as compared with the differences obtained under tensile stress conditions. Under tension, the cracks open and give rise to very large strength reductions.

The following estimates of m have been made from available data:

Coal subjected to compression	$5 < m < 10$
Coal subjected to tension	$10 < m < 50$
Rock subjected to compression	$2 < m < 5$
Rock subjected to tension	$5 < m < 10$

While these estimates must be treated with extreme caution, they do enable one to arrive at an order of magnitude for the specimen size which is acceptable.

Hence, for coal subjected to compression, the specimen size should lie between 10 and 100 times the average cleat spacing. Since the cleat spacing may be of the order of 2 inches, the specimen size required to provide a reasonable estimate of the in situ strength of coal should lie between 20 and 200 inches.

Because of the large value of m for coal subjected to tension, it is probably impractical to attempt to determine a value of the in situ tensile strength of coal. In the author's opinion, no serious error would be involved if the tensile strength of coal in situ is assumed to be zero.

In the case of rock subjected to tension or compression, assuming an average value of 5 for m, the specimen size should be approximately 20 times the grain size in order that the strength of the specimen should be within 10% of the in situ strength. Since, for most of the hard rocks with which this study is

primarily concerned, the grain size can be measured in fractions of an inch, specimens whose dimensions are measured in inches are acceptable.

The preceding discussion has been based on mean strength values for any given specimen size. Obviously, in a material such as rock, there is an appreciable scatter around the mean and it is necessary to consider the distribution of strength results within any given sample.

As in the case of the size effect, very little experimental evidence with permits accurate evaluation of the strength distribution is available.

Protodiakonov[299] has analysed the results of compressive tests on Deep Dufferin coal obtained by Evans and Pomeroy[118] and has found that the distribution of strength results is adequately defined by a normal Gaussian distribution. Wiid, who has carried out tests on a South African sandstone*, has found that the strength results within a given sample have a slightly skew distribution; there being a predominance of weaker results.

The author feels that a skew distribution is a more realistic reflection of in situ conditions since, in the laboratory, those specimens with very low strength do not survive the specimen preparation process and are therefore excluded from the sample. Consequently, when normal specimen sampling, based on the survival and appearance of specimens, is practised, it must be realised that the mean in situ strength is probably lower than the mean strength obtained in the laboratory.

If it is assumed that the cracks from which fracture initiates are randomly distributed throughout the specimen, it can be anticipated that the variation in strength will decrease with increasing specimen size.

13.5 Specimen preparation

Reliable results can only be obtained from laboratory strength tests on rock specimens if sufficient care is exercised in the preparation of these specimens. Experience has shown that poor

---

* WIID, B.L. Unpublished CSIR internal report on the influence of moisture on the strength of rock.

specimen preparation can cause a large amount of scatter in strength results.

Since the specimens used by the CSIR are all cut from diamond drilled core, the first important step in specimen preparation is the drilling process. It has been found that very light drilling machines, driven by approximately 3 horsepower motors and hand fed, are not suitable for the drilling of core from which test specimens are to be cut. The structure of these light machines is generally to flimsy to prevent vibration of the core barrel during drilling and the core obtained with these machines is neither straight nor of a uniform diameter. Such core requires grinding of the cylindrical surfaces.

The drilling machine used by the Rock Mechanics Division of the National Mechanical Research Institute is a heavy duty hydraulic feed machine, illustrated in Figure 30. In this machine, the drill chuck is driven by a ten horsepower motor through a five speed gear-box. The feed rate and thrust are independently adjustable and can be maintained at a constant level. Hence, for a given rock type the optimum drilling speed, feed rate and thrust can be determined experimentally and maintained throughout the drilling programme.

The frame of the machine, which is designed for drilling deep holes for prospecting, is very rigid and the core recovered with this machine is extremely straight and parallel. This core requires no further grinding of its cylindrical surfaces.

With the exception of coal and rocks which disintegrate when wet, all drilling is carried out wet. Water under pressure is fed into the core barrel, through a water swivel, and provides cooling of the cutting edge as well as removal of the pulverised material.

In the case of rocks which cannot be drilled wet, compressed air is fed through the barrel and provides cooling and dust removal. A vacuum system attached to a collar which surrounds the core barrel is used to collect the dust forced out by the compressed air.

Compression test specimens are cut from the core by means of

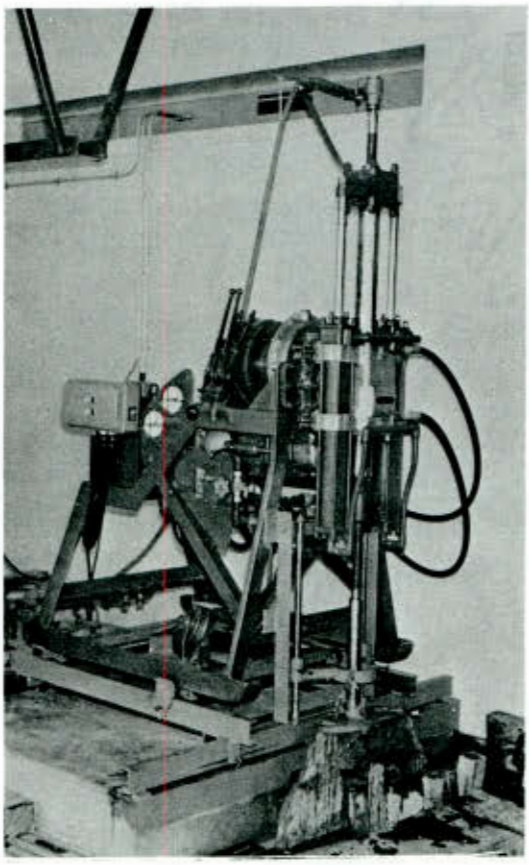

FIGURE 30

Hydraulic feed drilling machine used
for specimen preparation

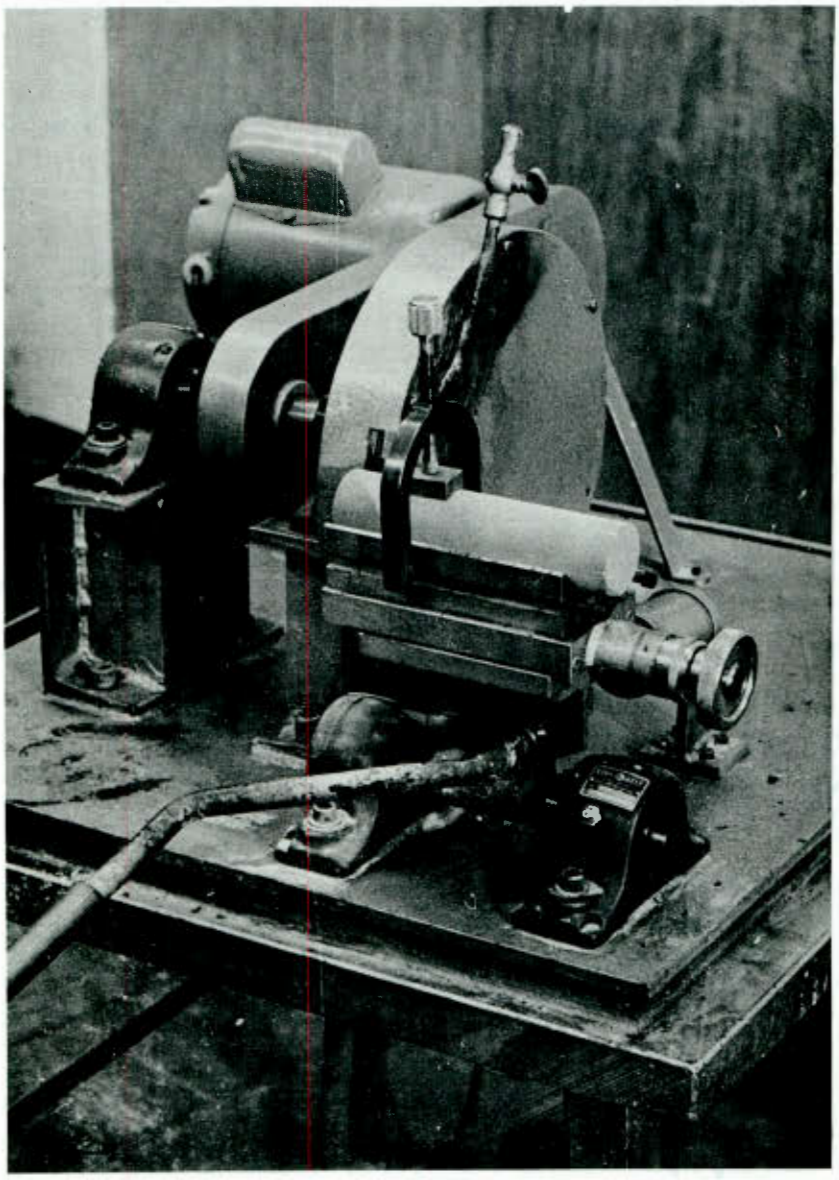

FIGURE 31

Grinding machine used for specimen end preparation

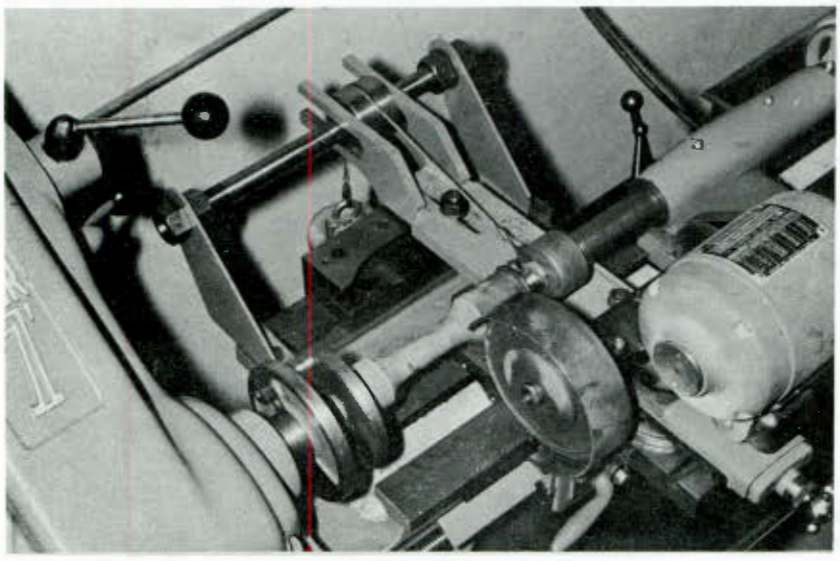

FIGURE 32

Apparatus for preparation of tensile specimens

a diamond saw and the ends are then ground in the machine illustrated in Figure 31. In this machine, the core is held in an accurately aligned Vee block which is moved across the face of a diamond impregnated cup wheel.

Tension test specimens are ground from core specimens in the lathe illustrated in Figure 32*. A diamond impregnated wheel, driven by a tool-post grinder is used to grind the specimen profile. This profile is generated by means of a template along which the tool-post is driven by the lead-screw.

13.6 Conclusions on the strength testing of rock specimens

The Mohr fracture envelope for a typical South African quartzite is illustrated in Figure 33. The results included in this diagram were obtained with the apparatus and using the techniques discussed above. These results can be regarded as typical of the results which have been obtained in the large number of tests carried out by the Rock Mechanics Division during the past three years.

The scatter of the results plotted in Figure 33 is encouragingly small but it must be remembered that these specimens have survived the preparation process and cannot be regarded as a random sample. In addition, these specimens were cut from standard EX core (0.85 inch diameter) and their strength must be considered in relation to the size-strength relationship given in Figure 29.

Ideally, all strength testing is aimed at establishing the strength of rock in situ in order to provide a rational basis for the design of mine excavations. With this aim in view, it is interesting to consider to what extent the results presented in Figure 33 can be accepted as representative of the strength of the quartzite in situ.

On the basis of the discussion presented earlier in this section and using a fair amount of imagination, the hypothetical fracture diagrams presented in Figures 34 and 35 have been con-

---

* The equipment for grinding the ends of compression specimens and the profile of the tension specimens was designed by Mr J.B. Kennard, Principal Technician in the Rock Mechanics Division of the National Mechanical Engineering Research Institute.

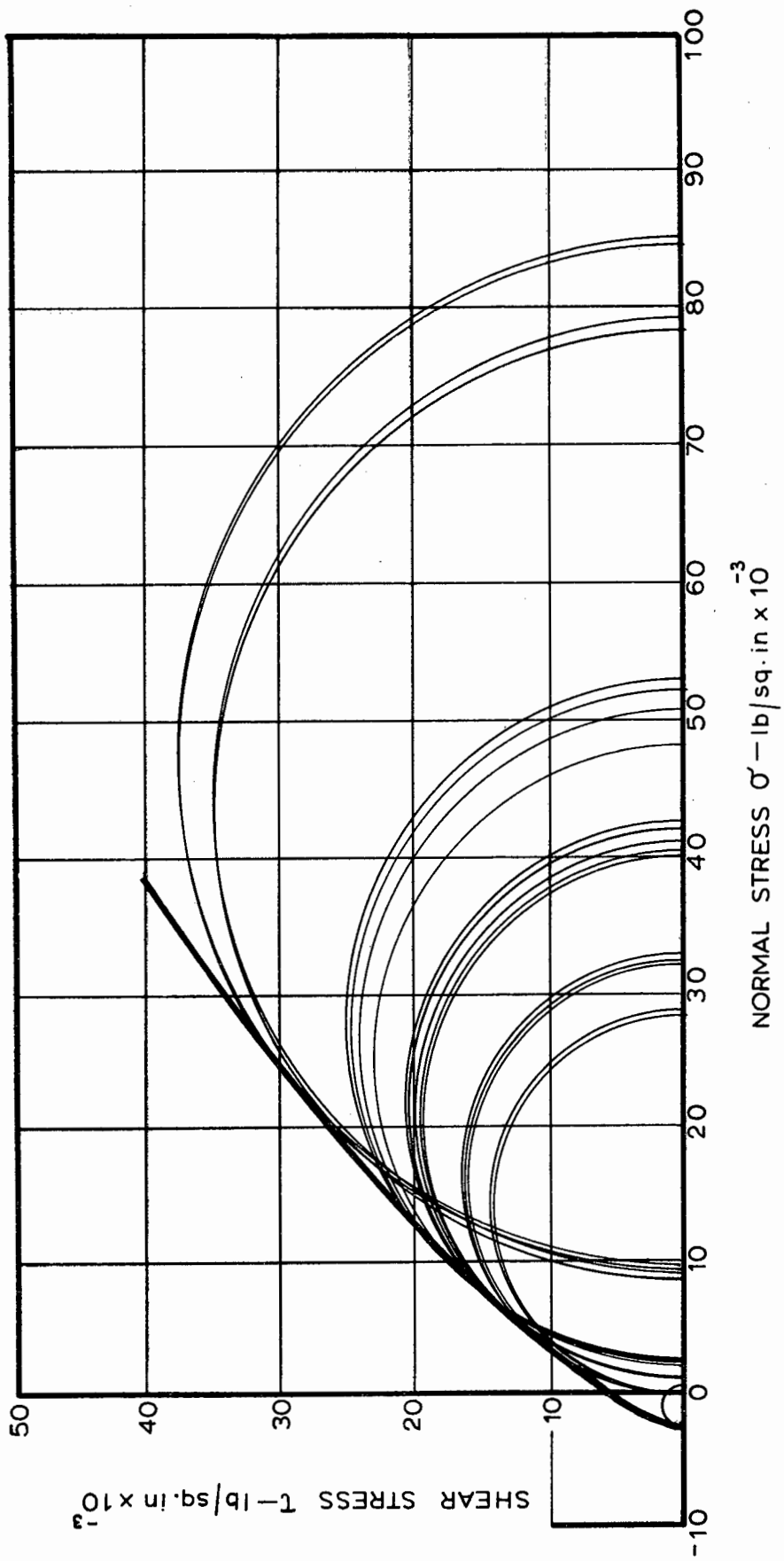

FIGURE 33

Mohr fracture diagram for typical Witwatersrand quartzite

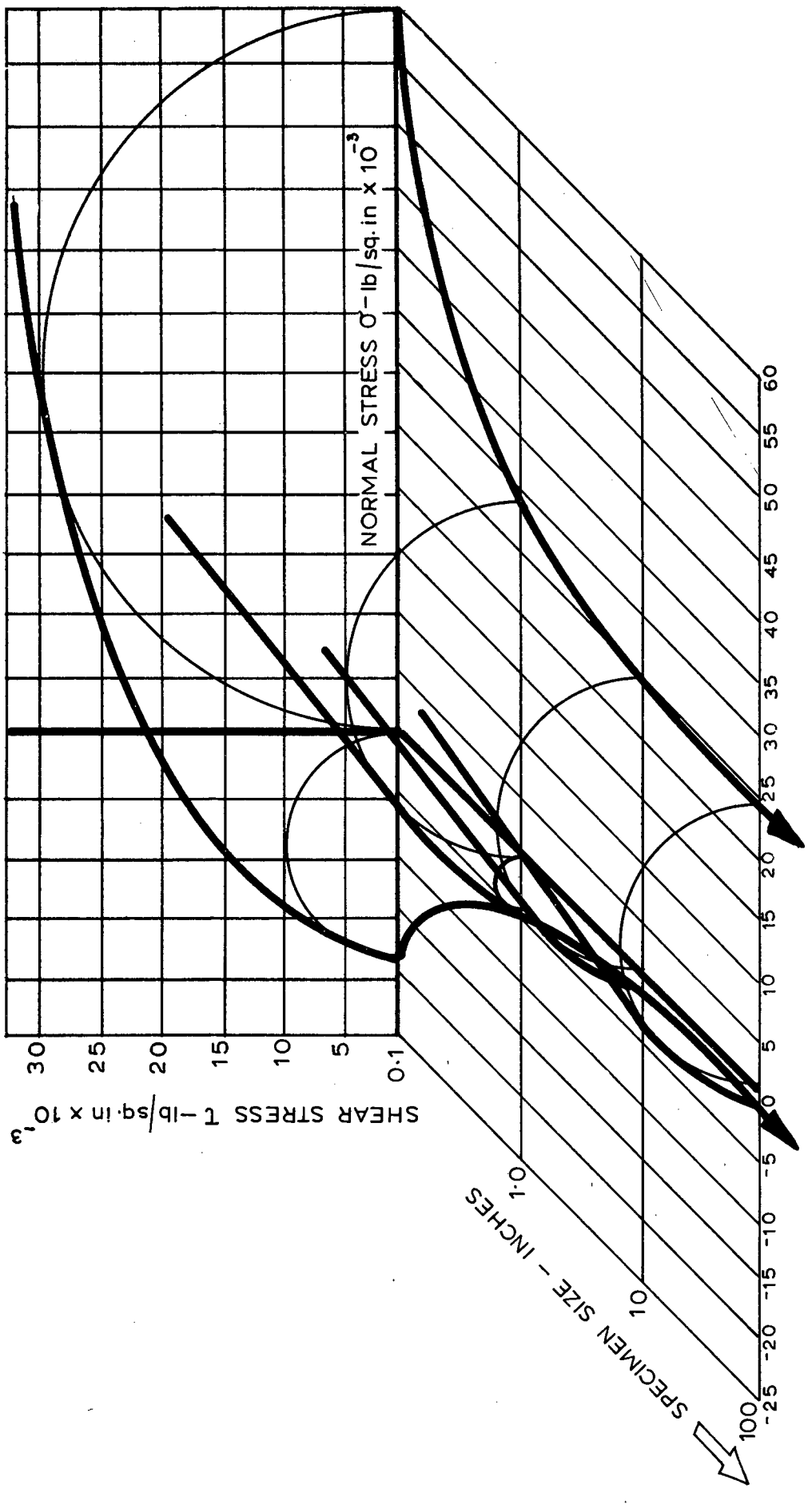

FIGURE 34

Probable influence of specimen size upon the Mohr fracture diagram for quartzite

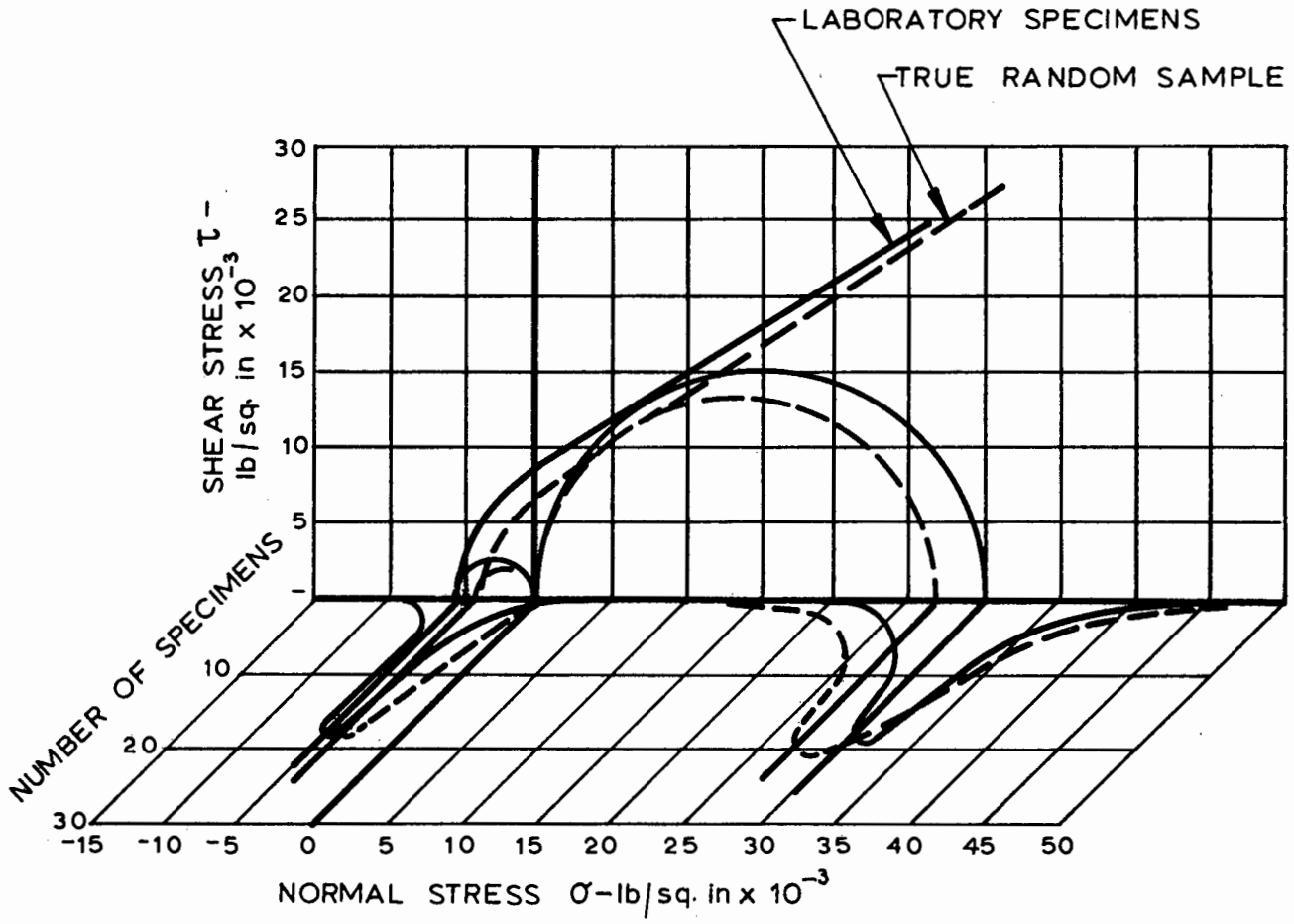

FIGURE 35

Hypothetical distribution of strength values
for a typical hard rock sample

structed. These diagrams purport to show how the properties of rock obtained from tests on a normal laboratory specimen are related to the overall fracture behaviour of the material.

Figure 34 illustrates the influence of specimen size upon the Mohr fracture diagram of a hard rock such as quartzite. The values presented in this figure have been estimated from Protodiakonov's relationship given in Figure 29. It has been assumed that tests on a 1 inch diameter specimen given a mean uniaxial tensile strength of approximately 4 000 lb/sq. in and a mean uniaxial compressive strength of approximately 30 000 lb/sq. in.

From the earlier discussion, it can be anticipated that the uniaxial tensile strength is more size dependent than the uniaxial compressive strength. Hence the uniaxial tensile strength rises sharply as the specimen size decreases. Protodiakonov[299] has assumed that, if it were possible to test tensile specimens which were so small that no cracks or flaws could be contained within the specimen, the uniaxial tensile and compressive strengths would be equal. Under these conditions failure would occur as a result of plastic flow within the crystal. Since there is no experimental evidence to support or contradict this postulate, it must remain unchallenged but it can be stated that failure in this realm of specimen size is of little practical interest to the engineer.

Protodiakonov's postulate does, however, have one important bearing upon the present problem in that it implies that the slope of the Mohr envelope must change with specimen size. Obviously this must be true in the region where one of the principal stresses is tensile. However, in the author's opinion, once the specimen is large enough to contain a number of randomly oriented grain boundary cracks, the slope of the Mohr envelope, in the compressive stress region of the diagram, will remain constant.

In Figure 35, the distribution of strength values for a given specimen size is illustrated. It is assumed that approximately 150 results are available for uniaxial tensile and compressive tests and that the scatter is due only to the distribution of inherent flaws in the specimens, i.e. the test conditions are

assumed to be perfect.

The solid lines in Figure 35 indicate the results of tests on normal laboratory specimens while the dotted lines illustrate the results which would probably be obtained from a true random sample of specimens. The difference is due to the fact that weaker specimens do not survive the preparation process and are therefore excluded from the laboratory sample.

While the reader will readily appreciate the present lack of adequate information for the complete evaluation of the fracture properties of a particular rock, it will also be obvious that laboratory testing procedures afford a realistic first approximation of these properties. Until more data becomes available, particularly from reliable large scale tests, small scale tests in the laboratory must remain the primary source of practical rock fracture data.

In the case of hard rock, this laboratory data is considered sufficiently accurate to permit its use in the design of mine excavations. However, in the case of materials such as coal, laboratory testing of small specimens can only be used with confidence if a few reliable large scale measurements are available and can be used as a basis for extrapolating the laboratory results.

14. INFLUENCE OF ADDITIONAL FACTORS UPON ROCK FRACTURE

In the preceding sections of this study it has been assumed that the element of rock under consideration contains a large number of randomly oriented cracks. These cracks are assumed to be initially closed and the factors which influence their behaviour, namely the cohesive strength and the coefficient of internal friction, are assumed to be constants.

Before going on to discuss the practical application of the original and modified Griffith's theories, it is necessary to consider whether the above assumptions are justified and to what extent any deviation from the assumed behaviour can be explained theoretically.

The influence of the following additional factors upon rock fracture will be considered in this section:

1. Anisotropy
2. Cracks which are initially open
3. Pore pressure
4. Environment and
5. Rate of loading.

14.1 The influence of anisotropy upon rock fracture

The successful application of the original and modified Griffith's criterion to the prediction of rock fracture depends upon the fact that most rocks contain a large number of randomly oriented cracks from which fracture can initiate. Strength tests on materials such as quartzite have not revealed any significant anisotropy.

On the other hand, materials such as slate exhibit a very marked anisotropy and the assumption that the inherent cracks are randomly oriented is not valid.

In a recent paper[193], the author assumed that slate contains two distinct crack systems*:

---

* During a visit to America, just before the presentation of this paper, the author found that Professor W.F. Brace and Dr J.B. Walsh, working at the Massachusetts Institute of Technology, had adopted an identical approach to that used by the author. Their paper[359] was written and presented almost simultaneously with the author's - neither group being aware of the other's efforts.

(a) Large cracks which are preferentially oriented along bedding planes and

(b) A randomly oriented matrix of grain boundary cracks which are probably several times smaller than the bedding plane cracks.

The bedding plane cracks are referred to as primary cracks and the grain boundary cracks are termed secondary cracks.

In deciding upon the stress required to initiate fracture in a particular specimen of slate, it is necessary to consider the orientation of the primary cracks and to determine whether the tensile stresses induced at the tips of these primary cracks are higher than those which occur at the tips of the most favourably oriented secondary cracks.

14.1.1 Fracture initiation from open primary cracks

Consider an isolated open primary crack oriented at an angle ψ to the direction of the major principal applied stress σ_1. Assuming that fracture initiates according to the original Griffith theory, the stress conditions for fracture initiation can be deduced from equations (18 b) and (23):

$$2\sigma_{tp} = \frac{1}{2}\sigma_1\{(1+k) - (1-k)\cos 2\psi\} - \sigma_1\sqrt{\frac{1}{2}\{(1+k^2) - (1-k^2)\cos 2\psi\}} \quad \ldots\ldots\ldots (65)$$

where σ_{tp} is the lowest uniaxial tensile strength of a specimen containing an open primary crack, i.e. the tensile strength measured on a specimen containing a crack oriented at $\psi = 0$.

Since the uniaxial tensile strength is difficult to determine experimentally, equation (65) can be written in terms of the lowest uniaxial compressive strength σ_{cp} which is determined on a specimen containing a primary crack inclined at 30° to the direction of σ_1 (from equation (19)).

According to the original Griffith's theory, the uniaxial tensile and compressive strengths are related by the following equation (from equation (41)): eqn 29.

$$\sigma_{cp} = -8\sigma_{tp} \quad \ldots\ldots\ldots\ldots\ldots (66)$$

Substituting into equation (65):

$$\frac{\sigma_1}{\sigma_{cp}} = \frac{1}{\sqrt{8\left\{(1+k^2)-(1-k^2)\cos 2\psi\right\}} - 2\left\{(1+k)-(1-k)\cos 2\psi\right\}} \quad \ldots\ldots (67)$$

The solution to equation (67), for various values of k and ψ, is presented graphically in Figure 36.

14.1.2 Fracture initiation from initially closed primary cracks

If the primary cracks are initially closed and if fracture initiates according to the modified Griffith's theory, the conditions for fracture initiation can be deduced from equations (23) and (31):

$$2\sigma_{tp} = -\frac{1}{2}\sigma_1\left\{(1-k)\sin 2\psi - \mu\left[(1+k) - (1-k)\cos 2\psi\right]\right\} \quad \ldots\ldots (68)$$

Expressing equation (68) in terms of the lowest uniaxial compressive strength, determined on a specimen inclined at $\arctan 1/\mu$ to the direction of the major principal applied stress σ_1 (from equation (42)):

$$\frac{\sigma_1}{\sigma_{cp}} = \frac{\sqrt{1+\mu^2} - \mu}{(1-k)\sin 2\psi - \mu\left[(1+k) - (1-k)\cos 2\psi\right]} \quad \ldots\ldots (69)$$

Note that equations (68) and (69) are only applicable when the normal stress across the crack (σ_{xx}) is compressive. The limits of validity and the transition between the original and modified Griffith theories have been fully discussed in section 8 of part I of this study and only the most important aspects of these limits need be considered here.

Since it is considered likely that the coefficient of

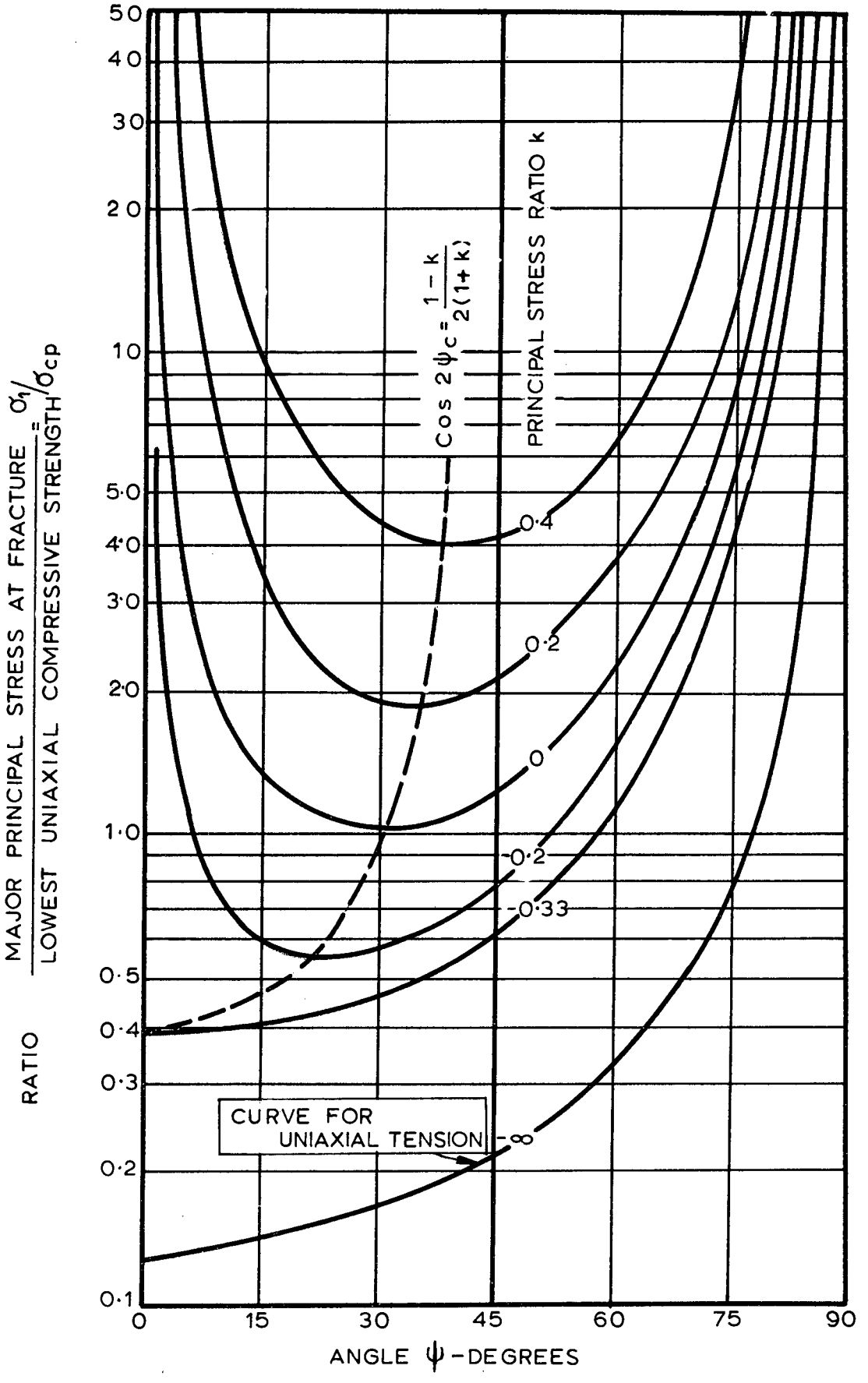

FIGURE 36

Fracture initiation from a single open Griffith crack inclined at an angle ψ to the major principal stress direction

friction on closed primary cracks would be less than unity, the most important limit of validity is that defined by equation (38) of section 8.3

$$k = \frac{-1}{2\sqrt{1 + \mu^2} + 2\mu + 1} \quad \ldots\ldots\ldots\ldots (38)$$

This equation defines the value of k at which the transition from the original to the modified Griffith's theory occurs in a material in which $\mu < 1.00$.

For values of k which are larger than that defined by equation (38), equations (68) and (69) are applicable to the prediction of fracture initiation.

For values of k smaller than that defined by equation (38), the original Griffith's theory must be used to predict fracture initiation.

Equation (65) defines the stress conditions for fracture initiation, according to the original Griffith's theory, in terms of the uniaxial tensile strength σ_{tp}. However, equation (67), which predicts fracture initiation from an open crack in terms of the lowest uniaxial compressive strength σ_{cp}, is not valid for cracks which are initially closed and which open when $\sigma_{xx} < 0$.

The relationship between the lowest uniaxial compressive and tensile strengths for a rock containing initially closed cracks is defined by equation (42):

$$\sigma_{cp} = \frac{-4\sigma_{tp}}{\sqrt{1 + \mu^2} - \mu} \quad \ldots\ldots\ldots\ldots\ldots (42)$$

Substituting this relationship into equation (65):

$$\frac{\sigma_1}{\sigma_{cp}} = \frac{\sqrt{1 + \mu^2} - \mu}{\sqrt{2\left[(1+k^2)-(1-k^2)\cos 2\psi\right]} - \left[(1+k)-(1-k)\cos 2\psi\right]} \quad \ldots (70)$$

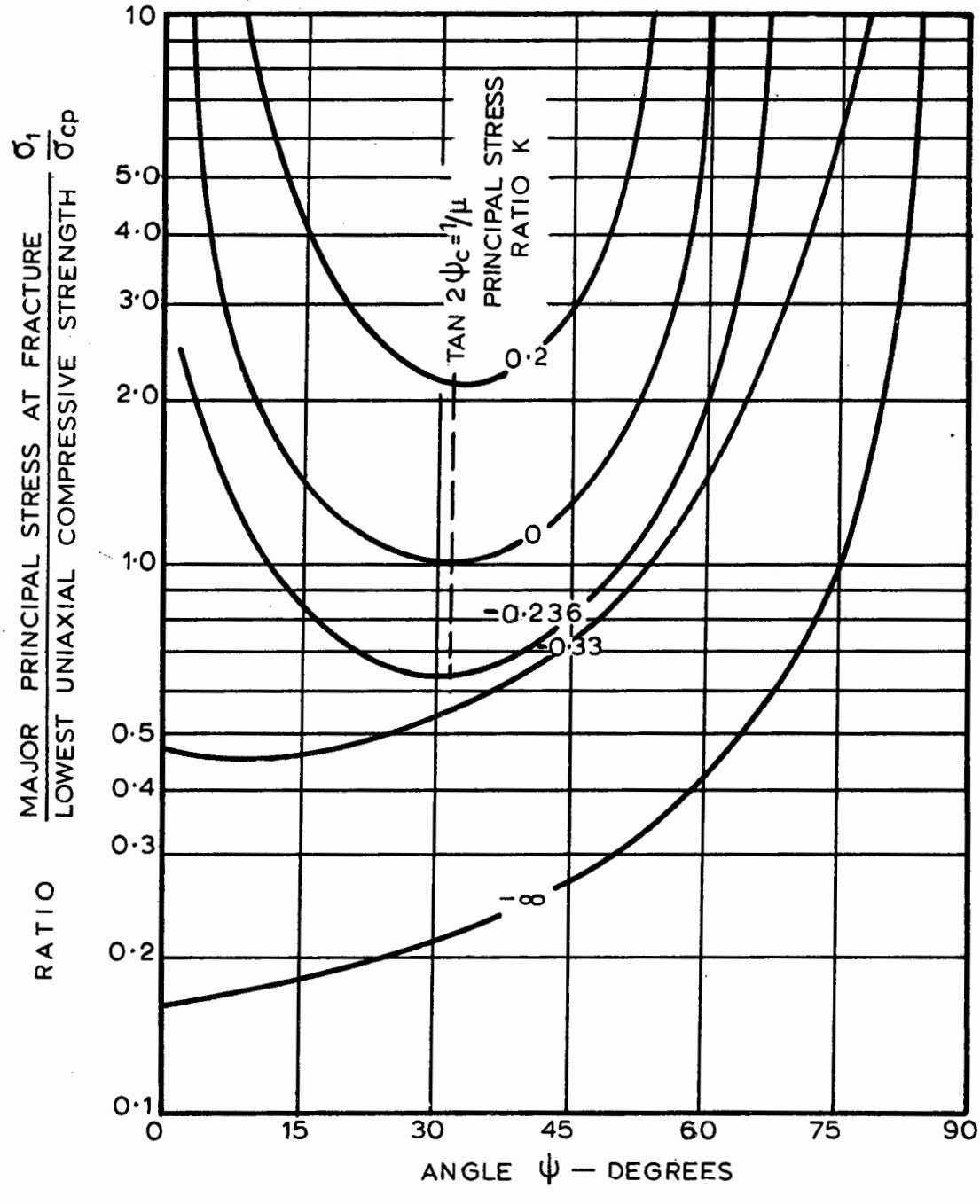

FIGURE 37

Fracture initiation from an initially closed Griffith's crack with a coefficient of friction $\mu = 0.5$ and inclined at an angle ψ to the direction of the major principal stress σ_1

Figure 37 illustrates the relationship between the stress required to initiate fracture and the inclination ψ of an initially closed primary crack which has a coefficient of internal friction $\mu = 0.5$. In this figure, the curves for $k < -0.236$, the limit of validity for $\mu = 0.5$ from equation (38), have been calculated from equation (69) while, for $k < -0.236$, the curves have been calculated from equation (70).

14.1.3 Fracture initiation from secondary cracks

In this analysis, it has been assumed that the secondary crack system in slate consists of a randomly oriented matrix of grain boundary cracks. Fracture initiation from these cracks can be predicted by either the original or the modified Griffith's theory, depending upon whether the cracks are open or closed, and these crack systems will not exhibit any directional effects, i.e. fracture is assumed to initiate from critically oriented cracks within the random matrix.

Fracture initiation from secondary cracks will occur when the tensile stresses at the tips of the critically oriented cracks exceed the tensile stresses at the tips of the longer preferentially oriented primary cracks. The stress level at which this transition occurs depends upon the relative lengths of the secondary and primary cracks and must be determined experimentally.

From equations (67) and (69), it can be deduced that compressive fracture initiation cannot occur from primary cracks which are inclined at $\psi = 0^{\circ}$ or $\psi = 90^{\circ}$. Hence the stresses required to initiate fracture from the secondary cracks can be determined from compressive tests on specimens parallel to or normal to the bedding planes.

14.1.4 Experimental study of the fracture of slate

The results of triaxial compression and tension tests carried out on EX specimens of slate, obtained from a quarry near Pretoria, are listed in Table III.

In order to determine whether the primary and secondary

TABLE III

FRACTURE DATA FOR A SOUTH AFRICAN SLATE

UNIAXIAL TENSILE TESTS

(a) Tensile strength perpendicular to bedding planes ($\psi = 0^{\circ}$), σ_{tp} = 660 and 570 lb/sq. in average 615 lb/sq. in

(b) Tensile strength parallel to bedding planes ($\psi = 90^{\circ}$) σ_{ts} = 2780 and 3000 lb/sq. in average 2880 lb/sq. in.

TRIAXIAL COMPRESSION TESTS

$\sigma_3/\sigma_1 = k$	k = 0 (uniaxial)	k = 0.113	k = 0.171
ψ	σ_1 lb/sq. in	σ_1 lb/sq. in	σ_1 lb/sq. in
0	17 600 21 600	39 200 36 000	55 700 49 300
15	6 900 8 700	18 300 30 000	34 200 39 000
30	4 500 4 150	7 300 -	8 730 7 840
45	5 540 6 560	13 900 11 000	15 000 16 300
60	11 850 11 600	24 600 19 400	29 600 32 400
75	16 000 16 600	31 200 31 900	41 400 42 900
90	15 600 16 700	30 600 -	41 700 39 300

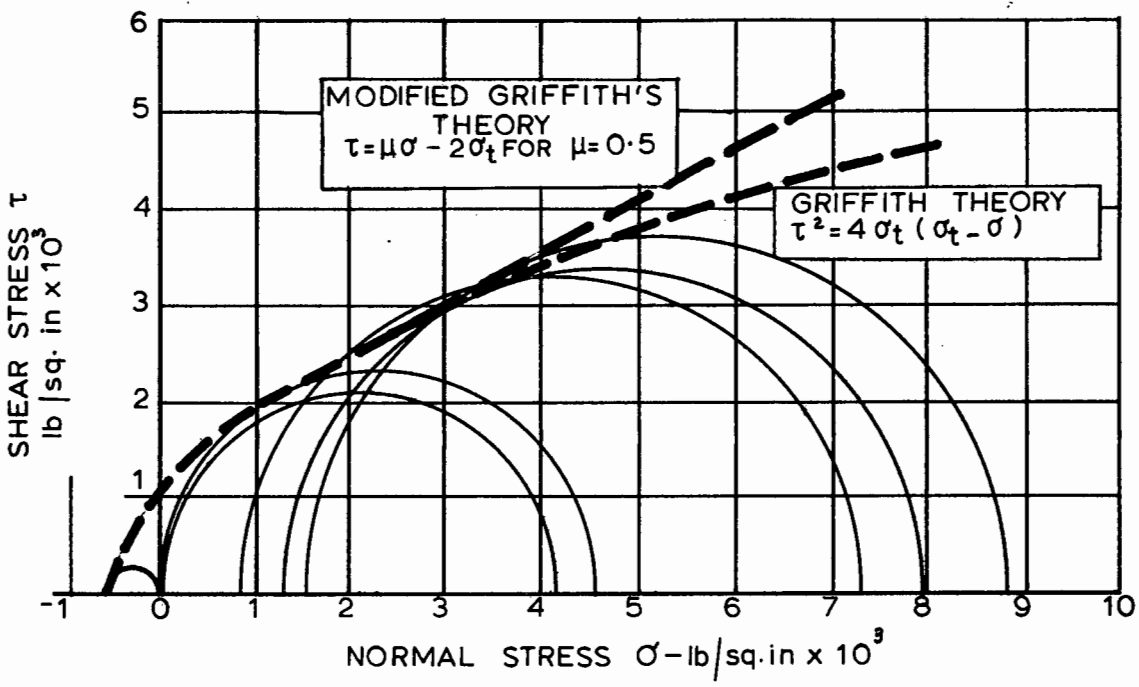

FIGURE 38

Mohr fracture diagram for primary crack system of slate

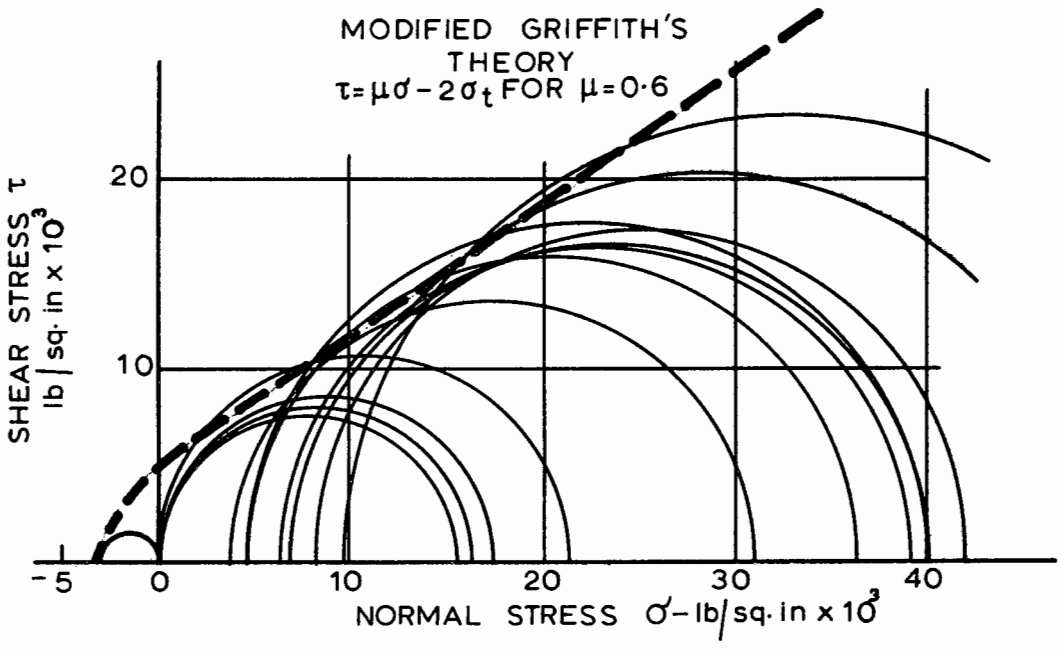

FIGURE 39

Mohr fracture diagram for secondary crack system of slate

cracks of this sample of slate are initially open or closed, some of the results listed in Table III are plotted as Mohr circles in Figures 38 and 39.

Data for the primary crack system has been obtained from the lowest strength values included in Table III, i.e. compressive strengths for $\psi = 30^{\circ}$ and the tensile strength for $\psi = 0^{\circ}$. Data for the secondary crack system is obtained from the highest strength values listed in Table III, i.e. compressive strengths for $\psi = 0^{\circ}$ and 90° and tensile strength for $\psi = 90^{\circ}$.

From Figure 38, it is difficult to decide whether fracture initiation from the primary cracks is more accurately predicted by the original Griffith's theory or by the modified Griffith's theory for $\mu = 0.5$. From subsequent analysis, presented in Figure 40, it appears that the modified Griffith's theory is the correct choice.

From Figure 39 it appears that the secondary crack behaviour can be adequately predicted by the modified Griffith's theory, using $\mu = 0.6$.

In Figure 40, the strength values listed in Table III are compared with the behaviour predicted by the modified Griffith's theory, assuming that both crack systems are initially closed and using $\mu = 0.5$ for the primary cracks and $\mu = 0.6$ for the secondary cracks. For the sake of clarity, the results for $k = 0.113$ have been omitted from Figure 40.

14.1.5 Discussion on the effects of anisotropy

From the agreement between the measured and predicted influence of bedding plane orientation, illustrated in Figure 40, it can be concluded that the effects of anisotropy can be predicted on the basis of the Griffith theory*.

The preceding discussion is based upon the assumption

---

* Walsh and Brace[359] used Donath's results[100] to check their theoretical predictions and found similar agreement to that illustrated in Figure 40.

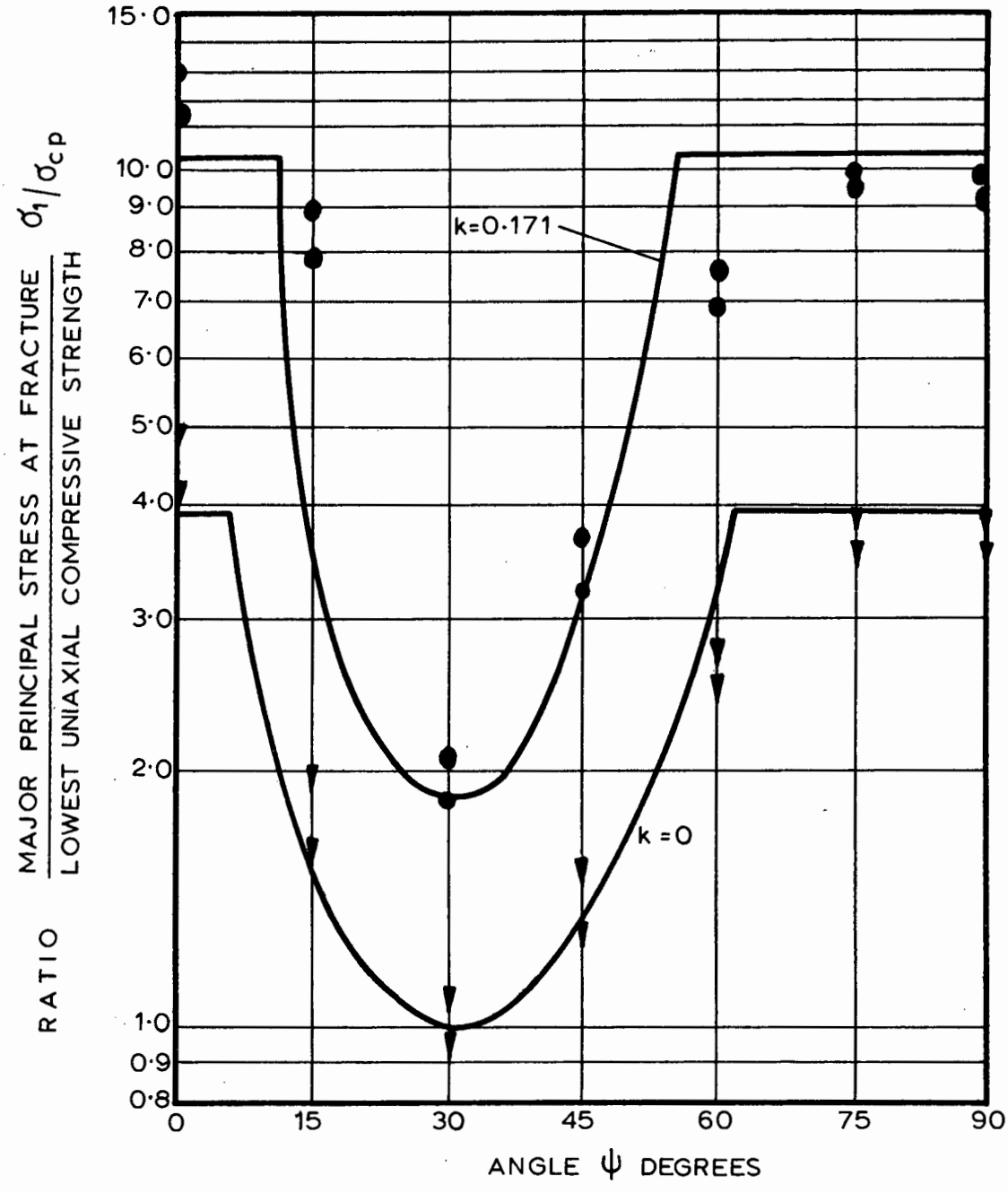

FIGURE 40

Comparison between measured and predicted influence of bedding plane orientation upon the strength of slate

that only two distinct crack systems are present in an anisotropic material such as slate. Obviously, these concepts could be extended to cover the case of two or more major crack systems such as those found in coal which contains cleats as well as bedding planes.

An important conclusion which can be drawn from this discussion is that it is not correct to conclude that a rock is macroscopically isotropic if its compressive strength parallel to the bedding planes is the same as that normal to the bedding planes. This conclusion can only be reached if no strength reduction is detected on specimens in which the bedding planes are inclined at approximately 30° to the major principal compressive stress direction or if the tensile strength is the same for specimens parallel to and normal to the bedding planes.

14.2 The influence of initially open cracks upon rock fracture

In part I of this study it was assumed that cracks in rock are initially closed and the frictional effects on the crack surfaces occur as soon as the normal stress σ_{xx} across the crack becomes compressive.

While, in the author's opinion, this assumption is probably justified for most hard rocks, it is also possible that some rocks contain cracks which are initially open and which close at a critical value of the normal stress $\sigma_{xx} = \sigma_{cr}$.

McClintock and Walsh[249] considered this as the most general case and the modified theory reviewed in part I of this study is a special case obtained from their equations when $\sigma_{cr} = 0$.

When crack closure occurs at $\sigma_{xx} = \sigma_{cr}$, the net normal compressive stress σ_n which is transmitted across the closed crack illustrated in Figure 2 is given by

$$\sigma_n = \sigma_{xx} - \sigma_{cr}.$$

The resulting frictional shear resistance τ_n is then

$$\tau_n = \mu (\sigma_{xx} - \sigma_{cr}).$$

Substituting this value into equation (29)

$$\sigma_\eta = \frac{2\eta (\sigma_{xz} - \mu (\sigma_{xx} - \sigma_{cr}))}{\xi_o^2 + \eta^2} \quad \ldots\ldots\ldots\ldots (71)$$

Following the same procedure as that used in the derivation of the modified Griffith's fracture criterion for initially closed cracks (section 7 of part I), the critical crack orientation for cracks which are initially open and which close when $\sigma_{xx} = \sigma_{cr}$ is found to be

$$\text{Tan } 2\psi_c = {}^1/_\mu \quad \ldots\ldots\ldots\ldots\ldots\ldots (32)$$

This equation is identical to that for the initially closed cracks.

The fracture initiation criterion for initially open cracks which close when $\sigma_{xx} = \sigma_{cr}$ is given by

$$\sigma_1 = \frac{-4\sigma_t}{\sqrt{1+\mu^2}\,(1-k) - \mu(1+k) + \mu\,\sigma_{cr}} \quad \ldots\ldots\ldots\ldots (72)$$

Obviously, this equation is only valid for $\sigma_{xx} > \sigma_{cr}$ and, for $\sigma_{xx} < \sigma_{cr}$, the original Griffith's criterion, equation (24 b) must be used to predict fracture initiation.

The transition from the original to the modified fracture criterion for a material containing initially open cracks can be determined by following the procedure set out in section 8 of part I. For the purpose of this discussion it is adequate to consider this transition in terms of the Mohr fracture envelope.

The equation to the Mohr envelope, corresponding to the

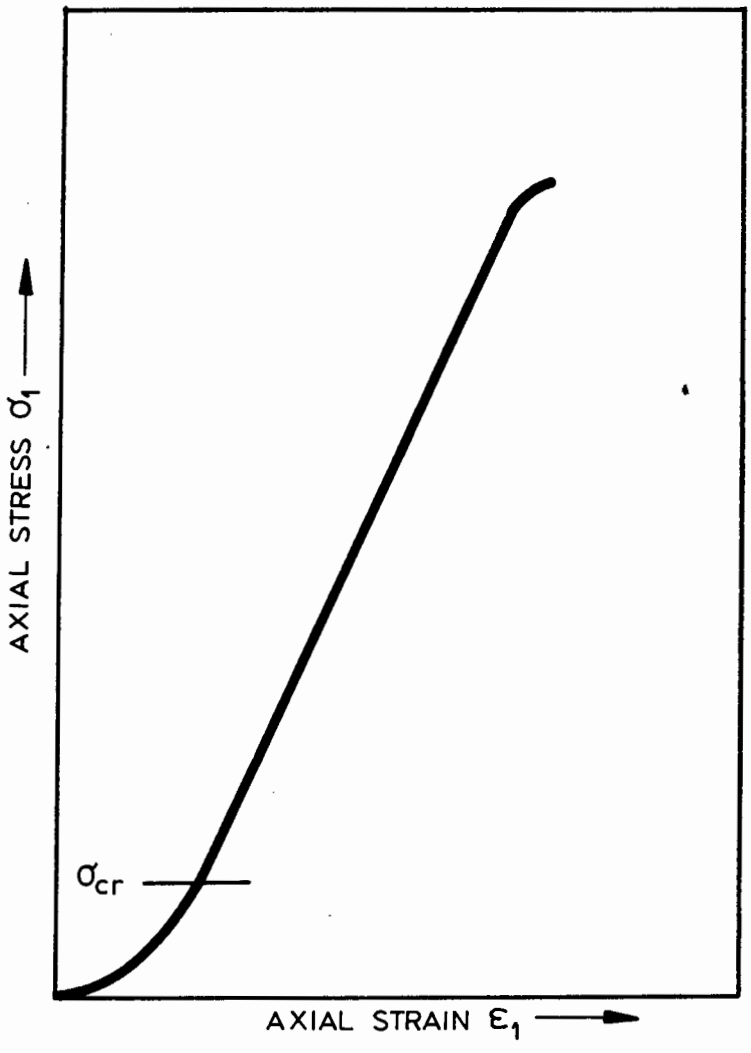

FIGURE 41

Hypothetical axial stress-strain relationship for a rock containing initially open cracks

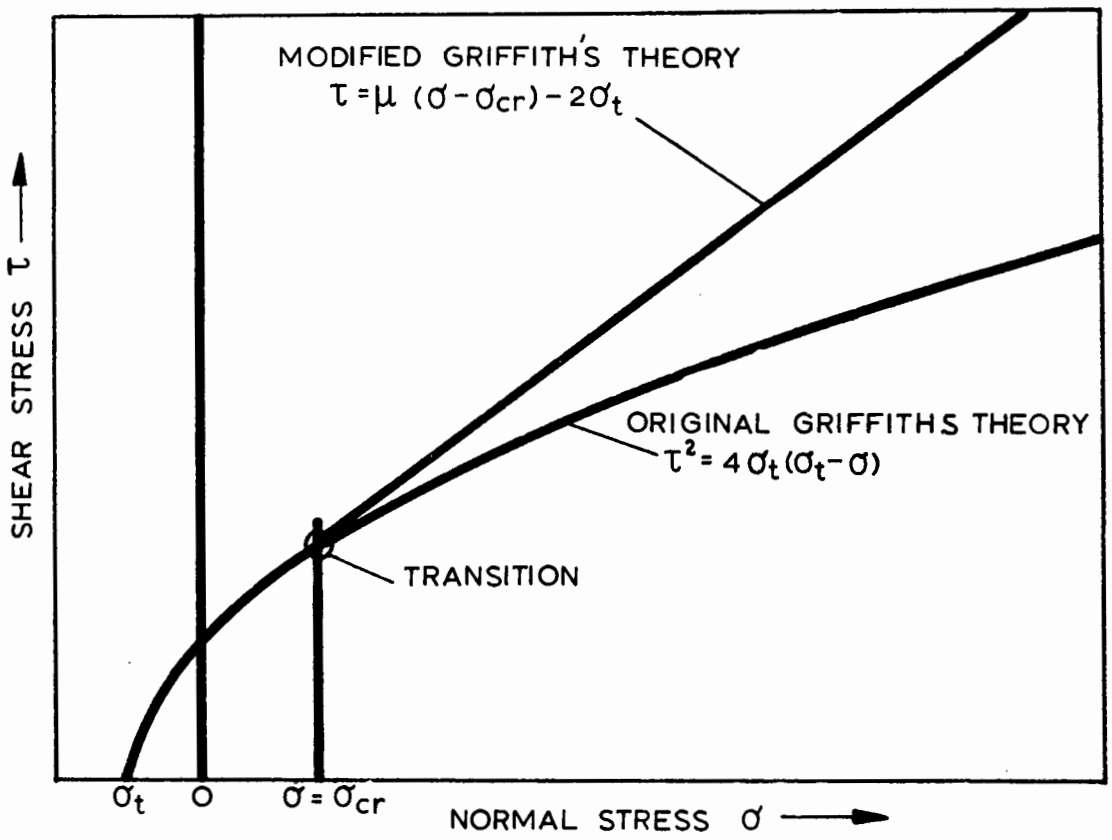

FIGURE 42

Hypothetical Mohr fracture diagram for a rock containing initially open cracks

criterion defined by equation (72), is

$$\tau = \mu (\sigma_{xx} - \sigma_{cr}) - 2\sigma_t \quad \ldots\ldots\ldots\ldots (73).$$

The transition from the Mohr envelope defined by equation (50), for the original Griffith's theory, to that defined by equation (73) occurs at $\sigma = \sigma_{xx} = \sigma_{cr}$.

In discussing McClintock and Walsh's modification to Griffith's theory, Brace[52] suggests that a rough measure of the critical stress σ_{cr} can be obtained from the axial stress-strain curve for a rock specimen. The application of this suggestion is illustrated by means of the hypothetical example given in Figures 41 and 42.

A material containing initially open cracks which close when $\sigma_{xx} = \sigma_{cr}$ will give the type of axial stress-strain curve illustrated in Figure 41. The slope of the curve will gradually increase as the cracks close and the stiffness of the specimen increases.

An approximate measure of σ_{cr} is given by the stress level at which the axial stress-strain curve becomes linear*.

The Mohr fracture envelope for a material with initially open cracks which close when $\sigma_{xx} = \sigma_{cr}$ is illustrated in Figure 42 and it will be noted that, theoretically, a sudden change in the slope of the envelope occurs at $\sigma_{xx} = \sigma_{cr}$.

The above discussion, included primarily for the sake of completeness, has been dealt with rather superficially since, in the author's experience on the behaviour of hard rocks, stress-strain behaviour such as that illustrated in Figure 41 is considered the exception rather than the rule. In most hard rocks, σ_{cr} is sufficiently close to zero for it to be neglected without introducing any significant error.

---

* Since the cracks close sequentially according to their orientation, this assumption is obviously an oversimplification. However, the detailed analysis of the effects of crack closure upon the stress-strain behaviour of rock, discussed in recent publications by Brace[385] and Walsh[386], [387], exceeds the scope of this study and the above assumption is accepted as sufficiently accurate for the purposes of the present discussion.

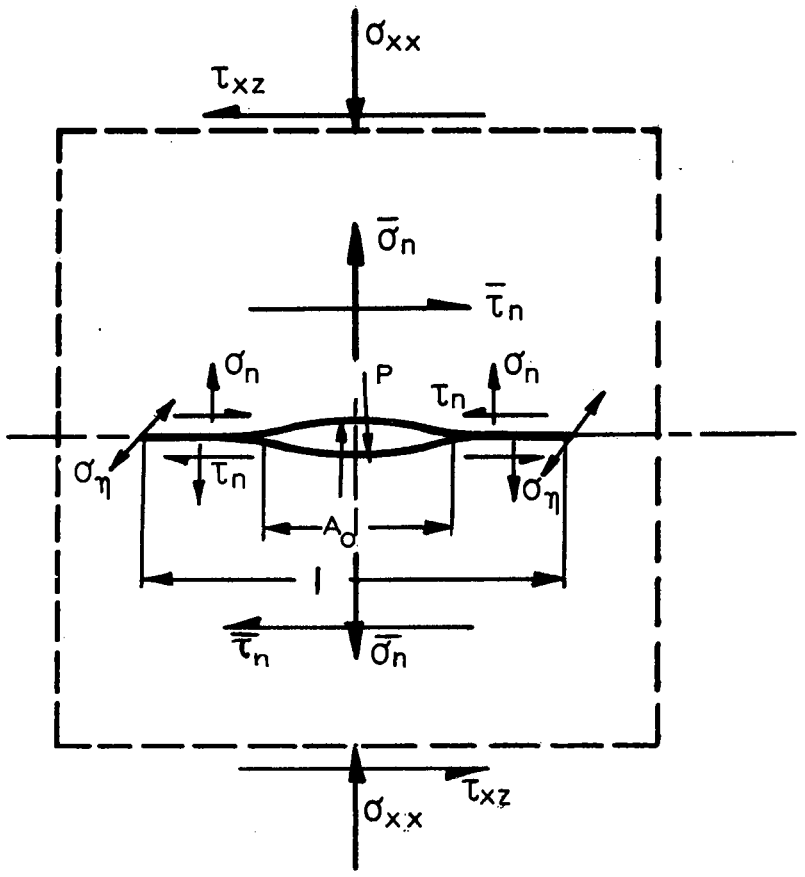

FIGURE 43

Stresses acting upon a crack subjected to pore pressure according to McClintock and Walsh

14.3 The influence of pore pressure upon rock fracture

In many underground situations, the rock is subjected to fairly high fluid pressure from water which has entered the area through fissures and faults. If sufficient time has been allowed for this water to permeate the rock, the internal pressure acting on the crack surfaces within the rock can have a significant influence upon the fracture behaviour of the rock*. It is interesting to consider to what extent this influence can be predicted on the basis of the Griffith's fracture theory.

In discussing the effects of pore pressure, McClintock and Walsh[249] assumed that the crack is acted upon by the stress system illustrated in Figure 43.

Considering the case of an initially closed crack of unit area subjected to an internal pressure P which forces the crack open over a central area A_o.

The average normal stress $\bar{\sigma}_n$ across the crack is related to the normal stress σ_n and the pressure P by the following equation.

$$\bar{\sigma}_n = \sigma_{xx} = (1 - A_o)\,\sigma_n + A_o\,P \quad \ldots\ldots\ldots (74).$$

Note that, since the crack is assumed to be initially closed, the critical stress σ_{cr} required to close the crack is zero and hence $\sigma_{xx} = \bar{\sigma}_n$.

The average frictional shear resistance $\bar{\tau}_n$ which must be overcome before sliding of the crack surfaces can occur is given by

$$\bar{\tau}_n = (1 - A_o)\,\tau_n = (1 - A_o)\mu\,\sigma_n \quad \ldots\ldots\ldots (75)$$

From equations (74) and (75)

---

* In this discussion it is assumed that the presence of water does not influence the strength of rock unless it is under pressure. The difference between the strength of wet and dry rock will be discussed in section 14.4 of this study.

$$\bar{\tau}_n = \mu (\sigma_{xx} - A_o P) \quad \ldots\ldots\ldots\ldots (76)$$

Using the same argument as presented in section 7 of part I, the net shear stress which is effective in inducing the tensile stress at the crack tip is now

$$\tau_{xz} - \mu (\sigma_{xx} - A_o P).$$

Substituting this value into equation (29):

$$\sigma_\eta = \frac{2\eta (\tau_{xz} - \mu (\sigma_{xx} - A_o P))}{\xi_o^2 + \eta^2} \quad \ldots\ldots\ldots (77)$$

Note that this equation is identical to equation (71) if $A_o P$ is substituted for σ_{cr}. Hence, by analogy with the argument presented in section 14.2, the fracture initiation criterion for an initially closed crack, subjected to an internal pressure P, can be written as

$$\sigma_1 = \frac{-4\sigma_t}{\sqrt{1+\mu^2}\,(1-k) - \mu(1+k) + \mu A_o P} \quad \ldots\ldots\ldots\ldots (78)$$

The corresponding Mohr envelope is defined by

$$\tau = \mu (\sigma - A_o P) - 2\sigma_t \quad \ldots\ldots\ldots\ldots\ldots\ldots (79)$$

Obviously, equations (78) and (79) are only valid when $\sigma_{xx} > A_o P$.

For smaller values of σ_{xx}, the original Griffith's theory must be used but this theory must be modified to allow for the effects of the pressure P.

When the normal stress σ_{xx} is smaller than the pressure P, the crack will be forced completely open, i.e. $A_o \to 1$. Under

these conditions, there will be no frictional effects on the crack surfaces but the normal stress σ_{xx} acting across the crack will now become $(\sigma_{xx} - P)$.

Following the same procedure as that outlined in part I, the fracture criterion can be expressed in the form of a Mohr envelope defined by the following equation

$$\tau^2 = 4\sigma_t (\sigma_t - (\sigma - P)) \quad \ldots\ldots\ldots\ldots (80)$$

The transition from equation (80) to equation (79) depends upon the value of A_o. In the case of porous materials such as limestone and sandstone, it can be anticipated that the whole crack will be open i.e. $A_o \to 1$. Under these conditions the transition will occur at $\sigma = P$. The fracture behaviour of the material will be governed by the same equations as for the material without pore pressure except that the effective stress $(\sigma - P)$ must be used instead of the normal stress σ.

A recent survey on the effects of pore pressure on rock fracture* confirms that the concept of an "effective" stress, as defined above, is generally accepted as the most reliable basis for the prediction of the effects of pore pressure on the fracture of porous rocks.

In the case of very dense rocks in which the cracks can be expected to remain almost completely closed except at very high pore pressures, equations (78) and (79) show that, under triaxial compressive stress conditions, for $A_o \to 0$ the rock strength will be almost independent of pore pressure.

14.4 The effect of environment upon rock fracture

The fracture theory, reviewed in part I of this study, postulates that rock fracture is dependent upon two basic material constants - the molecular cohesive strength and the coefficient of internal friction. In considering whether it is justified to accept these

---

* NICOLYASEN, O. The note of fluid pressure in the failure of of rock and other porous media. Unpublished report, Bernard Price Institute of Geophysical Research, July 1965.

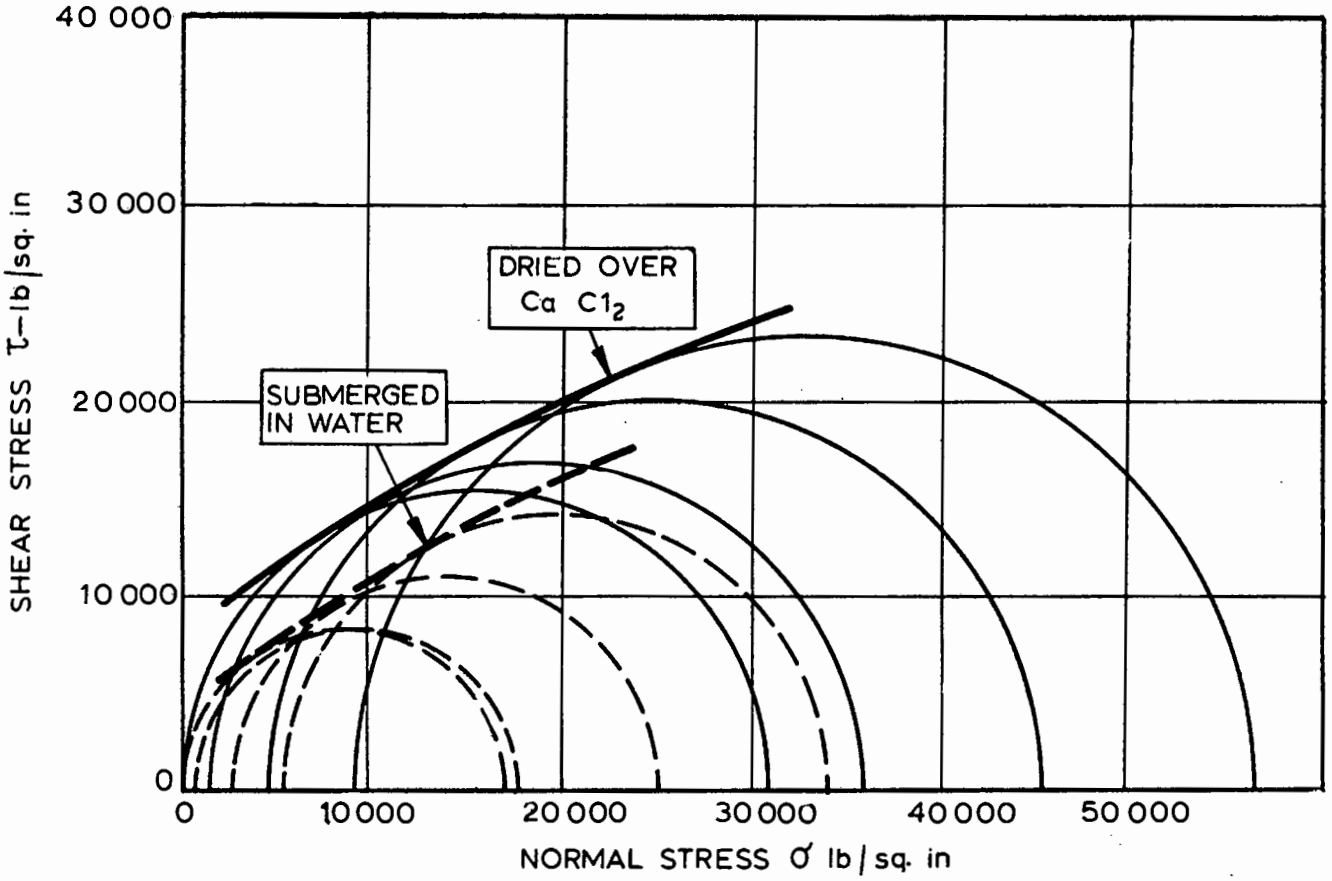

FIGURE 44

Mohr fracture envelopes showing the effect of moisture on the compressive strength of quartzitic shale (from Colback and Wiid)

parameters as constants, it is necessary to consider to what extent they may be influenced by the temperature and humidity environment of the specimen.

Available literature contains virtually no information on the influence of temperature on the strength of rock. Although it can be anticipated that the molecular cohesive strength may be temperature sensitive, it is unlikely that the resulting change in strength would be significant within the normal range of temperatures encountered in practical rock mechanics problems.

In the author's opinion, the influence of temperature upon the strength of rock would only become significant at very low temperatures, when an effect similar to low temperature brittleness in steel may occur, and at very high temperatures when the melting point of certain constituents is approached. It must be emphasised that these are purely opinions and are not based upon any experimental evidence.

The influence of moisture upon the strength of rock has been dealt with in a recent paper by Colback and Wiid[83]. In contrast to previous workers, who have tended to regard the influence of moisture as unimportant, these authors found that the moisture content of a specimen has a pronounced influence upon its strength.

The Mohr envelopes for a quartzitic shale, under "wet" and "dry" conditions, are reproduced, from Colback and Wiid's paper, in Figure 44. This particular material was found to have a mean "dry"* strength of 30 900 lb/sq. in and a mean "wet"** strength of 17 100 lb/sq. in. The same ratio of strengths was found in the case of a quartzitic sandstone.

Examination of Figure 44 shows that the Mohr envelopes are very nearly parallel and this implies that the coefficient of internal friction μ is not significantly influenced by the moisture content of the specimen. This in turn suggests that the molecular cohesive strength σ_o (from equation (23) of part I) is moisture sensitive.

---

* Dried oven calcium chloride for 120 days

** Submerged in water for 120 days.

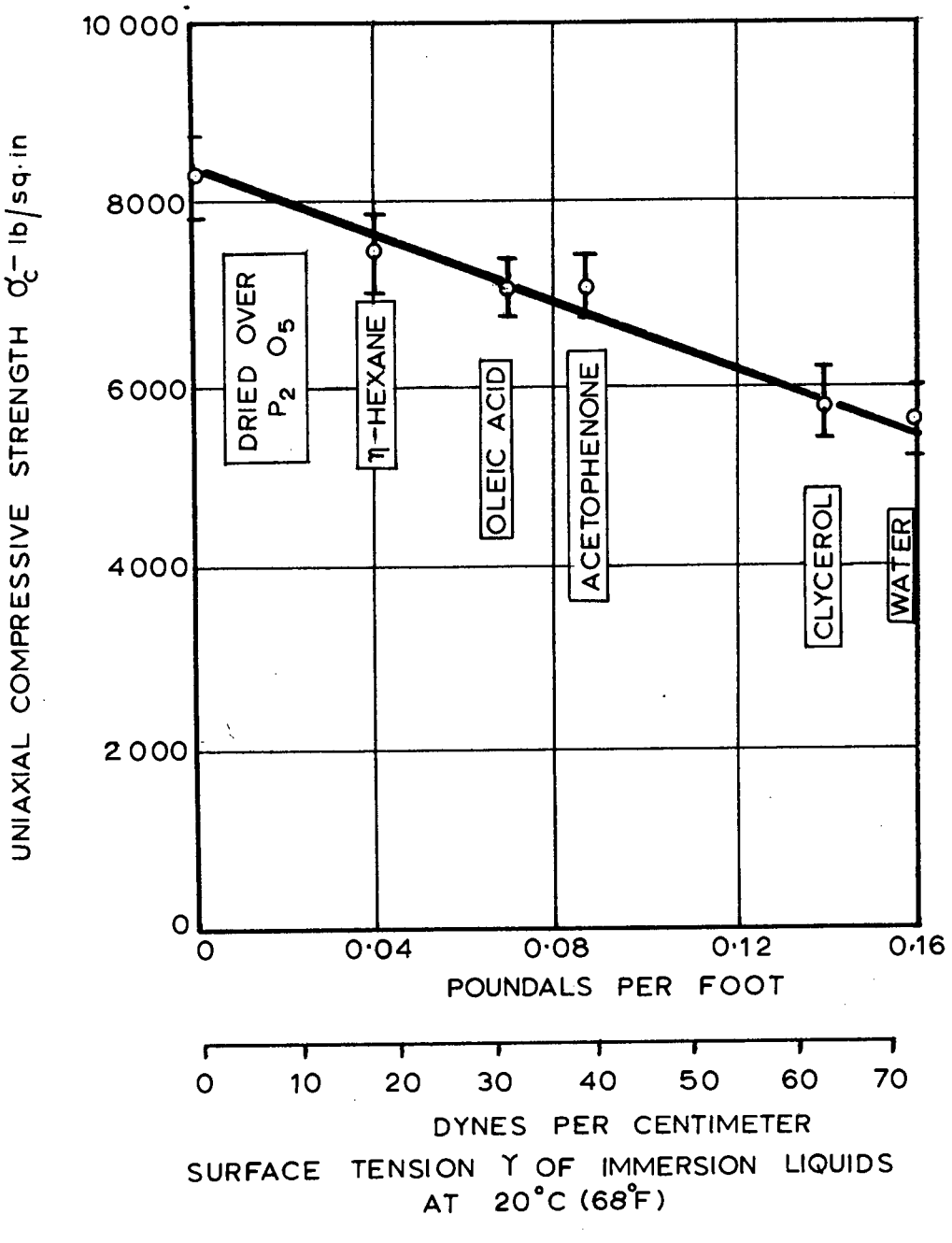

FIGURE 45

The influence of the surface tension of immersion liquids upon the uniaxial compressive strength of quartzitic shale (from Colback and Wiid)

According to Orowan[286], the molecular cohesion of a solid is related to its surface energy by equation (1) (page 4 of part I):

$$\sigma_o = \sqrt{\frac{2\gamma E}{a}} \quad \ldots\ldots\ldots\ldots\ldots\ldots (1)$$

Since it is unlikely that the Young's modulus E or the atomic plane spacing a would be moisture sensitive, the change in strength must be attributed to a change in the surface energy γ with changing moisture content.

Strong evidence in support of this conclusion is presented in Figure 45 which is reproduced from Colback and Wiid's paper. In this figure, the uniaxial compressive strengths of quartzitic sandstone specimens are plotted against the surface tension (surface energy) of the liquids in which these specimens were immersed. The resulting curve clearly illustrates the reduction in the strength of the rock with increasing surface tension of the immersion liquid and it can be concluded that this effect is due to a reduction in the surface energy of the rock.

From the results presented by Colback and Wiid it must be concluded that the strength of rock can only be adequately defined if the moisture content of the specimen or the relative humidity of the environment can be specified. The influence of moisture can only be neglected if tests on "wet" and "dry" specimens show no significant strength difference.

In the case of materials such as coal, the influence of moisture* is regarded as so important that the CSIR currently conducts triaxial tests on coal in the actual working area in order that the specimens need not be removed from their environment.

14.5 The influence of rate of loading upon rock fracture

In spite of the fact that most rock mechanics workers acknowledge

---

* Apart from the well known weathering characteristics of coal.

that the properties of rock are time-dependent, this aspect of rock behaviour is probably the least understood of all rock mechanics phenomena.

This ignorance is due primarily to the difficulties of accurate measurement at very high rates of loading or, at the other extreme, over long periods of time. In addition, the scatter in results which can be obtained in tests at various rates of loading makes meaningful analysis very difficult.

The quartzitic shale used by Colback and Wiid for their studies on moisture content was also used, by the author, for time-dependent fracture studies. A constant load was applied to the specimen, under constant temperature and humidity conditions, and it was found that, if the load was high enough, the specimen would fail after some period of time had elapsed. However, at a given load level, this time could vary from two minutes to two weeks. Obviously, the determination of a statistically significant time-dependent strength relationship for such a material would require the testing of an impossibly large population of specimens.

It is believed that the properties of rock must be studied under three distinct loading rate conditions:

(a) Under conditions in which the total load is applied within a few milliseconds such as in percussive drilling or blasting.

(b) Under conditions in which the total load is applied over a period of a few minutes as in normal laboratory testing.

(c) Under conditions in which the total load is maintained for a long period, perhaps years, as in normal mining situations.

The meager experimental evidence which is available suggests that the strength of hard rock may vary by as much as 20% over this range of loading rates. However, since the study of the time-dependent behaviour of rock represents a research field in itself, the only logical approach which can be adopted at present is to use a standard loading rate in all laboratory testing

in the hope that, in time, these results can be correlated with the behaviour at different loading rates.

14.6 Conclusions on the effects of additional factors upon rock fracture

The discussion presented in the preceding pages shows that the fracture theory, reviewed in part I of this study, is only applicable to the prediction of rock fracture behaviour if certain limitations are specified.

(a) The rock should be macroscopically isotropic i.e. its uniaxial compressive strength should be the same for compression specimens drilled at 30° to the bedding planes as it is for those normal or parallel to the bedding planes.

(b) The inherent cracks should be initially closed, i.e. the axial stress-strain curve should be linear from very low stress levels upwards to near the stress at fracture.

(c) If the specimen is in contact with a fluid under pressure, the influence of this pore pressure should be taken into consideration.

(d) The temperature and humidity conditions under which the tests are carried out should be specified and should be as near to in-situ conditions as possible. The specimens should be stored under controlled conditions for a period which is sufficient to allow the moisture content in the specimen to become stable (depending upon the porosity of the material).

(e) The rate at which the load is applied to the specimen should be constant and should be the same for all specimens tested.

If the material is found to be anisotropic or to have a non-linear axial stress-strain curve, the test results can be interpreted in terms of the discussion presented in sections 14.1 and 14.2 of this study.

Practical experience has shown that, provided the above factors are taken into account in the interpretation of the results of laboratory tests on rock properties, the amount of experimental scatter normally associated with rock fracture studies can be reduced to a minimum. The application of these results to the analysis of practical rock fracture problems will be considered in part III of this study.

PART III - THE APPLICATION OF GRIFFITH'S THEORY TO THE ANALYSIS OF ROCK FRACTURE IN A COMPLEX STRESS FIELD

The considerations presented in parts I and II of this study are concerned with the fracture behaviour of single cracks and of small laboratory specimens in which the stress field is assumed to be uniform. Unless it can be demonstrated that this work is applicable to the analysis of fracture in complex stress fields such as those which occur around mining excavations, its value will be limited to that of an interesting academic exercise.

The detailed analysis of the fracture of the material surrounding a circular excavation in a plate model, presented in the following sections, is an attempt to evaluate the potential and the problems involved in applying Griffith's theory to the prediction of rock fracture in a complex stress field.

15. FRACTURE OF THE MATERIAL AROUND A CIRCULAR HOLE

15.1 The stress distribution around a circular hole

The stress distribution around a circular hole was calculated by Kirsch[226] and his equations for the radial, tangential and shear stress are listed in Figure 46. From these equations it is clear that the maximum uniaxial tensile and compressive stress occur on the hole boundary, on the vertical and horizontal diameters (at $\theta = 0^{\circ}$ and 90°). The variation of these stresses, for various applied stress ratios ($^{Q}/P$) is illustrated in Figure 47.

Since the uniaxial tensile strength of hard rock is usually approximately one tenth of the uniaxial compressive strength (see Figure 11), it can be anticipated that tensile fracture will occur in the roof and floor of the circular excavation for applied stress ratios of $^{Q}/P < 0.25$. For $^{Q}/P > 0.25$, fracture will initiate as a result of the uniaxial compressive stress in the sidewalls of the excavation.

15.2 Tensile fracture of the roof and floor of a circular excavation

In order to study the initiation and propagation of tensile fracture in the roof and floor of a circular excavation, a photoelastic study was carried out in which the cracks were simulated

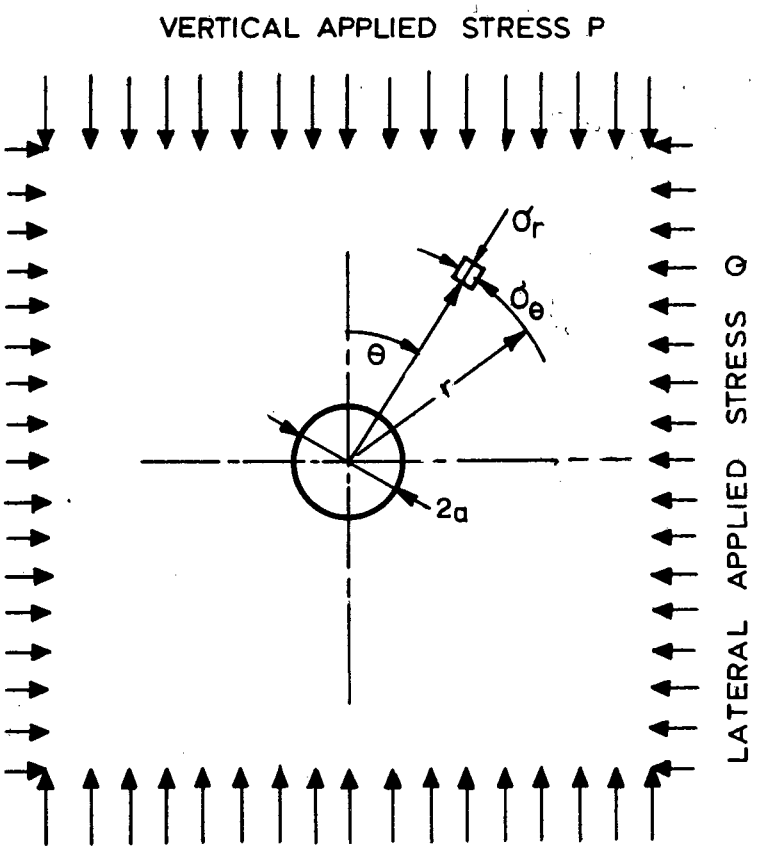

RADIAL STRESS

$$\sigma_r = \tfrac{1}{2}\left[(P+Q)(1-a^2/r^2) + (P-Q)(1-4\,a^2/r^2+3\,a^4/r^4)\cos 2\theta\right]$$

TANGENTIAL STRESS

$$\sigma_\theta = \tfrac{1}{2}\left[(P+Q)(1-a^2/r^2) - (P-Q)(1-3\,a^4/r^4)\cos 2\theta\right]$$

SHEAR STRESS

$$\tau_{r\theta} = -\tfrac{1}{2}\left[(P-Q)(1+2\,a^4/r^4-3\,a^4/r^4)\sin 2\theta\right]$$

FIGURE 46

Theoretical stress distribution around a circular hole in a biaxial stress field

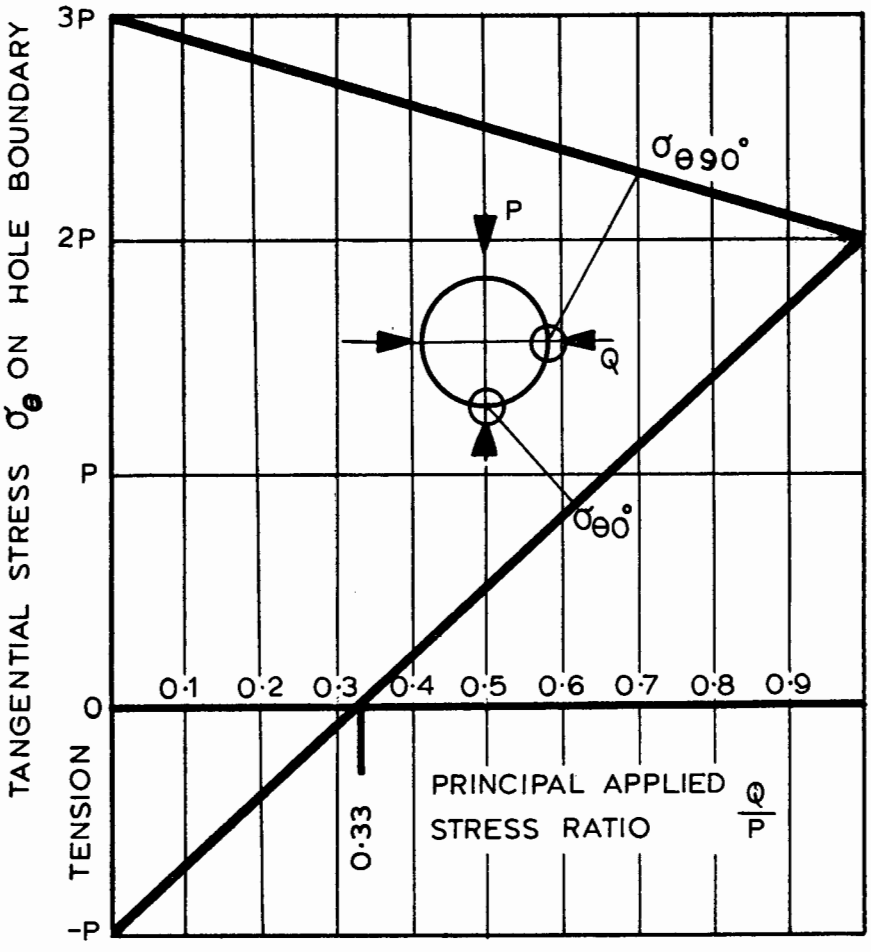

FIGURE 47

Boundary stresses on vertical and horizontal hole diameters for various ratios of applied stress

by means of fine saw cuts in Columbia resin (CR 39) models. These models were subjected to biaxial compressive loads and the photoelastic patterns studied in the 12 inch diameter lens polariscope illustrated in Figure 48.

The propagation of the roof and floor cracks was simulated by extending the saw cuts in the models. A detailed study of the stresses around the crack tip revealed the following behaviour:

For very short cracks, the tensile stress at the crack tip was several times higher than that which existed on the boundary of the hole before the crack was initiated. As the crack length increased, the tensile stress at the crack tip decreased. The rate of decrease with increasing crack length was found to depend upon the applied stress ratio $^{Q}/P$.

At a certain crack length, the stress at the crack tip became zero and further extension of the simulated crack resulted in the stress at the tip becoming compressive. Assuming that crack propagation would cease when the stress at the crack tip becomes zero, it was concluded that cracks of a certain length, depending upon the applied stress ratio $^{Q}/P$, would form and would not propagate further.

The photoelastic analysis described above suffered from several disadvantages; the most serious being the finite radius of the simulated crack tip. Consequently it was decided to use models of brittle materials which could be induced to fracture under high loads.

Glass plate models, 5 inches square by $\frac{1}{8}$ inch thick containing $\frac{3}{8}$ inch diameter central circular holes, were loaded in a 30 ton biaxial loading frame. This frame, loaded by means of two hand operated hydraulic jacks, was much less sophisticated than the biaxial loading machine described in Appendix III, but was found to be adequate for this type of study.

An isochromatic pattern in a glass plate model, in which tensile cracks have been induced, is illustrated in Figure 49. This particular photograph was taken at an applied vertical stress P of 30 000 lb/sq. in and at an applied stress ratio of $^{Q}/P = 0.166$. The apparent width of the crack is due to reflections from the

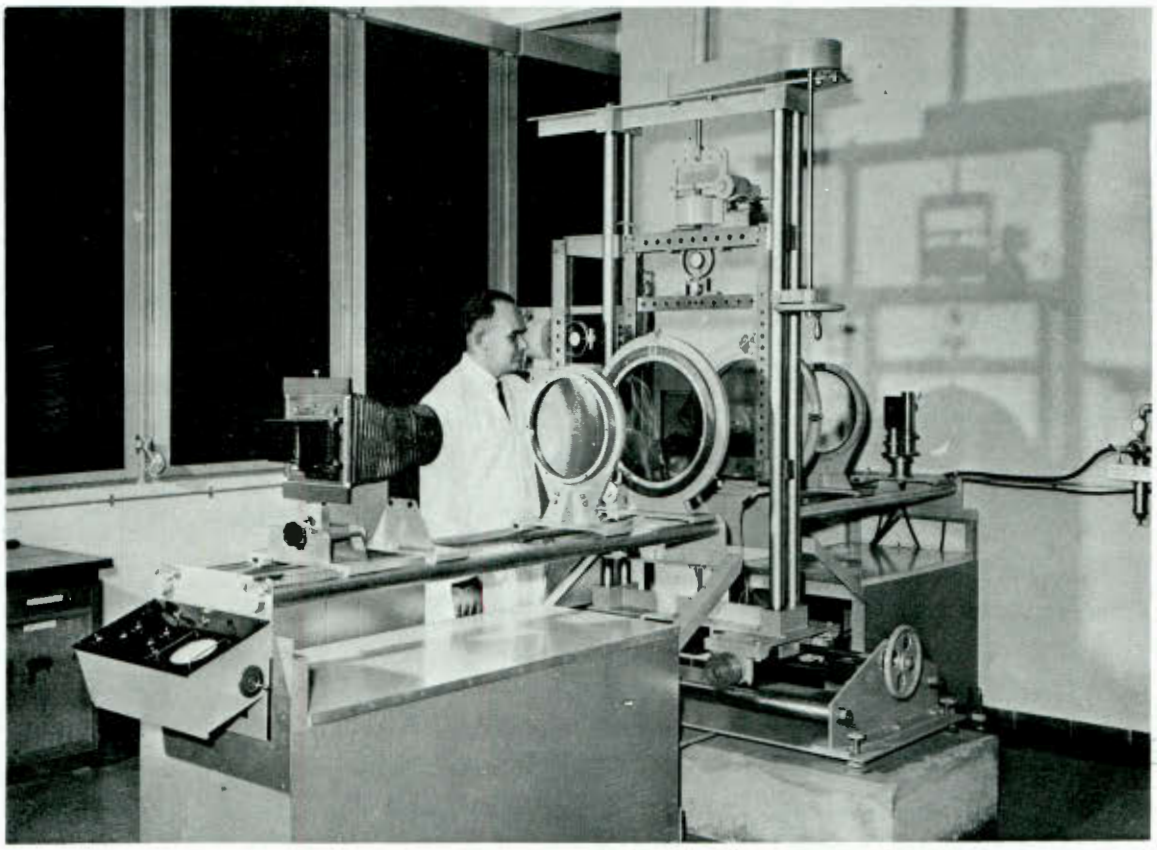

FIGURE 48

Photoelastic polariscope used for studies
of fracture propagation

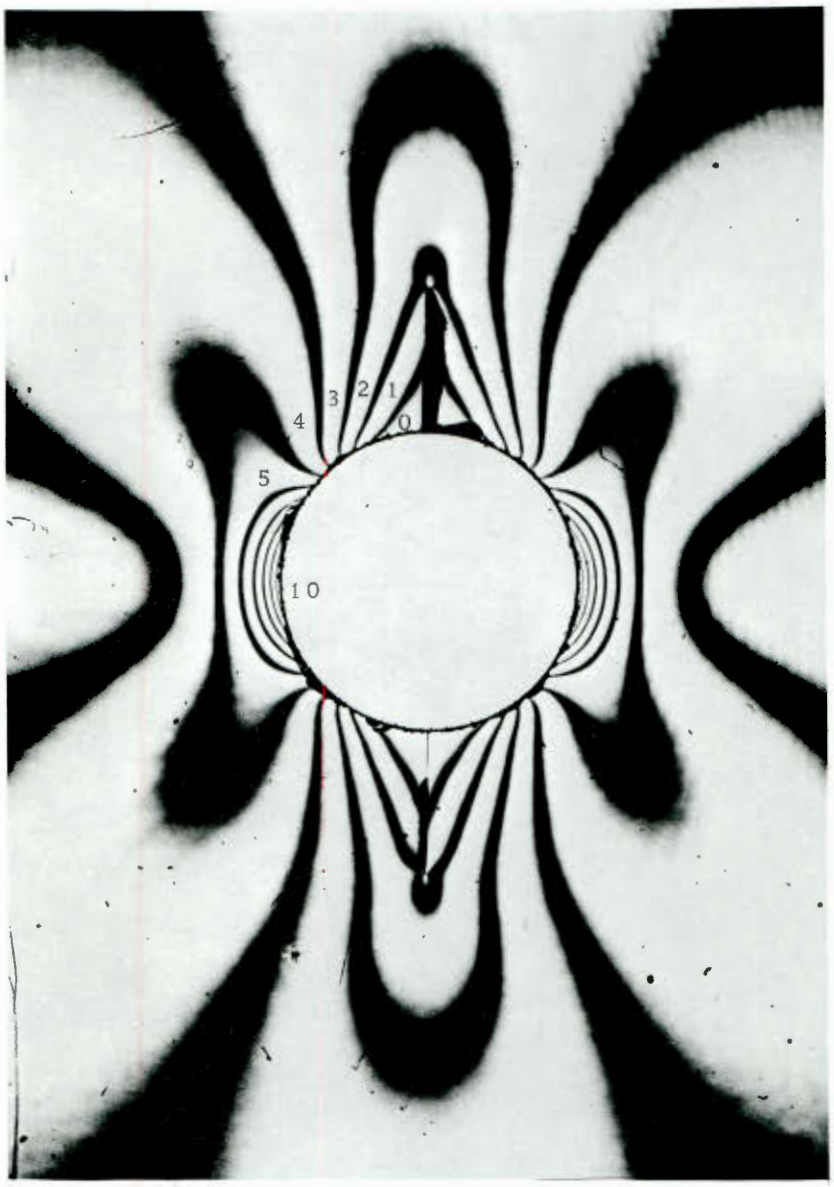

FIGURE 49

Photoelastic isochromatics in a glass plate containing a circular hole from which tensile cracks have propagated

$\frac{Q}{P} = 0.166$

crack surface.

As anticipated from the earlier photoelastic study, the stable crack length was found to be related to the applied stress ratio Q/P. This relationship, determined experimentally from the glass models, is illustrated in Figure 50.

In order to verify that the same behaviour occurs in hard rock, models were prepared from fine grained quartzite and loaded in the same way as the glass models. The results of these tests are included in Figure 50.

From the consistency of the results presented in Figure 50 it can be concluded that the cracks which form in the roof and floor of a circular excavation in a biaxial stress field, where $Q/P < 0.33$, will propagate to a length which depends upon the applied stress ratio. These tests showed that, once the crack had reached the length indicated in Figure 50, no further propagation would occur, even if the applied stress level was increased to several times the level at which fracture had initiated.

15.3 Failure initiation from the sidewalls of a circular excavation

Practical experience suggests that the most serious type of fracture which occurs around mining excavations is that which initiates in the compressive stress zones in the sidewalls. In order to study this type of fracture, it was decided to use rock plate models which could be loaded to destruction. The details of the plate model are given in Figure 51.

15.3.1 Model material

The material chosen for these model studies was a highly silicious fine-grained granite aplite which occurs in the mines of the central Witwatersrand of South Africa and which is known locally as chert dyke.

This material was chosen because it is free from major geological features such as bedding planes and because its behaviour is a close approximation to that of an ideal isotropic elastic solid. A typical stress-strain curve for this material is illustrated in Figure 52.

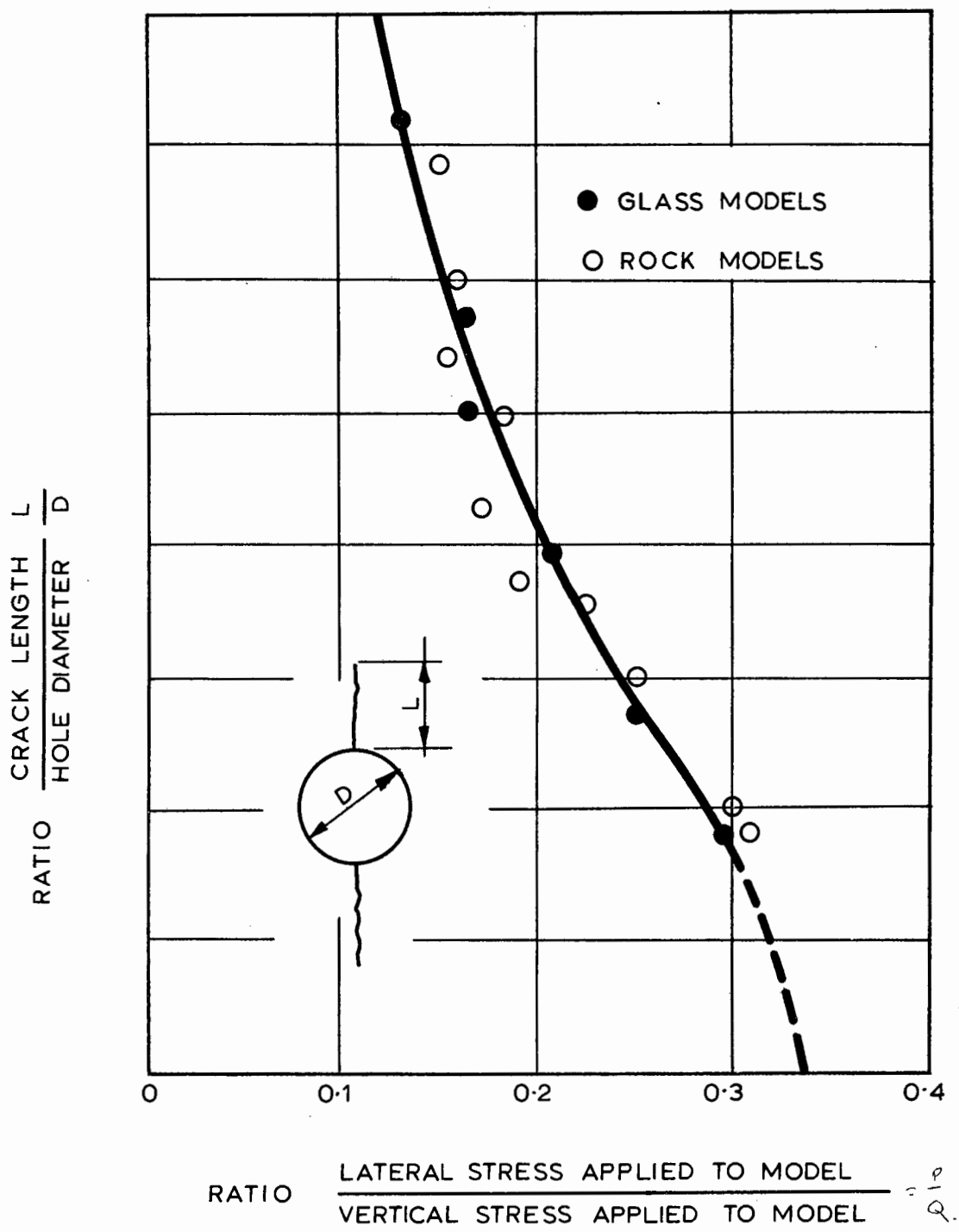

FIGURE 50

Influence of applied stress ratio upon length of tensile cracks in the roof and floor of a circular excavation

Hole dia ?
Is the ratio $\frac{L}{D}$ constant for different values of D and same Q/P ?

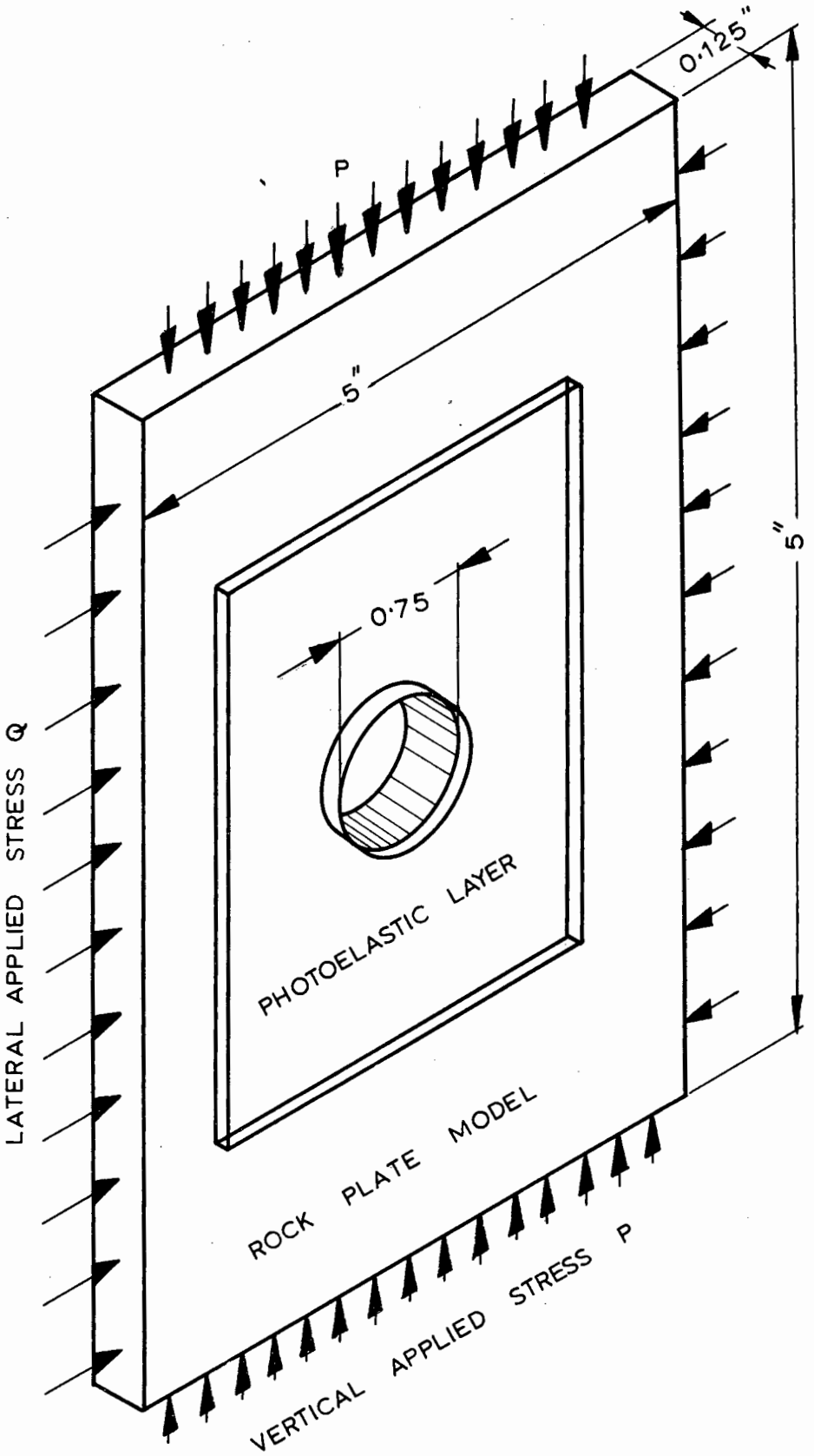

FIGURE 51

Rock plate model used to study fracture of the material around a circular hole

The triaxial fracture data for chert dyke material is presented, as a Mohr fracture diagram, in Figure 53. The strength values used in constructing this Mohr diagram are listed in Table IV. In addition to results obtained by the CSIR, this fracture data includes the results of tests carried out by Professor W.M. Brace of Massachusetts Institute of Technology's Department of Geology and Geophysics*.

In fitting the fracture envelope to the Mohr circles shown in Figure 53, the theoretical considerations discussed in part I of this study were only used as a guide; the actual fitting was done statistically**. The relationships between the major principal stress σ_1 and the principal stress ratio k (Figure 54) and the critical crack orientation ψ_c and the principal stress ratio k Figure 55) were determined graphically from the Mohr fracture envelope.

Note that the curves presented in Figures 53 to 55, representing the behaviour of a real material, bear a striking resemblance to the corresponding theoretical curves given in Figures 9, 4 and 3.

The average properties of the chert dyke material used in this model study are summarised below***.

Uniaxial tensile strength σ_t = 5 000 lb/sq. in
Uniaxial compressive strength σ_c = 85 000 lb/sq. in
Young's modulus E = 12 x 10^6 lb/sq. in
Poisson's ratio ν = 0.2
Approximate coefficient of internal friction μ = 1.08

---

* Details of the specimens and apparatus used by Professor Brace for triaxial testing of rock are given in a recent publication[52].

** PRETORIUS, J.P.G. Unpublished CSIR internal report, 1965; The technique used is to fit a general parabola to the σ_1 vs σ_3 plot by the method of least squares and then to transform this curve into a Mohr envelope. (Cf. reference 18).

*** This data is more complete than that used by the author in a paper published in 1964[194] and the study of the fracture of the material around a circular hole presented in the following sections is based upon the data presented in Figures 53 to 55.

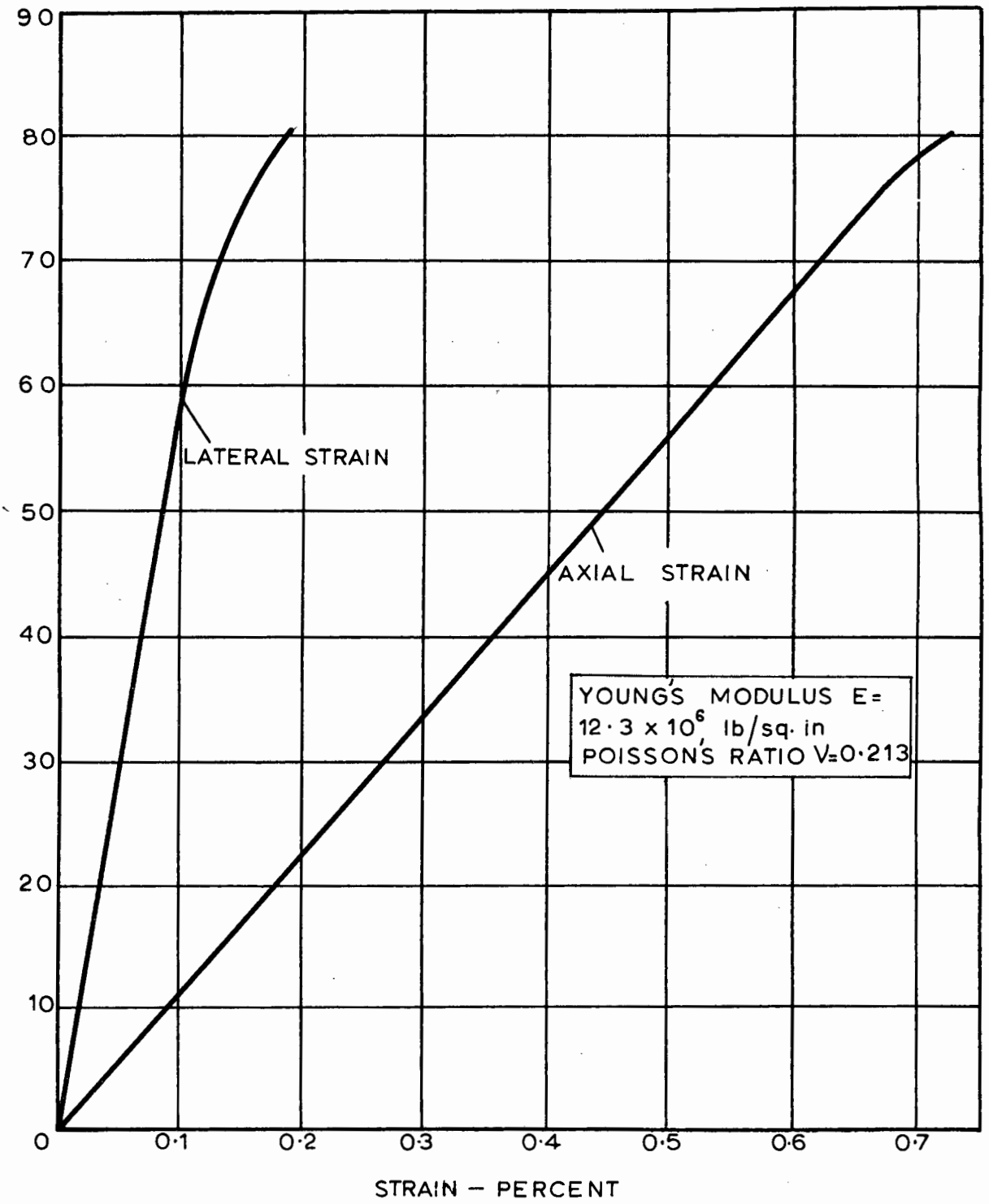

FIGURE 52

Stress-strain behaviour of chert dyke specimen subjected to uniaxial compression

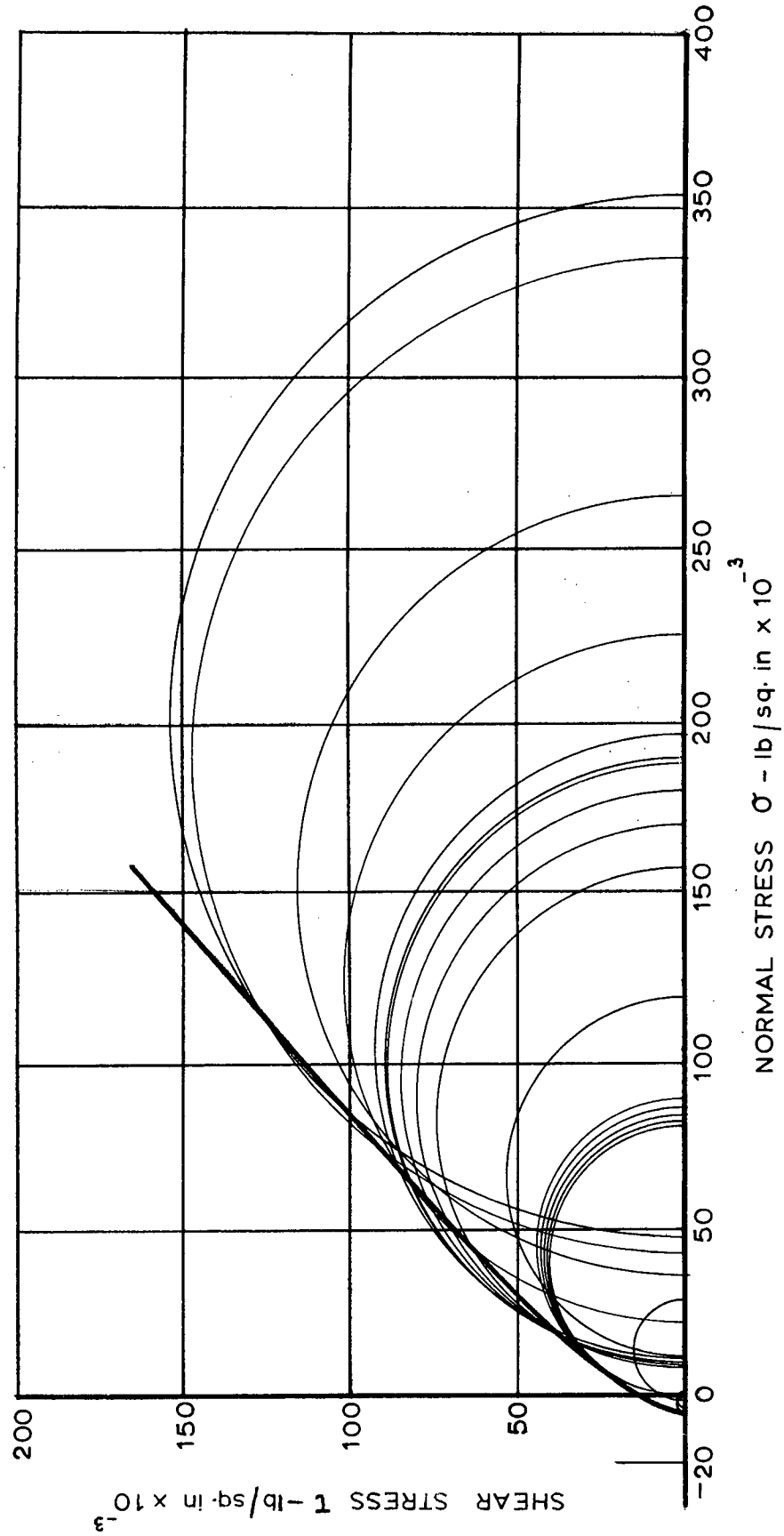

FIGURE 53

Mohr fracture diagram for chert dyke material

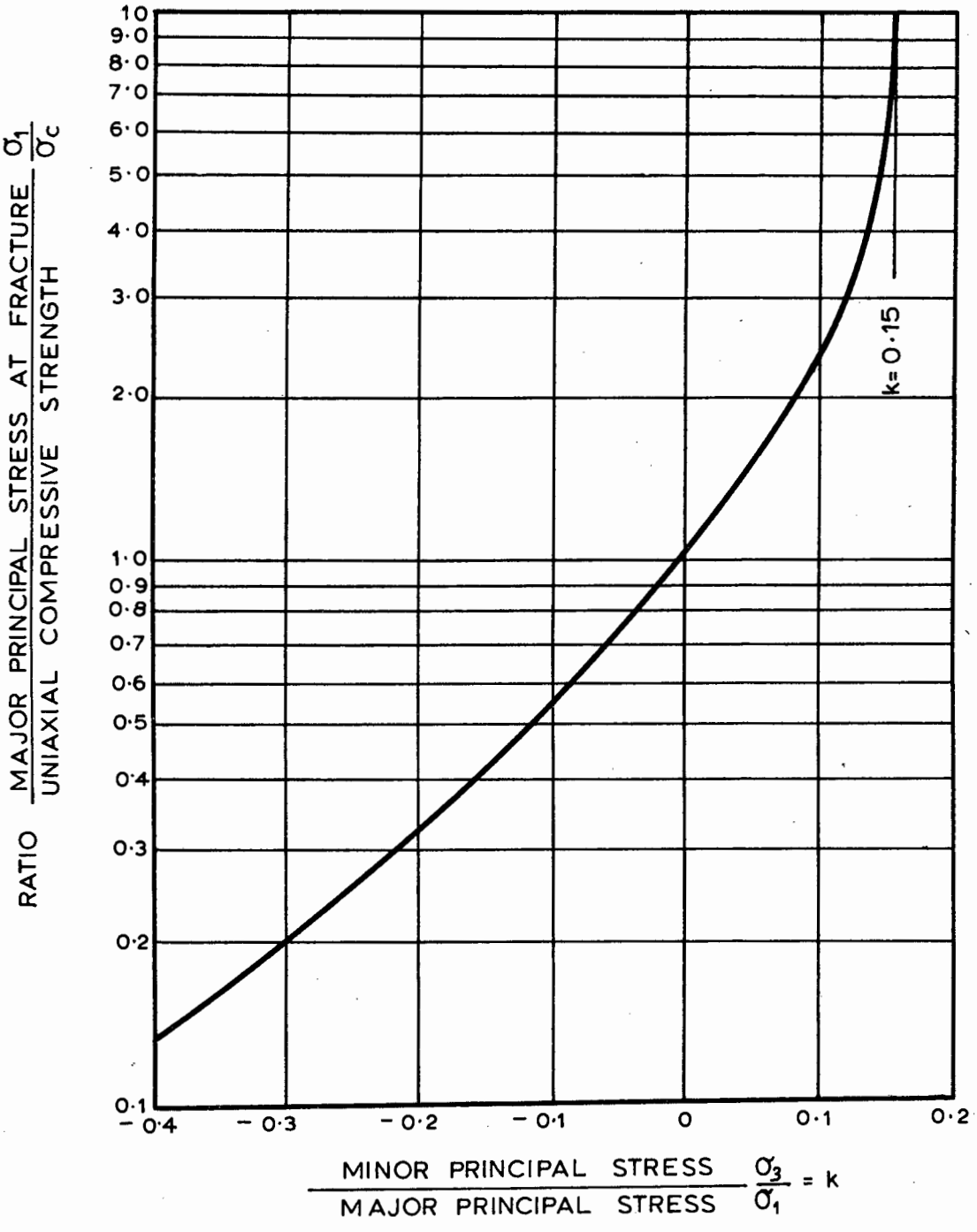

FIGURE 54

Relationship between major principal stress and principal stress ratio at fracture for chert dyke material

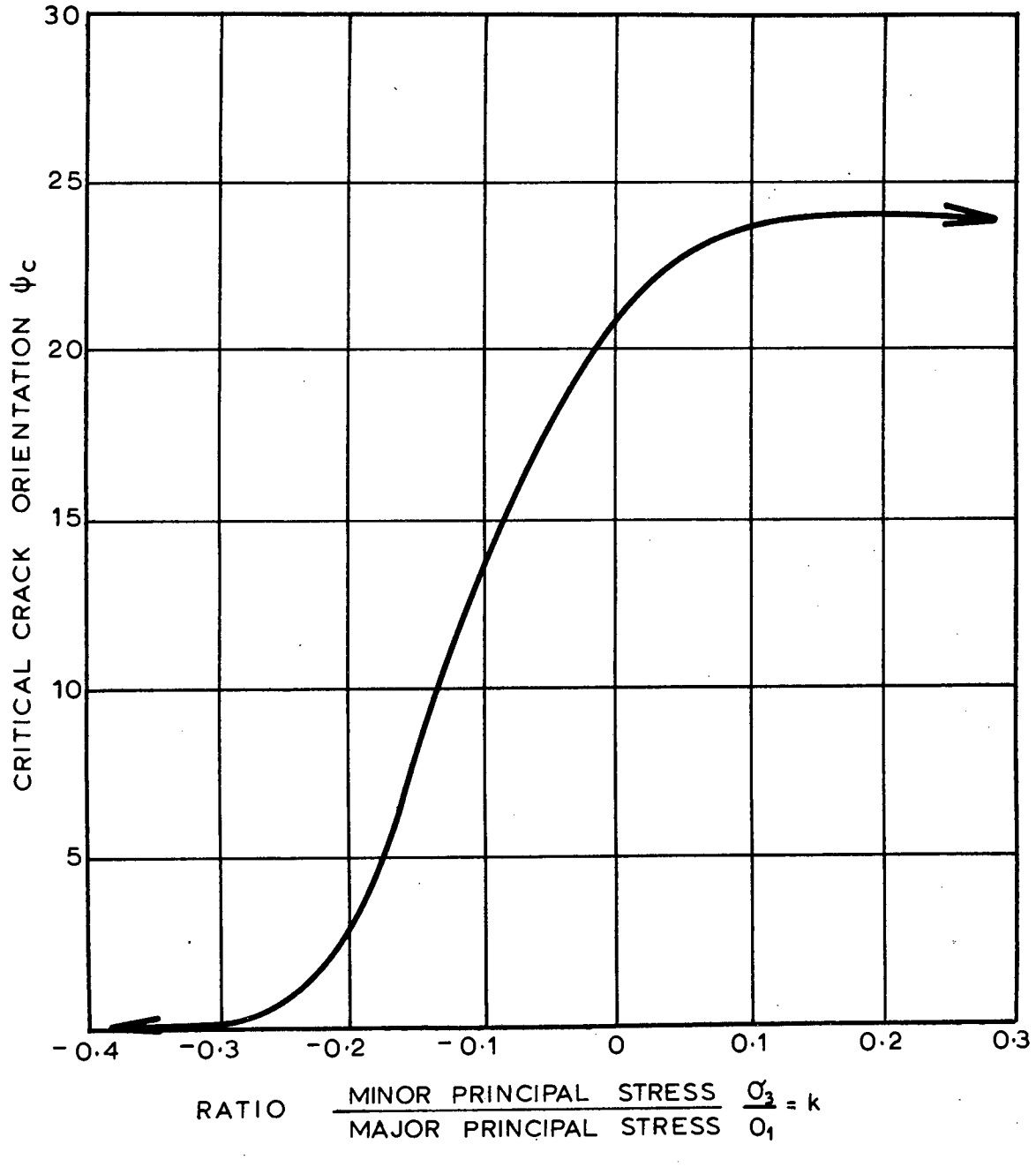

FIGURE 55

Relationship between the critical crack orientation and the principal stress ratio for chert dyke material

TABLE IV

TRIAXIAL FRACTURE DATA FOR CHERT DYKE MATERIAL

Major Principal Stress σ_1 lb/sq. in.	Minor Principal Stress σ_3 lb/sq. in.	Tested by
0	-5050	CSIR
330	-3120	CSIR
460	-4320	CSIR
28 600	-1900	MIT
88 600	0	CSIR
82 100	0	CSIR
86 000	0	CSIR
80 800	0	CSIR
84 000	0	CSIR
84 200	0	CSIR
87 600	0	MIT
89 000	0	MIT
118 000	11 300	MIT
118 000	11 300	MIT
156 700	8 400	CSIR
169 400	9 100	CSIR
178 900	9 500	CSIR
185 000	9 800	CSIR
186 900	9 100	CSIR
195 000	10 300	CSIR
224 000	21 000	MIT
264 000	35 000	MIT
333 000	41 600	MIT
352 000	47 200	MIT

15.3.2 Loads applied to the model

A theoretical consideration of the virgin stress which can occur in rock which is free from tectonic forces[92] suggests that the horizontal stress may be of the order of one quarter of the vertical stress, depending upon the Poisson's ratio of the material and the degree of horizontal restraint imposed by the surrounding rock.

Under these applied stress conditions, tensile fracture of the roof and floor of excavations such as haulages can be anticipated. Consequently, in planning this model study, it was considered necessary to apply stresses which would induce this tensile fracture. Practical considerations finally lead to the choice of a ratio of lateral to vertical applied stress ($^{Q}/P$ in Figure 51) of 0.15.

Since no facilities were available for the application of stress or restraint normal to the model surface approximately plane stress conditions existed in the models[340].

In analysing the fracture of the material around the circular hole in the model, it is necessary to compare this fracture behaviour with that which would occur under plane strain conditions which are likely to exist in the rock surrounding an underground excavation.

15.3.3 Fracture under plane stress and plane strain conditions

Under plane stress conditions, the stress normal to the plate surface σ_n is zero and hence the minor principal stress in the model plane σ_q is only algebraically smallest of the three principal stresses when it is tensile (negative). Hence

$$\sigma_n = 0 = \sigma_3 \text{ when } \sigma_q > 0; \quad \sigma_q = \sigma_2$$

$$\sigma_n = 0 = \sigma_2 \text{ when } \sigma_q < 0; \quad \sigma_q = \sigma_3.$$

Since fracture is dependent upon the algebraically greatest and smallest of the three principal stresses, σ_1 and σ_3 respectively, fracture in a model under plane stress conditions will occur as a result of the stresses σ_p and σ_q in

the model plane where $\sigma_q < 0$. In regions where $\sigma_q > 0$, fracture will occur as a result of the uniaxial compressive stress conditions $\sigma_p = \sigma_1$, $\sigma_n = 0$.

Under plane strain conditions, which can be assumed to occur in the material surrounding a long horizontal excavation such as a haulage, the strain parallel to the axis of the excavation is zero, i.e. $\varepsilon_n = 0$. The induced stress normal to the model plane σ_n is then dependent upon the principal stresses σ_p and σ_q in the model plane:

$$\sigma_n = \nu(\sigma_p + \sigma_q) \quad \ldots\ldots\ldots\ldots\ldots (81)$$

Under these cnnditions

$$\sigma_q = \sigma_3 \text{ when } \frac{\sigma_q}{\sigma_p} < \frac{\nu}{1-\nu} \quad \ldots\ldots\ldots (82)$$

Substituting $\nu = 0.21$ (from Figure 52) into equation (82):

$$\sigma_q = \sigma_3 \text{ when } {}^{\sigma_q}/_{\sigma_p} < 0.26$$

From Figure 54, fracture of this material can only occur for ${}^{\sigma_q}/_{\sigma_p} = k < 0.15$ hence, for this particular material under plane strain conditions, fracture will not be influenced by the stress σ_n which is parallel to the hole axis*.

15.4 Fracture analysis

The steps involved in the analysis of fracture in the material surrounding a circular excavation were as follows:

(a) The principal stresses σ_p and σ_q, the principal stress ratio ${}^{\sigma_q}/_{\sigma_p}$ and the principal stress directions in the material surrounding a circular hole in a plate subjected to a vertical applied stress P and a

---

* The possibility of inducing plane strain conditions in models is discussed in Appendix III.

lateral applied stress Q = 0.15 P were calculated by means of the equations presented in Figure 46.

(b) From the principal stress ratio σ_q/σ_p distribution and the fracture locus presented in Figure 54, the magnitude of the major principal stress $\sigma_p = \sigma_1$ required to initiate fracture at any point in the model was determined*.

(c) Division of this value of σ_1 by the stress concentration factor σ_1/P at that point gave the value of the vertical applied stress P which was required to initiate fracture at that point in the model. This value of P was expressed in multiples of the uniaxial compressive strength σ_c of the material.

(d) From the principal stress trajectories and the critical crack orientations ψ_c, from Figure 55, the distribution of critical crack orientations in the model was established.

(e) From the distribution of the vertical applied stress P required to initiate fracture and the critical crack orientations ψ_c in the model, the most likely fracture path in the material surrounding the hole was established.

(f) This fracture path was cut into a plastic photoelastic model by means of a fine saw and the redistribution of stress associated with this simulated fracture propagation was analysed photoelastically. Separation of the principal stresses was carried out by means of the conducting paper analogy described in Appendix V.

(g) Having established the stress distribution and the principal stress trajectories for the new excavation geometry, the entire fracture analysis as described above was repeated.

The complete analysis of fracture initiation and propagation in the rock surrounding a circular hole is presented in Figures 56 to 61.

---

* This analysis was done for both plane stress and plane strain conditions.

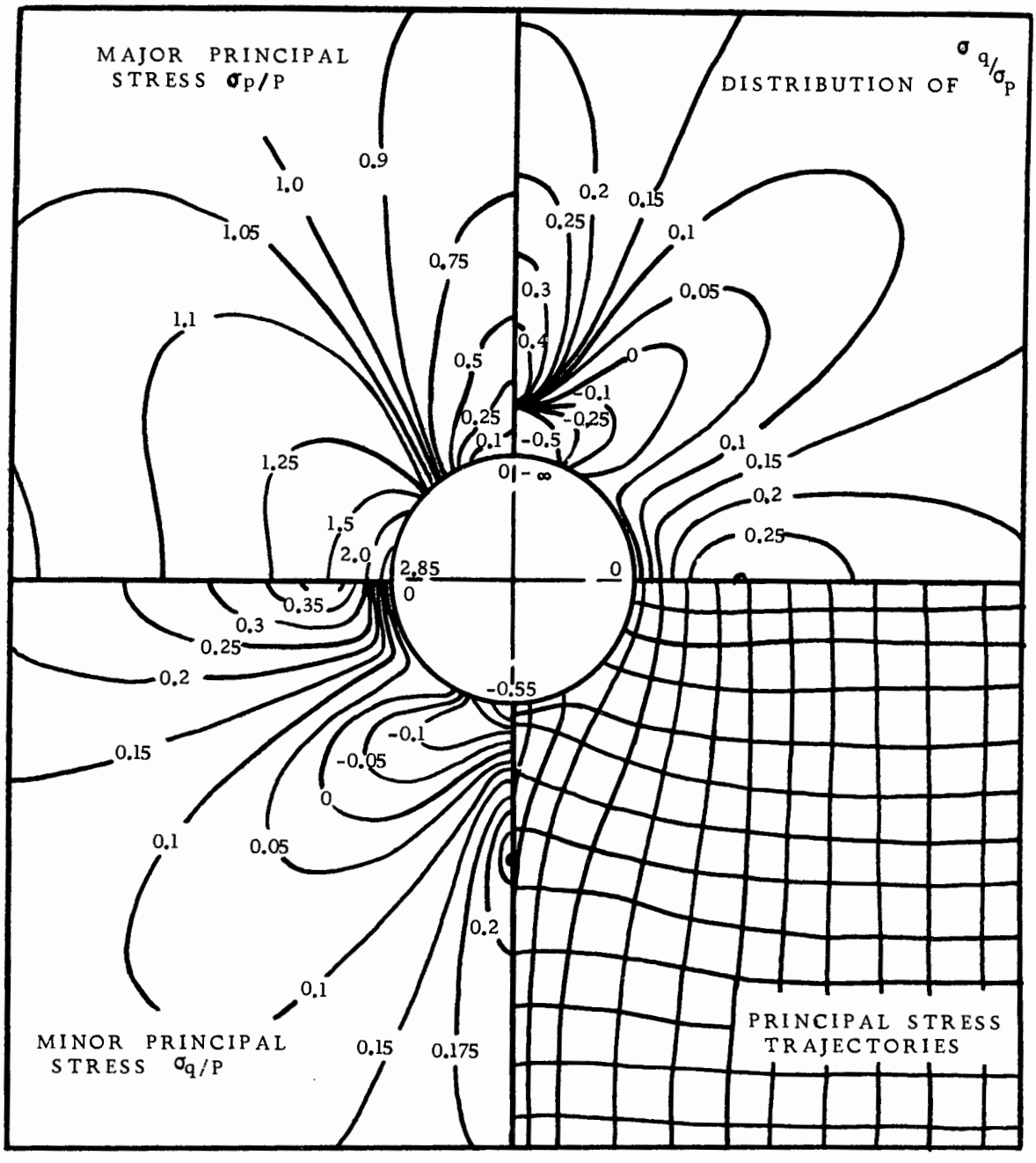

FIGURE 56

Distribution of principal stresses and principal stress trajectories in the material surrounding an unfractured hole

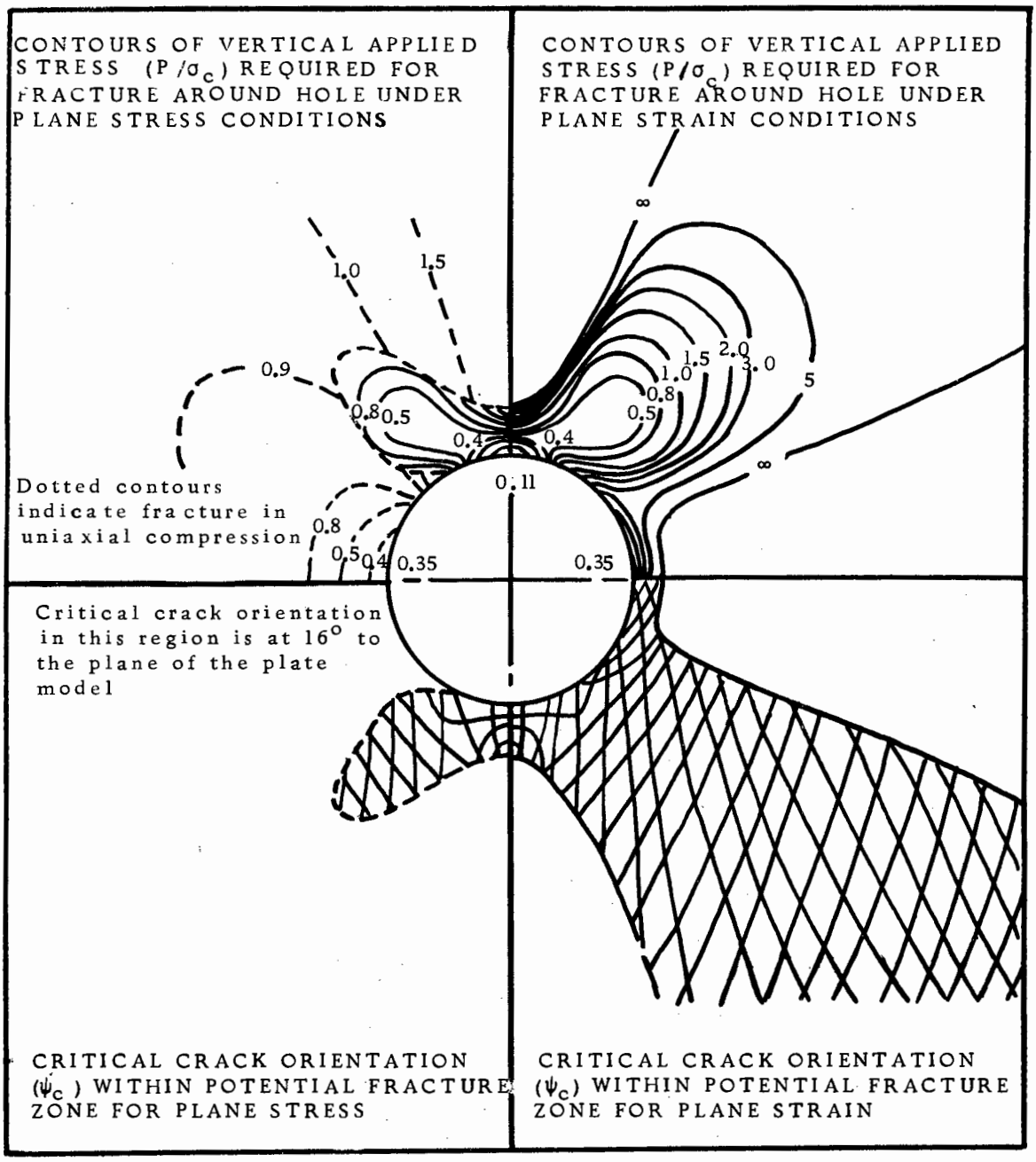

FIGURE 57

Fracture contours and critical crack orientations in the material surrounding an unfractured hole

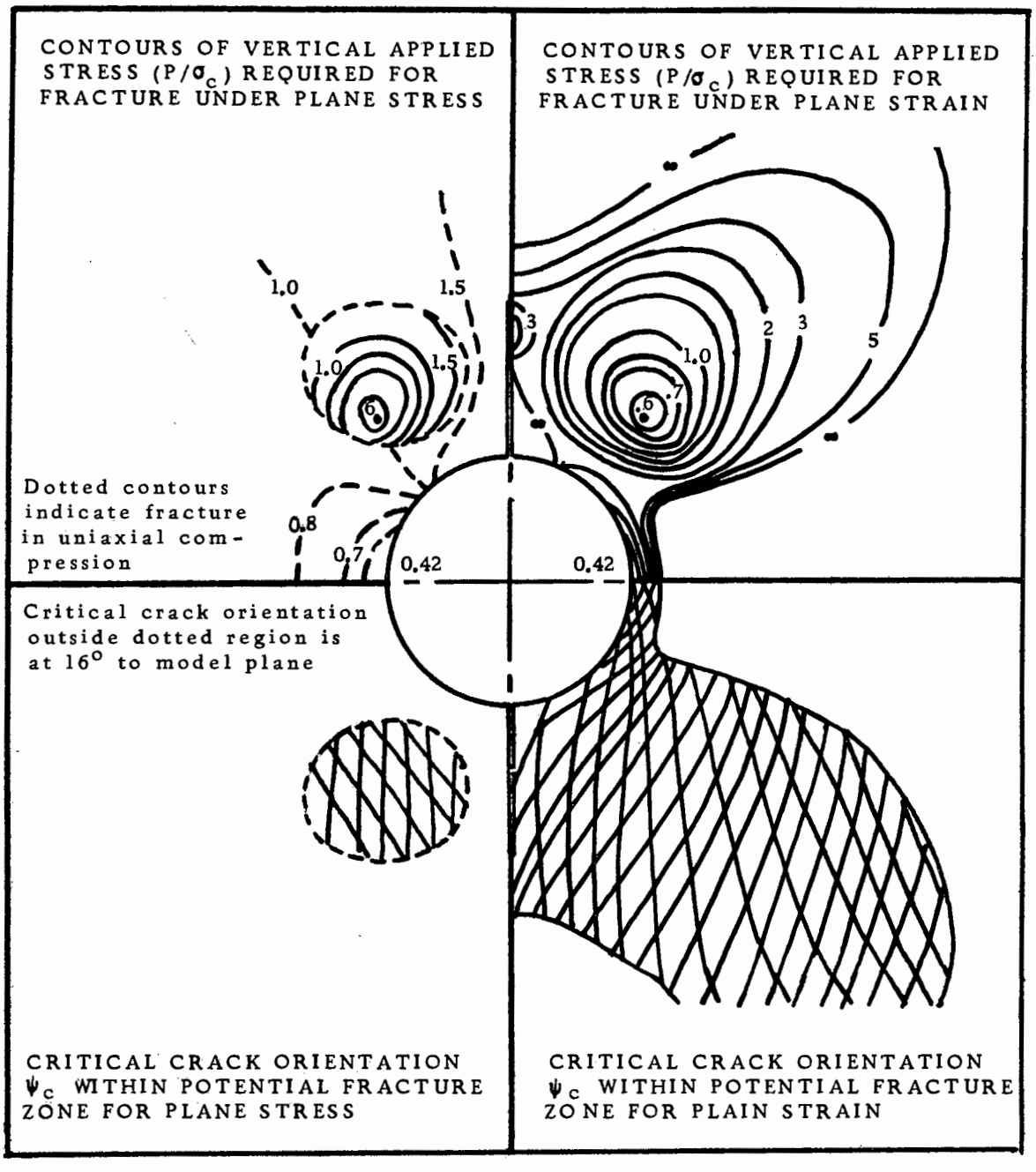

FIGURE 59

Fracture contours and critical crack orientations in the material surrounding a hole with roof and floor cracks

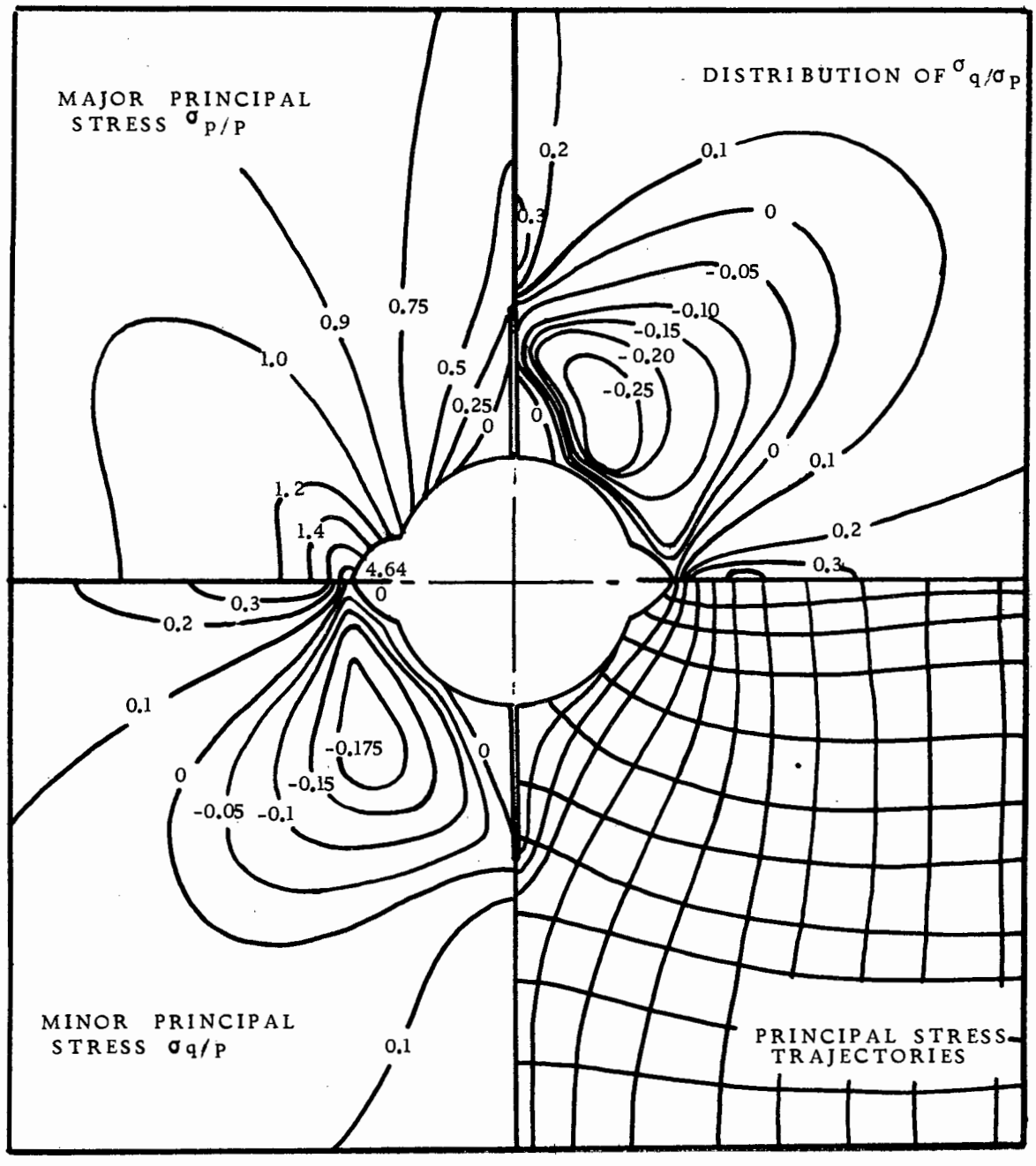

FIGURE 60

Distribution of principal stresses and principal stress trajectories in the material surrounding a hole with roof and floor cracks and sidewall fracture

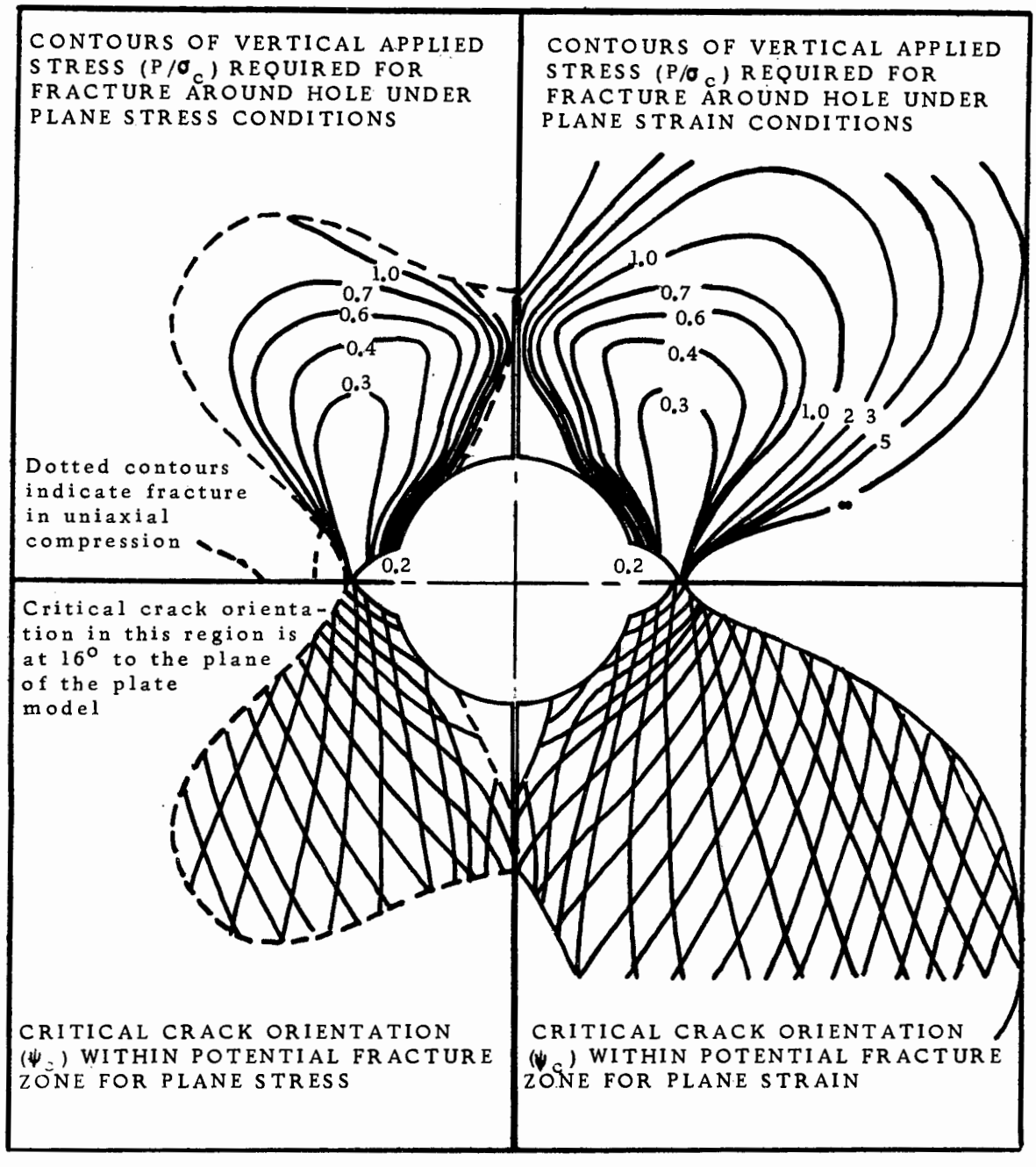

FIGURE 61

Fracture contours and critical crack orientations in the material surrounding a hole with roof and floor cracks and sidewall fracture

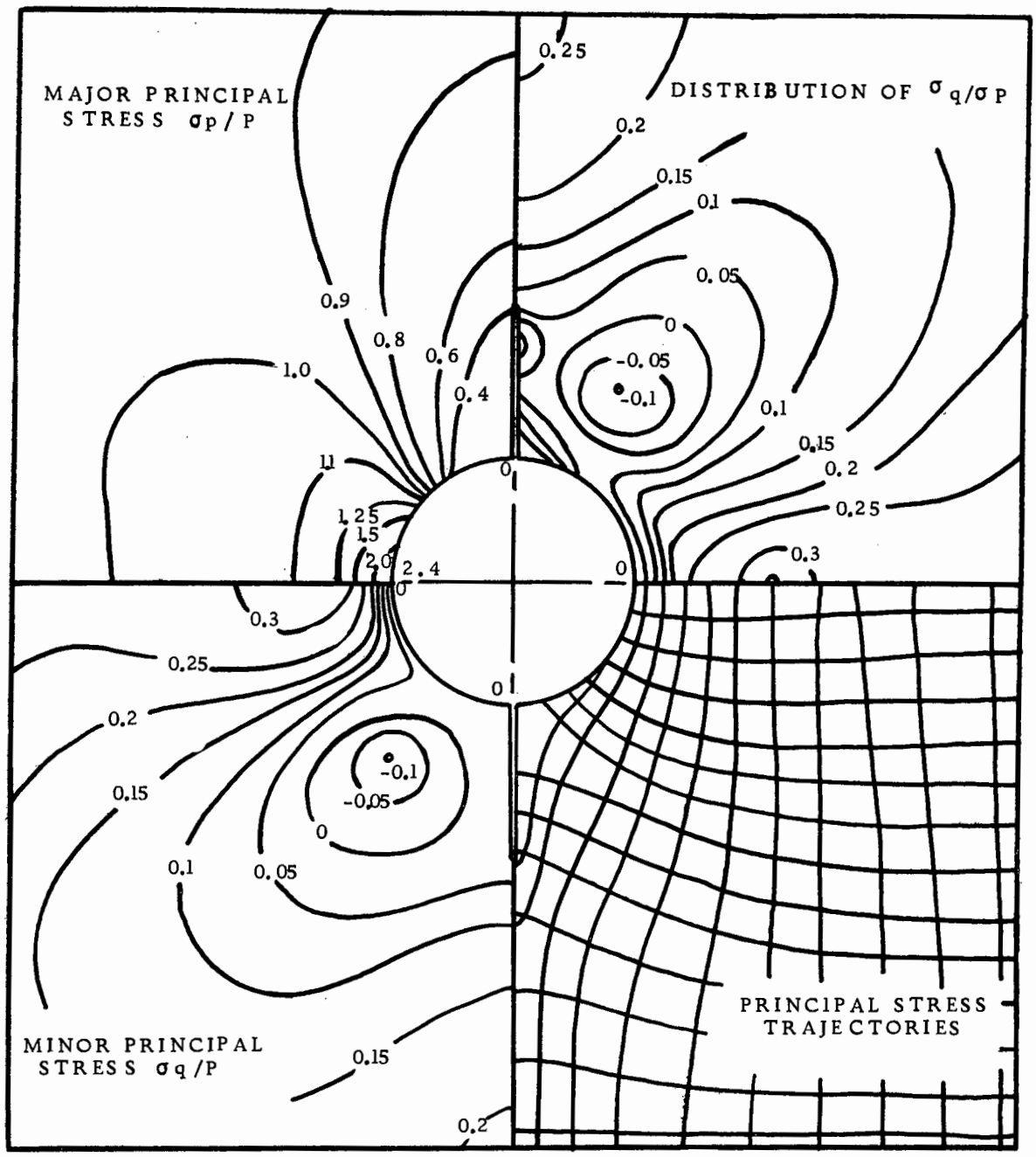

FIGURE 58

Distribution of principal stresses and principal stress trajectories in the material surrounding a hole with roof and floor cracks

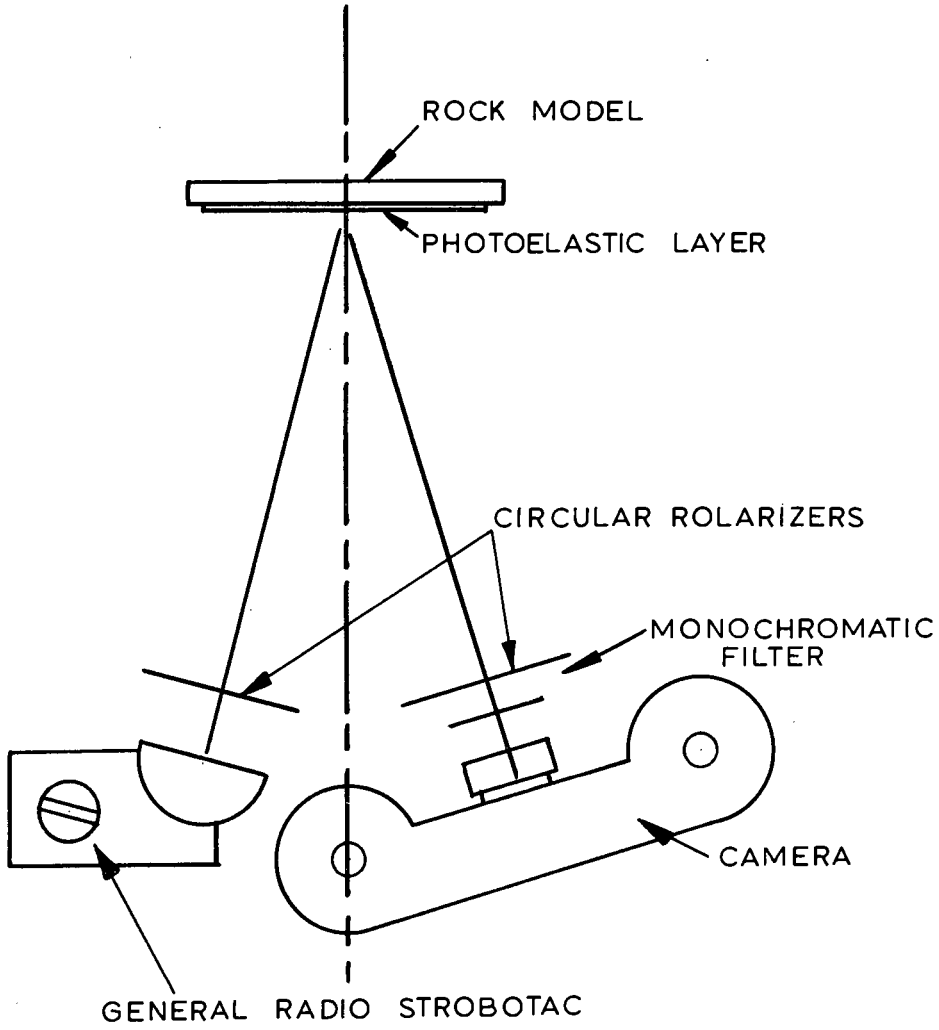

FIGURE 62

Arrangement for photography of photoelastic patterns during fracture of a rock plate model

15.5 Experimental study of fracture around a circular hole

The chert dyke plate model, illustrated in Figure 51, had one face covered with a layer of photoelastic material, bonded onto the model face by means of reflective cement*. The photoelastic pattern induced in the birefringent layer during loading of the model was photographed by means of the photographic arrangement illustrated diagrammatically in Figure 62**.

An oscillograph camera, fitted with a 50 mm Leica Summicron f2 lens, was run at a film speed of approximately 5 inches per second. A General Radio Strobotac was set to flash at 5 flashes per second at maximum flash intensity (2-3 microsecond flash duration). Since the camera shutter was kept open and the experiment was carried out in a darkened room, the film recorded the photoelastic fringe patterns at $^1/_5$ second intervals and the flash duration was sufficiently short to prevent blurring of the image due to movement of the film and propagation of the fracture.

A number of photographs, selected from the film exposed in one such experiment, are reproduced in Figure 63.

These photoelastic patterns were used to give a qualitative indication of fracture initiation and propagation in the model. This information is compared with the predicted behaviour, illustrated in Figures 56 to 61 in the following section.

Ideally, the information contained in the photographs reproduced in Figure 63 should have been used for the fracture analysis. However, separation of the principal stresses from these maximum shear strain contours represents a formidable experimental task which was not considered justified for this study.

15.6 Comparison of predicted and observed fracture in the material surrounding a circular hole

15.6.1 Tensile fracture in the roof and floor

The theoretical fracture contours presented in Figure 57 show

---

* Commercially available Budd Photostress type S material, 1 millimeter thick, and Budd reflective epoxy cement was used for this study.

** General Radio Handbook of High Speed Photography page 36.

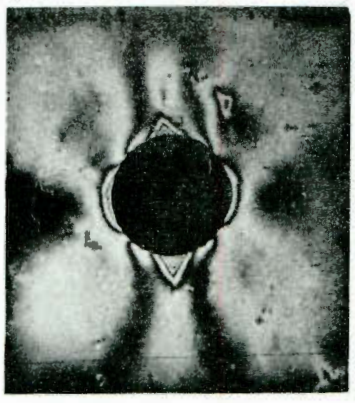

$P/\sigma_c = 0.30$

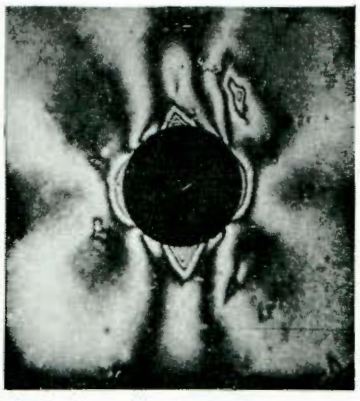

$P/\sigma_c = 0.35$

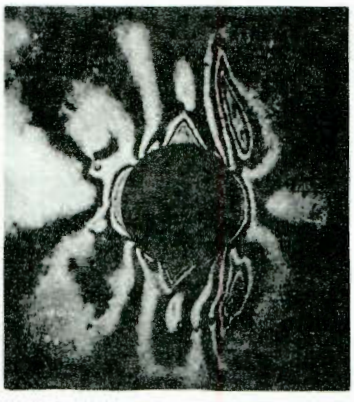

$P/\sigma_c = 0.38$

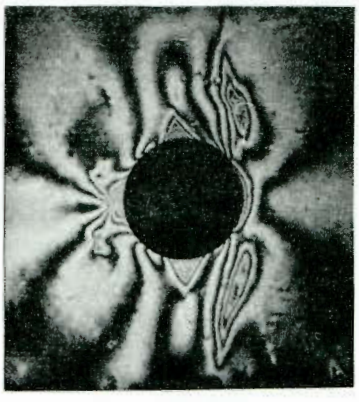

$P/\sigma_c = 0.40$

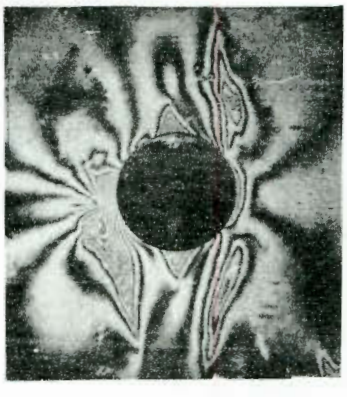

$P/\sigma_c = 0.42$

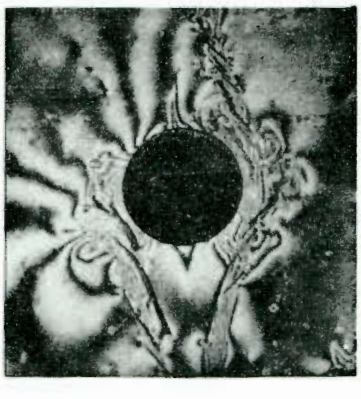

Failure $P/\sigma_c = ?$ — study for $P/\sigma_c = 0.4$ — model is [illegible]

FIGURE 63

Fracture propagation in the rock surrounding a circular hole in a plate model subjected to biaxial loading

that fracture of the roof and floor of the excavation should occur when the vertical applied stress $P/\sigma_c = 0.11$. In the chert dyke model, fracture at these points occurred at $P/\sigma_c = 1.07$, i.e. approximately 3% lower than predicted.

From the critical crack orientations shown in Figure 57, it can be anticipated that the roof and floor cracks will propagate along the vertical axis of symmetry of the model and the photoelastic patterns, reproduced in Figure 63, show this to be the case.

Note that, having formed, these roof and floor cracks show no tendency to propagate until complete failure of the model occurs. The stable crack length (from Figure 63) is found to be approximately 0.3 times the diameter of the hole as compared with 0.6 predicted from Figure 50. This discrepancy is attributed to the reinforcing effect of the photoelastic layer.

15.6.2 Fracture remote from the boundary of the opening

One of the most important consequences of the formation of the roof and floor cracks is the redistribution of stress which occurs in the material adjacent to the cracks. Particularly important is the isolated zone of tensile stress which is shown in Figure 58.

Figure 59 shows that fracture initiation in this zone, remote from the boundary of the excavation, can be expected to occur at $P/\sigma_c = 0.6$.

Figure 63 shows that fracture has initiated one of the four points, where fracture can be anticipated, at $P/\sigma_c = 0.30$ and that, at $P/\sigma_c = 0.38$, fracture is well developed in two of these regions.

While the qualitative agreement between the predicted and observed fracture initiation in the material remote from the hole boundary is remarkable, the early onset of failure is difficult to explain. It is believed that this discrepancy is due primarily to the inherent variation in the tensile strength of the material. The presence of a longer than

average "Griffith crack" within an isolated region of tensile stress can exert a significant influence upon the fracture behaviour in that region.

In contrast to the roof and floor cracks which do not propagate beyond their initial stable length, the failure remote from the hole boundary propagates with increasing stress level. The direction of fracture propagation is in good agreement with the critical crack orientations shown in Figure 59.

15.6.3 Fracture of the sidewalls of the circular opening

The fracture contours presented in Figure 59 show that fracture of the sidewalls of the circular opening can be anticipated at $P/\sigma_c = 0.42$. The photoelastic patterns reproduced in Figure 63 reveal that fracture of one sidewall occurred at $P/\sigma_c = 0.40$ while the other sidewall appears to be protected by the cracks remote from the boundary.

In analysing this fracture, it was assumed that the material within a wedge shaped region in the sidewall would be completely crushed and would not carry any stress. The shape of this wedge shaped region was determined from the critical crack orientations in this region (Figure 59) and from observations from previous model studies (Figure 64).

The photoelastic analysis of the stress distribution in a model with roof and floor cracks and sidewall fracture gave the results illustrated in Figure 60. A feature of these results is the further increase in the tensile stress in the region remote from the excavation boundary.

As a result of the sharp point formed by the wedge of fractured material in the sidewall, the stress concentration in this region rises sharply. The fracture contours plotted in Figure 61 show that the vertical applied stress required to propagate this fracture is $P/\sigma_c = 0.2$. Since fracture in the sidewall initiated at $P/\sigma_c = 0.4$, the increased stress concentration results in an unstable condition in which the fracture will propagate without any further

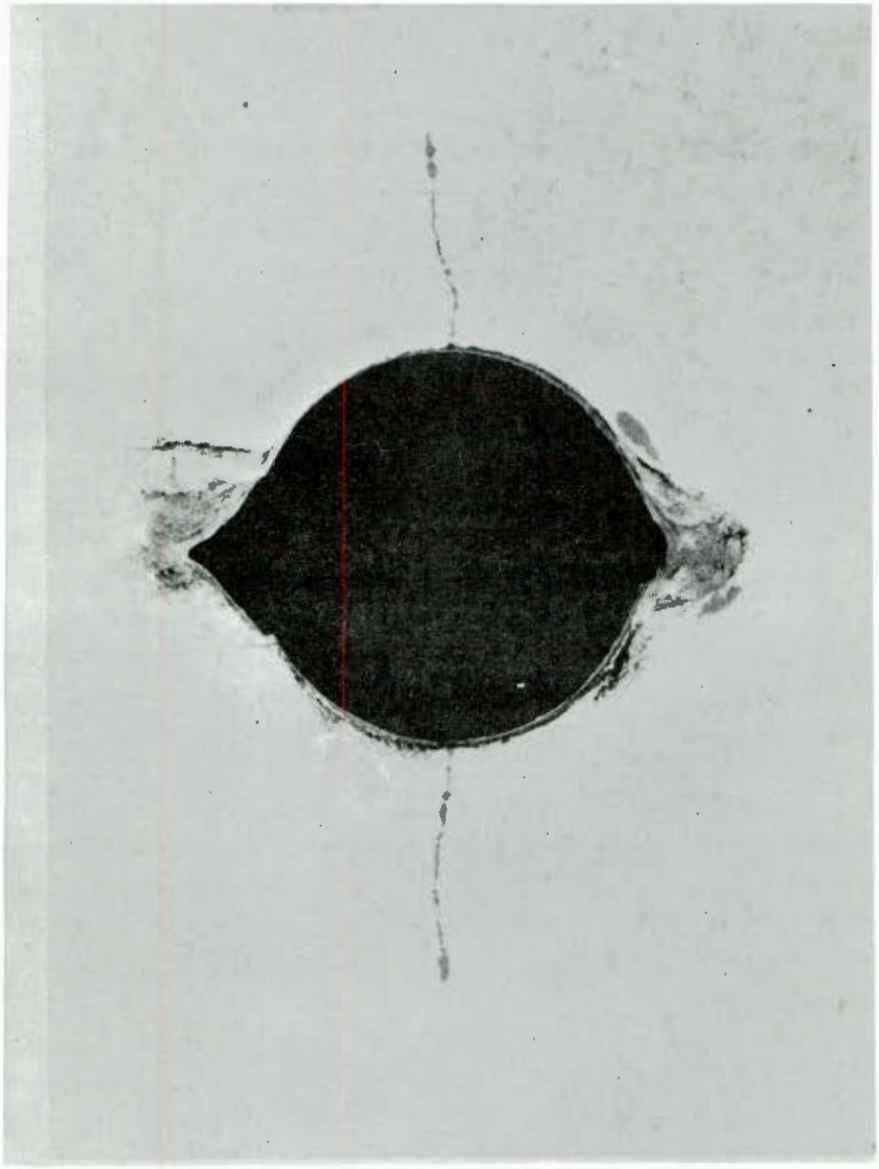

FIGURE 64

Fracture in the roof and floor and sidewalls of a circular hole in a rock plate model

increase in applied stress*.

In deciding upon the direction in which this fracture is liable to propagate the large zone of potential weakness ($^{P}/\sigma_{c}$ = 0.3) running parallel to the vertical axis of symmetry of the model (Figure 61) must be compared with the very high stress gradient along the horizontal axis of symmetry. Vertical rather than horizontal fracture propagation must be favoured because of the greater probability of having favourably oriented cracks in the larger volume of material. The presence of a fairly high horizontal tensile stress in this region (Figure 60) must also favour vertical fracture propagation.

Figure 63 shows that an abrupt change in the direction of fracture propagation occurred at $^{P}/\sigma_{c}$ = 0.42. As anticipated from the preceding discussion, the direction of fracture propagation is vertical rather than horizontal.

Considerable violence accompanied this final unstable fracture process and the final photograph in the series, taken $^{1}/5$ second after that at $^{P}/\sigma_{c}$ = 0.42, shows the model in the process of complete disintegration.

15.7 Discussion on the fracture of the material around a circular hole

The analysis presented in the preceding sections shows that the initiation and propagation of rock fracture in a complex stress field can be predicted if sufficient information on the fracture mechanism of the rock material and on the stress redistribution associated with fracture propagation is available.

A study of the predicted and observed fracture behaviour in the rock surrounding the circular hole reveals that fracture initiation and propagation occurs in regions in which the minor principal stress is either zero or tensile ($\sigma_{3} \leq 0$). Since Griffith's fracture theory offers a reliable basis for the

---

* The assumption that the material in the failed region is incapable of supporting any stress may be an oversimplification of actual conditions[388, 389].

prediction of rock fracture under these stress conditions, it becomes an important tool in the analysis of rock fracture phenomena in complex stress fields.

A feature of the fracture analysis presented in Figures 56 to 61 is the significant redistribution of stress which is associated with fracture propagation. These changes in the stress distribution are such that prediction of the final fracture pattern from the initial stress distribution in the unfractured material is not possible. Consequently, an understanding of rock fracture phenomena in complex stress fields requires a knowledge of the complete stress distribution at each stage in the fracture process.

Since the fracture mechanism of hard rock is governed by the ratio of the principal stresses acting upon the element under consideration, it is necessary to know the distribution of the individual principal stresses throughout the rock body. This requirement represents a major difficulty in the analysis of rock fracture problems since currently available techniques for the determination of individual principal stresses are difficult and time consuming.

The technique adopted by the author in this study suffers from the additional disadvantage that the boundary conditions must be drastically oversimplified in order to permit the application of the conducting paper analogy. Hence any load carrying capacity of the fractured material must be neglected and this may result in serious errors in the prediction of the final fracture pattern.

Ideally, the photoelastic patterns illustrated in Figure 63 could be used for the fracture analysis but, since the rock fracture mechanism bears no direct relationship to the maximum shear strain distribution in the material, this analysis would present formadible experimental difficulties.

It is evident that the analysis of rock fracture problems in mining and civil engineering will only be practical if the techniques adopted in this study can be considerably simplified. This simplification can only be successfully done if the basic mechanism governing rock fracture is adequately understood and it is believed that the Griffith's theory, reviewed in part I of this study, provides the basis for this understanding.

16. CONCLUSIONS

It has been shown that Griffith's theory of brittle fracture, modified to account for the effects of crack closure in compression, provides a reliable basis for the prediction of fracture in hard rock under static stress conditions.

Additional factors such as anisotropy, pore pressure and environment can exert a significant influence on rock strength but, provided that these factors are taken into account in the interpretation of rock fracture data, their influence can be explained on the basis of the Griffith's theory.

The Griffith's theory is particularly useful in the analysis of rock fracture in a complex stress field since it defines fracture behaviour under conditions in which the minor principal stress is tensile or zero. The study of fracture initiation and propagation in the rock surrounding a circular hole in a biaxial stress field has shown that the entire fracture process is associated with these stress conditions.

The redistribution of stress which occurs as a result of fracture propagation in a complex stress field has been shown to be a problem of major importance in the understanding of rock fracture phenomena. It is concluded that the successful analysis of practical rock fracture problems will depend upon the development of experimental techniques, particularly model studies, which can incorporate the effects of this stress redistribution.

---oooOooo---

APPENDIX A1

COMPLETE DERIVATION OF EQUATIONS GOVERNING FRACTURE INITIATION ACCORDING TO THE ORIGINAL GRIFFITH'S THEORIES

The tangential stress σ_η on the boundary of an elliptical crack, due to the application of the stresses σ_{xx} and τ_{xz} shown in Figure 1, is given by

$$\sigma_\eta = \frac{\sigma_{xx}\,(\text{Sinh } 2\xi_o + e^{2\xi_o}.\ \text{Cos } 2\eta - 1) + 2\tau_{xz}\, e^{2\xi_o}.\ \text{Sin } 2\eta}{\text{Cosh } 2\xi_o - \text{Cos } 2\eta} \quad ..(15)$$

Series expansion of the hyperbolic and trigonometric terms in this equation gives:

$$\text{Sinh } 2\xi_o = 2\xi_o + \frac{(2\xi_o)^3}{3!} + \frac{(2\xi_o)^5}{5!} + \ldots\ldots$$

$$e^{2\xi_o} = 1 + 2\xi_o + \frac{(2\xi_o)^2}{2!} + \frac{(2\xi_o)^3}{3!} + \ldots\ldots$$

$$\text{Cosh } 2\xi_o = 1 + \frac{(2\xi_o)^2}{2!} + \frac{(2\xi_o)^4}{4!} + \ldots\ldots$$

$$\text{Cos } 2\eta = \text{Cosh } i\,2\eta = 1 + \frac{(i2\eta)^2}{2!} + \frac{(i2\eta)^4}{4!} + \ldots\ldots$$

$$\text{Sin } 2\eta = \frac{\text{sinh } i\,2\eta}{i} = \frac{1}{i}\left\{ i2\eta + \frac{(i2\eta)^3}{3!} + \frac{(i2\eta)^5}{5!} + \ldots \right\}$$

Substitution of these expansions into equation (15) and, since both ξ_o and η are small at the crack tip, ignoring terms of the second order and higher which appear in the numerator, gives:

$$\sigma_\eta = \frac{\sigma_{xx}\left(2\xi_o + (1 + 2\xi_o) - 1\right) + 2\tau_{xz}\cdot(1 + 2\xi_o)\,2\eta}{(1 + 2\xi_o^2) - (1 - 2\eta^2)}$$

$$\sigma_\eta = \frac{2(\sigma_{xx}\cdot\xi_o + \tau_{xz}\cdot\eta)}{\xi_o^2 + \eta^2} \quad \ldots\ldots\ldots\ldots\ldots\ldots (16)$$

Note that the sign of ξ_o does not change and hence the sign of equation (16) depends upon the sign of η and of the normal stress σ_{xx}. When σ_{xx} is compressive (positive), the stress at the crack tip can only be tensile (negative) when η is negative and when $\tau_{xz}\cdot\eta > \sigma_{xx}\cdot\xi_o$.

Partial differentiation of equation (16) with respect to η gives

$$\frac{\partial\sigma_\eta}{\partial\eta} = \frac{2\tau_{xz}(\xi_o^2 + \eta^2) - 2(\sigma_{xx}\cdot\xi_o + \tau_{xz}\cdot\eta)\,2\eta}{(\xi_o^2 + \eta^2)^2}$$

The maximum and minimum values of σ_η occur when $\partial\sigma_\eta/\partial\eta = 0$ hence

$$\tau_{xz}\cdot\eta^2 + 2\sigma_{xx}\xi_o\cdot\eta - \tau_{xz}\xi_o^2 = 0.$$

Solving for η

$$\eta = -\xi_o \left\{ \frac{\sigma_{xx} \pm \sqrt{\sigma_{xx}^2 + \tau_{xz}^2}}{\tau_{xz}} \right\}$$

Substitution of these values of η into equation (16) gives the maximum and minimum values of σ_η, denoted by σ_N, as

$$\sigma_N = \frac{2\left(\sigma_{xx}\,\xi_o - \xi_o \left(\sigma_{xx} \pm \sqrt{\sigma_{xx}^2 + \tau_{xz}^2}\right)\right)}{\xi_o^2 \left\{ 1 + \left(\frac{\sigma_{xx} \pm \sqrt{\sigma_{xx}^2 + \tau_{xz}^2}}{\tau_{xz}} \right)^2 \right\}}$$

$$\sigma_N \cdot \xi_o = \frac{\tau_{xz}^2 \left(\pm \sqrt{\sigma_{xx}^2 + \tau_{xz}^2} \right)}{(\tau_{xz}^2 + \sigma_{xx}^2) \pm \sigma_{xx} \sqrt{\sigma_{xx}^2 + \tau_{xz}^2}}$$

Note that, from physical reasoning, this equation can only have two roots and hence it simplifies to

$$\sigma_N \cdot \xi_o = \frac{\tau_{xz}^2}{\sigma_{xx} \pm \sqrt{\sigma_{xx}^2 + \tau_{xz}^2}}$$

$$\sigma_N \cdot \xi_o = \frac{\left(\sigma_{xx} + \sqrt{\sigma_{xx}^2 + \tau_{xz}^2} \right)\left(\sigma_{xx} - \sqrt{\sigma_{xx}^2 + \tau_{xz}^2} \right)}{\sigma_{xx} \pm \sqrt{\sigma_{xx}^2 + \tau_{xz}^2}}$$

$$\sigma_N \cdot \xi_o = \sigma_{xx} \pm \sqrt{\sigma_{xx}^2 + \tau_{xz}^2} \qquad \ldots\ldots\ldots\ldots\ldots\ldots \quad (17)$$

Since it has been postulated that fracture occurs as a result of the tensile stress at the crack tip, only the negative solution of the above equation need be considered. Hence

$$\sigma_o \cdot \xi_o = \frac{-(\sigma_1 - \sigma_3)^2}{4(\sigma_1 + \sigma_3)} \quad \ldots\ldots\ldots\ldots (20)$$

which is only valid for $\sigma_3/\sigma_1 > -0.33$.

Fracture under uniaxial tensile stress conditions

Substitute $\sigma_1 = 0$ in equation (18)

$$\sigma_N \cdot \xi_o = \sigma_3 \left\{ \tfrac{1}{2}(1 + \text{Cos } 2\psi) \pm \sqrt{\tfrac{1}{2}(1 + \text{Cos } 2\psi)} \right\} \quad \ldots (21)$$

Maximum tensile stress occurs at the crack tip when the bracketted term on the right hand side of equation (21) is a maximum i.e. when Cos $2\psi = 1$ or $\psi = 0$.

Hence

$$\sigma_o \cdot \xi_o = 2\sigma_3 \quad \ldots\ldots\ldots\ldots\ldots (22)$$

Denoting the uniaxial tensile strength of the material by σ_t, equation (22) can be written as

$$\sigma_o \cdot \xi_o = 2\sigma_t \quad \ldots\ldots\ldots\ldots\ldots (23)$$

Fracture for $\sigma_3/\sigma_1 < -0.33$

When $\sigma_3/\sigma_1 = -0.33$, Cos $2\psi = 1$ from equation (19). Substituting this value into equation (18) gives

$$\sigma_o \cdot \xi_o = 2\sigma_3 \quad \ldots\ldots\ldots\ldots\ldots (25)$$

Since this is identical with equation (22), it can be deduced that fracture for $\sigma_3/\sigma_1 < -0.33$ occurs when

$$\sigma_3 = \sigma_t \quad \ldots\ldots\ldots\ldots (26)$$

Expressing equation (20) in terms of the uniaxial tensile strength σ_t from equation (23)

$$\sigma_t = -\frac{(\sigma_1 - \sigma_3)^2}{8(\sigma_1 + \sigma_3)} \quad \ldots\ldots\ldots (24).$$

APPENDIX II

APPARATUS FOR THE APPLICATION OF UNIFORMLY DISTRIBUTED TENSILE LOAD TO THE EDGES OF PLATE MODELS

The apparatus for applying uniformly distributed uniaxial tension to the edges of a 6 inch square plate model is illustrated in Figure A1.

Distribution of the load is achieved by means of a "whipple tree" arrangement of pin-jointed segments. The eight small segments which transmit the load onto the model are bonded onto the model edge with epoxy resin cement.

The model is loaded and the stress distribution studied photoelastically in the 12 inch diameter lens polariscope of the National Mechanical Engineering Research Institute, described in a 1961 publication by the author[195].

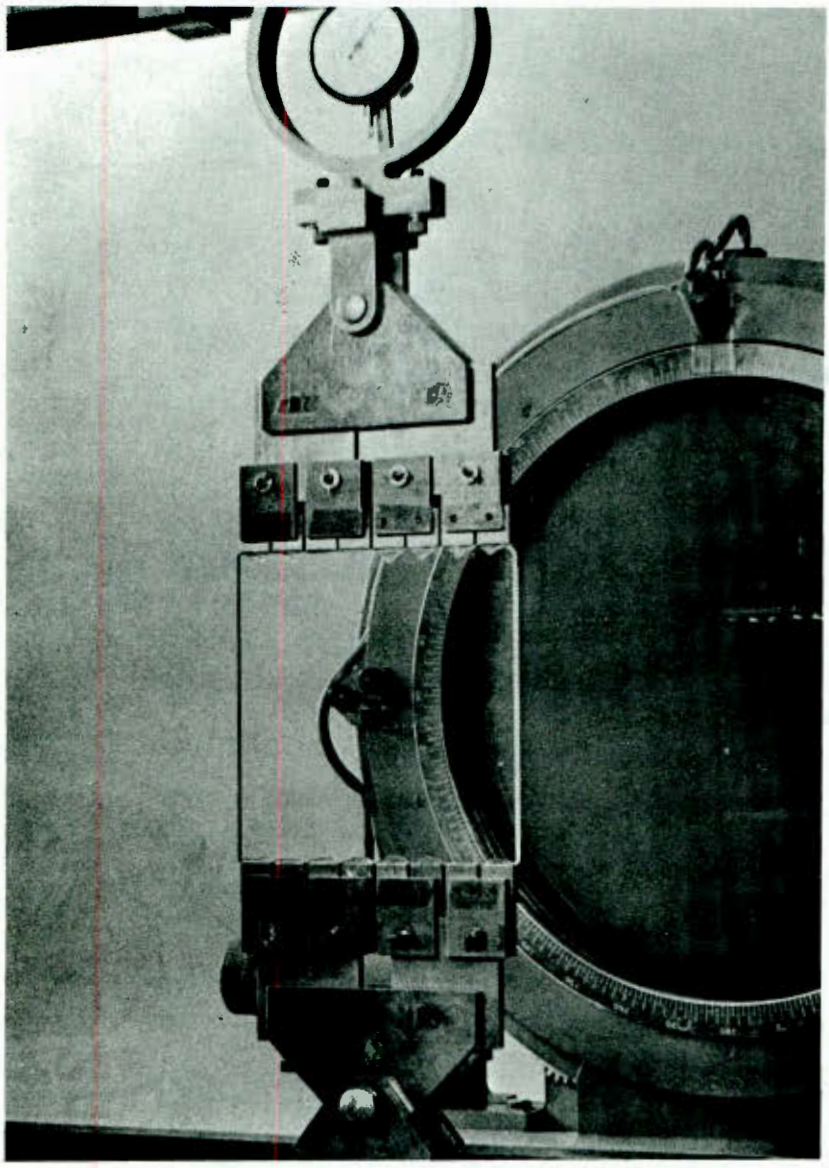

FIGURE A 1

Apparatus for subjecting plate models
to uniaxial tension

APPENDIX III

APPARATUS FOR SUBJECTING PLATE MODELS TO UNIFORMLY DISTRIBUTED BIAXIAL COMPRESSION

The apparatus described in this Appendix was designed primarily for model studies of the type described in Part III of this study. However, it has also proved useful in the fundamental fracture studies discussed in section 12 of Part II.

1. DESIGN REQUIREMENTS

The basic requirements, upon which the design of this apparatus was based, are as follows:

(a) The apparatus is required to apply uniformly distributed loads to the edges of 6 inch square x $\frac{1}{4}$ inch thick plate models.

(b) The load distribution should not change with increasing load, even if the deformation of the edge of the model is fairly severe.

(c) The vertical and horizontal loads should bear a constant ratio to one another throughout the loading cycle.

(d) Since hard rock models are to be loaded to destruction, the apparatus should be capable of applying loads of the order of 100 000 lb.

(e) Provision must be made for load or restraint to be applied to the faces of the model to prevent buckling and to induce plane strain conditions.

2. LOAD DISTRIBUTION MECHANISM

The load distribution mechanism, which was found to meet most of the requirements outlined above, involves the use of loading elements such as that illustrated diagrammatically in Figure A2.

The half inch thick semi-circular segment is attached to the outer frame by means of eight copper-beryllium leaf springs. These springs keep the segment in place and restrain it from

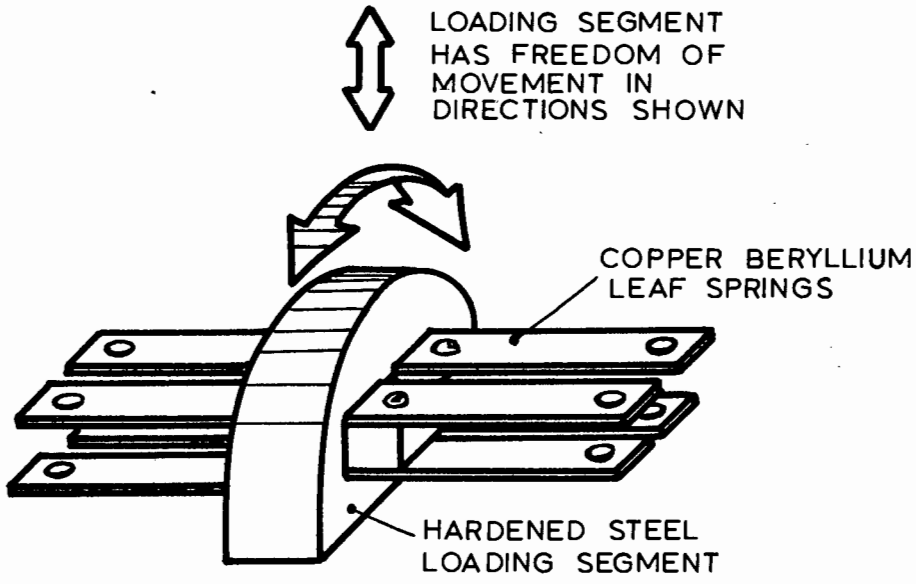

FIGURE A 2

Basic loading segment used to distribute load in the bi-axial loading apparatus

movement in all except the directions indicated on Figure A2.

Eight small segments rest on the edge of the model and these are loaded through four larger segments. These, in turn are loaded through two even larger segments which transmit the load from the largest main segment through which the load is applied. The complete assembly is illustrated in Figure A3 and in the photograph reproduced in Figure A4.

The individual segments, designed photoelastically, are machined from EN 25 steel, hardened and tempered to an ultimate strength of approximately 140 000 lb/sq. in. The copper beryllium springs are screwed onto projections on the sides of the segments as illustrated in Figure A4.

A strip of $^{1}/_{32}$ inch thick gasket material and a strip of 0.005 inch steel shim are placed between the eight small segments and the edge of the model. The gasket material compensates for small irregularities such as particles of grit which find their way between the loading elements and the model edge. The steel shim, placed between the gasket material and the model edge, prevents extrusion of the gasket material from inducing tensile stresses in the plate edge and thereby causing the model to split parallel to its faces.

The frame, which carries the four stacks of loading segments, is split diagonally as illustrated in Figure A4. Removal of the eight Allen screws, which hold the two halves together, permits the model to be rapidly and accurately located in the frame. The dimensions of the model are slightly greater than the free distance between the opposite sets of loading segments and hence, when the frame is reassembled, the model is held in place by the deformed copper-beryllium springs.

Experience has shown that, even if the model is severely cracked and deformed, the loading arrangement described above will maintain a uniform distribution of the load on the model.

3. PROVISION OF RESTRAINT NORMAL TO THE MODEL PLANE

It is necessary to provide restraint normal to the model plane in

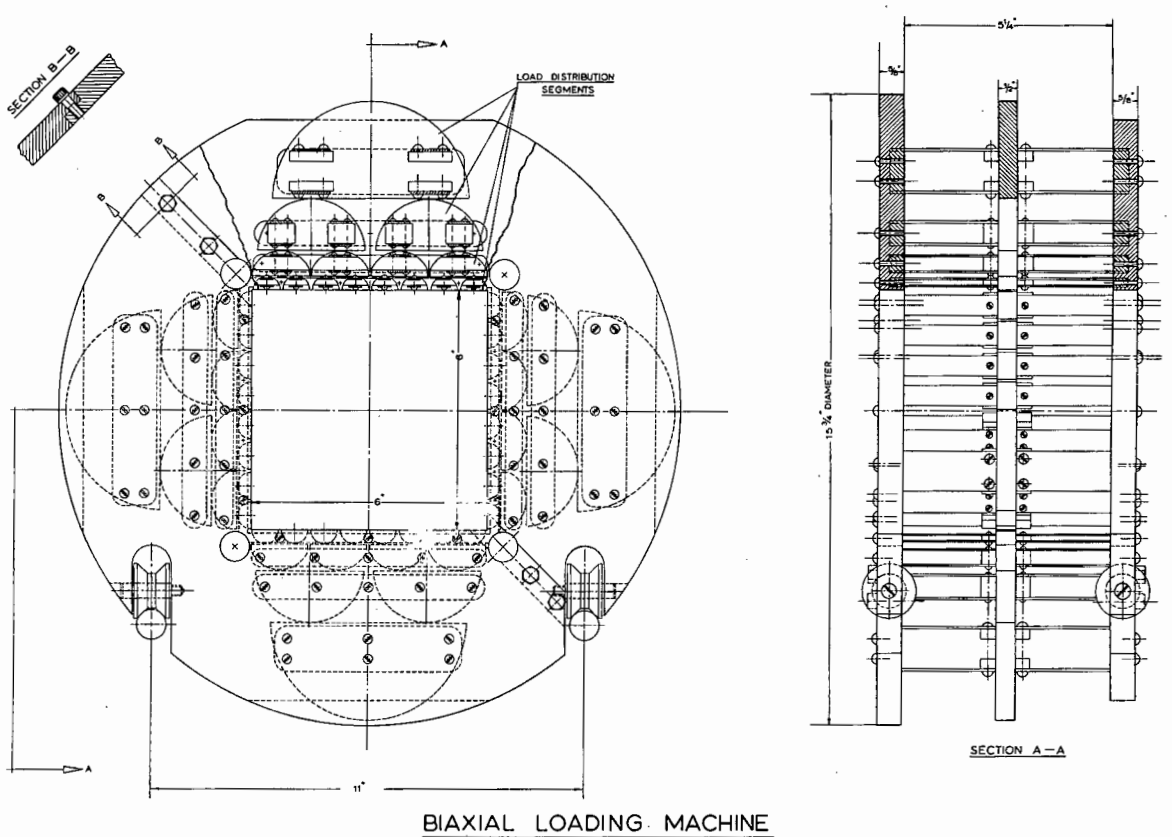

FIGURE A 3

Details of biaxial loading frame

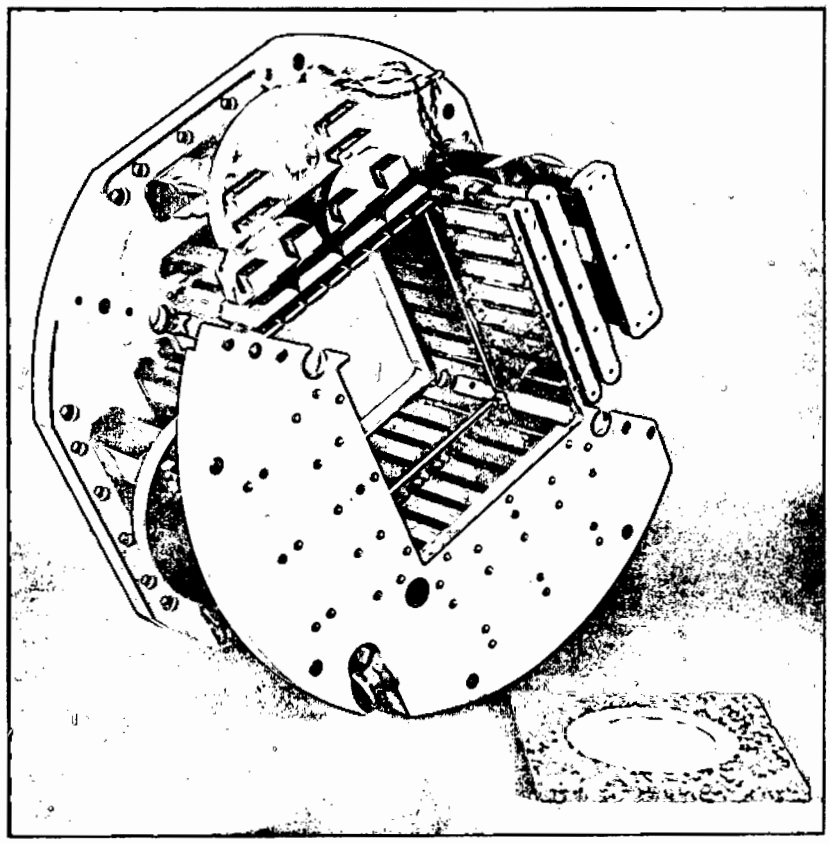

FIGURE A 4

Partially dismantled biaxial loading frame showing details of the load distribution mechanism

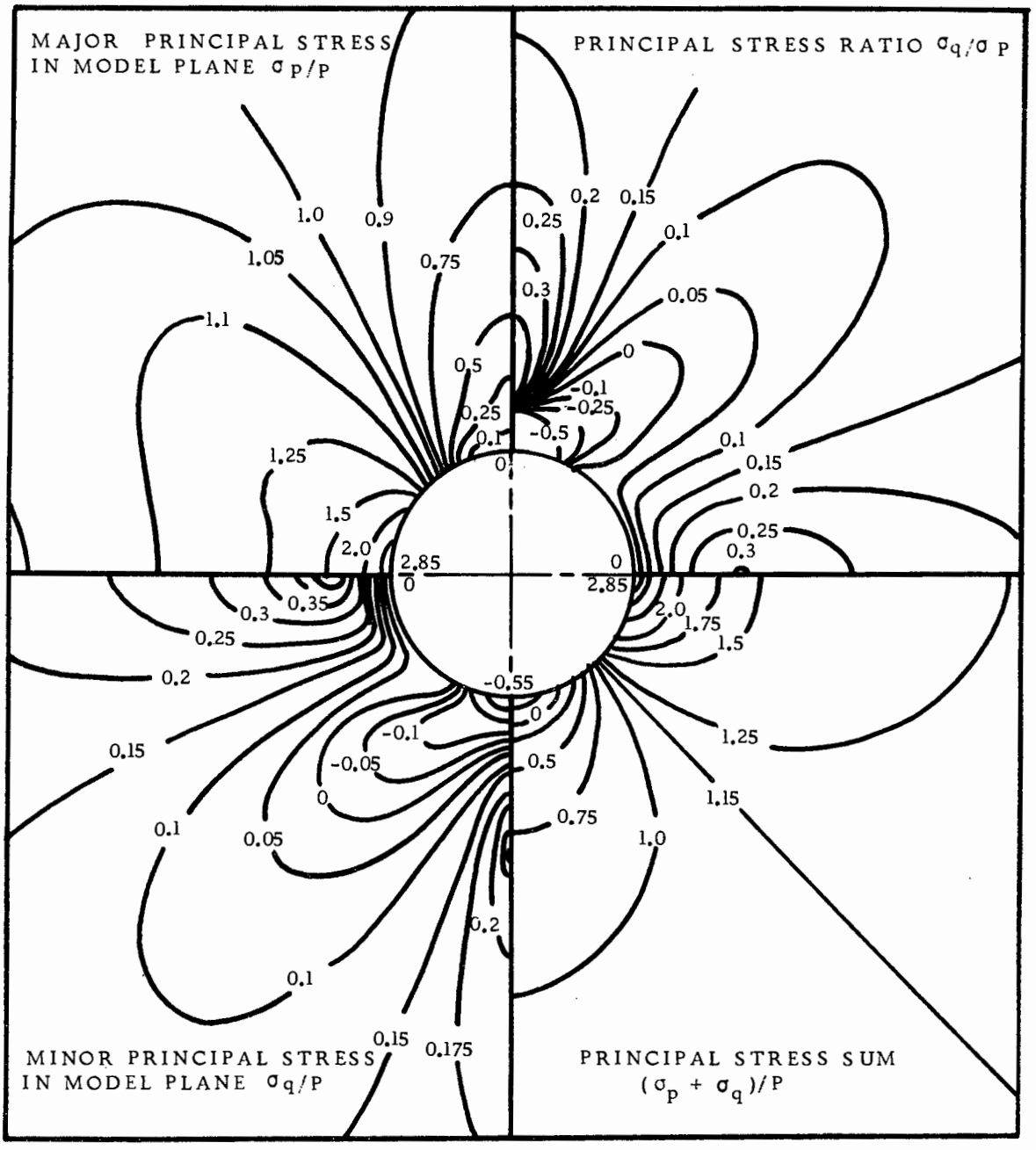

FIGURE A 5

Principal stress distribution in a plate model subjected to a vertical applied stress P and a horizontal applied stress of 0.15 P

order to

(a) Prevent buckling of the model.

(b) Induce approximately plane strain conditions in area where both principal stresses in the model plane are compressive.

Since the first requirement is likely to be automatically satisfied if the second can be met, only the latter requirement need be considered in detail. The problems involved and the possible means of solution are best dealt with by means of a practical example.

Consider the case of a plate model, containing a central circular hole, subjected to a vertical applied stress P and a lateral applied stress 0.15 P. The major and minor principal stresses in the model plane are defined as σ_p and σ_q respectively and the principal stress normal to the model plane as σ_n. The distributions of the principal stresses in the model plane, the principal stress ratio σ_q/σ_p and the principal stress sum $(\sigma_p + \sigma_q)$ are illustrated in Figure A5.

3.1 Fracture under plane stress conditions

Under plane stress conditions the stress normal to the plate surface σ_n is zero. Consequently the minor principal stress in the model plane is only algebraically smallest of the three principal stresses when it is tensile. Hence

$$\text{for } \sigma_n = 0, \quad \sigma_q = \sigma_3 \quad \text{when } \sigma_q < 0.$$

$$\text{and} \quad \sigma_n = 0 = \sigma_3 \quad \text{when } \sigma_q > 0$$

Since, according to the fracture theory postulated in part I of this study, fracture occurs as a result of the combination of the principal stresses σ_1 and σ_3, it follows that, when $\sigma_q > 0$, fracture will depend on the normal stress σ_n. This type of fracture cannot be regarded as representative of that which occurs around an underground excavation.

3.2 Fracture under plane strain conditions

Under plane strain conditions, the thickness of the plate remains constant.

Hence

$$\varepsilon_n = 0$$

and $$\sigma_n = \nu (\sigma_p + \sigma_q)$$

Since the value of Poisson's ratio for most hard rocks is small, approximately 0.15, it will be seen from Figure A5 that σ_n is not always greater than σ_q. However, when $\sigma_n < \sigma_q$, the principal stress ratio σ_3/σ_1 is generally larger than 0.2. From section 8.5 in part I it can be deduced that hard rocks will not fracture at such high principal stress ratios and hence the fact that $\sigma_n < \sigma_q$ in certain areas is of little practical importance.

When $\sigma_n > \sigma_q$, $\sigma_q = \sigma_3$ and fracture will occur as a result of the stresses in the model plane.

While this deduction is only strictly true for the particular example considered, experience suggests that it will also be generally true for most of the models which will be loaded in this machine.

3.3 Application of stress normal to the model plane

A possible means of achieving the fracture conditions outlined above is to apply a stress normal to the model plane. Obviously this stress cannot vary continuously across the model surface and hence a uniformly distributed stress has to be chosen to satisfy the requirements of section 3.2.

Suppose that a uniformly distributed normal stress σ_n of 0.3 P can be applied to the surface of the model considered earlier. From Figure A5 it will be seen that $\sigma_n > \sigma_q$ except in small regions where, in any case, $\sigma_3/\sigma_1 > 0.2$.

On the top and bottom of the hole, $\sigma_p = 0$ and hence $\sigma_n = 0.3\ P = \sigma_1$. However since $\sigma_3/\sigma_1 = -0.55/0.3 < -0.33$, the tensile fracture of the roof and floor of the excavation will not be influenced (see section 6.2.4 of Part I).

From this discussion it can be deduced that, provided care is exercised in choosing the constant normal stress σ_n which is applied to the plate surface, fracture conditions identical to those which apply under plane strain can be induced in the model.

Application of a uniform hydraulic pressure to the model surface does not present too many practical difficulties. Some form of membrane would be required in order to prevent the hydraulic fluid from entering the model material. The design of this membrane would present the greatest difficulty since it would be required to span the excavation and to remain intact during the fracturing of the model. In addition, since it is desirable to observe the fracture process in the model, this membrane should be transparent.

3.4 Application of restraint normal to the model plane

An alternative method for inducing plane strain conditions in the model is to provide restraint which will prevent the model from becoming thicker. Obviously it would be very difficult to prevent the model from becoming thinner but, since this can only occur when one of the principal stresses in the model plane is tensile, no practical advantage would have been gained if this were achieved.

In order to prevent the model from becoming thicker, very rigid restraint must be applied normal to the plate surface. It may be possible to provide sufficient restraint by clamping the model between two thick sheets of armourplate glass, held in steel frames and tied together by means of high tensile bolts. In designing the frame illustrated in Figure A4, space was left for such a restraining device.

The principal difficulty associated with this type of restraint is the friction force which would occur between the glass and model surfaces. It may be possible to minimise these by inserting thin sheets of low friction material such as polytetrafluroethylene* between the glass plates and the model.

At the time of writing, neither of the methods described in sections 3.3 or 3.4 have been tried in practice. However, it is

---

* Commercially available under the trade names "Teflon" or "Fluon".

felt that the practical difficulties associated with these techniques will be overcome in time and that a solution to the problem of inducing conditions equivalent to plane strain in the model will be found.

4. LOAD APPLICATION

The complete loading frame, in which the load distribution frame described in section 2 of this Appendix is loaded, is illustrated in Figure A6.

Two vertical and two horizontal jacks apply the load onto the four main segments of the load distribution arrangement. These four jacks are held between two $^{3}/_{4}$ inch thick steel rings by means of high tensile bolts. The entire system is designed to operate at a maximum hydraulic pressure of 10 000 lb/sq. in. At this pressure the jacks will each exert a maximum thrust of 100 tons. Since this magnitude of load has not been found necessary in the model studies carried out to date, a 5 000 lb/sq. in variable volume hydraulic pump is used to generate the hydraulic pressure for the jacks. However, should it prove necessary, a 10 000 lb/sq. in pump is also available.

Four jacks rather than two have been used in order to eliminate any transfer of load from the vertical to the horizontal system or vice versa. The design of the jack cylinder and piston is diagrammatically illustrated in Figure A7.

The main cylinder, the bore of which is ground, is designed to withstand a maximum hydraulic pressure of 10 000 lb/sq. in. In the case of the horizontal jacks, a secondary cylinder can be screwed into the main cylinder as illustrated in Figure A7. A range of such secondary cylinders, having different inside diameters and matched pistons, is available.

When the vertical cylinders are fitted with pistons which slide on the walls of the main cylinder and the horizontal jacks are fitted with smaller pistons which move in secondary cylinders, a constant ratio of vertical to horizontal applied load is achieved with a common oil pressure supply.

The moving seal illustrated in Figure A7 was adapted from a

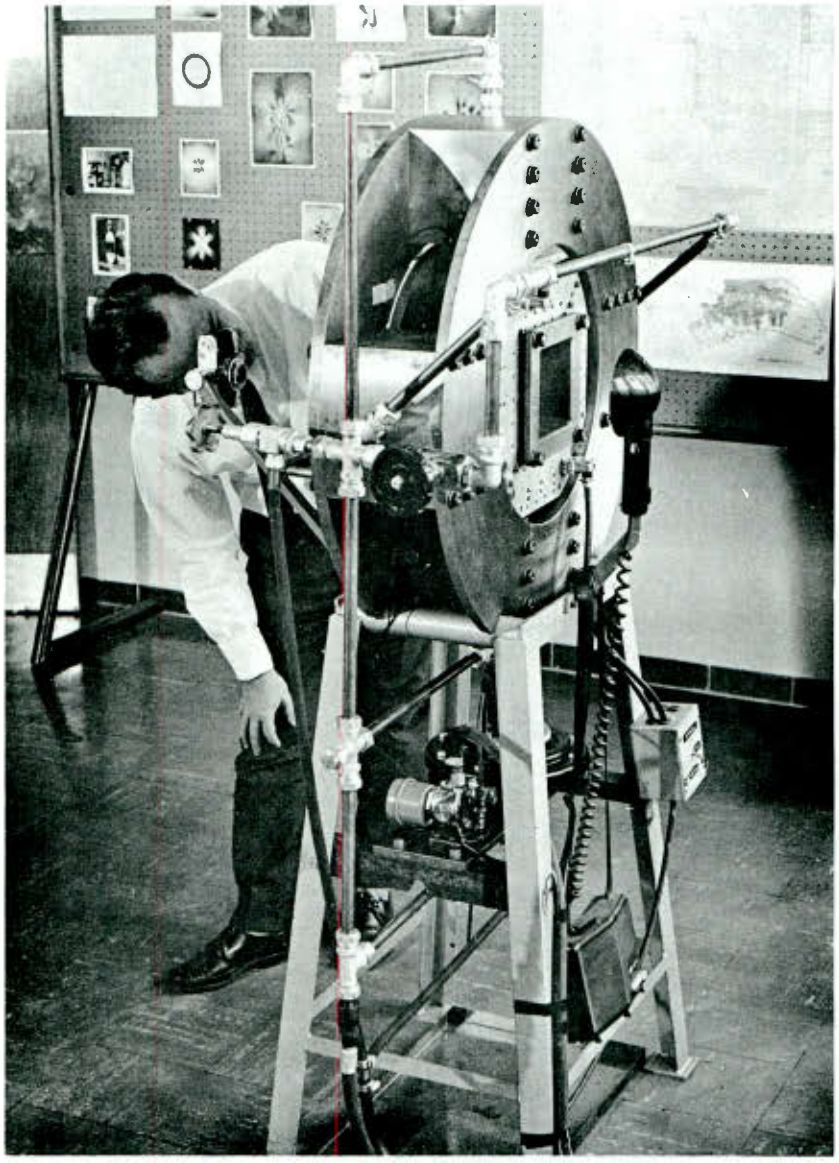

FIGURE A 6

Apparatus for subjecting plate models
to biaxial compression

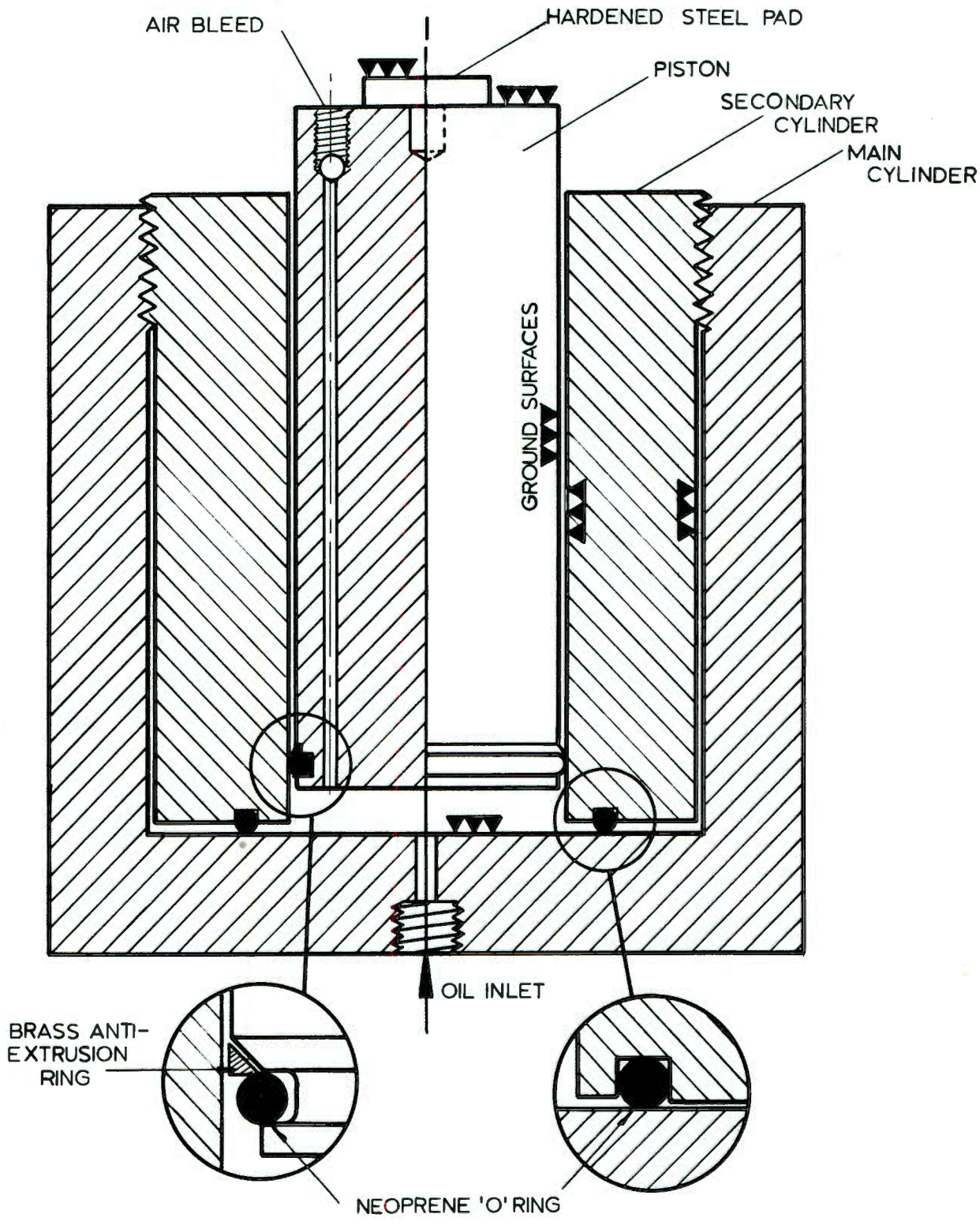

FIGURE A 7

Details of hydraulic jack design.

design evolved by the National Engineering Laboratory of the Department for Scientific and Industrial Research in Britain. This seal depends upon a wedge-shaped anti-extrusion ring for its high pressure sealing. This ring is made from a soft metal such as brass in order that the ground cylinder walls are not scored. Experience has shown that this seal is effective for pressures of up to 50 000 lb/sq. in (the maximum used by the author in triaxial testing on rock) and that it has very low friction characteristics. Measurements have shown that the loss due to friction is generally less than 1% of the applied hydraulic pressure.

5. HYDRAULIC CIRCUIT

The complete hydraulic circuit used in the biaxial loading machine described above is illustrated in Figure A8.

The pressure is generated by means of a variable volume 5 000 lb/sq. in pump which is driven at 900 revolutions per minute. by a 3 horsepower motor. The pump has five pistons driven by means of a swash-plate. The volume delivered is controlled by changing the swash-plate angle and hence the pump stroke. The flow can be reversed by altering the swash-plate setting and this is useful for drawing the pistons back into the cylinders after a test has been completed.

In normal operation the volume delivery is fixed at a convenient value and control of the pressure is achieved by means of a bypass needle valve. It has been found that very accurate control of the load is possible if care is taken in the choice of the pump delivery.

The oil pressure is delivered to all four loading jacks as illustrated in Figure A8. For uniaxial testing, the horizontal jacks can be isolated by means of a high pressure valve. For biaxial loading, the secondary piston and cylinder sets described in the previous section are fitted into the horizontal jacks.

In order to provide sudden relief of the load when the model fails, a diaphragm actuated high pressure valve is incorporated in the circuit. This diaphragm valve is kept closed by means of compressed air which is supplied through a solenoid valve. When the movement of the vertical jack exceeds a preset valve, a micro-

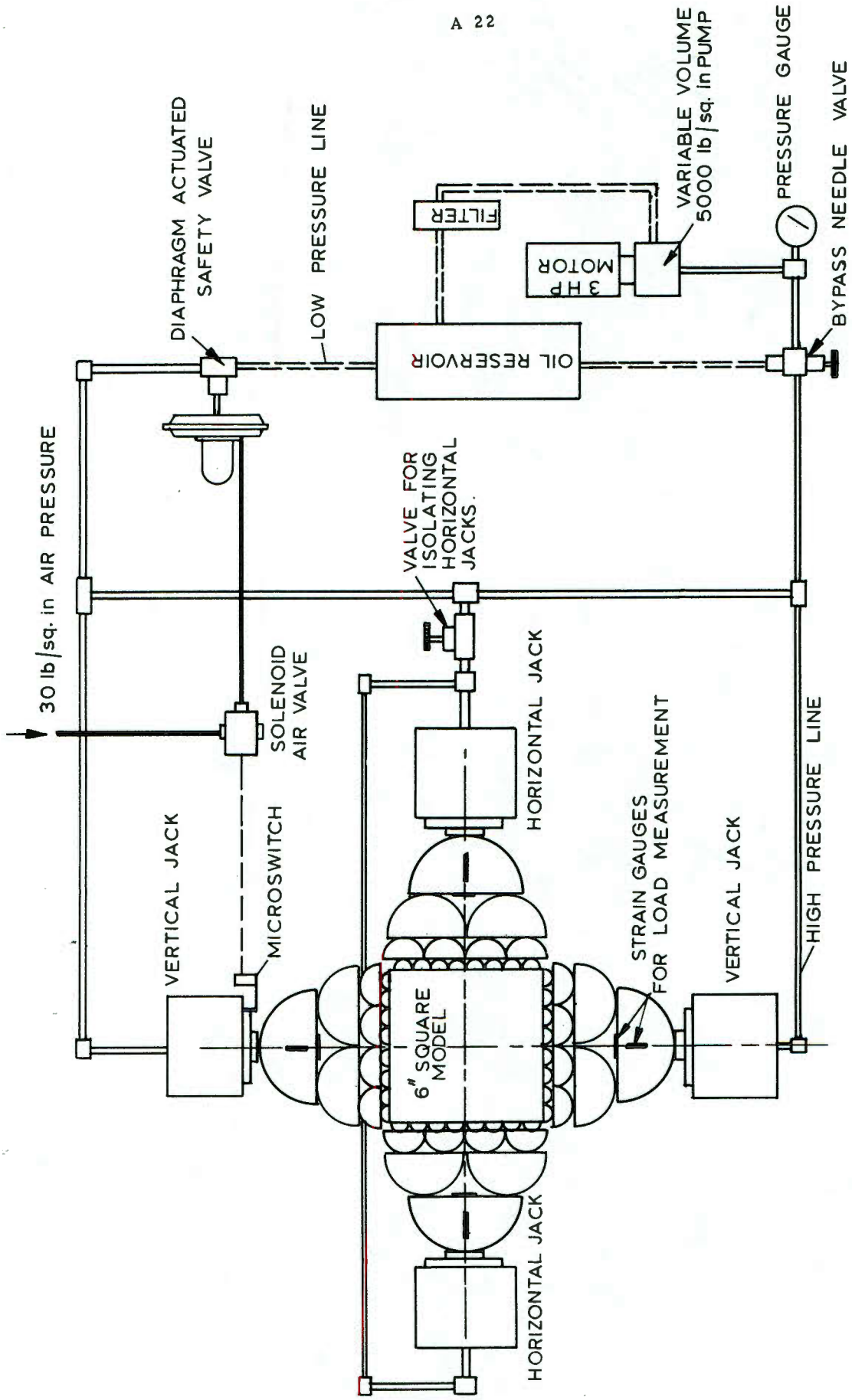

FIGURE A 8

Hydraulic circuit for biaxial loading machine

switch is actuated and this operates the solenoid valve and thereby relieves pressure on the diaphragm valve.

6. LOAD MEASUREMENT

In order to measure the load applied to the model, strain gauges are attached to the main loading segments at the positions indicated in Figure A8. These gauges are connected in a Wheatstone bridge and the resistance change with load measured by means of a digital voltmeter (10 microvolt resolution). This measuring system has been calibrated to give direct load readout in tens of pounds.

7. EXAMPLES OF LOADING ACCURACY

Probably the most sentitive test for the loading accuracy in a machine of this type is given by the photoelastic pattern around a circular hole in a plate subjected to equal vertical and horizontal loads. The theoretical isochromatics (maximum shear stress loci) are circles, concentric with the hole in the model. The photoelastic isochromatics obtained by subjecting a glass plate model, containing a central circular hole, to hydrostatic compression are illustrated in Figure A9.

A further example of the accuracy of load distribution which can be achieved with this machine is illustrated in Figure A10. This figure shows the photoelastic isochromatics induced in a glass plate, containing a central square hole, subjected to hydrostatic compression. The symmetry of this pattern gives a good indication of the loading accuracy.

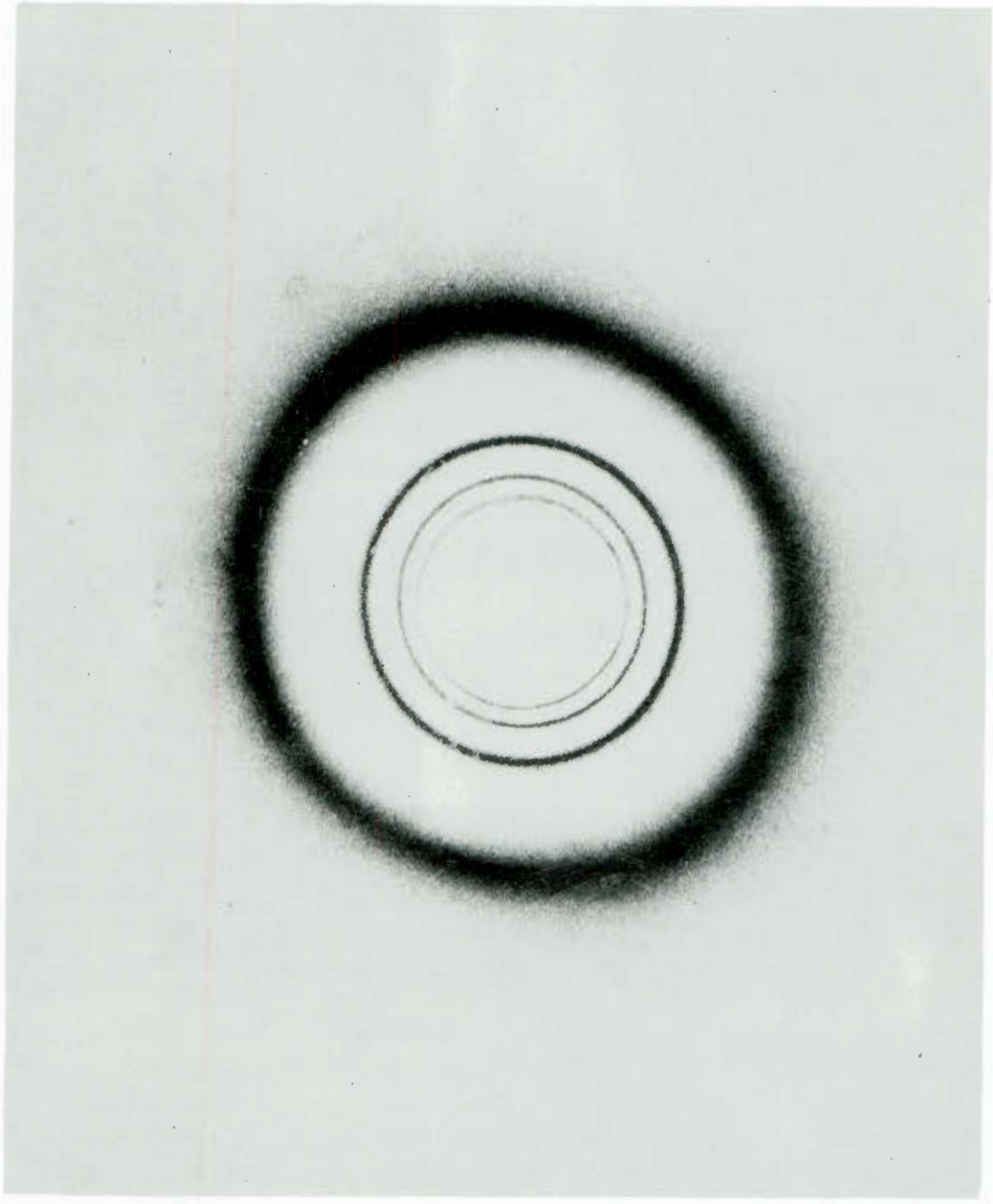

FIGURE A 9

Photoelastic isochromatics around a circular hole in a hydrostatic stress field

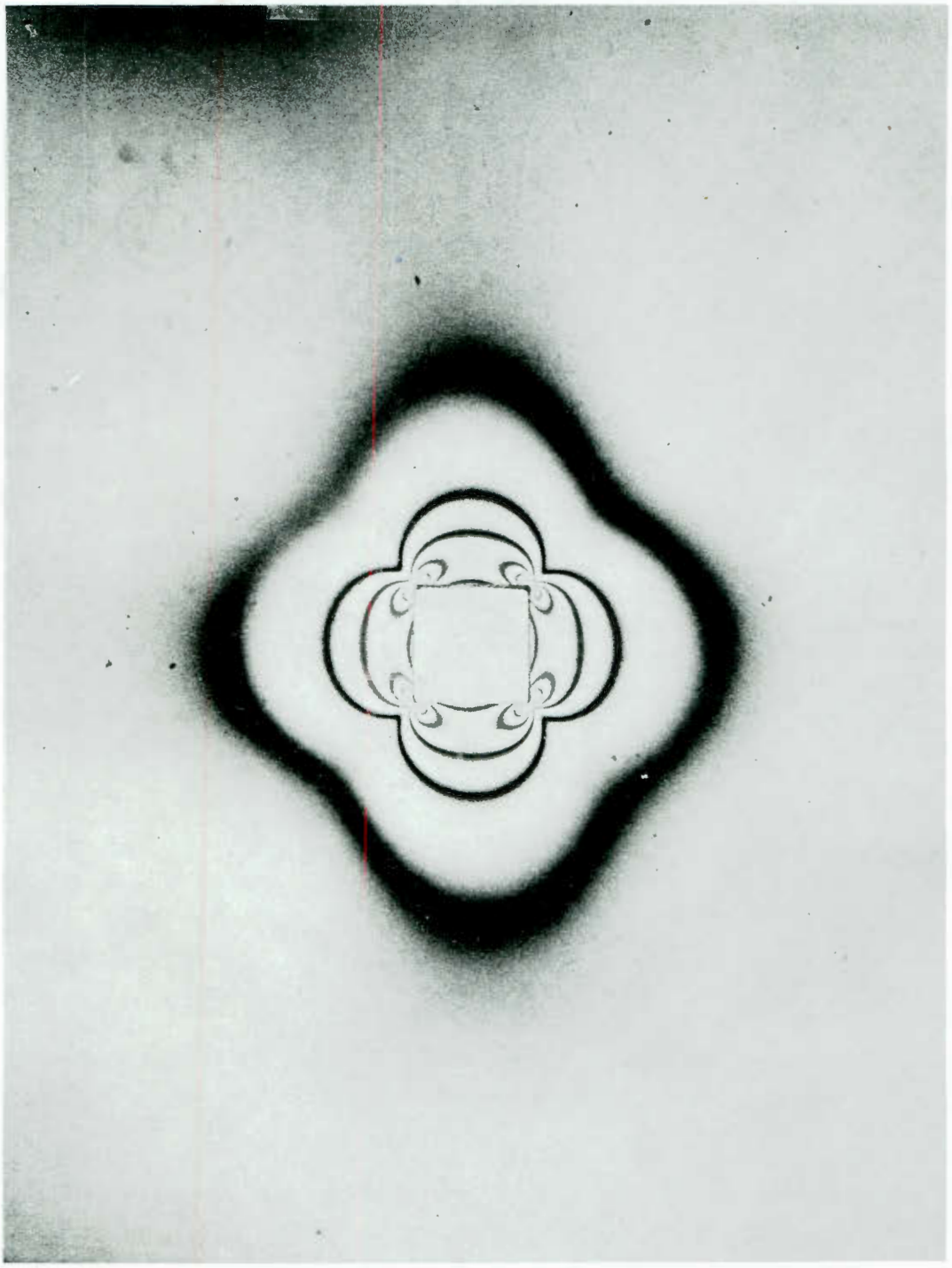

FIGURE A 10

Photoelastic isochromatics around a
square hole in a hydrostatic stress field

APPENDIX IV

APPARATUS FOR TRIAXIAL COMPRESSION TESTING OF ROCK SPECIMENS

The principal requirements for triaxial compression testing of rock specimens were considered in Section 13 of this study. This appendix describes the details of the triaxial apparatus designed by the author and used in the Rock Mechanics Division of the National Mechanical Engineering Research Institute.

1. PRINCIPLES OF OPERATION

The principal features of the triaxial apparatus are illustrated diagrammatically in Figure A11.

The specimen, of diameter D_s, is loaded axially by means of a load piston, diameter D_L. The specimen and load piston are loaded in series with an oil pressure piston and cylinder, diameter D_p, and the pressure generated therein is used to apply lateral pressure onto the specimen.

The intermediate and minimum principal stresses (σ_2 and σ_3) induced in the specimen are equal to the oil pressure P and are given by

$$\sigma_2 = \sigma_3 = P \frac{4L}{\pi D_p^2}$$

The axial principal stress σ_1 in the specimen is given by the net load on the specimen divided by its cross-sectional area. The net load is given by the total applied load L less the force exerted upon the load piston by the oil pressure acting on the annular area resulting from the difference between the load piston diameter D_L and the specimen diameter D_s.

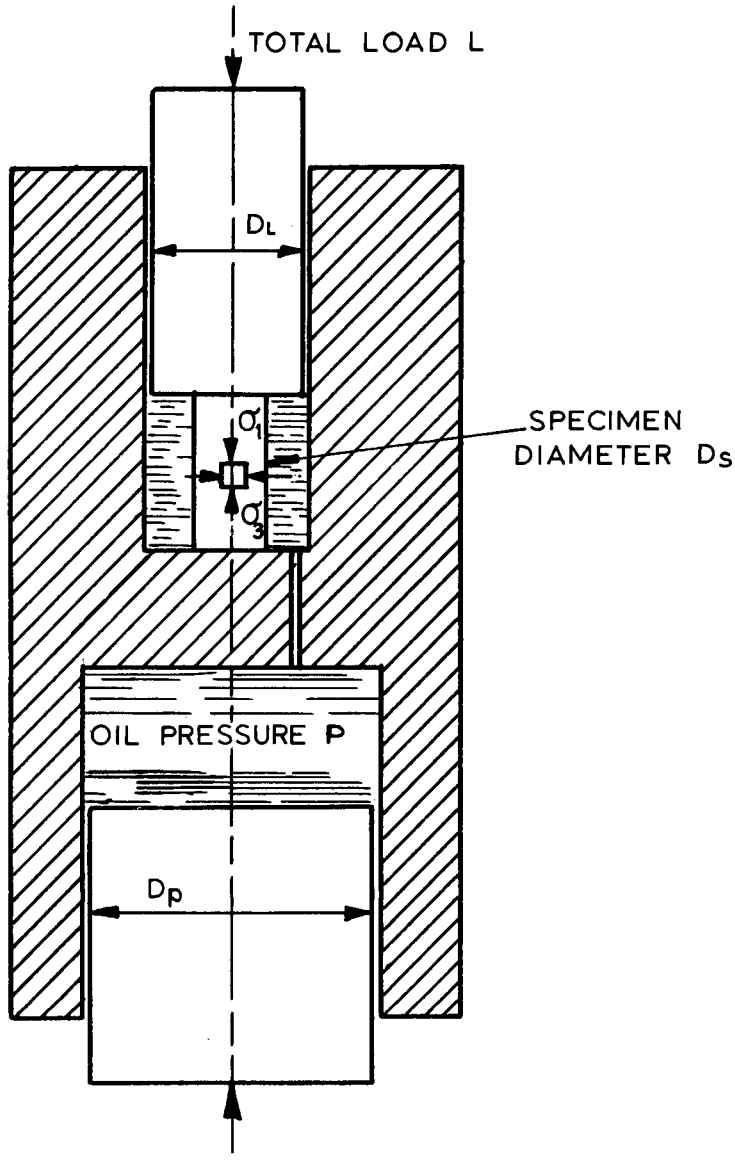

FIGURE A 11

Principles of operation of triaxial apparatus

Hence

$$\sigma_1 = \frac{L - \frac{4L}{\pi D_p^2}\left\{\pi/4\,(D_L^2 - D_s^2)\right\}}{1/4\,\pi D_s^2}$$

or

$$\sigma_1 = \frac{4L}{\pi}\left\{\frac{D_p^2 - D_L^2 + D_s^2}{D_p^2\, D_s^2}\right\}$$

The principal stress ratio σ_3/σ_1 is given by

$$\frac{\sigma_3}{\sigma_1} = \frac{D_s^2}{D_p^2 - D_L^2 + D_s^2}$$

2. CHOICE OF PRINCIPAL STRESS RATIOS

From the triaxial test results presented in Figure 11, it is evident that fracture of hard rocks will only occur within a fairly narrow range of principal stress ratios. It is considered unlikely that hard rocks, of the type with which this study is primarily concerned, can be induced to fail at $\sigma_3/\sigma_1 > 0.25$ at stress levels attainable in this apparatus.

In order to cover the range $0 < \sigma_3/\sigma_1 < 0.25$, the following principal stress ratios have been chosen:

0, $1/40$, $1/20$, $1/12$, $1/9$, $1/6$, $1/4$.

3. STRESS CONDITIONS IN EX SPECIMENS

Practical considerations led to the choice of a total load L of 100 tons. From considerations of the probable strength of hard rock specimens under triaxial stress conditions (Figure 11) it was decided that specimens should be cut from standard EX diamond drilled core (0.85 inches diameter). The load piston diameter D_L was chosen as 2.00 inches. But this is dependent on $D_s = D_L$ (see pg 80).

From considerations of commerically available 'O' rings, the

piston diameters listed in Table A1 were chosen to give the pressure ratios listed above. Also listed in Table A1 are the actual principal stress ratios and the maximum stresses induced in the specimen at an applied load L of 100 tons.

TABLE AI

STRESS CONDITIONS FOR D_s = 0.85 inches and D_L = 2.00 ins.							
Nominal ratio σ_3/σ_1	0	$^1/_{40}$	$^1/_{20}$	$^1/_{12}$	$^1/_9$	$^1/_6$	$^1/_4$
Piston diameter D_p ins.	-	5.500	4.250	3.568	3.125	2.750	2.500
Actual ratio σ_3/σ_1	-	0.027	0.049	0.076	0.112	0.169	0.243
σ_3 max lb/sq in. at	-	8 440	14 120	20 000	26 100	33 600	40 700
σ_1 max L = 100 tons	351 000	315 000	290 000	263 000	234 000	200 000	168 000

In practice, the diameter of a specimen produced by a standard diamond core barrell depends upon the hardness of the rock and the wear of the drill. Consequently, the actual specimen diameter is measured by means of a micrometer and the actual principal stresses σ_1 and σ_3 are calculated from a set of tables which have been prepared for this purpose.

In addition to the apparatus described above, similar apparatus for testing BX (1.66 inch diameter) and NX (2.13 inch diameter) core is also available. This equipment is used for testing soft rocks and coal and the practical procedure is identical to that outlined above.

4. DESIGN DETAILS

A detailed drawing of the complete triaxial machine is reproduced in Figure A12.

The design of the specimen and plattens was discussed in section 13.2 and the detailed application of this design is

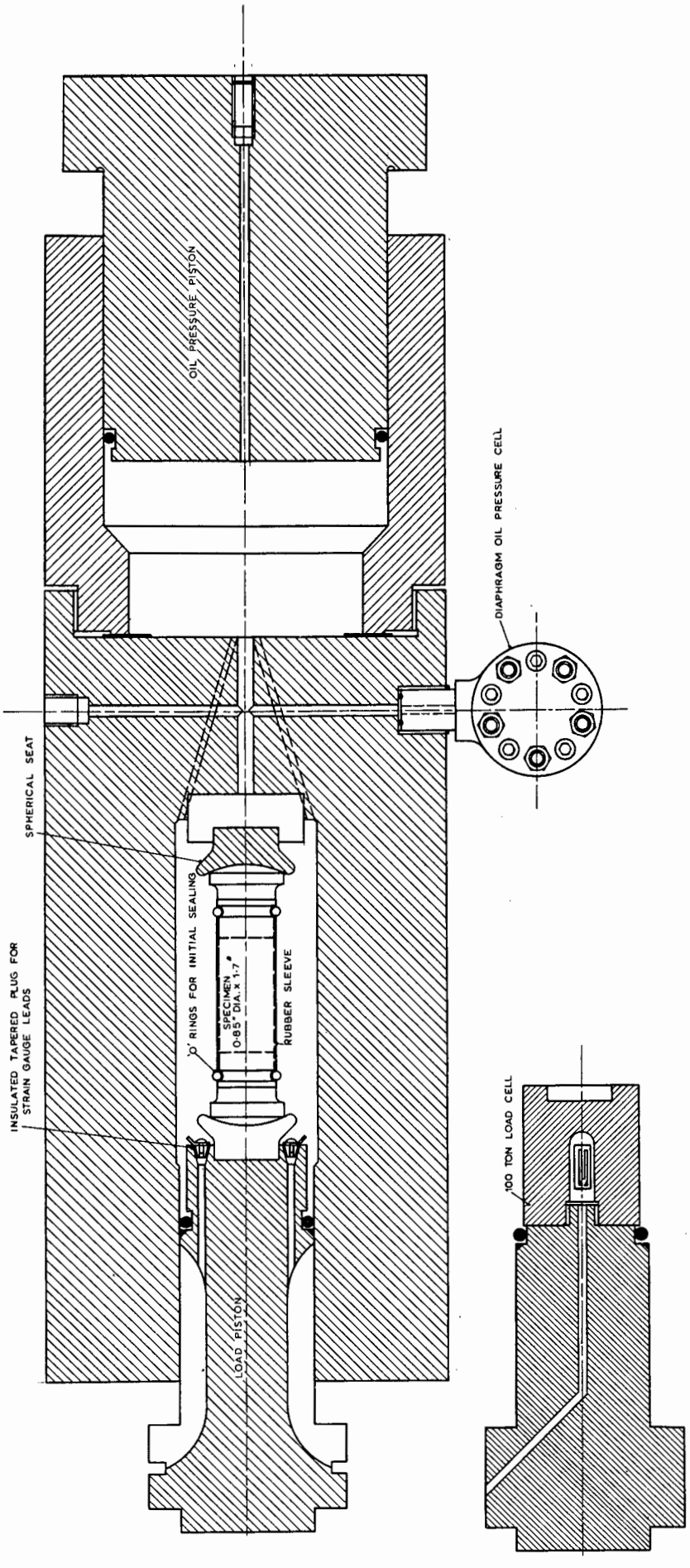

FIGURE A 12

Details of triaxial compression testing machine

illustrated in Figure A12. Note that spherical seats have been provided on both plattens in order to minimise eccentricity of loading due to slight imperfections in the preparation of the specimen.

The specimen is sleeved in a 0.020 inch thick latex rubber sleeve and, in order to prevent deterioration of this sleeve during the test, commerical hydraulic brake fluid is used as the pressure fluid.

The different pressure ratios, listed in Table A1, are achieved by replacing the pressure piston and cylinder with another set of different diameter.

Two load pistons are available, one fitted with a load cell to measure the axial load on the specimen and the other drilled to allow 8 strain gauge leads to be brought out from the specimen. Both pistons are illustrated in Figure A12.

The steel used for the construction of this machine conforms to the British Standard specifications of EN 30B steels. The pistons and cylinders have been heat treated to give an ultimate tensile strength of 120 000 lb/sq. in and, under these conditions, the steel retains a reasonable measure of ductility which is necessary for the safe design of high pressure units. The cylinders have been designed to withstand stresses 20% higher than those listed in Table A1.

The plattens and spherical seats were machined from a 1% carbon tool steel and hardened to 60 Rockwell C before grinding and lapping. The spherical seats were lapped with diamond paste and are numbered so that they are always used in matched pairs.

5. SEALING ARRANGEMENTS

The moving seals used on the load and pressure pistons are identical to those used in the biaxial machine, described in Appendix III.

The design of the seal between the pressure cylinder and the body of the triaxial apparatus is illustrated in Figure A13. This design was suggested to the author by Professor G.T. van Rooyen of the University of Pretoria.

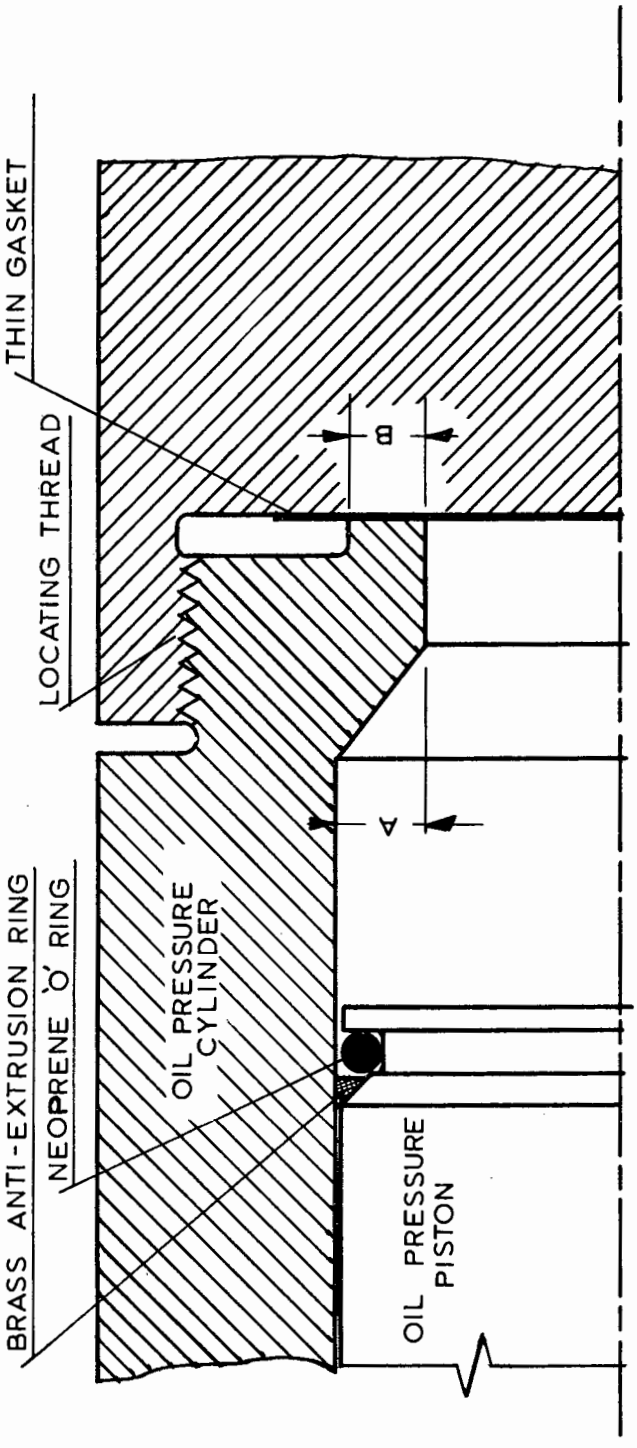

FIGURE A 13

Details of sealing arrangements used on triaxial apparatus

The oil pressure cylinder is attached to the test cell body by means of a loosely fitting thread - designed only to provide location and initial sealing. A thin impregnated paper gasket is placed between the sealing face and the test cell body.

Once the load is applied and an oil pressure generated in the pressure cylinder, this joint becomes self sealing since the area A is greater than the area B and hence the sealing pressure on the gasket is always greater than the pressure of the oil trying to escape. This sealing arrangement has proved completely reliable in hundreds of tests carried out with the apparatus.

6. LOAD AND PRESSURE MEASUREMENT

Because of the very low frictional losses in the pressure and load piston sealing devices, the stresses induced in the specimen are generally within 1% of the stresses calculated on the basis of the equations presented in Section 1 of this appendix. Consequently, it is sufficient to measure only the oil pressure or the load on the specimen.

Although Figure A12 shows that provision has been made for both measurements, practical experience has shown that measurement of the oil pressure is most convenient. This is achieved by means of the pressure capsule illustrated in Figure A14. Four such pressure measuring units are available for maximum pressures of 2 000, 5 000, 12 500 and 35 000 lb/sq. in. and the choice of the range used for a particular test depends upon the estimated strength of the material and the sensitivity required.

7. EXTERNAL LOAD APPLICATION

Two methods of load application are possible with this apparatus :

(a) External loading by means of a jack and
(b) Restraining the pistons from moving outwards and pumping oil under pressure into the system.

The second alternative has the advantage of giving a more compact overall unit and is being considered for use in the field. However, in the laboratory, it is advantageous to apply the load externally by means of a jack since the rate of loading can be

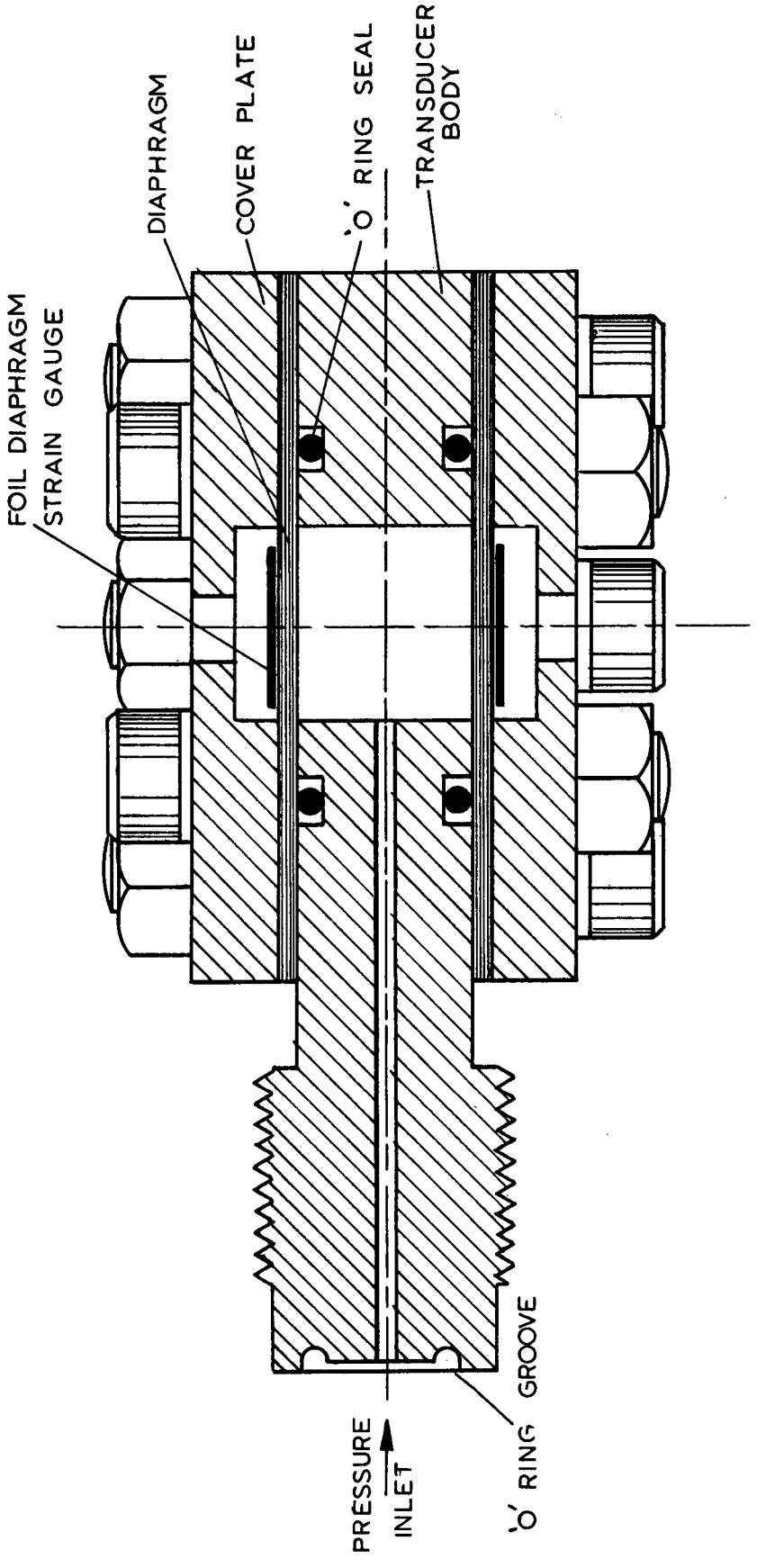

FIGURE A 14

Section through oil pressure transducer

more accurately controlled.

The 100 ton jack and hydraulic circuit used by the Rock Mechanics Division is illustrated diagrammatically in Figure A15. Note that the hydraulic circuit is similar to that used for the biaxial loading machine.

8. STRAIN MEASUREMENT

Measurement of the axial and lateral strains in the specimen will be carried out by means of strain gauges. Although no such measurements have been carried out at the time of writing, it is not anticipated that any major difficulties will be encountered since the techniques to be used have already been extensively investigated by Brace[52] and Milligan*.

9. DATA RECORDING AND PROCESSING

Since a study of the properties of rock involves a large number of tests, the collection and processing of the data must be carefully considered. Experience has shown that data recorded by means of X-Y recorders requires a large amount of accurate and therefore expensive manual processing. When rock properties testing is carried out on a simi-routine basis, as is the case at the CSIR, manual processing of the data becomes impractical and uneconomical.

In order to overcome the difficulties of rock properties data processing, the system, illustrated diagrammatically in Figure A17 and described hereunder, was evolved.

Four items of information are recorded:

(a) The time in seconds from the commencement of the test

(b) The hydraulic pressure P

(d) The axial strain in the specimen ε_1 and

This was not done for the tests reported here!

---

* MILLIGAN, R.V. The effects of high pressure on foil strain gages. Paper No. 803, SESA Spring Meeting, Seattle, May 8-10, 1963.

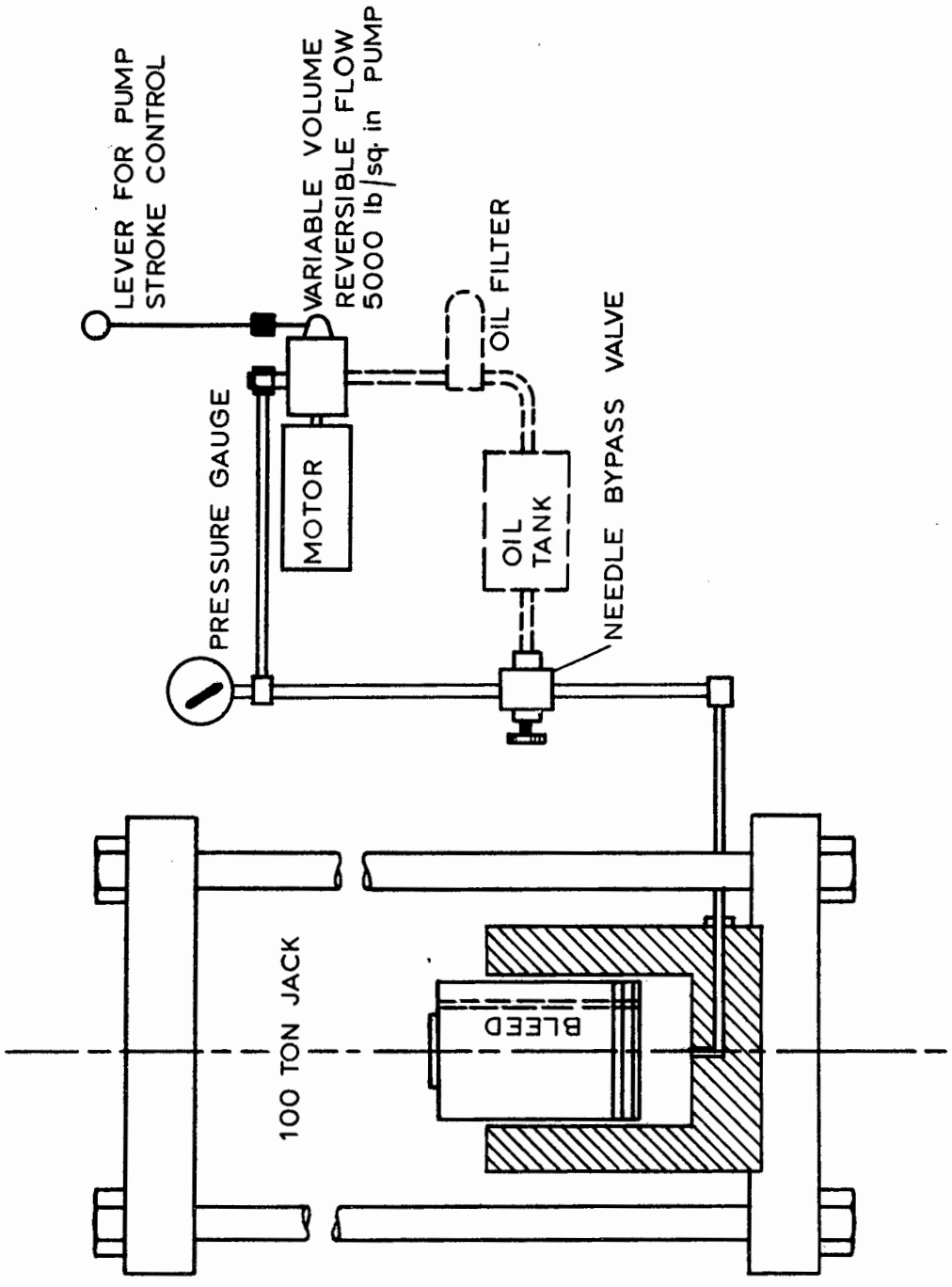

FIGURE A 15

Hydraulic circuit and 100 ton jack for loading triaxial apparatus

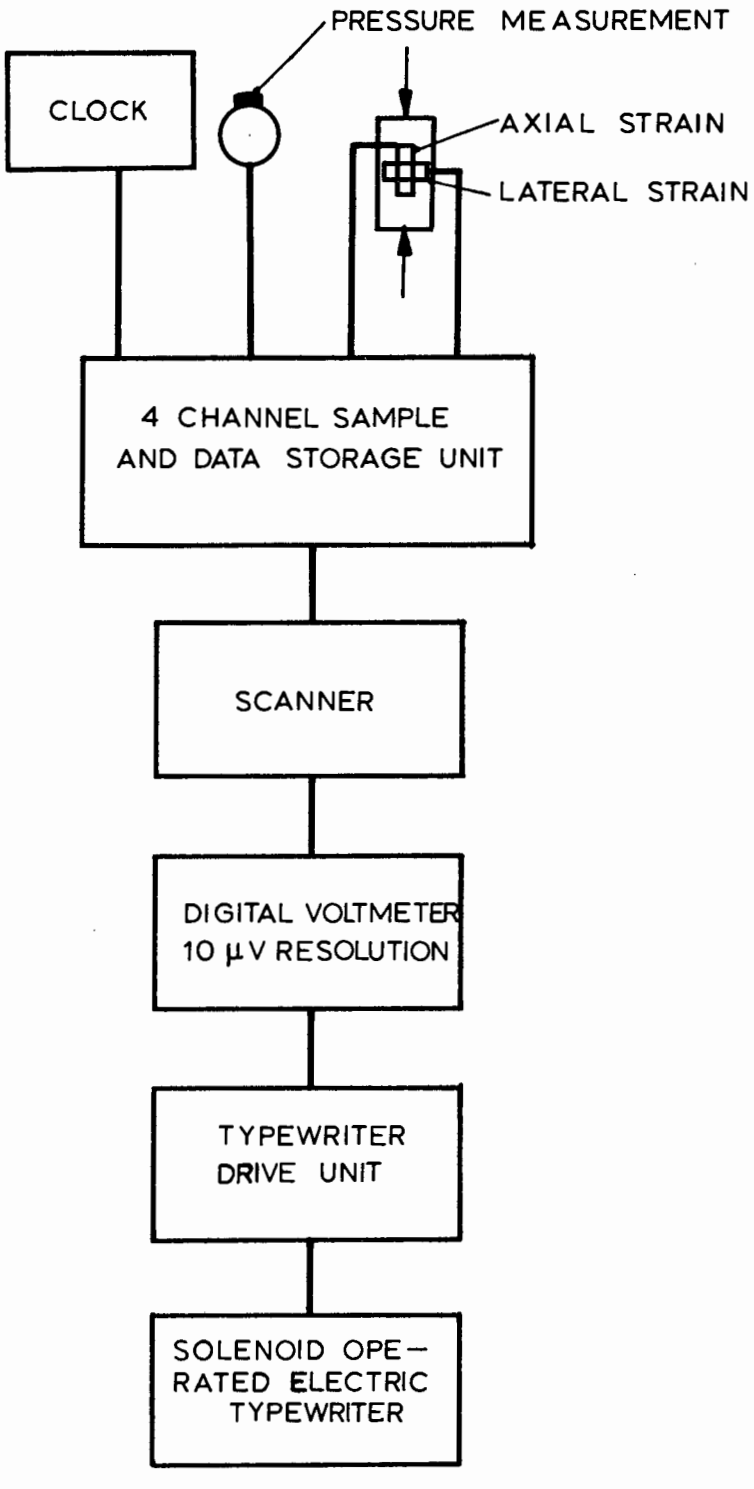

FIGURE A 16

Block diagram of data collection system
for triaxial tests on rock specimens

(d) The lateral strain in the specimen $\varepsilon_2 = \varepsilon_3$.

The clock, which generates a voltage directly proportional to time up to 1 000 seconds, is used to record the rate of loading.

The strain gauge circuits used to measure pressure, axial strain and lateral strain are all temperature compensated full Wheatstone bridge circuits.

The four items of information are sampled simultaneously and the voltages transferred onto high stability mylar film capacitance storage units.

A scanner then transfers these stored signals to the digital voltmeter which actuates a solenoid operated electric typewriter through a typewritten drive unit.

The scanning speed can be varied to suit the test conditions, its maximum speed being governed by the 16 character per second speed of the typewriter. At maximum sampling speed, each channel is sampled every two seconds*.

This sampling speed is adequate for the type of tests currently carried out by the Rock Mechanics Division.

Print out of the data by a typewriter was chosen in preference to punched tape because it provides directly interpretable information during the test.

This typed data is then punched onto cards and processed on the CSIR's IBM computor. High order polynomials are fitted to the axial and lateral stress-strain data by means of a standard programme. Once these curves have been mathematically defined they can be differentiated to give the tangent modulus at any stress level, divided to give the Poisson's ratio at any stress level and integrated to give the strain energy.

Since these processes involved the use of very simple programmes, the complete stress-strain data from a test can be

---

* The electronic design of the clock, sample unit and scanner was carried out by Dr D.H. Naude. Construction of most of the equipment was done by Mr A. van Jaarsvelt. Dr Naude and Mr Van Jaarsvelt are members of the CSIR's National Institute for Mathematical Sciences.

evaluated in a few seconds of computor time.

APPENDIX V

CONDUCTING PAPER ANALOGY FOR DETERMINATION OF THE PRINCIPAL STRESS SUM DISTRIBUTION

Application of the fracture theory discussed in this study requires a knowledge of the individual principal stresses σ_1, σ_2 and σ_3 at any point in the material surrounding an excavation. The photoelastic technique affords an accurate and convenient means for the determination of the principal stress difference in any plane in the model[197]. Separation of the principal stresses requires that the principal stress sum in this plane should also be known. The conducting paper analogy has been found particularly useful for the determination of this principal stress sum.

The sum of the principal stresses σ_p and σ_q in a plane in an isotropic elastic stressed body which is free from body forces is distributed according to Laplace's equation:

$$\frac{\partial^2(\sigma_p + \sigma_q)}{\partial x^2} + \frac{\partial^2(\sigma_p + \sigma_q)}{\partial y^2} = 0$$

The conducting paper analogy depends upon the fact that the voltage distribution in a uniformly conducting plane is also governed by Laplace's equation:

$$\frac{\partial^2 V}{\partial x^2} + \frac{\partial^2 V}{\partial y^2} = 0$$

Consequently, if voltages are applied to the boundary of a uniformly conducting sheet which is cut into the shape of the stressed model, the voltage at any point in the conducting sheet will correspond to the sum of the principal stresses at that point in the model. The values of the applied boundary voltages are determined from the boundary fringe orders in the photoelastic model.

Figure A17 illustrates the circuit used for the determination of the principal stress sum distribution by means of the conducting paper analogy.

The model is cut from commercially available 'Teledeltos' conducting paper. In the case of a model which contains one or more axis of symmetry, only that portion of the model bounded by this axis or axes and the loaded boundary need be considered. Hence, in the case of a circular hole, only one quarter of the model, as illustrated in Figure A17, need be studied.

The voltage applied to the loaded boundary corresponds to the sum of the applied principal stresses P and Q. The voltages applied to the boundary of the excavation correspond to the tangential stresses on this boundary, determined from the photoelastic isochromatic patterns. Note that, in order to approximate semi-infinite conditions, the hole diameter should be less than one-fifth of the side length of the conducting paper model.

A commercially available transistorized strain indicator has been found particularly suitable for measuring the voltage at any point in the model by a null-balancing method. The model and potential divider are arranged as a four arm Wheatstone bridge. Probing the model unbalances the bridge and it is brought back into balance by the internal potentiometer of the strain indicator.

The strain indicator supplies a $1\frac{1}{2}$ volt 1 000 cycle per second alternating voltage across terminals A and C. The galvanometer measures between terminals B and D. The 10 kΩ potentiometer shunts the galvanometer for control of the sensitivity. The 500 kΩ resistor in series with the probe prevents excessive current flow through probe. Connection between the wires and the conducting paper model is made with commercially available silver conducting paint.

A comparison between the distributions of the principal stress sum in the material surrounding an unfractured circular hole, determined by means of the conducting paper analogy and calculated from Kirsch's equations, showed that a maximum error of approximately 3% could be obtained if sufficient care was exercised in applying the correct boundary voltages.

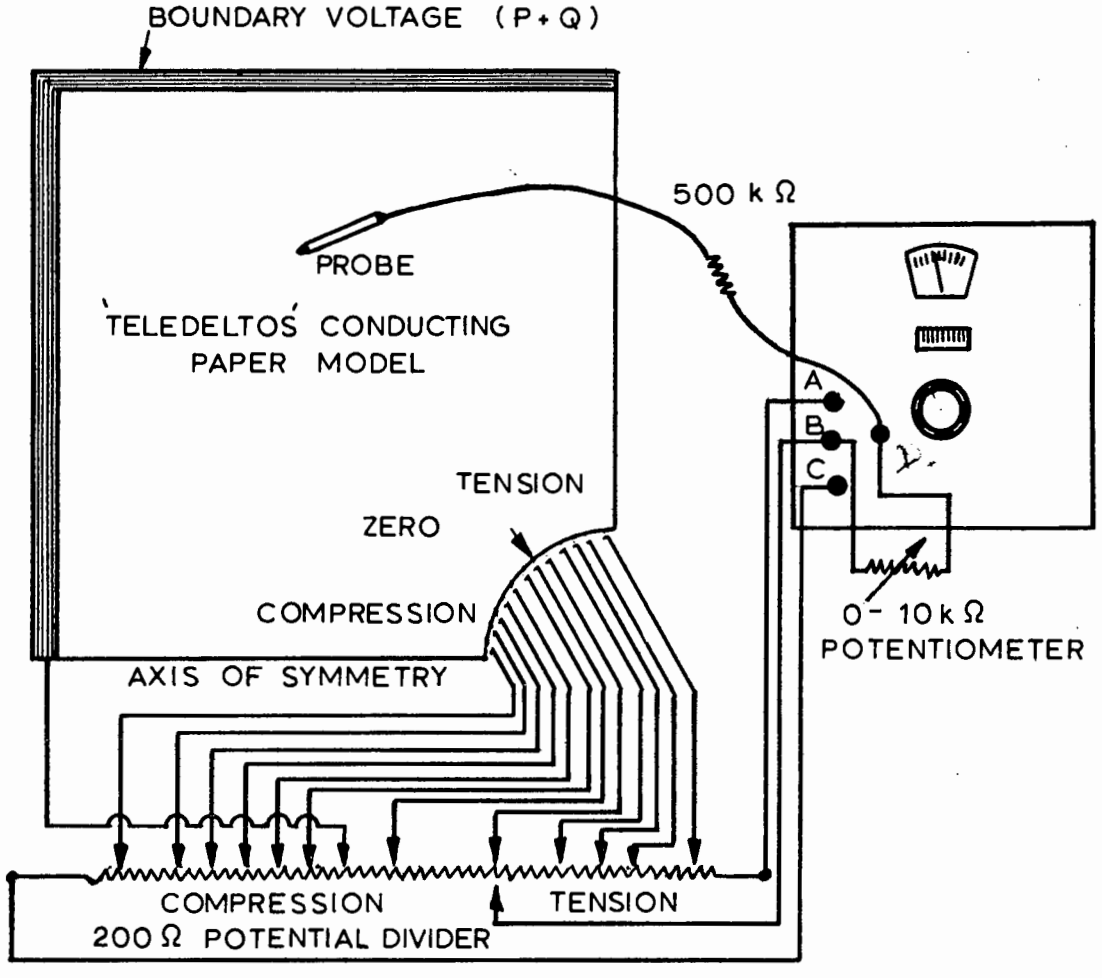

FIGURE A 17

Circuit for conducting paper analogy
used for determination of the principal
stress sum distribution

BIBLIOGRAPHY

1. ADAMS, F.D. An experimental investigation into the action of differential pressure on certain minerals and rocks, employing the process suggested by Professor Kick. J. Geol, Vol. 18, 1910, pp. 489-525

2. ADAMS, F.D. and BANCROFT, J.A. On the amount of internal friction developed in rocks during deformation and on the relative plasticity of different types of rocks. J. Geol, Vol. 25, 1917, pp. 597-658

3. ADAMS, F.D. and COKER, E.G. An investigation into the elastic constants of rocks, more especially with reference to cubic compressibility. Carnegie Instn. Washington. Publ. 46, 1906, 69 p

4. ADAMS, L.H. and WILLIAMSON, E.D. On the compressibility of minerals and rocks at high pressures. J. Franklin Inst., Vol. 195, 1923, pp. 475-529

5.* ADLER, L. Failure in geologic material containing planes of weakness. AIME Trans., Vol. 226, 1963, pp. 88-94

6. AHLVIN, R.G. Waterways experiment station large triaxial apparatus. Highway Research Board, Washington. D.C., Bull. 141, 1956, p. 19

7.* AKROYD, T.N.W. Ultimate loads in rock and concrete. Construction. May 1960, p. 672

8. AKROYD, T.N.W. Concrete under triaxial stress. Mag. Concrete Res., Vol. 13, no. 39, 1961, pp. 111-118

9. AKROYD, T.N.W. Failure mechanism of saturated concrete. Engineering, 1961, pp. 658-659

10. ANONYMOUS. Summarized proceedings of a conference on the mechanics of rupture, Southampton, April 1961. British J. Appl. Phys, Vol. 13, 1962, pp. 141-144

11. ANZO, Z. On the stresses in a gravitating elastic body having a circular hole near to its horizontal surface. Tech. Rep. Kynshu Imp. Univ, Vol. 12, no. 3, 1937

12. ARCHARD, J.P. Elastic deformation and laws of friction. Proc. Royal Soc. Series A, Math. and Phys. Sciences no. 1233, Vol. 243, 1957

13. AUDEREGG, F.O., WELLER, R. and FRIED, B. Tensíon specimen shape and apparent strength. Proc. Amer. Soc. Test. Nat, Vol. 39, 1939, pp. 1261-1269

14. BACON, L.O. A method of determining dynamic tensile strength of rock at minimum loading. U.S. Bur. Min. Rep. Inv. 6067, 1962

---

* Items marked with an asterisk were used by the author during the course of this research project.

15.* BALLA, A. Stress conditions in triaxial compression. J. Soil Mech. and Foundations Div., Proc. Amer. Soc. Civil Engrs, Vol. 86, no. SM 6, 1960, pp. 57-84

16.* BALLA, A. Stress conditions in the triaxial compression test. Proc. 4th Intnl. Conf. on Soil Mech. and Foundation Engg., London, Vol. 1, Div 1-3a, Butterworth Scientific Publications, 1957

17.* BALMER, G. Shearing strength of concrete under high triaxial stress - computation of Mohr's envelope as a curve. U.S. Bur. Reclamation. Struct. Res. Lab. Rep. no. SP-23, 1949

18.* BALMER, G. A general analytical solution for Mohr's envelope. American Soc. Testing Matls, Vol. 52, 1952, pp. 1260-1271

19.* BALSLEY, J.R. Deformation of marble under tension at high pressure. Trans. Amer. Geophys. Union, Vol. 22, 1941, pp. 519-525

20. BALSLEY, J.R. Tension in rock specimens. Trans. Amer. Geophys. Union, Part II, 1941, p. 519

21. BANVILLE, M. Physical properties of mine rock. Canada Dept. Mines and Tech. Surveys - Tech. Memo no. 61/57-MIN Fuels Div. Copy no. 15, 1957

22. BANVILLE, M. Physical properties of mine rock uniaxial compression studies - Report no. 8. Canada Dept. Mines and Tech. Surveys, Tech. Memo no. 63/57-MIN Fuels Div. Copy no. 18, 1957

23.* BARENBLATT, G.I. On some basic ideas on the theory of equilibrium cracks, forming during brittle fracture. Problems of Continuum Mechanics, ed. Radok. Published by Soc. for Ind. and Appl. Maths., Philadelphia, 1961, pp. 21-38

24. BARENBLATT, G.I. and KHRISTIANOVICH, S.A. Ob obrushchenii krovli pri gornykh vyrabotkakh. Izv. AN SSSR, Otd. Tekhn. N. no. 11, 1955, pp. 73-86

25. BARENBLATT, G.I. On some problems on the theory of elasticity, arising in the study of the mechanism of hydraulic fracture of an oil-bearing strata. PPM; Journal of Mathematics and Mechanics, New York, 1956, pp. 475-486

26. BARENBLATT, G.I. On the formation of horizontal cracks during hydraulic fracturing of oil-bearing strata. Izv. AN SSSR, Otd. Tekhn. N. no. 9, 1956, pp. 101-105

27.* BECKMAN, R.T. Compressive strength versus length-diameter ratios of potash specimens. U.S. Bur. Min. Rep. Inv. 6339, 1963, 15 p

28. BENARI, M.M. Rheology of granular material II : A method for the determination of the intergranular cohesion. Britt. J. Applied Phys. Vol. 12, no. 9, 1961

29. BERENBAUM, R. The strength of irregularly-shaped specimens of coal. National Coal Board, Scientific Dept. M.R.E. Rep. no. 2082, 1957

30. BERENBAUM, R. The shatter breakage of deep duffryn coal. Nat. Coal Board, M.R.E. Rep. no. 2128, 1959

31. BERENBAUM, R. The breakage of irregular lumps of pentremawr anthracite in uniaxial compression. Nat. Coal Board, M.R.E. Rep. no. 2138, 1959

32. BERENBAUM, R. Shatter characteristics of M.R.E. representative coals. Nat. Coal Board, M.R.E. Rep. no. 2136, 1959

33.* BERENBAUM, R. and BRODIE, I. Measurement of the tensile strength of coal : A critical assessment and the application of a new technique. Nat. Coal Board, M.R.E. Rep. no. 2109, 1958

34. BERENBAUM, R. and BRODIE, I. The tensile strength of coal. J. Inst. Fuel, 1959

35. BERENBAUM, R. and BRODIE, I. Measurement of the tensile strength of brittle materials. Brit. J. appl. Phys, Vol. 10, 1959, pp. 281-287

36. BERENBAUM, R. Coal shatter tests. Colliery Guard, 1962, pp. 435-442

37.* BERRY, D.S. An elastic treatment of ground movement due to mining. I. Isotropic ground. J. Mech. Phys. Solids, Vol. 8, 1960, pp. 280-292

38.* BERRY, D.S. and SALES, T.W. An elastic treatment of ground movement due to mining. II. Transversely isotropic ground. J. Mech. Phys. Solids, Vol. 9, pp. 52-62

39.* BERRY, D.S. and SALES, T.W. An elastic treatment of ground movement due to mining. III. Three-dimensional problem, transversely isotropic ground. J. Mech. Phys. Solids, Vol. 10, 1962, pp. 73-83

40. BIOT, M.A. Theory of elasticity and consolidation for a porous anisotropic solid. J. Appl. Phys, Vol. 26, no. 2, 1955, pp. 182-185

41. BLAIR, B.E. Physical properties of mine rock. Part III. U.S. Bur. Min. Rep. Inv. 5130, 1955, 69 p

42. BLAIR, B.E. Physical properties of mine rock. Part IV. U.S. Bur. Min, Rep. Inv. 5244, 1956, 69 p

43.* BLAKEY, F.A. Some considerations of the cracking or fracture of concrete. Civil Engng, London, 1957

44. BLANKS, R.F. and McHENRY, D. Large triaxial testing machine. U.S. Bur. of Reclamation, Eng. News Record, Aug. 1945

45.* BÖKER, R. Die mechanik der bleibenden formänderung in kristallinisch aufgebauten korpern. Ver. Deut. Ing. Mitt. Forch, Vol. 175, 1915, pp. 1-51

46. BOOZER, G.D., HILLER, K.H. and SERDENGECTI, S. Effects of pore fluids on the deformation behaviour of rock subject to triaxial compression. Rock Mechanics edited by Fairhurst, Pergamon Press, New York, 1963, pp. 579-626

47.* BOSKHOV, S. Some mathematical and model guides in the analysis of underground mine stress problems. Columbia Univ, School of Mines, 1956

48. BOSSCHART, R.A.J. Elasticity and strength of concrete. D.S.I.R. Bldg. Res. Sta. Lib. Comm no. 794, Transladed from Dutch, 1957, 11 p

49.* BRACE, W.F. An extension of Griffith theory of fracture to rocks. J. Geophys. Res, Vol. 65, no. 10, 1960, pp. 3477-3480

50.* BRACE, W.F. and BOMBOLAKIS, E.G. A note on brittle crack growth in compression. J. Geophys. Res, Vol. 68, no. 12, 1963, pp. 3709-3713

51.* BRACE, W.F. Dependence of fracture strength of rocks on grain size. Penn. State. Univ. Mineral Expt. Sta. Bull. no. 76, 1961, pp. 99-103

52.* BRACE, W.F. Brittle fracture of rocks. State of Stress in Earth's Crust, ed. Judd, American Elsevier Publishing Company, New York, 1964, pp. 111-180

53. BRACE, W.F. and WALSH, J.B. Some direct measurements of the surface energy of quartz and orthoclase. American Mineralogist, Vol. 47, 1962, pp. 1111-1122

54.* BRACE, W.F. Behaviour of quartz during indentation. J. Geology, Vol. 71, no. 5, 1963, pp. 581-595

55.* BREDTHAUER, R.O. Strength characteristics of rock samples under hydrostatic pressure. American Soc. Mech. Engrs. Trans. Vol. 79, 1957, pp. 695-708

56.* BRESLER, B. and PISTER, K.S. Failure of plain concrete under combined stress. Proc. Amer. Soc. civ. Engrs, Paper 674, Vol. 122, 1957, p. 1049

57.* BRIDGMAN, P.W. The physics of high pressure. G. Bell and Sons, London, 1958, 445 p

58. BRIDGMAN, P.W. The failure of cavities in crystals and rocks under pressure. American J. Sci, Vol. 45, 1918, pp. 243-268

59. BRIDGMAN, P.W. Shearing phenomena at high pressure of possible importance for geology. J. Geol, Vol. 44, 1936, pp. 653-669

60. BRIDGMAN, P.W. and LARSEN, E.S. Shearing experiments on some selected minerals and mineral combinations. American J. Sci, Vol. 36, 1938, pp. 81-94

61. BRIDGMAN, P.W. The high-pressure behaviour of miscellaneous minerals. American J. Sci, Vol. 37, 1939, pp. 7-18

62. BRIDGMAN, P.W. Breaking tests under hydrostatic pressure and conditions of rupture. Phil. Mag, Vol. 24, 1912, pp. 63-80

63. BROCK, J.S. Analytical determination of the stresses around square holes with rounded corners. David W. Taylor Model Basin Rep. 1149, Nov. 1957, 29 p

64.* BRODE, H. Rock mechanics considerations in the design of underground protective structures. Proc. Intnl. Conf. State of Stress in Earth's Crust. Santa Monica, May 1963. In press.

65. BRODIE, I. and BERENBAUM, R. A study of the breakage of coal by surface indentation. National Coal Board, Sci. Dept. M.R.E. Rep. no. 2108, 1958

66. BROWN, P.D. and SHAW, J.R. Young's Modulus rock. The in-situ measurement of Young's modulus for rock by a dynamic method. Geotechnique, Vol. III, no. 7, 1953, pp. 283-286

67.* BUCKY, P.B. Use of models for the study of mining problems. Amer. Inst. Min. Metall. Engrs, Tech. Publ. 425, 1931, 28 p

68. BUCKY, P.B. The application of barodynamics for mining problems. Iron and Coal Trades Rev. Aug. 9, 1940

69. BUCKY, P.B. A practical way of attacking the problem of structure and ground support. Engl. Elect. J. July 1941

70.* BUCKY, P.B. and FENTRESS, A.L. Application of principles of similitude to design of mine workings. Trans. Amer. Inst. Min. Engrs, Vol. 109, 1934, p. 25

71.* BUCKY, P.B., SOLAKIAN, A.G. and BALDIN, L.S. Centrifugal method of testing models. Civil Engng, Vol. 5, no. 5, 1935, pp. 287-290

72. BURKE, S.P. and PARRY, V.F. Mechanism of outburst in coal mines. Colliery Guard, Vol. 150, 1935, p. 482

73. CAMERON, E.L. Physical properties of some Canadian mine rocks. Canadian Inst. Min. Trans, Vol. 62, 1954, pp. 506-509

74.* CAUDLE, R.D. and CLARK, G.B. Stresses around mine openings in some simple geologic structures. Illinois Eng. Exp. Station Bull. no. 430

75. CHEATHAM, J.B. Indentation analysis for rock having a parabolic yield envelope. Int. J. Rock Mech. Mining Sci, Vol. 1, 1964, pp. 431-440

76. CHECHULIN, B.B. On the statistical theory of brittle strength. U.S. Bureau of Ship's Translation no. 603, 1956

77.* CLARK, G.B. and CAUDLE, R.D. Failure of homogeneous rock under dynamic compressive loading. Proc. Intnl. Conf. State of Stress in Earth's Crust. Santa Monica, May 1963. In press

78. CLAUDING, D.P. Comparison of Griffith's theory and Mohr's failure criterion. Quart. Colorado School of Mines, Vol. 54, 1959, pp. 285-296

79.* COATES, D.F. Classification of rocks for rock mechanics. Unpublished paper

80. COATES, D.F., UDD, J.E. and MORRISON, R.G.K. Some physical properties of rocks and their relationship to uniaxial compressive strength. Unpublished paper

81.* COATES, D.F. Rock mechanics applied to the design of underground installations to resist ground shock from nuclear blasts. Rock Mechanics edited by Fairhurst, Pergamon Press, New York, 1963, pp. 535-562

82.* COFFIN, L.F. Jr. The flow and fracture of a brittle material. J. Appl. Mech. 1950, pp. 233-248

83.* COLBACK, P.S.B. and WIID, B.L. The influence of moisture content on the compressive strength of rock. To be presented to the Third Canadian Symposium on Rock Mechanics, Toronto, January 1965

84.* COOK, N.G.W. The basic mechanics of rockbursts. J. S.A. Inst. Min. and Metall, Oct. 1963, pp. 71-81

85.* COOK, N.G.W. A study of failure in the rock surrounding underground excavations. Ph.D. Thesis, Univ. Witwatersrand, 1962, 130 p

86.* COOK, N.G.W. The seismic location of rockbursts. Rock Mechanics edited by Fairhurst, Pergamon Press, New York, 1963, pp. 493-516

87.* CORLETT, A.V. and EMERY, C.L. Prestress and stress redistribution in rocks around a mine opening. Canadian Min. and Metall. Bull, Vol. 62, 1959, pp. 186-198

88.* CORNET, I. and GRASSI, R.C. A study of theories of fracture under combined stresses. ASME Paper no. 60-MET-4, April 1960

89.* CORTEN, H. and PARK, F. Fracture. International Science and Technology, No. 15, March 1963, pp. 24-36

90. D'APPOLONIA, E. and NEWMARK, N.M. A method for solution of the restrained cylinder under axial compression. Proc. 1st U.S. Conf. of Appl. Mech. American Soc. Mech. Eng. 1951, pp. 217-226

91.* DENKHAUS, H.G., HILL, F.G. and ROUX, A.J.A. A review of recent research into rockbursts and strata movement in deep level mining in South Africa. Ass. Min. Mngrs. S. Africa, Circ. 8, 1958, also Trans. Inst. Min. Metall. London. Bull. 629, Vol. 68, 1959, pp. 283-309

92.* DENKHAUS, H.G. The application of the mathematical theory of elasticity to problems of stress in hard rock at great depth. Ass. Min. Mngrs. S. Africa, Vol. 1958/59, 1958, pp. 271-310

93.* DENKHAUS, H.G., ROUX, A.J.A. and GROBBELAAR, C. A study into the mechanical properties of rock with special reference to their bearing on the occurrence of rockbursts. S. African Mech. Engr. Vol. 8, 1958, pp. 67-85

94.* DENKHAUS, H.G. The significance of some properties of rock in relation to the problem of rockbursts in deep mining. Intnl. Cong. Strata Control, Leipzig, October 1958

95.* DENKHAUS, H.G. and HILL, F.G. The conditions of the ground around excavations in hard rock at great depth. Intnl. Conf. Strata Control, Paris, May 1960

96.* DENKHAUS, H.G. Model studies in rock mechanics. Intnl. Bur. Rock Mech. Leipzig, Nov. 1961

97.* DENKHAUS, H.G. A critical review of the present state of scientific knowledge related to the strength of mine pillars. J. S.A. Inst. Min. and Metall, Vol. 62, no. 2, 1962, pp. 59-75

98.* DIXON, J. and BIRON, C. The photoelastic analysis of the distribution of stresses around mining excavations. King's College Univ. School Min. Res. Publ, Vol. 2, 1954, pp. 40-56

99.* DONATH, F.A. Experimental study of the shear failure of anisotropic rocks. Geol. Soc. America. Bull, Vol. 72, 1961, pp. 985-990

100.* DONATH, F.A. Strength variation and deformation behaviour in anisotropic rock. Proc. Intern. Conf. State of Stress in Earth's Crust, Santa Monica, June 1963, in press, pp. 5-1-9

101. DRUCKER, D.C. Coulomb friction, plasticity and limit loads. Paper 53 - A 57. Amer. Soc. Mech. Engr.

102.* DUCKWORTH, W.H. and RUDNICK, A. The strength of ceramic materials. Batelle Tech. Rev, Vol. 10, no. 4, 1961

103. DUDA, S.J. Elastische Wellen im anisotropen Medium nach einer makroseismischen Untertage-Messung. Geophysical Prospecting, Vol. VIII, 1960, pp. 429-444

104.* DUGAN, W.G. Strength of a brittle material subjected to biaxial stress. M.Sc. Thesis, Univ. of Illinois, 1941

105.* DULANEY, E.N. and BRACE, W.F. Velocity behaviour of a growing crack. Jnl. Appl. Phys, Vol. 31, no. 12, 1960

106.* DURELLI, A.J., PHILLIPS, E.A. and TSAO, C.H. Introduction to the theoretical and experimental analysis of stress and strain. Mc Graw - Hill Book Co., Inc. 1958

107. DURELLI, A.J. and JACOBSEN, R.H. Development and application of brittle material method of stress analysis and study of brittle failure problems. Armour Res. Foundation Project no. 90-1081 J final rept. 1952, 90 p

108.* DUVALL, W.I. Stress analysis applied to underground mining problems. Part I: Stress analysis applied to single openings. U.S. Bur. Min, Rep. Inv. 4192, 1948

109. EDGERTON, H.E. and BARSTOW, F.E. Further studies of glass fracture with high speed photography. J. Amer. Ceramic Soc, 24, 131, 1941

110.* EMERY, C.L. Strain energy in rocks. Proc. Intnl. Conf. State of Stress in Earth's Crust, Santa Monica, May, 1963, in press

111.* EMERY, C.L. Photoelastic coatings on granular materials. Inst. Physics. London, April, 1960, 15 p

112.* EMERY, C.L. The strain in rocks in relation to mine openings. Mining Eng. October 1960, pp. 54-61

113.* EMERY, C.L. Testing rock in compression. Mine and Quarry Engng, Vol. 26, no. 4, 1960, pp. 164-168 and 196-202

114.* EPSTEIN, B. Statistical aspects of fracture problems. J. Appl. Phys. Vol. 19, 1948, pp. 140-147

115. EVANS, W.H. The strength of undermined strata. Inst. Min. and Metall. Trans. Vol. 50, 1940-41, pp. 475-532

116. EVANS, I. A theory of the basic mechanics of coal ploughing. National Coal Board, M.R.E. Rep. no. 2151, 1959

117. EVANS, I. and MURRELL, S.A.F. Wedge penetration into coal. Colliery Engng. 1962, pp. 11-16

118.* EVANS, I. and POMEROY, C.D. The strength of coal in uniaxial compression. National Coal Board, M.R.E. Rep. no. 2035, 1956

119. EVANS, I. and POMEROY, C.D. The compressive strength of rectangular blocks of coal. National Coal Board, M.R.E. Rep. no. 2077, 1957

120. EVANS, I., POMEROY, C.D. and DAVIES, R. An apparatus for assessing the in-situ strength of coal. Colliery Engng, 1959, pp. 234-240

121. EVANS, I., POMEROY, C.D. and BERENBAUM, R. The compressive strength of coal. Colliery Engng. Vol. 38, 1961, pp. 75-80, 123-127, 172-176

122. EVANS, I. The tensile strength of coal. Colliery Engng, 1961, pp. 428-434

123. EVANS, R.H. Elasticity and plasticity of rocks and artificial stone. Proc. Leeds Phil. and Lit. Soc, Vol. 3, 1936, pp. 145-158

124.* EVERLING, G. Gesteinsmechanische Untersuchungen und Grundlagen zur Ermittlung des Gebirgsdruckes aus Bohrlochverformungen. Glückauf, Heft 7, 1960, S.390-409

125.* EVERLING, G. Das Endflächenproblem beim Druckversuch. Bergbau-Archiv, Heft 1, 1961, S.27-37

126.* EVERLING, G. Model tests concerning the interaction of ground and roof support in gate-roads. Int. J. Rock Mech. Mining Sci, Vol. 1, 1964, pp. 319-326

127. EVISON, F.F. The seismic determination of Young's modulus and Poisson's ratio for rocks in situ. Geotechnique, 1956, pp. 118-123

128. FELBECK, D.K. and OROWAN, E. Experiments on brittle fracture of steel plates. Weld. J. Supp., Vol. 34, Nov. 1955, pp. 570-575s.

129. FILON, L.N.G. On the elastic equilibrium of circular cylinders under certain practical systems of load. Phil. Trans. A, Vol. 198, 1902, pp. 147-233

130. FITZPATRICK, J. Biaxial device for determining the modulus of elasticity of stress-relief cores. U.S. Bur. Min. Rep. Inv. 6128, 1962

131. FOOTE, P. A laboratory investigation of the effect of cleat orientation and tensile strength on coal ploughing. National Coal Board, M.R.E. Rep. no. 2186, 1961

132.* FREDERICK, D. and GRACIA, M.A. The theoretical behaviour of an inelastic model material. Bull. Virginia Polytech. Inst. Engng. Exp. Sta. series no. 85, Vol. 46, no. 8, 1953, 32 p

133.* FRIEDMAN, M. Petrofabrics. Proc. Intnl. Conf. State of Stress in Earth's Crust, Santa Monica, May 1963, in press

134.* FUMAGALLI, E. Matériaux pour modèles réduits et installations de charge. RILEM Bull. Vol. 8, September, 1960

135.* FUMAGALLI, E. Suitable materials for static and dynamic tests on model concrete dams. Cement and Concrete Assoc. Fifth Congress on Big Dams, Paris, 1955

136. GADDY, F.L. A study of the ultimate compressive strength of coal as related to the absolute size of the cubical specimens tested. Virginia Polytechnic Inst. Bull. 112, 1960

137. GELLER, L.B. Impact strength measurements on selected rocks - Jet piercing research project. Dept. Mines and Tech. Surveys, Internal Rep. FMP-60-175 - MECH, 1960

138. GILMAN, J.J. Direct measurement of the surface energy of crystals. J. Appl. Phys, Vol. 31, 1960, pp. 2208-2218

139.* GILVARY, J.J. Fracture of brittle solids. I. Distribution function for fragment size in single fracture (theoretical). J. Appl. Phys, Vol. 32, no. 3, 1961, pp. 391-399

140. GOLDER, H. and AKROYD, T. An apparatus for triaxial compression tests at high pressures. Geotechnique, Vol. 4, 1954, p. 131

141. GORANSON, R. Fracture and flow in stressed solids. Trans. Amer. Geophys. Union, Part II, 1940, p. 698

142.* GORDON, J.E., MARSH, D.M. and PARRAFT, M.E.M.L. On the strength and structure of glass. Proc. roy. Soc. Series A, no. 1256, Vol. 249, 1959

143.* GRAMBERG, J. The axial cleavage fracture in brittle materials at compressive loading. Technological Univ. Delft, Rock Mechanics Rep. no. 1.07, 1952, 36 p

144. GREENLAND, B.J. Rock mechanics. Colliery Guard, 1961, pp. 346-348

145. GREENSPAN, M. Effect of a small hole on the stresses in a uniformly loaded plate. Quarterly Appl. Math, Vol. 2, 1944, pp. 60-71

146. GREENWALD, H.P., AVINS, S. and RICE, G.S. Compressibility and bearing strength of coal in place : Tests of lateral compression of Pittsburgh coal bed. U.S. Bur. Min., Tech. Publ. 527, 1933

147. GREENWALD, H.P., HOWARTH, H.C. and HARTMAN, I. Experiments on the strength of small pillars of coal in the Pittsburgh bed. U.S. Bur. Min. Tech. Publ. 605, 1939, also U.S. Bur. Min., Rep. Inv. 3575, 1941

148. GREENWALD, H.P. and HOWARTH, H.C. Compression tests of roof-salt slabs supported by potash salt pillars. U.S. Bur. Min., Rep. Inv. 3386, 1938, 16 p

149. GREGORY, A.R. Shear wave velocity measurements of sedimentary rock samples under compression. Rock Mechanics edited by Fairhurst, Pergamon Press, New York, 1963, pp. 439-472

150.* GRIFFITH, A.A. The phenomena of rupture and flow in solids. Phil. Trans. Royal Soc. (London), A.Vol. 221, 1921, pp.163-198

151.* GRIFFITH, A.A. Theory of rupture. First Int. Cong. Appl. Mech, Delft, 1924. Technische Boekhandel en Drukkerij J. Waltman Jr, 1925, pp. 55-63

152. GRIFFITH, J.H. Physical properties of typical American rocks. Iowa Eng. Exper. Sta. Bull. 161, 1937, 56 p

153.* GRIGGS, D. and HANDIN, J.H. Observations of fracture and a hypothesis of earthquakes. Geol. Soc. of America Mem, Vol. 79, 1960, pp. 347-364

154.* GRIGGS, D., TURNER, F.J. and HEARD, H.C. Deformation of rocks at 500° to 800°C. Geol. Soc. America Mem, Vol. 79, 1960, pp. 39-104

155. GRIGGS, D.T. and KENNEDY, G.C. A simple apparatus for high pressures and temperatures. American J. of Sci., Vol. 254, 1956

156. GRIGGS, D.T. An experimental approach to dynamic metamorphism. American Geophysical Union, Trans, Part I, 1941

157.* GRIGGS, D.T. Creep of rocks. J. Geology, Vol. 47, 1939, pp. 225-245

158.* GROBBELAAR, C. Some properties of rock from a deep level mine of the Central Witwatersrand. Ass. Min. Mngrs. S. Africa, Vol. 1958/9, Sept. 1958, pp. 311-330

159. GROSS, B. Mathematical structure of the theories of visco elasticity. Brazil Nat. Inst. Technology, Rio de Janero, 1953

160. GUCER, D.E. and GURLAND, J. Comparison of the statistics of two fracture modes. J. Mech. and Phys. Solids, Vol. 10, 1962, pp. 365-374

161.* GURNEY, C. The effective stress concentration at the end of a crack having regard to the atomic constitution of the materials. RAE Rpt. No. Mat 10, Rpts. and Mem. no. 2285, Dec. 1945, 5 p.

162.* GURNEY, C. and ROWE, P.W. The effect of radial pressure on the flow and fracture of reinforced plastic rods. RAE Rpt. No. Mat. 5, Rpts. and Mem. no. 2283, May 1945, 10 p

163.* GURNEY, C. and ROWE, P.W. Fracture of glass rods in bending and under radial pressure. RAE Rpt. No. Mat. 8, Rpts. and Mem. no. 2284, Nov. 1945, 5 p

164. GYSS, E.E. and DAVIS, H.E. The hardness and toughness of rocks. Min. and Met. (American), Vol. 8, June 1927, pp. 261-263

165.* HANDIN, J. and FAIRBAIRN, H.W. Experimental deformation of Hasmark dolomite. Geol. Soc. America. Bull. Vol. 66, 1955, pp. 1257-1274

166. HANDIN, J. and HAGER, R.V. Jr. Experimental deformation of sedimentary rocks under confining pressure : tests at room temperature on dry samples. American Ass. Petrol. Geologists Bull, Vol. 41, 1957, pp. 1-50

167. HANDIN, J. and HAGER, R.V. Jr. Experimental deformation of sedimentary rocks under confining pressure : tests at high temperature. American Ass. Petrol. Geologists Bull. Vol. 42, 1958, pp. 2892-2934

168.* HANDIN, J., HIGGS, D.V. and O'BRIEN, J.K. Torsion of Yule marble under confining pressure. Geol. Soc. America Mem. 79, 1960, pp. 245-274

169.* HARDY, H.R. Jr. Preliminary study into the possibilities of correlating the variation in compression and fracture modulus with variations in chemical and structural composition of mine rock samples. Canada Dept. Mines and Tech. Surveys - Rep. no. TM 27/56 - Fuels Div. Copy no. 10, 1956

170.* HARDY, H.R. Jr. Studies to correlate the compression modulus and Poisson's ratio values for mine rock as determined by SR-4 type resistance strain gauges and the Marten's mirror extensometer. Ottawa Dept. Mines and Tech. Surveys - Rep. no. TM 50/56, Copy no. 16, 1956

171. HARDY, H.R. Jr. Physical properties of mine rock under short period uniaxial compression : Part I: Results of McGillioray Mine, Coleman, Alberta. Canada Dept. Min Tech. Survey, Rep. FRL-243, Fuels Div, 1957

172. HARDY, H.R. Jr. Hardness tests on selected rock specimens using the Taber Dyhedron Dynamic Diamond tester and their correlation with other physical properties. Canada Dept. Mines and Tech. Survey, Tech. Memo no. 52/57-MIN, Copy no. 19, 1957

173. HARDY, H.R. Jr. and WALKER, F. Physical properties of mine rock and minerals uniaxial compression studies. 9. Initial studies to determine the physical properties of coal under short period uniaxial compression. Canada Dept. Mines and Tech. Surveys, Tech. Memo no. 69/57-MIN, Fuels Div. 1957

174.* HARDY, H.R. Standardized procedures for the determination of the physical properties of mine rock under short period uniaxial compression. Dept. Mines and Tech. Survey, Canada, Rep. no. FRL 242, 1957

175. HARDY, H.R. Jr. Physical properties of mine rock and minerals time-strain studies. 4. Development of new apparatus for maintaining constant stress on rock specimens during time-strain tests. Canada Dept. Mines and Tech. Surveys, Fuels Div. Tech. Memo 18/58-MIN, 1958

176.* HARDY, H.R. Jr. Time-dependent deformation and failure of geologic materials. Canada Dept. Mines and Tech. Surveys; Tech. Memo 25/59-MIN, 1959

177. HARDY, H.R. Jr. and LACHARITE, N. Physical properties of mine rock and minerals uniaxial tensile studies. 1. Initial studies of the tensile properties of mine rock specimens. Canada Dept. Mines and Tech. Surv. Fuels Div. Tech. Memo 17/58-MIN, 1958

178. HARDY, H.R. Jr. and MACLEAN, M.J. Physical properties of mine rock and minerals uniaxial compression studies. 10. Determination of the mathematical equations of stress-strain curves for some sedimentary rocks. Canada Dept. Mines and Tech. Surv. - Fuels Div. - Tech. Memo. 16/58-MIN, 1958

179. HARRIS, A.J. Failure of concrete under compound stress. The Engineer, 1946, p. 569

180. HARRISON, E., KIESCHNIK, W.F. Jr, and McGUIRE, W.J. THE mechanics of fracture induction and extension. Trans. AIME, 201, T.P. 3916

181. HASHIN, Z. The moduli of an elastic solid reinforced by rigid particles. Bull. Res. Council of Israel, Section C, Vol. 5C, no. 1

182.* HAST, N. The measurement of rock pressure in mines, Sveriges Geol. Under. Årsbok, Vol. 52, 1958, 183 p

183.* HEARD, H.C. Transition from brittle fracture to ductile flow in Stolenhofen limestone as a function of temperature, confining pressure and interstitial fluid pressure. Geol, Soc. America Mem. Vol. 79, 1960, pp. 193-226

184.* HILL, F.G. and DENKHAUS, H.G. Rock mechanics research in South Africa with special reference to rockbursts and strata movement in deep level gold mines. Seventh Commonwealth Min. Metall. Congr. Johannesburg, 1961

185.* HIORNS, F.J. and VENABLES, J. Propagation of fracture in brittle solids. B.C.U.R.A. Bull. Vol. 25, no. 10, Part II, 1961, pp. 369-408

186. HIORNS, F.J. Mechanical tests on coal. Fuel, Vol. 32, 1953, p. 113

187.* HIRAMATSU, Y. and OKA, Y. Stress around a shaft or a drift excavated in ground being in three-dimensional stress state. Internationales Büro für Gebirgsmechanik, 1961

188. HOBBS, D.W. The strength and stress-strain characteristics of Oakdale coal under triaxial compression. Geol. Mag, Vol. 97, 1960, pp. 422-435

189.* HOBBS, D.W. The strength and stress-strain characteristics of the M.R.E. representative coals under triaxial compression. National Coal Board, MRE Rep. no. 2198, 1961, 24 p

190. HOBBS, D.W. The strength of oakdale coal under triaxial compression. National Coal Board, Sci. Dept. M.R.E. Report no. 2150, 1959

191. HOBBS, D.W. The strength of coal under biaxial compression. National Coal Board, M.R.E. Report no. 2179, 1960

192. HOBBS, D.W. The tensile strength of rocks. Int. J. Rock Mech. Mining Sci., Vol. 1, 1964, pp. 385-396

193.* HOEK, E. Fracture of anisotropic rock. J. S. African Inst. Min. and Met., Vol. 64, no. 10, 1964, pp. 510-518

194.* HOEK, E. Rock fracture around mining excavations. Proc. 4th Intnl. Conf. on Strata Control and Rock Mech. New York, 1964. In press. also CSIR Rock Mech. Special Rep. no. 58, 1963

195.* HOEK, E. Experimental study of rock stress problems in deep level mining. Experimental Mechanics. Edited by Rossi Pergamon Press, London, 1963, pp. 177-193

196.* HOEK, E. Analysis of the stress, strain and displacements in the material surrounding a cylindrical hole in a semi-infinite body subjected to tri-axial loading. CSIR Rock Mech. Special Rep. no. 42, 1961, 15 p

197.* HOEK, E. and BERNER, G. The use of photoelasticity for experimental stress analysis. CSIR Special Rep. N 222, 1961, 30 p

198.* HOEK, E. and BIENIAWSKI, Z.T. Application of the photo-elastic coating technique to the study of the stress redistribution associated with plastic flow around notches. S. African Mech. Engr. Vol. 12, no. 11, 1963, pp. 275-287

199.* HOEK, E. and BIENIAWSKI, Z.T. A large field reflection polariscope. S. African Mech. Engr. Vol. 12, no. 8, 1963, pp. 222-226

200. HOLLAND, C.T. Mineral content, a factor in weathering of mine roof. Mining Congress J, 1956, pp. 49-54

201.* HORI, M. Statistical aspects of fracture in concrete. RILEM Bull. Part I - Vol. 11, June 1961, pp. 73-81, Part II - Vol. 16, Sept. 1962, pp. 39-46

202. HORIBE, T. and KOBAYASHI, R. Physical and mechanical properties of coal measure rocks under triaxial pressure. Proc. Intnl. Conf. Strata Control. Paris, 1960, pp. 175-186

203.* HOSKINS, J.R. Design and construction of a basic geo-mechanics laboratory. Ph.D. Thesis, University of Utah, 1962, 130 p.

204. HUBBERT, M.K. and RUBEY, W.W. Role of fluid pressure in mechanics of overthrust faulting. Geol. Soc. America. Bull. 70, 1959, pp. 165-206

205. HUBBERT, M.K. Mechanical basis for certain familiar geologic structures. Geol. Soc. America Bull, Vol. 62, 1951, pp. 355-372

206. HUBBERT, M.K. and WILLIS, D.G. Mechanics of hydraulic fracturing. Trans. AIME, Preprint 686-G

207.* INGLIS, C.E. Stresses in a plate due to the presence of cracks and sharp corners. Trans. Inst. Naval Architects, London, Vol. 55, Part I, 1913, pp. 219-230

208.* IRWIN, G.R. Fracture mechanics. Proc. 1st Symp. on Naval Struct. Mech. Edited by Goodier and Hoff, Pergamon Press, New York, 1960

209.* ISAACSON, E. de St. Q. Rock pressure in mines. Mining Publications Ltd., London, 1962, 260 p

210.* ISAACSON, E. de St. Q. Stress waves resulting from rock failure. Bull. Min. Ind. Expt. Sta., Penn. State Univ., Vol. 76, 1961, pp. 153-161

211. ISAACSON, E. de St. Q. Research into the rockburst problem on the Kolar goldfield. Mine & Quarry Engng, Vol. 23, no. 12, 1957

212. IVISON, D.C.K. Determination of some physical properties of McGillivray and International mine rock. Canada Dept. Mines and Tech. Surv. - Tech. Memo no. 6057-MIN, Copy no. 16, 1957

213.* JACOBI, O. and EVERLING, G. Model tests illustrating the effects of different roadway supports. Intern. Conf. on Strata Control, Paris, May 1960

214.* JAEGER, J.C. Elasticity, Fracture and Flow. John Wiley & Sons, New York, 1962 (2nd ed.) 208 p

215.* JAEGER, J.C. Rock failures at low confining pressures. Engineering, Vol. 189, 1960, pp. 283-284

216. JAEGER, J.C. The frictional properties of joints in rocks. Geofisica pure e applicata, Milano, Vol. 43, 1959, pp. 148-158

217. JAEGER, J.C. Punching tests on discs of rock under hydrostatic pressure. J. Geophysical Res. Vol 67, 1962, pp. 369-373

218. JAEGER, J.C. The distribution of stress round cylindrical openings. J. Chem. Metall. Min. Soc. S. Afr., Vol. 55, 1954, pp. 125-128

219. JOHNSON, R.P. Strength tests on scaled-down concretes suitable for models, with a note on mix design. Mag. Concrete Res, Vol. 14, no. 40, 1962, pp. 47-53

220. JOHNSTON, M.L. Pressure and rockburst from a practical point of view. Engng. & Min. J. 151, 1950, pp. 91-94

221. JONES, R. A method of studying the formation of cracks in a material subjected to stress. Brit. J. Appl. Phys, Vol. 3, 1952, pp. 229-232

222.* KERPER, M.J., MONG, L.E., STIEFEL, M.B. and HOLLEY, S.F. Evaluation of tensile, compressive torsional, transverse, and impact tests and correlation of results for brittle cermets. J. Res. Nat. Bureau of Standards, Vol. 61, no. 3, 1958, Res. Paper 2895

223. KIES, J.A. The strength of glass. Naval Research Lab. Report 5098, 1958, 26 p

224. KING, F.R. and TABOR, D. The strength properties and frictional behaviour of brittle solids. Roy. Soc. London, Proc. Ser. A, Vol. 223, 1954, pp. 225-238

225. KING, M.S. and FATT, I. Ultrasonic shear-wave velocity in rocks subjected to simulated overburden pressure. Geophysics, Vol. 27, no. 5, 1962, pp. 591-598

226.* KIRSCH, G. Die theorie der elastizität und die bedürfnisse der festigkeitslehre. Zeit. Ver. Deut. Ing., Vol. 42, no. 29, 1898, pp. 797-807

227. KNUTSON, C.F. and BOHOR, B.F. Reservoir rock behavior under moderate confining pressure. Rock Mechanics edited by Fairhurst, Pergamon Press, New York, 1963, pp. 627-660

228. KONTOROVA, T. and FRENKEL, J. A statistical theory of brittle strength of real crystals. D.S.I.R. translation no. 13, from J. Tech. Phys. U.S.S.R. Vol. 11, no. 3, 1941, pp. 174-183

229. KUSAKABE, S. On the modulus of rigidity of rocks. Publ. Earthquake Inv. Comm., Tokyo, no. 11, 1903

230. KUSAKABE, S. Modulus of elasticity of rocks. Publ. Earthquake Inv. Comm., Tokyo, no. 17, 1904

231. KVAPIL, R. The theory of the flow of loose and coarse substances. The S N T L Tech. Digest no. 10

232. KVAPIL, R. und LUFFER, K. Beitrag zur Frage der Spannungsverteilung in würfelförmigin Probekörpern bei triaxialer Beanspruchung. Bergakademie, Sonderdruck aus Heft 11, 1960, 12 Jahrg. S. 587-594

233.* KVAPIL, R. Photoelasticimetric research in rock mechanics. The SNTL Tech. Digest, Vol. 2, no. 4, Czechoslovakia, Prague

234. KVAPIL, R. Concerning the theory of rock destruction. Intern. Strata Control Congress, Leipzig, 1958

235. LACHARITE, N. Determination of some tensile properties of mine rock and the effects of moisture on rock specimens and attached resistance type strain gages. Dept. Mines and Tech. Surveys, Fuels Div. Tech. Memo. 15/58-MIN 1958

236. LAFLAMME, C. Research on triaxial compression apparatus and determination of some physical properties of mine rock. Canada Dept. Mines and Tech. Surveys, Tech. Memo no. 68/57-MIN, Fuels Div. Copy no. 18, 1957

237. LARMOR, J. The influence of flaws and air-cavities on the strength of materials. Phil. Mag. and J. Sci., Vol. 33, Ser. 5, 1892, pp. 70-78

238. LAROCQUE, G.E. Measurement of the mechanical properties of eight rock types as part of the Jet Piercing Project. Canada Dept. Mines and Tech. Surveys, Internal Report FMP-60/37-MIN, 1960

239.* LEEMAN, E.R. and GROBBELAAR, C. A compressometer for obtaining the stress-strain curves of rock specimens up to fracture. J. Sci. Instr., Vol. 34, 1957, pp. 279-280

240.* LEEMAN, E.R. and GROBBELAAR, C. A lateral extensometer for the determination of the poisson's ratio of rock. J. Sci. Instr., Vol. 34, 1957, pp. 503-505

241.* LEEMAN, E.R. Some underground observations relating to the extent of the fracture zone around excavations in some central Rand mines. Ass. Min. Mngrs. S. Africa, Vol. 1958/59, 1958, pp. 357-384

242.* LEEMAN, E.R. Rockbursts in South African gold mines. New Scientist, Vol. 16, no. 308, 1962, pp. 79-82

243.* LELIAVSKY, S. Rock mechanics and the seventh congress on large dams. Rome, 1961. The Engineer, Aug. 10, 1962, pp. 228-232

244. LEON, A. Über die scherfestigkeit des betons. Beton und Eisen, Vol. 34, 1935, pp. 130-135

245. LIEBENBERG, A.C. A stress-strain function for concrete subjected to short-term loading. Mag. Concrete Res., Vol. 14, no. 41, 1962, pp. 85-90

246. LISOWSKI, A. Failure of rock cubic specimens in the light of the theory of elasticity. Acad. Polonaise Sci. Bull. Ser. Sci. Tech., Vol. 7, no. 5, 1959, pp. 341-351

247. LIVINGSTONE, C.W. Fundamentals of rock failure. Quart. Colorado Sch. Mines, Vol. 51, no. 3, 1956, pp. 1-11

248. MATSUSHIMA, S. On the flow and fracture of igneous rocks. Disaster Research Inst. Bull, no. 36, 1960, pp. 1-9

249.* Mc CLINTOCK, F.A. and WALSH, J.B. Friction on Griffith cracks in rock under pressure. Int. Cong. Appl. Mech., Berkeley, 1962, in press

250.* Mc HENRY, D. and KARNI, J. Strength of concrete under combined tensile and compressive stresses. J. American Conc. Inst., Proc. Vol. 54, 1958, pp. 829-839

251.* MENDES, F. de M. Comportamento mecânico de rochas xistos. (Mechanical behaviour of schistose rocks) Portugese with English synopsis. Dissertation to Instituto Superior Técnico, Lisbon, 1960, 243 p

252. MERRILL, H. and MORGAN, T.A. Method of determining the strength of a mine roof. U.S. Dept. Interior, Rep. of Invest. 5406, 1958

253. MIKLOWITZ, J. Elastic waves created during tensile fractures. Amer. Soc. Mech. Engrs. Paper no. 52-A-10, 1952

254. MILLARD, D.J., NEWMAN, P.C. and PHILLIPS, J.W. The apparent strength of extensively cracked materials. Proc. Phys. Soc. Section B, 1955, p. 723

255. MINDLIN, R.D. Gravitational stresses in bipolar co-ordinates. Proc. Fifth Internat. Congress Appl. Mech., 1939, pp. 112-116

256. MINDLIN, R.D. Stress distribution around a tunnel. Proc. Amer. Soc. Civ. Engrs., April 1939, pp. 619-642

257. MOHR, O. Abhandlung aus dem Gebiete der Technischen Mechanik. W. Ernst und Sohn, Berlin, 1914

258. MOHR, F. Gebirgsmechanik. Hermann Hubener Verlag. K.G. Goslav, 1963, 392 p

259. MORGANS, W.T.A. The elastic properties of coal. III. Static compression tests. National Coal Board, M.R.E. Report no. 2072, 1957

260. MORGANS, W.T.A. The elastic properties of coal. IV. Static bending tests. National Coal Board, Sci. Dept. M.R.E. Report no. 2078, 1957

261. MORGANS, W.T.A. and TERRY, N.B. Measurements of the static and dynamic elastic moduli of coal. Fuel, Vol. 37, no. 2, 1958

262.* MORRISSON, R.G.K. Synthetic rockbursts, part I. Canadian Min. Metall. Bull. Vol. 56, no. 613, 1963, pp. 394-396

263. MORRISON, R.G.K. and COATES, D.F. Soil mechanics applied to rock failure in mines. Canadian Inst. Min. Trans. Vol. 63, 1955, pp. 405-411

264. MORRISON, R.G.K. Points of view on the rock-burst problem. Trans. Canad. Inst. Min. Met., Vol. 42, 1939, pp. 443-460

265. MORRISON, R.G.K. Unsolved problem of rock bursts. Engng. and Min. J., Vol. 148, 1947, pp. 80-82

266. MORRISON, R.G.K. General theory of rock bursts. Eng. and Min. J., Vol. 148, no. 12, Dec. 1947, pp. 70-73, Vol. 149, no. 1, Jan. 1948, pp. 68-70, March pp. 66-72

267.* MULLER, L. Rock mechanics considerations in the design of rock slopes. Proc. Intnl. Conf. State of Stress in the Earth's Crust. Santa Monica, May 1963, in press

268. MULLER, L. Der Felsbau. Ferdinand Enke Verlag, Stuttgart, 1963, 624 p

269. MURDOCH, J.W. and KESLER, C.E. Effect of length to diameter ratio of specimen or the apparent compressive strength of concrete. A S T M no. 221, 1955

270.* MURRELL, S.A.F. The strength of coal under tri-axial compression. Mechanical Properties of Non-metallic brittle materials, ed. Walton, Butterworth Scientific Publications, London, 1958, pp. 123-145

271.* MURRELL, S.A.F. A criterion for brittle fracture of rocks and concrete under triaxial stress, and the effect of pore pressure on the criterion. Rock Mechanics. Proc. 5th Symposium on Rock Mech., Univ. Minnisota. Edited by Fairhurst. Pergamon Press, New York, 1963, pp. 563-578

272. MURRELL, S.A.F. The effect of high pressure on brittle fracture. Proc. Conf. on Physics and Chemistry of High Pressure. London, June 1962

273. MURRELL, S.A.F. A study of the mechanics of rock fracture in mining processes. Univ. Sheffield, Annual Rep. 1961

274.* MURRELL, S.A.F. and MISRA, A.K. Time-dependent strain or 'creep' in rocks and similar non-metallic materials. Trans. Inst. Min. Metall., Vol. 71, 1962, pp. 353-378

275.* MUSKHELISHVILI, N.I. Some basic problems of the mathematical theory of elasticity. 3rd Edition, translated by Radok J.R.M. P. Noordhoff Ltd, Groningen-Holland, 1953, p. 49

276. NABARRO, F.R.N. The modern atomic approach to the mechanical properties of solids. The S.Afr. Inst. Electr. Engr., 1955

277. NADAI, A. Theory of flow and fracture of solids. Vol. I. Mc Graw-Hill Book Co., Inc. New York, 1950, 572 p

278.* NEUBER, H. Kerbspannungslehre. Springer - Verlag, Berlin. Theory of notch stresses, David Taylor Model Basin Translation no. 74, 1945

279.* NEVILLE, A.M. Some aspects of the strength of concrete. Civ. Engng. and Public Works Rev. Part I in Vol. 54, no. 639, 1959, pp. 1153-1156, Part II in Vol. 54, no. 640, 1959, pp. 1309-1439

280. NISHIHARA, M. Stress-strain relation of rocks. Doshisha Engng. Rev., Vol. 8, no. 2, 1957, pp. 32-55

281.* OBERT, I., WINDES, S.L. and DUVALL, W.I. Standardized tests for determining the physical properties of mine rock. U.S. Bur. Mines. Rpt. Inv. no. 3891, 1946, pp. 1-67

282. OBERT, L. Effects of stress relief and other changes in stress on the physical properties of rock. U.S. Bur. Min., Rep. Inv. 6053, 1962

283.* ODE, H. Faulting as a velocity discontinuity in plastic deformation. Geol. Soc. America Mem. 79, 1960, pp. 293-321

284.* ODE, H. A note concerning the mechanics of artificial and natural hydraulic fracture systems. Quart. Colorado School of Mines. Vol. 51, no. 3, 1956, pp. 21-29

285. ONODERA, T.F. Dynamic investigation of foundation rocks in situ. Rock Mechanics edited by Fairhurst, Pergamon Press, New York, 1963, pp. 517-534

286.* OROWAN, E. Fracture and strength of solids. Rept. Prog. Phys., Vol. 12, 1949, pp. 185-232

287.* OROWAN, E. Mechanism of seismic faulting. Rock Deformation Geological Society of America, New York, 1960, pp. 323-345

288.* OROWAN, E. Energy criteria of fracture. Weld. J. Supp. Vol. 34, March 1955, p. 157s - 160s.

289. PATCHING, T.H. Tri-axial compression tests of fragmented coal. Canada Dept. Mines and Tech. Surveys, Internal Rep. FMP-60/68-MIN

290. PATERSON, M.S. Experimental deformation and faulting in Wombeyan marble. Geol. Soc. America Bull. Vol. 69, pp. 465-476

291. PENNINGTON, J.V. Rock failure in percussion. The Pet. Engineer, May, 1954, 26, 5, B-76

292. PHILLIPS, D.W. Further investigation of the physical properties of coal-measure rocks and experimental work on the development of fractures. Trans. Inst. Min. Engrs., Vol. 82, 1931/32

293. PICKETT, G. Application of the Fourier method to the solution of certain boundary problems in the theory of elasticity. J. Appl. Mech., American Soc. Mech. Eng., Vol. 11, A - 176, 1944

294. POMEROY, C.D. and MORGANS, W.T.A. The tensile strength of coal. Min. Res. Est., Report 2019, 1955

295. PRATIGNIC, K. Statistical studies related to the uniaxial rock testing program study of long term stability in the time-strain apparatus and the study of observed fractures in diamond drill core. Canada Dept. Mines and Tech. Surveys - Internal Rep. FMP-60/61-MIN, 1960

296. PRETORIUS, P.G.D. Some observations on rock pressure at depth on E.R.P.M. Ltd., Ass. Min. Mngrs. S. Africa, Vol. 1958/59, 1958

297.* PRICE, N.J. The strength of coal measure rocks in tri-axial compression. National Coal Board, MRE. Rpt. no. 2159, 1960

298. PRICE, N.J. The compressive strength of coal measure rocks. Colliery Engng, 1960, pp. 283-292

299.* PROTODYAKONOV, M.M. Methods of evaluation of cracks and strength of rock systems at depth. Proc. 4th Intern. Conf. Strata Control and Rock Mech., New York, May 1964, in press

300. PROTODYAKONOV, M.M. Concerning a uniform method of determining coal strength. Academy of Sciences Press, 1954

301.* PROTODYAKONOV, M.M. Determining of mechanical properties of rocks. Third International Conf. Strata Control, Paris, 1960

302.* PROTODYAKONOV, M.M. Mechanical properties and drillability of rocks. Rock Mechanics edited by Fairhurst, Pergamon Press, New York, 1963, pp. 103-118

303. RADMANOVICH, M. and HARGRAVES, A.J. The strength of, and the stresses in, coal and coal mine rocks. Proc. Australas. Inst. Min. Metall, no. 203, 1962, pp. 45-65

304.* RAPHAEL, J.M. Structural model investigations for Orville dam. Struct. and Matls. Research Rept. Ser. 100, issue 6, Univ. California, Berkeley, 1960, 164 p

305.* REINER, M. Deformation and flow. H.K. Lewis & Co. Ltd, London, 1949

306.* REINIUS, E. A theory of the deformation and the failure of concrete. Cement and Concrete Ass. Translation no. 63, from Swedish article in Betong, no. 1, 1955, 31 p

307.* REINKOBER, O. Die zerreissfestigkeit dünner quarzfäden. Physikalische Zeit. Vol. 32, 1931, pp. 243-250

308. REYNOLDS, H.R. Rock Mechanics. Crosby, Lockwood and Son Ltd., London, 1961, 136 p

309. RICE, G.S. Bumps in coal mines - theories of causes and suggested means of prevention or of minimising effects. Amer. Inst. Min Engrs. Tech. Publ. 609, 1935

310. RICHART, F.E., BRANDIZAEG, A. and BROWN, R.L. A study of the failure of concrete under combined compressive stresses. Bull. 185, Eng. Exp. Station, Univ. Illinois, Urbana, Ill. 1928

311. RITCHIE, A.G.B. The tri-axial testing of fresh concrete. Mag. Concrete Res., Vol. 14, no. 40, 1962, pp. 37-42

312.* ROBERTSON, E.C. Experimental study of the strength of rocks. Geol. Soc. America. Bull. Vol. 66, 1956, pp. 1275-1314

313.* ROBERTSON, E.C. Viscoelasticity of rocks. Proc. Intnl. Conf. State of Stress in Earth's Crust. Santa Monica, May 1963, in press

314.* ROBERTSON, E.C. Creep of Stolenhofen limestone under moderate hydrostatic pressures. Geol. Soc. America. Mem. 79, 1960, pp. 227-244

315.* ROBINSON, L.H. The effect of pore and confining pressure on the failure process in sedimentary rock. 3rd Rock Mech. Symposium, Colorado School of Mines, April 1959

316.* ROBINSON, L.H. The mechanics of rock failure. Quart. Colorado School of Mines, Vol. 54, 1959, pp. 177-200

317. ROCHA, M., SERAFIM, J.L. and DASILVEIRA, A.F. Deformability of foundation rocks. Lab. Nac. Eng. Civ., Publ. 82, 1956

318.* ROLFES, J.B. The behaviour of rock and the possible danger resulting from the use of singly set props in longwall mining. John Thompson Bull. no. 2. J. Thompson Africa (Pty) Ltd, Johannesburg, January 1964, 62 p

319.* ROS, M. and EICHINGER, A. Experimental study of theories of rupture. Non-metallic materials. Eidgenoss, Materialprufungsanstalt E.T.H., Zurich, no. 28, June 1928, 57 p

320.* ROUX, A.J.A., DENKHAUS, H.G. and LEEMAN, E.R. The stresses in and the condition of ground around mining excavations. Trans. Canadian Inst. Min. Metall., Vol. 59, 1956, pp. 19-26 also Coal and Base Minerals Southern Africa, Vol. 4 no. 6, 1956, pp. 34-40 and Vol. 4, no. 7, 1956, pp. 26-34

321.* SACK, R.A. Extension of Griffith's theory of rupture to three dimensions. Proc. Phys. Soc. London. Vol. 58, 1946, pp. 729-736

322. SADOWSKY, M.A. and STERNBERG, E. Stress concentration around a tri-axial ellipsoidal cavity. J. Appl. Mech., Vol. 16, 1949, p. A-149

323.* SALAMON, M.G. An introductory mathematical analysis of the movements and stresses induced by mining in stratified rocks. Univ. Durham, King's College, Mining Bull. no. 3, Vol. 9, Series: Strata Control/Res. no. 16

324. SALAMON, M.D.G. Elastic analysis of displacements and stresses induced by mining of seam or reef deposits. J. S. African Inst. Min. Metall, Vol. 64, nos. 4, 6 and 10 1964

325. SALMASSY, O.K., SCHWOPE, A.D. and DUCKWORTH, W.H. Statistical significance of the strength of brittle materials. American Ceramic Soc. Bull. Vol. 33, 1954, pp. 240-243

341.* SUTHERLAND, R.B. Some dynamic and static properties of rock. Rock Mechanics edited by Fairhurst, Pergamon Press, New York, 1963, pp. 473-492

342.* TANDANAND, S. and HARTMAN, H.L. Investigation of dynamic failure by high-speed photography. Rock Mechanics edited by Fairhurst, Pergamon Press, New York, 1963, pp. 1-32

343. TERPIGOREV, A.M. and PROTODYAKONOV, M.M. Destruction of coal and rock. Canada Dept. Mines and Tech. Surveys, Internal Rep. FMP-60/70-MIN, 1960

344. TERRY, N.B. The elastic properties of coal. VII. Some investigations and considerations relating to anisotropy. Nat. Coal Board, Sci. Dept. M.R.E. Rep. no. 2094, 1958

345. TERRY, N.B. The dependence of the elastic behaviour of coal on the microcrack structure. Fuel, Vol. 38, no. 2, 1959

346. TERZAGHI, K. Stress conditions for the failure of saturated concrete and rock. American Soc. Testing Matls. Proc., Vol. 45, 1945, pp. 777-801

347. TERZAGHI, K. and RICHART, F.E. Stresses in rock about cavities. Geotechnique, June 1952, pp. 57-90

348.* TIMOSHENKO, S. and GOODIER, J.N. Theory of elasticity. McGraw-Hill Book Co. Inc., New York, 1934

349. TOCHER, D. Anisotropy in rocks under simple compression. Trans. American Geophysical Union, Vol. 38, 1957, pp. 89-94

350. TOPPING, A.D. Rock strength : the condition of failure. World Oil. Vol. 141, 1955, pp. 109-117

351. TOPPING, A.D. The use of experimental constants in the application of theories of strength to rock. Conference on solid mechanics, Sept. 1955, Res. Bull. no. 129

352. TRUMP, R.P. and PATNODE, H.W. Laboratory demonstrations of the failure of materials under uniform loads. Rock Mechanics edited by Fairhurst, Pergamon Press, New York, 1963, pp. 661-676

353.* U.S. BUREAU OF RECLAMATION. Physical properties of some typical foundation rocks. U.S. Bur. Reclamation Concrete Lab. Rpt. no. SP-39, 1953, 150 p

354.* U.S. BUREAU OF RECLAMATION. Laboratory tests of rock cores from Fremont canyon tunnel area - Glendo unit - Missouri river basin project, Wyoming. U.S. Bur. Reclamation Lab. Rpt. C-945, 1960, 30 p

355. U.S. BUREAU OF RECLAMATION. A revised method of interpretation of tri-axial compression tests for the determination of shearing strength. U.S. Bur. Reclamation Structural Research Lab. Rep. SP-9, 1946

356. VANZANT, B.W. Dynamic rock penetration tests at atmospheric pressure. Rock Mechanics edited by Fairhurst, Pergamon Press, New York, 1963, pp. 61-92

357.* VON KARMÅN, T. Festigsversuche under allseitigem druk. Zeit. Ver. Deut. Ing., Vol. 55, 1911, pp. 1749-1757

358. WALDORF, S.K. A simple method of capping compression test samples. Amer. Soc. Test. Mat. Bull. no. 216, 1956

359.* WALSH, J.B. and BRACE, W.F. A fracture criterion for anisotropic rock. J. Geophysical Res. in press

360. WALTERS, E.J. Role of porosity in the deformation of rock materials. Univ. Durham, Mining Bull. no. 2, Vol. 9, Series: Strata Control/Res. no. 15

361.* WALTON, P. Micro- and macro-strength of glass : a review. Mechanical Properties of Non-metallic brittle materials. Edited by Walton. Butterworth Scientific Publications, London, 1958

362. WANE, M. Investigation of stress concentration around a cylindrical cavity in a semi-infinite elastic body. Canada Dept. Mines and Tech. Surveys - Tech. Memo 81/59-MIN, 1959

363.* WANTLAND, D. Geophysical measurements of rock properties in situ. Proc. Intnl. Conf. State of Stress in Earth's Crust. Santa Monica, May 1963. in press

364. WEIBULL, W. A statistical theory of the strength of materials. Proc. Roy. Swedish Inst. Eng. Res. no. 151, 1939, 45 p

365. WEISS, O. The theory of rockbursts and the possibilities of geophysical methods in predicting rockbursts on the producing mines of the Witwatersrand. J. Chem. Metall. Min. Soc. S. Afr., Vol. 38, 1938, pp. 273-329

366. WEISS, O. Experiments in the fracturing of Witwatersrand quartzites under direct pressure. J. Chem. Metall. Min Soc. S. Afr., Vol. 41, 1941, pp. 355-363

367.* WELLS, A.A. and POST, D. Dynamic stress distribution around a running crack. Proc. Soc. Exptl. Stress Anal. Vol. 16, 1958, pp. 69-96

368.* WELLS, A.A. Brittle fracture mechanics : a survey of published work. Aeronautical Res. Council. Rep. ARC 21508 CCP 75, 1959

369.* WILLIAMS, M.L. The stresses around a fault or crack in dissimilar media. Seismological Soc. America. Bull. Vol. 49, no. 2, 1959, pp. 199-204

370.* WILLIAMS, M.L., JESSEY, M.E. and PARMERTER, R.P. Some exploratory studies in stress wave propagation. Proc. Soc. Exp. Stress Anal., Vol. 17, no. 2, 1960

371. WINDES, S.L. Physical properties of mine rock part I. U.S. Bur. Min., Rep. Inv. 4459, 1949, 79 p

372. WINDES, S.L. Physical properties of mine rock part II. U.S. Bur. Min., Rep. Inv. 4727, 1950, 37 p

373. WUERKER, R.G. Influence of stress rate and other factors on strength and elastic properties of rocks. 3rd Rock Mech. Symposium, Colorado School of Mines, April 1959

374.* WUERKER, R.G. The status of testing strength of rocks. Trans. American Soc. Min. Engng., Nov. 1953, pp. 1108-1113

375.* WUERKER, R.G. Annotated tables of strength of rock. American Inst. Min. Engrs. Petrol. branch paper no. 663-9, 1959

376. WUERKER, R.G. Measuring the tensile strength of rocks. Mining Engng, 1955, 157 p

377. WUERKER, R.G. The shear strength of rocks. Min. Engng., 1959, pp. 1022-1026

378.* YI-YUAN YU. Gravitational stresses on deep tunnels. J. Appl. Mech., Vol. 19, 1952, pp. 537-542

379. YOKOBORI, T. Failure and fracture of metals from the standpoint of Stochastic theory. J. Physical Soc. Japan, Vol. 8, no. 1, 1953, pp. 104-106

380. ZHELTOV, Iu. P. and KHRISTIANOVITCH, S.A. On the mechanism of hydraulic fracturing of oil-bearing strata. Izv. AN SSSR, Otd. tekhn. n., no. 5, 1955, pp. 3-41

381. ZHELTOV, Iu. P. On the formation of vertical cracks in a strata by the help of a filtering fluid. Izv. AN SSSR. Otd. tekhn. n. no. 8, 1957, pp. 56-62

382. ZISMAN, W.A. Young's modulus and Poisson's ratio with reference to geological applications. Proc. Nat. Acad. Sci. (Geology), Vol. 19, 1933, pp. 653-686

ADDITIONAL REFERENCES

(in order of appearance in the text)

383. HOEK, E. and BIENIAWSKI, Z.T. Brittle fracture propagation in compression. Submitted for publication in the International Journal of Fracture Mechanics, 1965

384. HOEK, E. and BIENIAWSKI, Z.T. Fracture propagation mechanism in hard rock. Unpublished paper.

385. BRACE, W.F. Some new measurements of linear compressibility of rocks. J. Geophysical Res. Vol. 70, no. 2, 1965, pp. 391-398

386. WALSH, J.B. The effects of cracks on the uniaxial compression of rocks. J. Geophysical Res. Vol. 70, no. 2, 1965, pp. 399-411

387. WALSH, J.B. The effects of cracks on the compressibility of rock. J. Geophysical Res. Vol. 70, no. 2, 1965, pp. 381-389

388. COOK, N.G.W. A note on rockbursts considered as a problem of stability. S.A. Inst. Min. and Metall. Vol. 65, no. 8, 1965

389. DEIST, F.H. A non-linear continuum approach to the problem of fracture zones and rockbursts. S.A. Inst. Min. and Metall. Vol. 65, no. 10, May, 1965

390. HOEK, E. The design of a centrifuge for the simulation of gravitational force fields in mine models. S.A. Inst. Min. and Metall. Vol. 65, no. 9, 1965